ASSESSING THE IMPACTS OF CLIMATE CHANGE ON RIVER BASIN MANAGEMENT: A NEW METHOD WITH APPLICATION TO THE NILE RIVER

A Dissertation
Presented to
The Academic Faculty

by

Amy C. Tidwell

In Partial Fulfillment
of the Requirements for the Degree
Doctor of Philosophy in the
School of Civil and Environmental Engineering

Georgia Institute of Technology
December 2006

ASSESSING THE IMPACTS OF CLIMATE CHANGE ON RIVER BASIN MANAGEMENT: A NEW METHOD WITH APPLICATION TO THE NILE RIVER

Approved by:

Dr. Aris Georgakakos, Advisor
School of Civil and Environmental Engineering
Georgia Institute of Technology

Dr. Terry Sturm
School of Civil and Environmental Engineering
Georgia Institute of Technology

Dr. Phil Roberts
School of Civil and Environmental Engineering
Georgia Institute of Technology

Dr. Donald Webster
School of Civil and Environmental Engineering
Georgia Institute of Technology

Dr. Rong Fu
School of Earth and Atmospheric Sciences
Georgia Institute of Technology

Dr. Christa Peters-Lidard
NASA/GSFC

Date Approved: October 23, 2006

ACKNOWLEDGEMENTS

I wish to extend my deepest gratitude to the many people and organizations that have made this work possible. During my time at the Georgia Institute of Technology, I have benefited from the financial support of the Georgia Water Resources Institute, the National Science Foundation, the Food and Agriculture Organization of the United Nations, and the Georgia Tech President's office.

To my advisor, Dr. Aris Georgakakos, I have deep appreciation for overwhelming generosity of time, advice, and resources. His guidance has been an essential part of my intellectual and professional development.

To my colleagues at the Georgia Water Resources Institute and the Environmental Fluid Mechanics and Water Resources group, I am thankful for friendship, moral support, and many stimulating conversations over the years.

To my husband, George, I am truly grateful for unending love, patience, and support that has seen me through the trying times of the past five years. He has been my inspiration and given me the strength to persevere. I cannot thank him enough for what he has brought to my life.

TABLE OF CONTENTS

	Page
ACKNOWLEDGEMENTS	iii
LIST OF TABLES	x
LIST OF FIGURES	xiii
SUMMARY	xviii
CHAPTER	
Chapter 1: Introduction	1
1.1 Research Objective	2
1.2 Research Framework	2
Case Study System	3
1.3 Thesis Organization	3
Chapter 2: Literature Review	6
2.1 East African Climate	6
2.2 Hydrology	8
2.2.1 Equatorial Lakes	9
2.2.2 Ethiopian Basins	13
2.3 Climate Change Impact Assessments	14
2.3.1 Climate Scenario Methods	14
Global Climate Model Temperature and Precipitation	16
Regional Methods	17
2.4 African Climate Change Assessments	20
2.5 Literature Review Summary	22

Chapter 3: Future Climate Scenarios 24

3.1 Climate Data 26

3.2 Uncertainty Characterization 28

Climate Model Uncertainties 28

Climate System Unpredictability 28

Emissions Scenarios 29

Method Uncertainties 29

3.3 Statistical Basis for Assessing Model Skill 30

The Bootstrap 31

3.4 Lake Victoria 34

3.4.1 Model Skill 34

3.4.2. Bias Correction 39

3.4.3 Indicator Pixels 40

Spatial Relationships between Indicator and Target Pixels 40

3.4.4 Downscaling 43

3.4.5 Spatial Variability 45

3.4.6 Final Sequences 47

Temperature Assessment 52

Precipitation Assessment 54

3.5 Blue Nile 55

3.5.1 Model Skill 55

3.5.2 Bias Correction 57

3.5.3 Indicator Pixels 59

Precipitation 59

Temperature 63

3.5.4 Downscaling 66
3.5.5 Spatial Variability 68
3.5.6 Final Sequences 69
Temperature Assessment 70
Precipitation Assessment 71
3.6 Atbara 73
3.6.1 Indicators 73
3.6.2 Downscaling and Spatial Variability 74
3.6.3 Final Sequences 75
Temperature Assessment 77
Precipitation Assessment 78
3.7 Sobat 79
3.7.1 Indicator Pixels 80
3.7.2 Downscaling 83
3.7.3 Final Sequences 83
Temperature Assessment 86
Precipitation Assessment 87
3.8 Equatorial Lakes below Lake Victoria 88
3.8.1 Indicator Pixels 88
3.8.2 Downscaling 90
3.8.3 Final Sequences 91
Temperature Assessment 96
Precipitation Assessment 97
3.9 GCM Scenario Field Significance 98
3.10 Summary Remarks on Climate Scenarios 103

Chapter 4: Hydrologic Modeling 106

4.1 Lake Victoria 106

4.1.1 Lake Water Balance 107

Lake Evaporation 107

Watershed Evapotranspiration 109

4.1.2 Lake Victoria Hydrologic Model 111

4.1.3. Retrospective Climate and Hydrology Study 115

4.1.4 Hydrologic Impact Assessment 119

4.2 Blue Nile 123

4.2.1 Upper Blue Nile Hydrologic Model 124

4.2.2 Rivers Dinder and Rahad 129

4.2.3 Hydrologic Impact Assessment 130

4.3 Atbara 134

4.3.1 Atbara Hydrologic Model 134

4.3.2 Hydrologic Impact Assessments 138

4.4 Sobat 140

4.4.1 Sobat Hydrologic Model 141

4.4.2 Hydrologic Impact Assessment 145

4.5 Equatorial Lakes below Lake Victoria 147

4.5.1 Lake Kyoga and Lake Albert Hydrologic Models 148

4.5.3 Hydrologic Impact Assessment 151

4.6 Uncertainty in Hydrologic Scenarios 154

4.7 Summary Remarks on Hydrology 156

Chapter 5: Water Resources Assessments 159

5.1 Background 159

Equatorial Lakes 159

Sudd, Bahr el Ghazal, and Machar Marshes 159

White Nile 160

Blue Nile 160

Main Nile 161

5.2 Basin Development Scenarios 165

5.3 Assessment Methodology 166

5.3.1 Data Base 166

5.3.2 Water Resources Models 167

The Nile Decision Support Tool 167

Nile-DST Assessment Module 168

5.4 Scenario Assessments 169

5.4.1 Sensitivity of Water Supply Deficits to Climate Change 170

Scenario I: Current Development 170

Scenario II: Basin -wide Development 171

5.4.2 Sensitivity of Energy Generation to Climate Change 175

Scenario I: Current Development 175

Scenario II: Basin -wide Development 175

5.4.3 Sensitivity of River Flow and Reservoir Levels to Climate Change 180

Scenario I: Current Development 180

Scenario II: Basin -wide Development 181

5.5 Summary Remarks on Water Resources Assessments 188

Southern Nile 188

Eastern Nile 189

Main Nile 189

Chapter 6: Conclusions and Recommendations 191

6.1 Scientific Contributions 191

6.2 Application to the River Nile 193

Summary of Assessment Findings 193

6.3 Recommendations for Future Work 196

APPENDIX A: Temperature and Precipitation Spatial Relationships 199

APPENDIX B: Hydrologic Ensembles 238

APPENDIX C: Nile System Specifications 257

REFERENCES 260

LIST OF TABLES

Page

Table 3.1: Temperature significance testing results, α = 10% , α = 5% shown with *, α = 1% shown with **. 37

Table 3.2: Precipitation significance testing results, α = 10% , α = 5% shown with *, α = 1% shown with **. 38

Table 3.3: Projected temperature changes between final 30 years (2070-2099) and 30-year baseline (1961-1990). 53

Table 3.4: Projected percentage precipitation changes between final 30 years (2070-2099) and 30-year baseline (1961-1990). 54

Table 3.5: Blue Nile precipitation indicator sets. 60

Table 3.6: Blue Nile downscaling statistics. 66

Table 3.7: Projected temperature changes between the final 30 years (2070-2099) and the 30-year baseline (1962-1991). 71

Table 3.8: Projected precipitation changes between the final 30 years (2070-2099) and the 30-year baseline (1962-1991). 72

Table 3.9: Atbara precipitation indicator sets. 74

Table 3.10: Atbara downscaling statistics. 75

Table 3.11: Projected temperature changes between the final 30 years (2070-2099) and the 30-year baseline (1962-1991). 78

Table 3.12: Projected precipitation changes between the final 30 years (2070-2099) and the 30-year baseline (1962-1991). 79

Table 3.13: Sobat precipitation indicator sets. 82

Table 3.14: Sobat downscaling statistics. 83

Table 3.15: Projected temperature changes between the final 30 years (2070-2099) and the 30-year baseline (1962-1991). 86

Table 3.16: Projected temperature changes between the final 30 years (2070-2099) and the 30-year baseline (1962-1991). 87

Table 3.17: Projected precipitation changes between the final 30 years (2070-2099) and the 30-year baseline (1962-1991). 89

Table 3.18: Equatorial lakes precipitation indicator sets. 91

Table 3.19: Equatorial Lakes downscaling statistics. 97

Table 3.20: Projected temperature changes between the final 30 years (2070-2099) and the 30-year baseline (1962-1991). 98

Table 3.21: Equatorial Lakes field significance results for temperature shown with the number of significant pixels over the critical number of significant pixels. 101

Table 3.22: Equatorial Lakes field significance results for precipitation shown with the number of significant pixels over the critical number of significant pixels. 102

Table 3.23: Eastern Nile field significance results for temperature shown with the number of significant pixels over the critical number of significant pixels. 102

Table 3.24: Eastern Nile field significance results for precipitation shown with the number of significant pixels over the critical number of significant pixels. 103

Table 4.1: Lake Victoria hydrologic model coefficients. 113

Table 4.2: Changes in lake water balance terms between 2070 to 2099 and baseline period, expressed as percentage of net basin supply. 123

Table 4.3: Upper Blue Nile hydrologic model coefficients. 127

Table 4.4: Atbara hydrologic model coefficients. 136

Table 4.5: Sobat hydrologic model coefficients. 143

Table 4.6: Lake Kyoga and Lake Albert hydrologic model coefficients. 150

Table 4.7: Summary of flow scenarios for the Blue Nile, Atbara and Sobat river basins. 157

Table 4.8: Summary of NBS scenarios for the Equatorial Lakes. 158

Table C.1: Storage and outflow specifications for the Equatorial Lakes. 258

Table C.2: Existing and potential hydroelectric sites on the Victoria and Kyoga Niles. 258

Table C.3: Existing and potential hydroelectric sites on the Blue Nile and Atbara Rivers. 259

Table C.4: Storage and hydroelectric specifications for the Aswan Complex. 259

LIST OF FIGURES

Page

Figure 1.1: Climate scenario and impact assessment methodology. 4

Figure 2.1: Nile River Basin. 9

Figure 2.2: Illustration of the delta approach to future climate scenarios. 17

Figure 3.1: Nile Basin study regions (GCM gridin red, CRU grid in gray.) 26

Figure 3.2: Example of sampling distribution for $\hat{\theta}$ indicating a significant result (top) and an insignificant result (bottom). 34

Figure 3.3: Thirty-two HadCM3 nodes covering the Lake Victoria region. 35

Figure 3.4: Example of the relationship between temperature at regional pixel 16 and one of the Lake Victoria pixels. 41

Figure 3.5: Example of spatial aggregation using the CRU data set. 44

Figure 3.6: Example of season independent (top) and season dependent (bottom) downscaling relationships. 45

Figure 3.7: Illustration of the regionalization of an indicator pixel and subsequent downscaling. 46

Figure 3.8: Downscaled temperature sequences for the lake sub-areas with observed baseline shown in black. 48

Figure 3.9: Downscaled temperature sequences for the watershed sub-areas with observed baseline shown in black. 49

Figure 3.10: Downscaled precipitation sequences for the lake sub-areas with observed baseline shown in black. 50

Figure 3.11: Downscaled precipitation sequences for the watershed sub-areas with observed baseline shown in black. 51

Figure 3.12: Trendlines for the eight projected temperature sequences over the downscaled watershed area of pixel 2. 52

Figure 3.13: Blue Nile region (pixels of interest shown in yellow). 56

Figure 3.14: Frequency curves of historical precipitation (blue) and future precipitation under the HadA2a scenario. 63

Figure 3.15: An example of using frequency matching to select future model departures (*h* represents historical temperature departures, *m* the model departures, and *m'* the final model departures.) 65

Figure 3.16: Season dependent downscaling from Pixel 89 to watershed 1. 67

Figure 3.17: An example of very high correlations between large scale pixels and watershed sequences. 68

Figure 3.18: Temperature sequences for two sub-basins in the Upper Blue Nile (observed baseline shown in black). 69

Figure 3.19: Precipitation sequences for two sub-basins in the Upper Blue Nile (observed baseline shown in black). 70

Figure 3.20: Atbara region with pixels of interested highlighted in yellow. 73

Figure 3.21: Temperature sequences for two Atbara sub-basins (observed baseline shown in black). 76

Figure 3.22: Precipitation sequences for two Atbara sub-basins (observed baseline shown in black). 77

Figure 3.23: Sobat region with pixels of interested highlighted in yellow. 80

Figure 3.24: Temperature sequences for four Sobat sub-basins (observed baseline shown in black). 84

Figure 3.25: Precipitation sequences for four Sobat sub-basins (observed baseline shown in black). 85

Figure 3.26: Equatorial Lakes region with pixels of interest highlighted in yellow. 88

Figure 3.27: CRU pixels over the Equatorial Lakes. 90

Figure 3.28: Temperature sequences for the Lake Kyoga sub-basins (observed baseline shown in black). 92

Figure 3.29: Temperature sequences for the Lake Albert sub-basins (observed baseline shown in black). 93

Figure 3.30: Precipitation sequences for the Lake Kyoga sub-basins (observed baseline shown in black). 94

Figure 3.31: Precipitation sequences for the Lake Albert sub-basins (observed baseline shown in black). 95

Figure 3.32: Equatorial Lakes field with thirty-two pixels (yellow). 100

Figure 3.33: Eastern Nile field with fourteen pixels (yellow). 101

Figure 4.1: Predicted (Q/P) versus observations. 114

Figure 4.2: Predicted (Q) versus observations. 115

Figure 4.3: Lake sequences. 117

Figure 4.4: Watershed precipitation sequences. 118

Figure 4.5: Watershed evapotranspiration sequences. 118

Figure 4.6: Lake Victoria hydrologic sequences (lake precipitation, lake evaporation, watershed runoff, and net basin supply) for Hadley scenarios. 120

Figure 4.7: Lake Victoria hydrologic sequences (lake precipitation, lake evaporation, watershed runoff, and net basin supply) for Echam and Canadian scenarios. 121

Figure 4.8: Eight-member ensemble of Lake Victoria net basin supply with observed baseline shown in black. 122

Figure 4.9: Upper Blue Nile hydrologic units. 126

Figure 4.10: Observed (blue) and simulated (pink) Upper Blue Nile flows 128

Figure 4.11: Scatter plot of observed versus predicted Upper Blue Nile flows. 129

Figure 4.12: Relationship between monthly Border and Dinder flow. 130

Figure 4.13: Relationship between monthly Border and Rahad flow 130

Figure 4.14: Monthly Blue Nile flow sequences for eight climate scenarios. 131

Figure 4.15: Five-year moving average flows at Border. 131

Figure 4.16: Thirty-year mean monthly flows at Border. 132

Figure 4.17: Thirty-year mean monthly flows for the Dinder River. 133

Figure 4.18: Thirty-year mean monthly flows for the Rahad River. 133

Figure 4.19: Atbara hydrologic units. 135

Figure 4.20: Observed (blue) and simulated (pink) Atbara flows. 137

Figure 4.21: Scatter plot of observed versus predicted Atbara flows. 138

Figure 4.22: Monthly Atbara flow sequences for eight climate scenarios. 139

Figure 4.23: Five-year moving average flows for the Atbara River. 139

Figure 4.24: Thirty-year mean monthly flows for the Atbara River. 140

Figure 4.25: Sobat hydrologic units. 142

Figure 4.26: Observed (blue) and simulated (pink) Sobat flows. 144

Figure 4.27: Scatter plot of observed versus predicted Sobat flows. 145

Figure 4.28: Monthly Sobat flow sequences for eight climate scenarios. 146

Figure 4.29: Five-year moving average flows for the Sobat River. 146

Figure 4.30: Thirty-year mean monthly flows for the Sobat River. 147

Figure 4.31: Lake Kyoga and Lake Albert hydrologic units. 149

Figure 4.32: Observed (blue) and simulated (pink) Lake Kyoga net basin supply. 151

Figure 4.33: Observed (blue) and simulated (pink) Lake Albert net basin supply. 151

Figure 4.34: Five-year moving average net basin supply for the Lake Kyoga. 152

Figure 4.35: Five-year moving average net basin supply for the Lake Albert. 152

Figure 4.36: Thirty-year mean monthly NBS for Lake Kyoga. 153

Figure 4.37: Thirty-year mean monthly NBS for Lake Albert. 153

Figure 4.38: Had A2a Lake Kyoga net basin supply ensemble. 155

Figure 4.39: EchA2 Blue Nile flow ensemble. 156

Figure 4.40: HadB2 Blue Nile flow ensemble. 156

Figure 5.1: The Nile system with existing and planned development. 162

Figure 5.2: Mean annual water supply deficit. 173

Figure 5.3: Mean annual water supply deficit frequency curves. 174

Figure 5.4: Average annual energy generation. 177

Figure 5.5: Annual energy generation frequency curves (Scenario I). 178

Figure 5.6: Annual energy generation frequency curves (Scenario II). 179

Figure 5.7: Average annual river flow. 183

Figure 5.8: Monthly river flow frequency curves. 184

Figure 5.9: Monthly lake level at Lake Victoria. 186

Figure 5.10: Monthly reservoir elevation at High Aswan Dam. 187

Figure A.1: Lake Victoria Indicator-Target pixel temperature relationships (S 1). 200

Figure A.2: Lake Victoria Indicator-Target pixel temperature relationships (S 2). 201

Figure A.3: Lake Victoria Indicator-Target pixel precipitation relationships (S 1). 202

Figure A.4: Lake Victoria Indicator-Target pixel precipitation relationships (S 2). 208

Figure A.5: Lake Victoria temperature downscaling relationships. 215

Figure A.6: Lake Victoria precipitation downscaling relationships. 218

Figure A.7: Equatorial Lakes temperature downscaling relationships. 221

Figure A.8: Equatorial Lakes precipitation downscaling relationships. 226

Figure A.9: Sobat temperature downscaling relationships. 230

Figure A.10: Sobat precipitation downscaling relationships. 232

Figure A.11: Blue Nile temperature downscaling relationships. 234

Figure A.12: Blue Nile precipitation downscaling relationships. 235

Figure A.13: Atbara temperature downscaling relationships. 236

Figure A.14: Atbara precipitation downscaling relationships 237

Figure B.1: Lake Victoria net basin supply ensembles by scenario. 239

Figure B.2: Lake Kyoga net basin supply ensembles by scenario. 242

Figure B.3: Lake Albert net basin supply ensembles by scenario. 245

Figure B.4: Sobat River flow ensembles by scenario. 248

Figure B.5: Blue Nile flow ensembles by scenario. 251

Figure B.6: Atbara River flow ensembles by scenario. 254

SUMMARY

A framework is developed for the assessment of climate change impacts on water resources systems. The applied techniques include: quantifying global climate model (GCM) skill over a range of time scales; developing future climate scenarios based on GCM data that are found to skillfully represent the observed climate over an historical baseline period; and using the climate scenarios together with hydrologic and water resources models to make assessments of the potential impacts and implications of climate change on water resources systems. A statistical analysis of GCM skill in East Africa shows that temperature is well represented in the GCMs at monthly to annual time scales. Precipitation is found to be much less reliable in the models and shows skill in fewer seasons and nodes than temperature. Eight climate scenarios, stemming from three global climate models and two atmospheric emissions scenarios, project temperature increases between 2 and 5 ° Celsius by the year 2080. Precipitation projections vary widely across models as well as regionally. The scenarios project changes in precipitation from -38% to +42%.

The climate change impact methodology is applied to the Nile River Basin. It is shown that, in spite of widely varying precipitation projections, the major sub-basins of the Nile River will experience decreases in watershed runoff under all eight climate scenarios. Detailed water resources models are employed to assess the system wide response to the climate-induced hydrologic changes. The assessments indicate that water supply deficits will emerge by 2030 and continue to grow in frequency and magnitude by 2080. Additional impacts include reservoir depletion and reduced hydropower generation. An assessment of the river system response to basin development projects, including additional water storage and wetlands water conservation, indicates that adverse climate

impacts may be mitigated for 30 to 40 years. The assessments demonstrate the relevance of climate change considerations to water resources management and the development of water policy.

Chapter 1: Introduction

Current studies into the potential impacts of climate change remain largely uninformative to policy and decision makers in the water resources sector. Alarming trends in temperature and the potential for redistribution of fresh water has understandably led to concerns for the future availability of water resources. Although some projections suggest that significant climate change may occur over the same scales as water resources development and management, policy makers continue to rely heavily on the assumption that historical conditions will persist into the future. This is largely due to a lack of integrative tools with realism to tie climate to hydrology to water resources and yield meaningful information for decision makers.

Climate change impact assessments begin with developing scenarios of future climate. Typically, historical records of temperature and precipitation are adjusted according to some specified change, often based on the output of general circulation models (GCMs). The adjusted climate, or climate scenario, is then used to drive hydrologic models in the area of interest. Finally, the resulting hydrologic sequences are analyzed with respect to a baseline. Many of these studies are inconclusive due to conflicting trends across a number of climate scenarios, often showing potentially large runoff increases in some scenarios and significant drying in others. Thus previous climate and hydrologic scenarios tended to be most informative as aides to sensitivity studies rather than true impact projections.

From the water resources planning and management perspective, the more germane climate change issues relate not only to changes in basin outflow, but to how the coordinated response of an entire water system translates into tangible impacts.

Questions that may enter into the decision making process include: how will climate change affect the reliability of water supply and hydropower generation; what are the implications for drought and flood protection; what is the current and future system vulnerability and resilience; and what uncertainties underlie projected impacts?

1.1 Research Objective

This research aims to develop and demonstrate an integrative approach to climate, hydrology, and water resources modeling for assessing climate change impacts on water policy and water resources management. To this end, the major questions addressed in this work include:

- What is the information content of GCMs in specific regions, and how can model skill and relevance be quantified?
- What methodologies can be developed to extract regionally relevant information from these models?
- How can we account for uncertainty throughout the assessment process?
- Can integrative modeling (climate-hydrologic-water resources) be used to reach definitive conclusions regarding the implications of climate change for water resources management and suggest possible mitigation measures?

1.2 Research Framework

This research develops new methods to *(1)* assess the regional value of GCM predictions, *(2)* leverage regionally significant model aspects to generate plausible climate scenarios, *(3)* develop hydrologic models that are consistent with operational water resources models, and *(4)* use the climate scenarios in connection with the hydrologic and water resources models to assess the future response of the river basin under potential climate change. An important aspect of this work is uncertainty characterization stemming from

GCM output, regional assumptions in climate sequence development, downscaling, and hydrologic modeling. Therefore, the hydrologic series associated with each of the eight climate scenarios are themselves presented as ensembles based on the cumulative effect of uncertainties.

Case Study System

The Nile basin provides an interesting and important case study for this work. The river drains approximately 10 percent of the African continent and is vital to the economic development of the riparian countries. The primary water uses in the basin are water supply (agricultural, industrial, and urban) and energy generation. The majority of the basin remains largely undeveloped, and the primary source of employment is agriculture. At present, Egypt and Sudan represent nearly all of the consumptive use in the basin with 18.5 and 55.5 billion cubic meters per year, respectively. In light of an already stressed resource and a continent on the brink of rapid growth, effective climate change impact assessments may become critical to adaptive resource management strategies.

1.3 Thesis Organization

Following review of the relevant literature on climate, hydrology, and climate change impact assessments, Chapters 3 through 6 detail the methods and results of this research. The organization of the chapters closely follows the graphically depicted approach shown in Figure 1.1.

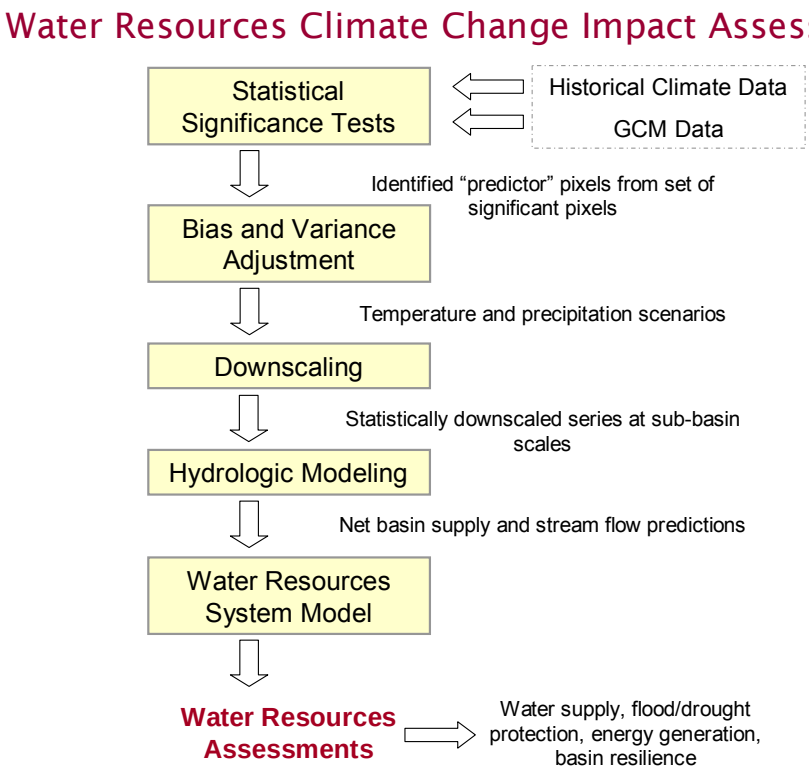

Figure 1.1: Climate scenario and impact assessment methodology.

Chapter 3 details the methods used to construct future climate scenarios. A novel statistical procedure is developed to test for significance of GCM temperature and precipitation series in the study regions. Model pixels demonstrating statistically significant skill are used, together with observed spatial relationships, as indicators of the regional climate and further developed into plausible climate scenarios. This process is applied to a total of eight GCM runs from three different modeling centers.

Following the above-mentioned GCM data analysis, Chapter 4 describes the development of hydrologic models for lakes Victoria, Kyoga, and Albert, and the Sobat, Blue Nile, and Atbara Rivers. The Lake Victoria hydrologic model is also used to test the hydrologic consistency of two methods for estimating evapotranspiration. After calibration, the

hydrologic models are used with the constructed climate scenarios to predict lake and river responses throughout the basins over the next 100 years.

The resulting hydrologic sequences are used as input to detailed water resources models to simulate the spatially distributed response of the Nile system to projected climate change. Chapter 5 describes the methods and results for climate change impact assessment of water resources. The Nile Decision Support Tool, developed at the Georgia Water Resources Institute, is used to simulate the system response and assess implications for water uses and users. Key findings are presented with respect to water supply deficits, hydropower generation, and river flows at representative points in the system. Finally, conclusions and recommendations are presented in Chapter 6.

Chapter 2: Literature Review

2.1 East African Climate

East African climate results from a complicated interplay of large scale atmospheric features such as monsoons and convergence zones, and highly heterogeneous local geographic features, such as steep topographic relief and large lakes. The region is influenced by two monsoons from the northeast and southeast of the continent, which in comparison to the Asian monsoons are relatively dry. In addition, westerly flow brings moist air from the Congo River Basin, which is associated with rainfall. The monsoonal flows are separated by the Inter-Tropical Convergence Zone (ITCZ), while the Congo Air Boundary separates the westerly from the easterly flow. Largely due to topography, easterly flow predominates to the east of the East African highlands, while westerly flow is influential to the west, including the lake plateau region.

Rainfall in East Africa is particularly variable and complex. Seasonal patterns range from a single rainy season to as many as three rainfall maxima, with average annual rainfall ranging from as much as 1800 millimeters in the mountains of Rwanda to less than 200 mm in the arid lowland regions of Sudan and Ethiopia. In the lake plateau, the extensive surface area of Lake Victoria itself strongly influences precipitation via the Lake Victoria Low. Nicholson (1996) points out that while the spatial heterogeneity and complexities of East African rainfall suggest local control over the mean climate, coherent spatial patterns of temporal variability implicate significant large scale control in the region. Correlations between region-averaged annual rainfall departures and smaller area series range from 50 to 80%. Principal component analyses from both Nicholson (1996) and Camberlin and Philippon (2002) also indicate spatial coherence in rainfall variability. Nyenzi (1988) found that the first eigenvector of the analysis explains

36% of the annual variance, while accounting for more than 50% of the short rain variance.

In the Equatorial Lakes region, the long rain season (Mar-May) is generally the more productive of the two rainy seasons. However, the short rains (Oct-Nov) demonstrate greater influence on inter-annual variability. In addition, variability of the short rains has been linked to ENSO and possibly even more strongly with SST in the Atlantic and Indian Oceans (Nicholson, 1996). Camberlin and Philippon (2002) underscore the greater difficulty with explaining the long rains. They found that even within the commonly defined long rains season, May does not demonstrate the same level of spatio-temporal consistency as the early season (Mar-Apr) and is therefore considered separately in the context of atmospheric dynamics.

Moving northeast of the lake plateau, the precipitation regime transitions from bi-modal to uni-modal. In the Ethiopian Highlands, the single rainy season is brought on with the passage of the ITCZ. Accordingly, the rainy season becomes progressively shorter in duration from south to north. In the southwestern portion of the highlands, the rains arrive around April-May and remain until as late as October. Near Lake Tana in the north, the rains do not materialize until June-July and remain through September. Temperature exhibits two annual minima and maxima. The onset of the summer rainy season acts to cool what would otherwise have been the warmest months of the year. Therefore, temperatures begin to increase during the Spring months, temporarily decrease during the rainy season, and again rise prior to the onset of Fall.

Additionally important characteristics of East African rainfall include non-random fluctuations in annual rainfall observed at scales of 2 to 6 years and the potential for extreme precipitation anomalies in individual years (Nicholson 1996). Nicholson (1996)

suggest that spectral peaks around 5 years may be associated with similar peaks of sea surface temperatures in the tropical Atlantic and Indian Oceans, which may ultimately be the link between East African rainfall and the ENSO phenomena. Extremely high precipitation in an individual year can lead to dramatic changes in Lake Victoria or severe flooding below the Blue Nile. One such occurrence was observed in 1961/62 and was responsible for a profound 2.5 m increase in the level of Lake Victoria.

2.2 Hydrology

The River Nile extends 6,700 kilometers through a drainage area equaling approximately 3 million square kilometers. The Nile Basin is shown in Figure 2.1. Although the foregoing discussion of East African climate reveals that some of this area is subject to very high rainfall, the average annual runoff from the basin is merely 30 millimeters. This low runoff is in large part due to the majority of Nile flow originating from a relatively small fraction of the basin. The two primary runoff producing regions in the Nile Basin are the lake plateau of equatorial East Africa and the Ethiopian, or Abyssinian, plateau. The following is an overview of the hydrology in these two regions.

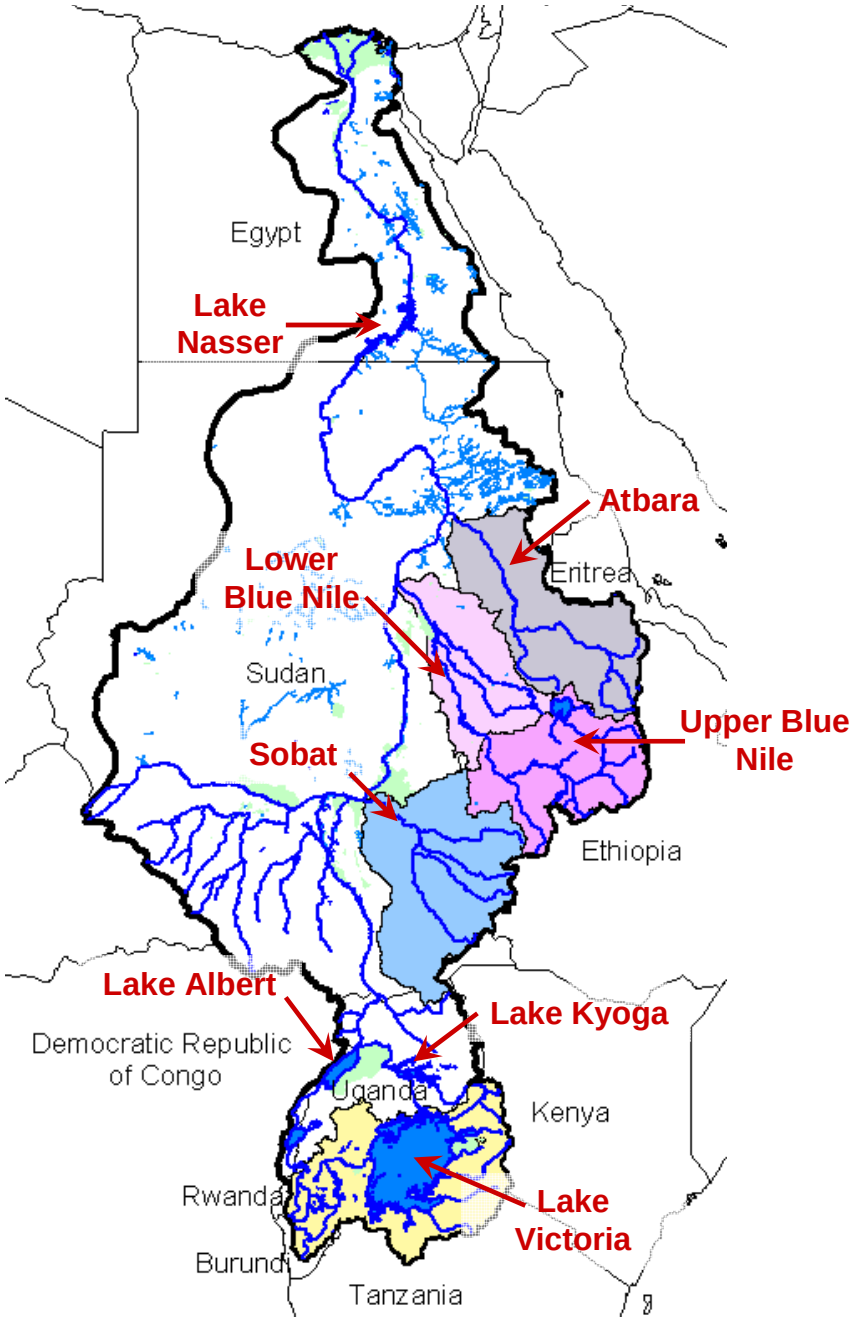

Figure 2.1: Nile River Basin.

2.2.1 Equatorial Lakes

Lake Victoria is a prominent feature in East African geography, climatology, and hydrology. The lake is located in the three countries of Uganda, Kenya and Tanzania,

with contributing watershed areas in Rwanda, Burundi and the Democratic Republic of Congo (DRC). With a lake surface of nearly 70,000 km^2 and total catchment area of approximately 193,000 km^2, the lake basin extends from 4° South to 1.3° North and 29° to 36° East. While the lake plateau lies at 1300 m elevation, highlands to the west and northeast reach elevations of 2500 m with some peaks reaching as high as 4500 m. Although much of the terrain is steep and rainfall is high in the lake region, watershed runoff is remarkably low due to the attenuating effects of many lake and wetland areas.

Lake water balance principally depends on lake rainfall and evaporation, watershed runoff, lake outflow, and change in lake storage. The Kagera basin, located west of the lake, is the largest tributary and accounts for approximately 1/3 of the total land contribution to the lake balance. The Kagera River basin spans approximately 60,000 km^2 and ranges between 1200 and 1600 m elevation with peaks reaching 4500 m. Although many of the tributaries are steep and annual rainfall ranges between 1000 and 1800 mm, substantial losses are incurred along a long and winding drainage path that encounters a series of lakes and swamps. The attenuating effect of the lakes and wetlands is manifest in the delayed flow peaks at various points in the Kagera drainage. The long rains arrive in the Kagera between February and May, leading to an upper tributary runoff peak in April. However, the peak does not develop until May in the middle portion of the basin and is further delayed until July for the lower reach of the river (Sutcliffe and Parks, 1999).

A series of smaller basins located in the northern, eastern, and southern portions of the lake watershed also contribute runoff to Lake Victoria and cumulatively account for twice the inflow contribution of the Kagera basin. As with the Kagera, all tributaries experience a bi-modal rainfall distribution, although there are some differences. The Nzoia basin to the northeast of the lake extends into the Kenyan highlands and exhibits

peaks closer to July-August than the western and southeastern basins. To the southeast, the two rainy seasons are markedly delineated with more influential dry seasons than in other parts of the lake region and lower base flow than both the Kagera and the northeastern tributaries. The other contributing tributaries have earlier peaks and lower base flows than the Kagera, but many of these tributaries also pass through swamps at the edge of the lake.

The watershed runoff into the lake is about 30% of the total lake water input (lake precipitation and watershed runoff). Given the vast lake area, precipitation over the lake is by far the largest input. Historically, however, lake precipitation and free surface evaporation have been quite close in magnitude and are largely offsetting. Due to the nonlinear relationship between precipitation and runoff, runoff variability is amplified with respect to the precipitation that drives it. In this regard, Sutcliffe and Parks (1999) note that early attempts to model lake fluctuations suffered from poor estimates of lake precipitation and from failure to properly estimate the true runoff variability and, consequently, the variability of the lake balance.

Precipitation over the lake is generally estimated from a small set of shoreline stations and from a few islands. However, the lake itself greatly influences rainfall, and lake precipitation is believed to be as much as 30% higher than along the shore. Studies of lake evaporation have investigated numerous estimation methods. Although the methods are reasonably close on an annual basis, monthly values may differ considerably. HYDROMET project lake evaporation estimates for the years 1969 and 1970 using the water balance and mass transfer techniques (WMO, 1974) varied 3 to 5% on an annual basis, but differed by as much as 30 to 60% in a given month.

Lake storage is very large and acts as a buffer between changes in lake water supply and lake outflow to the Nile river downstream. The impacts of changing lake inflows may not manifest as significant changes in outflow for several years (Sutcliffe and Parks, 1999).

Below Lake Victoria, the Upper Victoria Nile drops 105 m over its 130 km course toward Lake Kyoga. Kyoga is a shallow lake, only a few meters deep, surrounded by considerable wetlands with a combined surface area of 4,700 km^2. Much of its 75,000 km^2 drainage area is relatively flat valley, but with steeper mountainous terrain to the northeast. The average annual basin rainfall is nearly 1300 mm. Even so, the net water contribution of Lake Kyoga to Victoria Nile flows has historically been very low and often negative due to evaporative losses over the lake and wetlands (Sutcliffe and Parks 1999; Shahin 1985). From the outlet of Lake Kyoga, the Lower Victoria Nile, or Kyoga Nile, flows north and west, passing through a series of rapids and dropping 410 m along its course toward Lake Albert. Lake Albert has a surface area of approximately 5,300 km^2 and direct drainage basin of 17,000 km^2. In addition to the Victoria Nile, the lake also receives inflow from the Semliki River in the south, which drains an additional 30,500 km^2 that includes Lakes Edward and George. The direct rainfall and inflow from Albert's immediate basin is thought to be offset by evaporation over the lake surface. Therefore, the net contribution of Lake Albert to the main Nile flows is believed to be a result of the Semliki inflow (Shahin, 1985).

A number of factors complicate the study of Lake Albert water balance. Inflow and outflow from Lakes Kyoga and Albert are dominated by the volume originating at Lake Victoria making the additional lake balance terms small in comparison. There are inadequate flow measurements along the Lower Victoria Nile, and Lake Albert outflow is not directly measured but, rather, inferred from downstream measurements during

periods when intermittent tributaries are dry. Consequently, estimates of Lake Kyoga and Lake Albert net basin supplies are not independent of each other (Sutcliffe and Parks 1999).

Exiting Lake Albert, the river flows north into Sudan and is known as the Bahr el Jebel. Below the Sudan-Uganda border, the river receives seasonal flow from torrential streams before entering the Sudd, below Mongalla. The Sudd is a region of permanent swamps and seasonal wetlands, within which approximately half of the Bahr el Jebel flow is lost to evaporation. Beyond the Sudd, the river receives the Bahr el Ghazal at Lake No and is called the White Nile. Although the headwaters of the Bahr el Ghazal receive 1200-1400 mm of precipitation, nearly all of the runoff is lost in lower swamps, which ultimately results in negligible contributions to White Nile flow (Sutcliffe and Parks, 1999; Shahin, 1985).

2.2.2 Ethiopian Basins

The White Nile is joined by three additional tributaries, the Sobat, Blue Nile, and Atbara Rivers, all of which have their origins in the Ethiopian plateau. The Sobat River joins the White Nile prior to Malakal, nearly doubling the flow from the Sudd. This basin is comprised of two distinct tributaries, the Baro (41,400 km^2) and Pibor (109,000 km^2). The Baro originates in the Ethiopian plateau and is the more productive of the two branches. Portions of the Baro flow spill through a series of channels to large wetlands known as the Machar Marshes. Additionally, under high flow conditions, the river over flows its banks and inundates parts of the floodplain. The Pibor basin, albeit much larger, contributes considerably less flow. It drains portions of the Ethiopian plateau, the northeastern edge of the lake plateau, and the Sudan plain. Rainfall is usually low and the milder slope renders it liable to form swamps and wetlands.

The Blue Nile basin adjoins the Sobat to the north and drains rugged terrain through deep canyons cut into the Ethiopian plateau. The river undergoes a steep 900 kilometer decent from its source in Lake Tana at 1,829 meters elevation to the Sudan plain at 490 m. The river continues to flow across the flat plain for another 800 km and intercepts two smaller rivers, Dinder and Rahad, bringing the total drainage area to 324,500 km^2. At Khartoum, the Blue and White Niles converge to form the Main Nile. 84% of the annual runoff in the Blue Nile basin occurs between June and October, resulting from heavy rains during the single rainy season. 320 kilometers downstream of Khartoum, the Atbara River also flows from its headwaters in Ethiopia and has a drainage area of 112,400 km^2. The Atbara shares many characteristics with the Blue Nile, though the upper portion of its basin has an even greater slope, the rainy season is shorter, and it does not have a large lake at its source. Consequently, the Atbara River is even more strongly seasonal than the Blue Nile, often receding to little or no flow in the dry season. From the mouth of the Atbara, the Nile continues its course through flat terrain within an arid climate towards Aswan, Egypt.

2.3 Climate Change Impact Assessments

2.3.1 Climate Scenario Methods

There are two major components to any investigation aiming to assess hydrologic response under a changing climate. First, it is necessary to have an appropriate hydrologic model that performs well at the temporal scale of interest. Second, it is important to carefully consider how to create plausible scenarios of future climate to drive the hydrologic model. Global climate models (GCMs) are a commonly used tool to aide climate scenario development. GCMs are based on the physical laws describing the dynamics of the atmosphere and oceans, as represented by mathematical equations. The equations are solved on three-dimensional grids that typically have horizontal resolutions around 250 km and 10 to 30 vertical levels. Typical ocean models have horizontal

resolution around 125 to 250 km and vertical resolution between 200 and 400 m. Model time steps are typically around 30 minutes. Processes that occur on finer spatial or temporal resolutions are parameterized (IPCC, 2001). Although the climate models are based on the same physical laws, there are several ways in which the models may differ. Two examples of the source of the differences include differences in model resolution and the form of sub-grid scale process parameterization.

While global climate models (GCMs) are at present the most powerful and widely used means for exploring potential future climates, large uncertainties remain primarily with respect to modeling errors, climate unpredictability, and scenarios of future greenhouse gas and other emissions. Models differ in their representation of the climate sensitivity to changes in atmospheric greenhouse gas composition. Moreover, the inter-model differences in projected regional changes are much larger than the global scale differences even when models are forced with a common emission scenario. Therefore, it is incumbent on each impact assessment to determine the best methods for employing the available climate tools and address the inherent uncertainties.

Climate change impact studies abound in the literature; however, with the exception of the increased availability and use of regional climate models (RCM), little has changed in recent years with regard to how climate scenarios are constructed. Given the broad interest and concern for potential impacts of climate change, the Intergovernmental Panel on Climate Change (IPCC) has generated a wealth of technical information and guidance material related to the science of climate change. Here the focus is on methods for generating regional climate scenarios for impact assessments.

Global Climate Model Temperature and Precipitation

Surface temperature is generally represented quite well in models. Globally, model pattern correlations are consistently above 0.95. Removing the zonal component (dependence on latitude), the pattern correlations are generally between 0.7 to 0.8. Mean model biases are generally within 1 °C over the oceans and within 5 °C over land (IPCC, 2001; Achuta Rao et al., 2004).

In general, the large-scale structure of model precipitation is much better represented than absolute quantities, with zonal averages showing reasonable magnitudes and patterns (Achuta Rao et al., 2004). Spatial variance of model precipitation agrees well with observations, and pattern correlations range between 0.7 and 0.9. The pattern correlations, however, say nothing of model biases. Model mean precipitation in the tropics relates to Dec-Jan-Feb observations fairly well, but is seen to greatly underestimate Jun-Jul-Aug precipitation. Importantly, inter-model differences are quite large with respect to precipitation, and particularly so in areas of tropical convergence. Multi-model mean precipitation is shown in a number of studies to compare better with observations than any individual model (Achuta Rao et al., 2004)

The latest generation of coupled atmosphere-ocean GCMs have shown progress in their ability to represent such phenomena as ENSO, and many models are able to demonstrate ENSO-like sea surface temperature variability (IPCC, 2001). The ability of models to capture ENSO behavior could have bearing on modeled precipitation variability in some regions. Hulme et al. (2001) demonstrated that the two expected ENSO-precipitation relationships in Africa (East Africa from Oct-Nov and South Africa from Nov-Feb) do materialize to some extent in a control run of the HadCM2 model. However, the relationship strengths are underestimated and the spatial extent displaced with respect to observations.

Regional Methods

Although the recent generation of GCMs have improved over their early predecessors and appear to represent the general atmospheric circulation well at global scales, they are still not regarded as sufficiently reliable for direct application in regional climate studies. Instead, GCMs are typically used to generate change fields (IPCC, 1999), which are pixel by pixel differences, or deltas, between the modeled future climate and the modeled baseline climate (run with observed atmospheric forcing). The delta method assumes that climate changes are more reliably modeled than the absolute climate conditions, which exhibit significant modeling biases. Since the observed climate is known to vary considerably on inter-annual and multi-decadal scales, change fields are generally computed as changes in 30-year climatologies. The change fields are then applied to the observed baseline climate and the result used as a potential future climate scenario. Figure 2.2 illustrates the delta approach with respect to temperature.

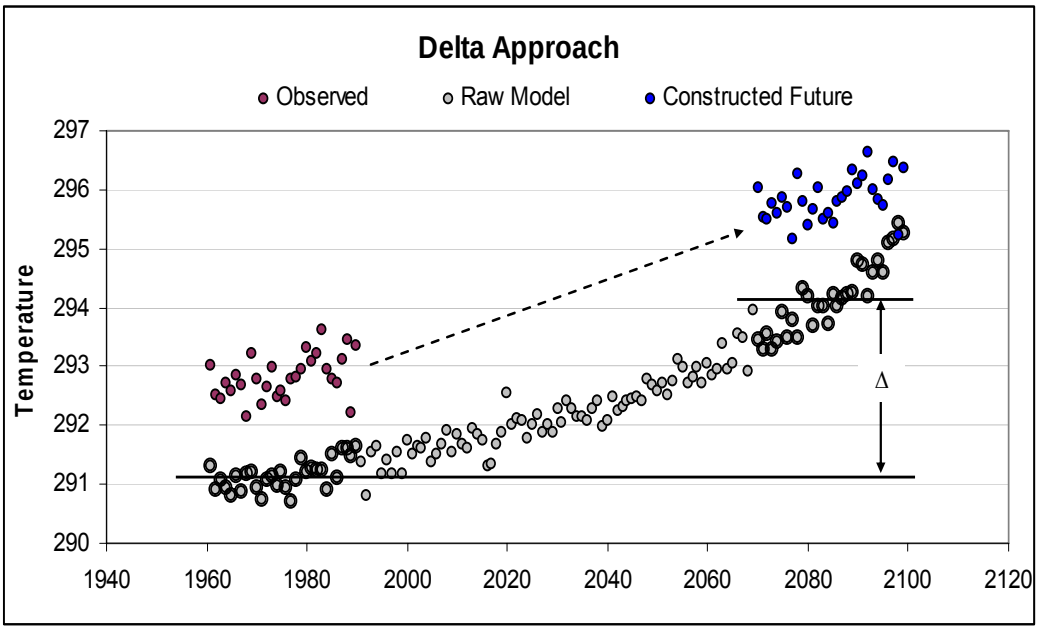

Figure 2.2: Illustration of the delta approach to future climate scenarios.

The advantages of the delta approach are that it bypasses the model mean climate biases by using modeled differences and that it is also a straightforward and relatively simple method to implement. The main disadvantages of this method are that *(1)* it does not retain any information about potential changes in climate variability, *(2)* the internal consistency of variables such as temperature and precipitation are lost in the averaging process, and *(3)* the results are applied uniformly over 30-year periods.

In recent years, the IPCC published a set of standard emission scenarios (IPCC, 2000) that have enabled the direct comparison of experimental results from different models. The IPCC Data Distribution Center has collected and archived experimental results associated with these scenarios for seven commonly used GCMs. The results can be obtained as monthly time series or as 30-year average change fields. The available scenarios, however, remain a limited set of potential climates.

In some cases it is desirable to specify the climate sensitivities under consideration as well as the range of emissions. Climate sensitivity is defined as the mean global temperature increase due to a doubling of atmospheric CO_2. A widely used approach is pattern scaling (IPCC, 1999; Mitchell, 2003), which basically extracts the pattern of climate response from a GCM, but normalizes it to the specified climate sensitivity. The pattern responses are then scaled according to a prescribed atmospheric composition associated with a specific time period, typically based on 30-year averages. This version of the delta approach enables greater flexibility for developing multiple scenarios of interest from a limited set of GCM change fields. The major assumptions inherent in pattern scaling are *(1)* patterns of response remain constant with time, and *(2)* patterns for variables other than temperature scale linearly with global warming (Mitchell, 2003; IPCC 1999). Precipitation patterns sometimes pose an additional complication as it is often difficult to identify a distinct change signal amidst high background, or natural

variability. Mitchell (2003) tested the assumptions of linearity of local and seasonal response patterns for temperature and precipitation. Mild nonlinearities were found to exist and patterns appear to have some time dependence both with respect to the length of warming and the rate at which change occurs.

It is often necessary to represent the regional climate response in greater spatial detail than is resolved by the coarse resolution GCMs. The simplest approach to representing such detail is to uniformly apply changes at large GCM nodes across finer scale observed data. This can be achieved in a number of ways, including applying the changes from the node nearest the study region or by interpolating changes from a number of nearby GCM nodes. However, due to large regional uncertainties, using a single node as the basis for impact assessment is not recommended (IPCC, 1999). Furthermore, depending on the region and variables involved, it may not be a reasonable assumption that small scale responses occur uniformly.

A range of downscaling techniques can be applied and are generally selected based on the requirements of the study. In some cases, simple regression models between upscaled climate and smaller areas may be sufficient. Methods may also incorporate circulation patterns and upper air data (IPCC, 1999). In other cases, the use of a regional climate model (RCM) may be warranted. RCMs use the larger GCM nodes as boundary conditions and then model the region at finer spatial scales. For this reason, the results of RCMs are still dependent upon the validity of the overriding GCM. Furthermore, the use of RCMs does not eliminate regional uncertainties and model biases; therefore, the delta approach is still commonly used with RCM results. Mearns et al. (2003) outline the advantages and disadvantages of using RCMs and provide guidance on the use of their output.

2.4 African Climate Change Assessments

Hulme et al. (2001) developed a set of climate scenarios for the African continent using change fields from 7 different models. They used pattern scaling to generate climate scenarios with a range of climate sensitivities and greenhouse gas concentrations. Change fields for the 30-year time period centered on the 2080s were used to scale to two additional time slices about the 2020s and 2050s. Four traces from one model (HadCM2) were explored for significance in temperature and precipitation change fields by using 1400 years of the model control run to estimate natural temperature and precipitation variability.

In all scenarios, continent wide temperature increases exceeded the estimates of natural variability and were considered significant. The scenarios project temperature increases over Africa of 2° to 6° C within 100 years. Precipitation scenarios were less conclusive. Under the low to moderate forcing scenarios, few areas indicated 'significant' changes in precipitation. Even under the more extreme forcing scenarios, with considerable areas of 'significant' precipitation changes, median model response is often less than the inter-model range of responses. The seasonal and spatial patterns of changes vary considerably. In equatorial Africa, Dec-Feb precipitation is estimated to increase, while near the Horn of Africa Jun-Aug precipitation experiences significant decreases.

Conway and Hulme (1996) used three climate scenarios in a study of the sensitivity of Nile river flows to potential climate change. One dry and one wet scenario were selected from GCM experiments, and a third scenario was constructed from a weighted average of seven models. The GCM equilibrium results were then normalized according to their individual climate sensitivities and scaled to a common 1° C global temperature increase specified for the year 2025. Seasonal temperature and precipitation changes were

calculated (but applied monthly) for eight GCM nodes around the Blue Nile basin and interpolated to a 10-minute grid, while a single node was used for Lake Victoria.

Simple water balance models for the Lake Victoria and Blue Nile basins were run with the perturbed climate of their respective basins and allowed to equilibrate. Simulated changes in runoff ranged from -8.7 to +15.3% for the Blue Nile and from -9.2% to +11.8% for Lake Victoria, with just one scenario predicting decreases in the two basins. While Lake Victoria demonstrated greater sensitivity to temperature changes than the Blue Nile, the study found that both were more susceptible to changes in precipitation than temperature. This and a companion study, (Conway et al., 1996) extrapolate these results to the other Nile basins, based on similarities to either Lake Victoria or the Blue Nile, to assess changes in main Nile flows at Egypt. It is worth noting that in this process runoff and losses from the equatorial lakes were assumed unchanged as was the percentage loss in the Sudd swamps and additional evaporative losses along channels and reservoirs. Under scenarios of increasing temperature such losses may in fact be quite important.

A more detailed modeling effort was undertaken by Yates and Strzepek (1998) in a climate change assessment for the Nile basin. Lumped hydrologic models and lake/swamp models for the entire Nile system were developed and calibrated on a monthly basis. Six different GCM experiments were used in the assessment. GCM temperature and precipitation changes were interpolated to a 0.5° x 0.5° grid for use with the hydrologic models. GCM projections of Lake Victoria temperature changes ranged from 2 to 2.7° C with precipitation changes between -0.2 to +26%. Blue Nile changes ranged from 2.2 to 3.7° C and -8.8 to +55% for temperature and precipitation, respectively. Modeled Blue Nile flows ranged from -32 to +133%, while Lake Victoria

flows ranged from -35 to +104%. The study concluded that river flows were especially susceptible to precipitation changes.

More recently, Tate et al. (2004) describe a climate change impact study for Lake Victoria using an annual lake water balance model and future climate scenarios generated by the UK Hadley GCM (HadCM3). The future climate scenarios are associated with the standardized greenhouse gas emission scenarios A2 and B2. A key assumption of the lake water balance model is that watershed runoff is a quadratic function of lake rainfall only. Namely, watershed runoff is not a function of watershed evapotranspiration. The study goes on to estimate percent changes of lake precipitation and evaporation from a control period (1961-1990 or 1931-1960) to a future period (2021-2050 and 2070-2099). Under both emissions and baseline periods, the 2021-2050 time period experiences falling lake levels, while the 2070 to 2099 period experiences rising lake levels. The authors acknowledge that their assessment includes several uncertainties and their results serve to identify the degree of Lake Victoria sensitivity to potential climate changes rather than representing future climate predictions. Arguably, the most critical weakness of the study is the assumption regarding watershed runoff. If watershed runoff is solely dependent upon lake rainfall and not watershed evapotranspiration (or temperature), the model is bound to over-estimate watershed runoff under increased temperature conditions. Thus, the lake basin supply results are overly optimistic.

2.5 Literature Review Summary

All methods and applications reviewed here are predicated on the delta approach to climate change. Reducing future climate scenarios to change fields of 30-year means imposes severe limitations to assessing true hydrologic and water resources impacts, as the temporal structure of the climate on inter-annual and decadal scales is lost. However, water resources impacts are primarily linked to wet and dry climate persistence on inter-

annual to decadal time scales. For example, the long response times of Victoria Nile flows and upper Nile system modulate main Nile response at multi-year to decadal scales.

Another important factor in climate change assessment studies is associated with limited access to observed hydrologic data, especially in Africa. In the absence of reliable data, the representation of the hydrologic system response introduces additional and significant uncertainties. To this end, a question yet to be answered is the relative magnitude and influence of the climate, hydrologic, and other uncertainty sources on the assessed impacts.

Finally, credible water resources impact studies require representative models of the various water resources users and uses. In this regard, previous studies mostly focus on climate and hydrology, with water resources given secondary attention. Practically useful climate change assessments can only be carried out by integrative modeling efforts that comprehensively represent the combined response of the climate, hydrology, and water resources at all relevant temporal and spatial scales.

Specifically for Lake Victoria and the Blue Nile, previous studies are largely inconclusive on long term climate change impacts, rendering them somewhat uninformative from a management standpoint.

Chapter 3: Future Climate Scenarios

GCM correspondence with observed temperature and precipitation fields varies considerably across the East African region. This is generally expected due to the coarse model resolution, 2.5 x 3.75 degrees, and the spatial heterogeneity of the East African climate. In light of this, the first step in the analysis is to identify areas where the models exhibit high correlation between GCM predictions and the observed climate. The underlying premise is that if a model is able to capture the climatic features and variability for the observed record then it is likely to continue to represent the climate response at those pixels in the future.

Ideally, the GCMs would demonstrate spatially and temporally extensive model skill and could then be applied as direct indicators of future climates. Unfortunately, however, GCMs have not yet reached this level of performance and, in fact, their skill is widely variable both spatially and seasonally. The general approach described in this chapter consists of the following steps: GCM data are evaluated against observed records to identify the regional strengths of each climate model scenario; the data which demonstrate strong statistical correlation with observed records is used to reconstruct the climate in areas where the models fail to capture the observed climate; finally, seasonal and spatial scales are reconciled according to the appropriate resolutions for each hydrologic application (e.g., Lake Victoria, Blue Nile, etc.)

The chapter begins with a description of the observed and model data used to carry out this work. This is followed by a discussion of uncertainties inherent in climate change scenarios and how those uncertainties are treated throughout this study. Section three lays out the statistical basis used to evaluate GCM performance. While methodologies

described here are general and can be applied in any region, the specific details for constructing climate scenarios directly depend on the results of the statistical analysis in each region. Therefore, the remaining sections address the region-specific methods. There are two distinct cases relative to precipitation scenarios, one is Lake Victoria, where climate model data are directly used on a 6-monthly time step, and the other is the Blue Nile, where an historical analog method is developed and applied at monthly resolution. We will first cover these areas and present the methods developed and then work through the rest of the regions which fall into one or the other case (Figure 3.1). The procedure for each basin involves selecting an appropriate method for inferring regional climate from an identified set of statistically significant indicators (i.e. pixels with skill), bias-correcting model temperature and precipitation sequences, downscaling to relevant hydrologic units, and characterizing method uncertainties.

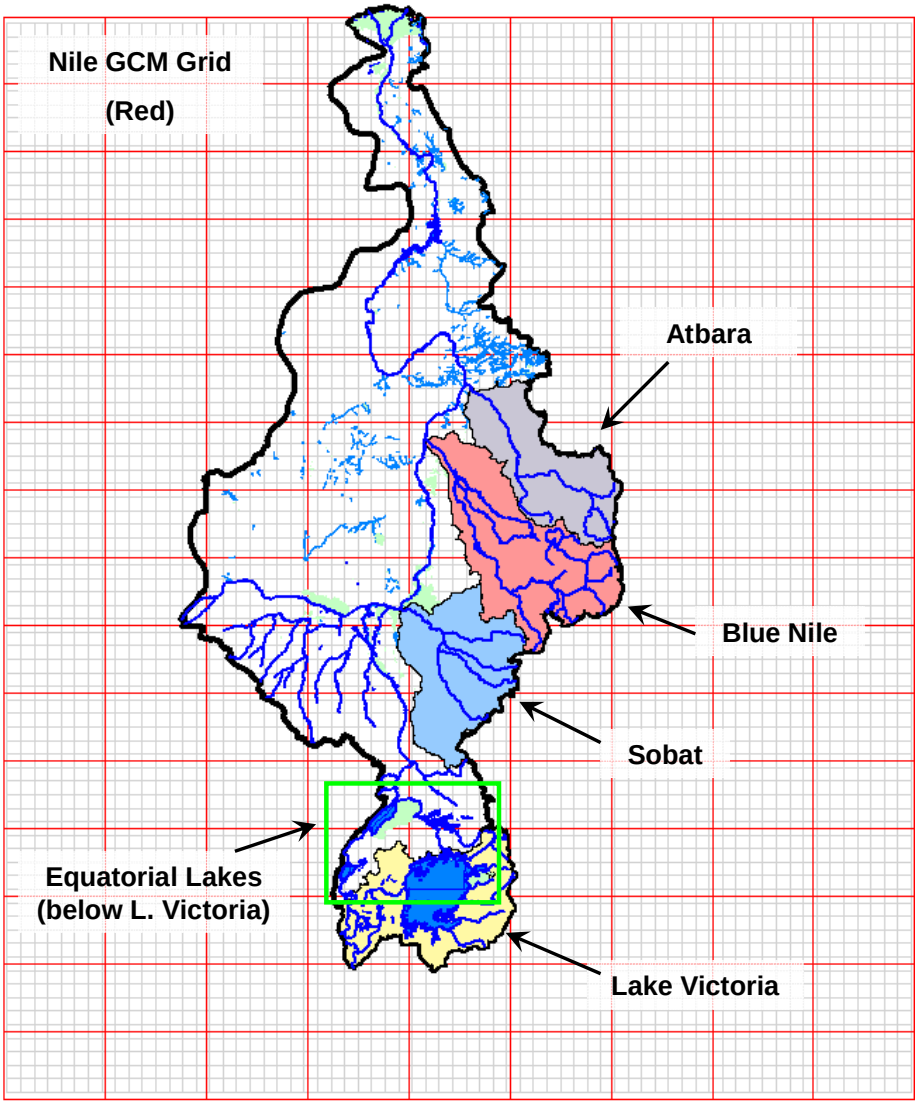

Figure 3.1: Nile Basin study regions (GCM gridin red, CRU grid in gray.)

3.1 Climate Data

Monthly temperature and precipitation data from commonly cited global climate models (GCMs) were obtained from the IPCC Data Distribution Center (DDC) website. The following GCM models were used in this work: the HadCM3 model (Pope et al., 2000; Gordon et al., 2000) developed at the Hadley Center; ECHAM4 (Roeckner et al., 1996; Oberhuber, 1993), developed at the Max Planck Institute for Meteorology; and the Canadian Center for Climate Modeling and Analysis' CGCM2 (Flato et al., 2000). The

HadCM3 model has a spatial resolution of 2.5 x 3.75 degrees, while ECHAM4 has resolution 2.8 x 2.8 and CGCM2 has resolution 3.75 x 3.75. In these evaluations, a common grid was used for all models by interpolating the ECHAM4 and CGCM2 data to the HadCM3 grid. This grid corresponds to the red pixels in Figure 3.1. This study incorporates a total of eight model runs, four obtained from HadCM3, two from ECHAM4, and two from CGCM2. Each model run is defined by three parameters: model (e.g., HadCM3), atmospheric forcing, and model initial conditions. Two standard emissions scenarios, developed through the IPCC Special Report on Emissions Scenarios (SRES) (IPCC, 2000), are used to force each of the three models. Each scenario represents a plausible projection of future greenhouse gas and sulfate emissions. Here, the SRES A2 and B2 scenarios are available for each model, with two additional HadCM3 SRES A2 traces also available. The three HadCM3 SRES A2 traces differ on with respect to model initial conditions. In following sections, the eight scenarios are commonly referred to as: HadA2a, HadA2b, HadA2c, HadB2, EchA2, EchB2, CanA2, and CanB2. The first three letters refer to the model, while the remaining characters identify the associated emissions scenario and, in the case of HadCM3, the individual trace.

Historical data are used to assess and adjust GCM output, establish regional spatial relationships, and develop input sequences for hydrologic model calibration. The primary observational data used for these purposes are the Climate Research Unit TS 2.0 monthly temperature and precipitation series (Mitchell et al., 2005). The data are provided on a 0.5 x 0.5 degree grid corresponding to the gray pixels in Figure 3.1. These data were found to correspond well with station data at several locations within the Nile Basin. Additional data sources used in the development of the Lake Victoria hydrologic model include World Meteorological Organization (WMO, 1974) and data from individual Nile countries.

3.2 Uncertainty Characterization

The work detailed here has incorporated information about uncertainty associated with the following sources: GCM model uncertainties, such as those related to formulation and parameterization; sensitive dependence of the climate system on initial conditions; scenarios of potential future atmospheric composition, based on projections of future human behavior; and uncertainties associated with the specific methods developed and implemented in this research.

Climate Model Uncertainties

Given a common set of initial conditions and atmospheric forcing, different models will produce different projections of the climate. The discrepancies exist due to the various ways in which models are formulated and how some physical processes are parameterized. This does not, however, imply that one model is necessarily correct, while another is incorrect. Rather, in any modeling application, there is uncertainty associated with the simplified representation of the true system.

The uncertainty directly related to climate modeling can be assessed by compiling the results of multiple climate models. As previously mentioned, this assessment utilizes three commonly used GCMs (HadCM3, ECHAM4, and CGCM2), which are publicly available through the IPCC DDC. These models were selected based on the availability of model baseline climate (1961-1990) and experimental runs from a common set of selected atmospheric forcing.

Climate System Unpredictability

Of the seven GCMs with archived data on the DDC website, only the HadCM3 was available with multiple traces for a common forcing scenario. Here three HadCM3 traces have been included from a single atmospheric forcing. The traces differ only by initial

conditions and are therefore included in this research as an indicator of uncertainty stemming from climate unpredictability.

Emissions Scenarios

At the heart of future climate and climate change assessments are underlying assumptions about atmospheric forcing. In an attempt to encourage standardized comparisons among climate change experiments and assessments, the Intergovernmental Panel on Climate Change (IPCC) has developed a series of potential emission scenarios as part of its Special Report on Emissions Scenarios (SRES) (IPCC, 2000). The SRES describes four families of scenarios, SRES A1, A2, B1 and B2, each of which is based upon differing assumptions about future economic development, population growth, environmental policies and technological change.

The two climate scenarios considered in this work stem from the SRES A2 and SRES B2 emissions. These runs were selected for several reasons, including: SRES A2 and B2 GCM output is most readily available through the IPCC Data Distribution Center; and, the future atmospheric compositions prescribed by these two scenarios span nearly the entire inter-quartile range for all scenarios developed as part of the SRES. Therefore, the A2 and B2 families are representative of a wide range of potential atmospheric forcing conditions.

Method Uncertainties

The total set of GCM climate scenarios includes: three HadCM3 A2 traces and one B2 trace; one each of ECHAM4 A2 and B2 runs; and one each of CGCM2 A2 and B2 runs. While the compilation of these 8 runs facilitates an appreciation for the uncertainties of climate modeling, taken alone they cannot confer information about subsequently introduced errors as part of the methods applied in this research. Therefore, each of the

above 8 model runs are expanded into ensembles of 20 traces that represent a range of potential sequences that may be expected in light of the unexplained variance of the spatial regressions (i.e., relationships between indicator pixels and targets and downscaling relationships) and, later, the hydrologic models. The methods for incorporating these sources of uncertainty are explicitly described later in the chapter.

3.3 Statistical Basis for Assessing Model Skill

Numerous studies of East African precipitation have found that interannual variability exhibits significant fluctuations at intervals of 3 to 5 years (Rodhe and Virji, 1976; Ogallo, 1979; Nicholson, 1996). Nicholson (1996) reports a dominant time scale for the East African region as a whole of 5 to 6 years, with additional significant spectral peaks at 3.5 and 2.3 years. Given the evidence for such temporal structure in rainfall and its relevance to East African hydrology and, consequently, the overall Nile River, a statistic was selected to test model performance with respect to multiple scales of model correlation with observed temperature and precipitation. The resulting statistic is defined as follows:

$$\theta = \sum_{i=1}^{5} \rho_i \ ,$$

where ρ_i is the correlation between model and observed data for the pixel of interest averaged over i years. Sample statistics, denoted $\hat{\theta}$, for each model are drawn from the historical period 1961 to 2000. High values of $\hat{\theta}$ indicate consistently good correspondence of model results and observed data over a range of time scales from one to five years.

It is important to understand the likelihood that a sample value, $\hat{\theta}$, would materialize purely by chance as opposed to model skill. However, because θ is not a simple statistic, such as the mean or variance, it cannot be evaluated for statistical significance

using standard statistical formulae, which also rely heavily on distributional assumptions. Therefore, a statistical test based on bootstrapping is implemented to overcome this obstacle (Efron and Tibshirani, 1993).

The Bootstrap

The statistical test consists of constructing the $\hat{\theta}$ sampling distribution, adjusting for possible estimator bias, and using the distribution to determine the probability that the test statistic is statistically different than zero. The basis for constructing the distribution is to apply resampling assuming that the realized sample represents the true population. That is, it is assumed that each member of the original sample of size *n* has a *1/n* probability of occurring. Then additional samples of size *n* can be drawn from the original data through the process of sampling with replacement. Each new sample yields a bootstrap replicate of θ, denoted $\hat{\theta}^*$. The process is repeated *B* times until a sufficiently detailed and accurate distribution of $\hat{\theta}$ can be estimated (Efron and Tibshirani, 1993). In the present context, the original sample, **X**, for a given pixel consists of pairs of historically observed and model data (temperature or precipitation) over the reference period 1961-2000:

$$\mathrm{X} = \begin{Bmatrix} h_1 & m_1 \\ h_2 & m_2 \\ \vdots & \vdots \\ h_{40} & m_{40} \end{Bmatrix}.$$

In this array, the (h_1, m_1) pair represents the historically observed variable, *h*, and corresponding model variable, *m*, over the pixel of interest for the year 1961, while (h_2, m_2) represents data for 1962 and so forth for a total of $n = 40$ sample pairs.

The basic resampling procedure described above assumes that each pair is independent of the others. However, this is not necessarily a valid assumption. In fact, the form of the test statistic used here is based on the opposing assumption that there should be some temporal structure in the data, extending at least to 5-year aggregations. A modified resampling method, known as the moving blocks bootstrap (Efron and Tibshirani, 1993, chapter 8), is employed in this study as follows. Instead of randomly selecting *n* pairs from the original data, 5-year blocks are randomly selected to fill the sample array. An example of the set of *B* bootstrap samples, and associated $\hat{\theta}^*$ s, generated using the moving block technique is shown below.

$$\mathrm{X}_1^* = \begin{Bmatrix} h_{23} & m_{23} \\ h_{24} & m_{24} \\ h_{25} & m_{25} \\ h_{26} & m_{26} \\ h_{27} & m_{27} \\ \vdots & \vdots \\ h_{8} & m_{8} \\ h_{9} & m_{9} \\ h_{10} & m_{10} \\ h_{11} & m_{11} \\ h_{12} & m_{12} \\ \vdots & \vdots \end{Bmatrix}, \quad \mathrm{X}_2^* = \begin{Bmatrix} h_{17} & m_{17} \\ h_{18} & m_{18} \\ h_{19} & m_{19} \\ h_{20} & m_{20} \\ h_{21} & m_{21} \\ \vdots & \vdots \\ h_{32} & m_{32} \\ h_{33} & m_{33} \\ h_{34} & m_{34} \\ h_{35} & m_{35} \\ h_{36} & m_{36} \\ \vdots & \vdots \end{Bmatrix}, \quad \cdots \quad \mathrm{X}_B^* = \begin{Bmatrix} h_{4} & m_{4} \\ h_{5} & m_{5} \\ h_{6} & m_{6} \\ h_{7} & m_{7} \\ h_{8} & m_{8} \\ \vdots & \vdots \\ h_{13} & m_{13} \\ h_{14} & m_{14} \\ h_{15} & m_{15} \\ h_{16} & m_{16} \\ h_{17} & m_{17} \\ \vdots & \vdots \end{Bmatrix} \quad \rightarrow \quad \hat{\theta}_1^*, \hat{\theta}_2^*, \cdots, \hat{\theta}_B^*$$

Again, if θ was a simple statistic with unbiased estimator $\hat{\theta}$, percentiles of the $\hat{\theta}$ distribution could be used directly to construct confidence intervals for the true quantity θ. However, it is not immediately obvious to what extent $\hat{\theta}$ may be biased and how this may influence estimates of its sampling error. To correct for the potential bias of the estimator, confidence intervals are constructed using Efron and Tibshirani's bias-corrected and accelerated (BCa) method, as prescribed in his chapter 14. This method uses the bootstrap itself to estimate the bias and uses a jackknife procedure to assess the rate at which the standard error changes with changing θ, called acceleration. Given a

sufficiently large number of bootstrap trials, B=1000 in this case, the confidence interval for a specified significance level α can be easily calculated.

The procedure described above results in confidence intervals for θ at each pixel in the region of interest. With this information it is possible to test the following hypothesis:

Null hypothesis, H_o: $\theta = 0$ Alternate hypothesis, H_a: $\theta \neq 0$.

If the (1-α) confidence interval of θ does not contain zero then the null hypothesis is rejected and the sample estimate $\hat{\theta}$ is said to be significant at level α (Figure 3.2).

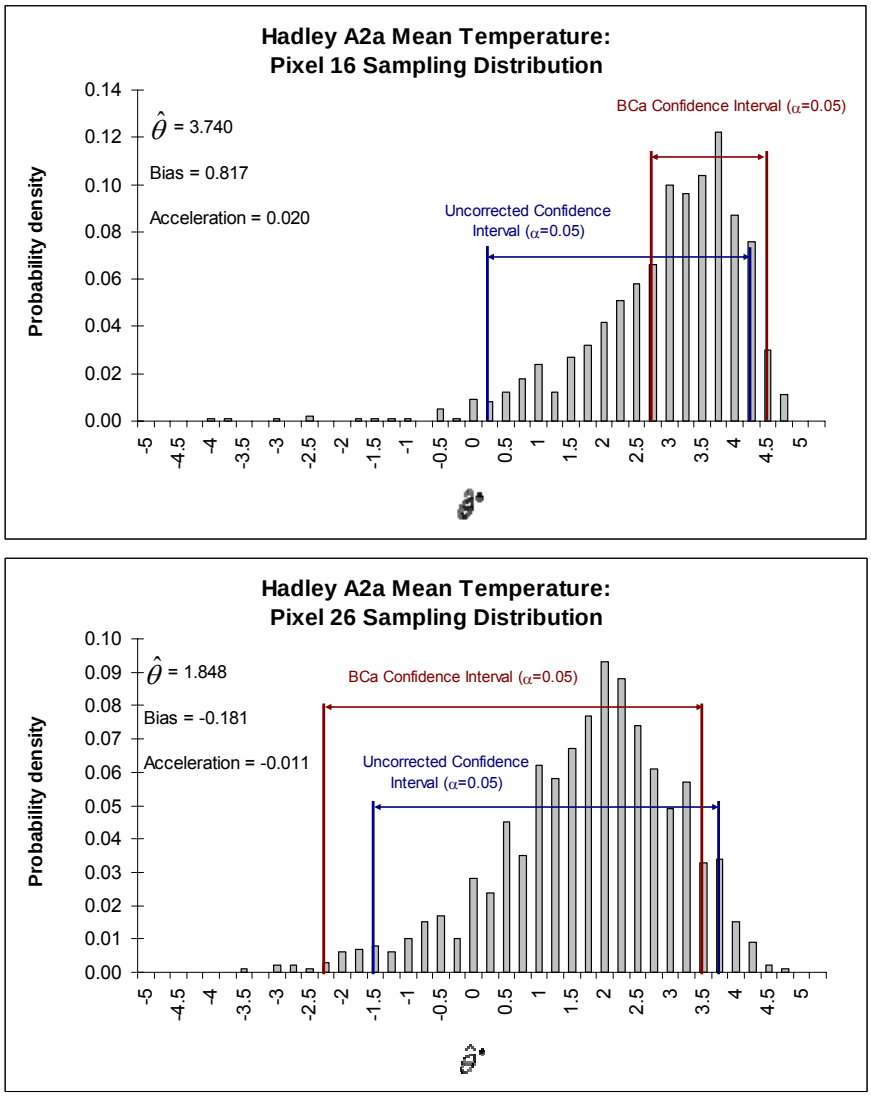

Figure 3.2: Example of sampling distribution for $\hat{\theta}$ indicating a significant result (top) and an insignificant result (bottom).

3.4 Lake Victoria

3.4.1 Model Skill

Thirty-two GCM pixels, approximately centered over Lake Victoria, were evaluated for agreement with the observed climate on a seasonal basis. Three considerations led to the seasonal definitions of January-June and July-December. First, the GCMs tend to more closely resemble the observed climate over longer aggregations, as indicated by detailed

correlation analysis. Secondly, as discussed later, while the hydrologic model developed for Lake Victoria was calibrated with monthly, three-monthly, and six-monthly data, only the six-monthly time step produced satisfactory results. Finally, the seasons are delineated to completely bound the long rains (Mar-Apr-May) in one season and the short rains (Oct-Nov-Dec) in the other.

The significance results for all thirty-two pixels are summarized in Tables 3.1 and 3.2. The tables communicate the following information: the total number of pixels passing at α levels 10%, 5%, and 1%; and the identity of each specific pixel passing at a given level. Note that while the pixels are numbered from 1 to 36, pixels 31-34 correspond to ocean pixels (Figure 3.3) and are therefore hatched in the summary tables.

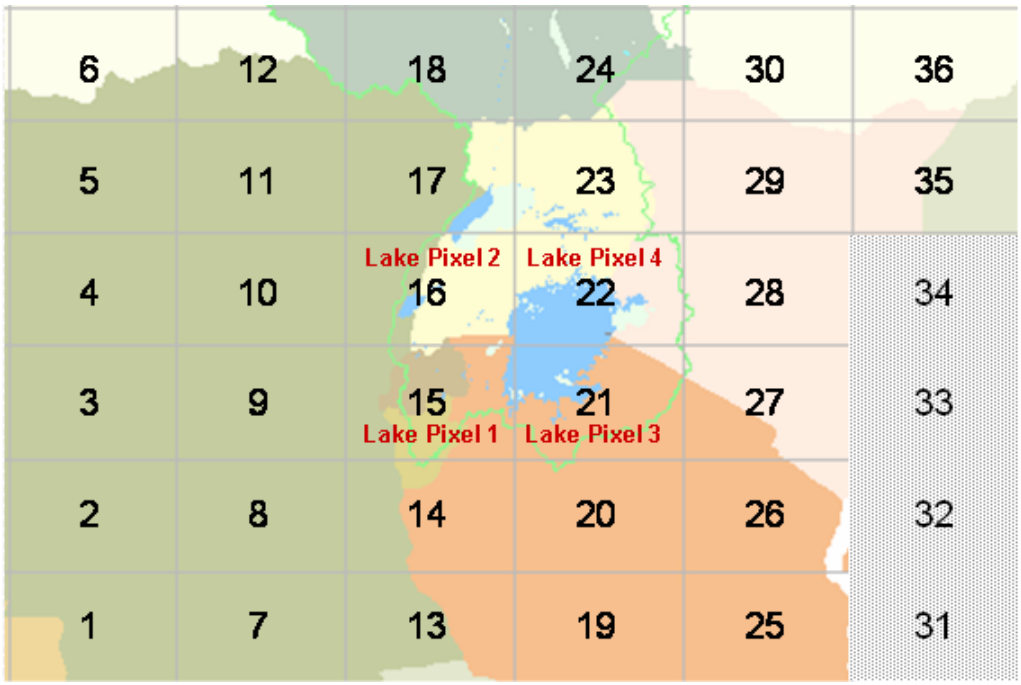

Figure 3.3: Thirty-two HadCM3 nodes covering the Lake Victoria region.

It is clear that temperature performs quite well over most of the region and in all three models. In the HadCM3 and CGCM2 runs most of the pixels that pass the test at the 10% level remain significant at 5%, with a remarkable number still significant at the 1% level. This is also true for ECHAM4 in season 1, though season 2 indicates fewer pixels passing at the 5% and 1% thresholds. Given that regional pixels 15, 16, 21, and 22 represent lake pixels 1-4 (Figure 3.3), it is seen that the entire lake region is significant for all HadCM3 and CGCM2 runs. ECHAM4 shows significance in both seasons for the western two lake pixels, while the eastern lake pixels are not as well represented.

Significant precipitation pixels are sparse for all models. The HadCM3 and ECHAM4 models, while not showing extensive lake coverage do indicate significance in some pixels at the margins of the lake area, all of which pass at either the 1% or 5% level. CGCM2 on the other hand shows a single season 1 pixel for the A2 and B2 runs and a single season 2 pixel for B2, all of which are located a considerable distance from the lake. The HadCM3 A2b run shows a remarkable 17 significant pixels in season 2, also covering the entire lake region, while none are significant in season 1. The overall results confirm that precipitation is much less reliable than temperature at the regional scale.

Table 3.1: Temperature significance testing results, $\alpha = 10\%$, $\alpha = 5\%$ shown with *, $\alpha = 1\%$ shown with **.

	Temperature																	
	Had A2a		Had A2b		Had A2c		Had B2		Ech A2		Ech B2		Can A2		Can B2			
	Season 1	Season 2	Season 1	Season 2	Season 1	Season 2	Season 1	Season 2	Season 1	Season 2	Season 1	Season 2	Season 1	Season 2	Season 1	Season 2		
Pixel/No. Passing	27/21/15	29/26/17	26/23/14	20/17/5	20/16/11	20/17/10	22/21/18	27/25/21	17/15/14	16/14/5	17/16/15	18/11/2	22/18/10	20/20/13	23/23/16	27/25/19		
1	1**	1**	1**	1**	1**	1*	1**	1**	1**	1**	1**	1**	1*	--	1**	1**		
2	2**	2**	2**	2**	2**	2**	2**	2**	2**	2**	2**	2*	2*	--	2**	2**		
3	3**	3*	3**	3*	3**	3**	3**	3**	3**	3	3**	3	3**	--	3**	--		
4	4**	4	4**	--	4**	4	4**	--	4**	--	4**	--	4*	--	4**	--		
5	--	--	--	--	5**	--	--	--	--	--	5	--	--	--	--	--		
6	--	--	--	--	6*	--	--	--	--	--	--	--	--	--	--	--		
7	7**	7*	7**	7	7**	7*	7**	7**	7**	7*	7**	7	7**	--	7**	7*		
8	8**	8*	8**	8*	8**	8**	8**	8**	8**	8*	8**	8*	8**	--	8**	8		
9	9**	9*	9**	--	9**	9*	9**	9*	9**	--	9**	--	9**	--	9**	9*		
10	10**	10*	10*	--	10*	--	10**	10*	10**	--	10**	--	10	10*	10*	10**		
11	11**	11	11*	--	11**	--	11**	--	11**	--	11**	--	--	11**	11*	11**		
12	12**	12*	12**	--	12**	12*	12**	12	12**	12*	12**	12*	--	12**	--	12**		
13	13*	13**	13**	13*	13*	13**	13**	13**	13**	13*	13**	13	13**	13*	13**	13**		
14	14**	14**	14**	14*	14*	14**	14**	14**	14**	14*	14**	14*	14**	14*	14**	14*		
15	15**	15**	15**	15*	15**	15**	15**	15**	15**	15*	15**	15*	15**	15*	15**	15**		
16	16**	16**	16**	16*	16*	16**	16**	16**	16**	16*	16**	16	16	16**	16*	16**		
17	17**	17**	17**	17**	17	17*	17**	17**	17*	17**	17**	17*	--	17**	--	17**		
18	18**	18**	18*	18**	--	18*	18**	18**	18	18**	18*	18**	--	--	--	--		
19	19*	19	19*	--	--	19**	--	19*	19	19*	--	19*	19*	19**	19**	19**		
20	20*	20**	20*	20*	--	20**	--	20**	--	20**	--	20*	20*	20*	20**	20**		
21	21*	21**	21*	21	21	21	21*	21**	--	--	--	21	21**	21**	21**	21**		
22	22*	22**	22*	22*	22	22**	22**	22**	--	--	--	--	22**	22**	22**	22**		
23	23	23**	23*	23**	--	23*	23*	23**	--	--	--	--	23**	23**	23**	23**		
24	24	24**	--	24*	--	--	24**	24**	--	--	--	24	24*	24**	24*	24**		
25	25*	25*	25*	--	--	--	25*	25**	--	25	--	--	25*	25**	25**	25**		
26	--	--	--	--	--	--	--	--	--	26*	--	26	--	26**	26*	26**		
27	27	27*	--	--	--	--	--	27	--	--	--	27*	27	27**	27*	27**		
28	--	28**	28	28*	--	--	--	28**	--	--	--	--	28	28**	--	28**		
29	--	29**	29	29*	29	--	--	29**	--	--	--	--	--	29*	--	29*		
30	30	30**	30**	30*	--	30	30	30**	--	--	--	--	30*	30*	30*	30*		
31	--	--	--	--	--	--	--	--	--	--	--	--	--	--	--	--		
32	--	--	--	--	--	--	--	--	--	--	--	--	--	--	--	--		
33	--	--	--	--	--	--	--	--	--	--	--	--	--	--	--	--		
34	--	--	--	--	--	--	--	--	--	--	--	--	--	--	--	--		
35	35	35**	--	35	--	--	--	35**	--	--	--	--	--	--	--	35		
36	36	36*	36	--	--	--	--	36*	--	--	--	--	--	--	--	36*		

Table 3.2: Precipitation significance testing results, $\alpha = 10\%$, $\alpha = 5\%$ shown with *, $\alpha = 1\%$ shown with **.

	Precipitation															
	Had A2a		Had A2b		Had A2c		Had B2		Ech A2		Ech B2		Can A2		Can B2	
	Season 1	Season 2	Season 1	Season 2	Season 1	Season 2	Season 1	Season 2	Season 1	Season 2	Season 1	Season 2	Season 1	Season 2	Season 1	Season 2
Pixel/No. Passing	0/0/0	6/3/0	0/0/0	17/10/7	4/2/0	2/1/0	1/1/1	4/3/1	2/0/0	0/0/0	3/3/2	2/1/0	1/0/0	0/0/0	1/0/0	1/1/0
1	--	--	--	--	--	--	--	--	--	--	--	1*	--	--	--	--
2	--	2	--	2	--	--	--	2	--	--	--	--	--	--	--	--
3	--	3*	--	--	--	--	--	3*	--	--	--	--	--	--	--	--
4	--	4	--	4	--	--	--	--	--	--	--	--	--	--	--	--
5	--	--	--	--	--	--	--	--	--	--	--	--	--	--	--	--
6	--	--	--	--	--	--	--	--	--	--	--	--	--	--	--	--
7	--	--	--	--	7	--	--	--	--	--	--	--	--	--	--	--
8	--	--	--	--	8*	--	--	--	--	--	--	--	--	--	--	--
9	--	9*	--	9**	--	--	--	9**	--	--	--	--	--	--	--	--
10	--	--	--	10**	--	--	--	--	--	--	--	--	--	--	--	--
11	--	--	--	--	--	--	--	--	--	--	--	--	--	--	--	--
12	--	--	--	--	--	--	--	--	--	--	--	--	--	--	--	12*
13	--	--	--	--	--	--	--	--	--	--	--	--	--	--	--	--
14	--	--	--	14	14*	--	--	--	--	--	--	--	--	--	--	--
15	--	15	--	15*	--	--	--	--	15	--	15**	--	--	--	--	--
16	--	--	--	16*	--	--	--	--	16	--	16**	--	--	--	--	--
17	--	--	--	--	--	--	--	--	--	--	17*	17	--	--	--	--
18	--	--	--	--	--	--	--	--	--	--	--	--	--	--	--	--
19	--	--	--	19	--	--	19**	--	--	--	--	--	--	--	--	--
20	--	--	--	--	--	20	--	--	--	--	--	--	--	--	--	--
21	--	--	--	21**	--	--	--	--	--	--	--	--	--	--	--	--
22	--	--	--	22**	--	--	--	--	--	--	--	--	--	--	--	--
23	--	23*	--	23**	--	--	--	23*	--	--	--	--	--	--	--	--
24	--	--	--	24*	--	--	--	--	--	--	--	--	--	--	--	--
25	--	--	--	25	25	--	--	--	--	--	--	--	--	--	--	--
26	--	--	--	--	--	--	--	--	--	--	--	--	--	--	--	--
27	--	--	--	27	--	27*	--	--	--	--	--	--	--	--	--	--
28	--	--	--	28**	--	--	--	--	--	--	--	--	--	--	--	--
29	--	--	--	29**	--	--	--	--	--	--	--	--	--	--	--	--
30	--	--	--	--	--	--	--	--	--	--	--	--	30	--	30	--
31	--	--	--	--	--	--	--	--	--	--	--	--	--	--	--	--
32	--	--	--	--	--	--	--	--	--	--	--	--	--	--	--	--
33	--	--	--	--	--	--	--	--	--	--	--	--	--	--	--	--
34	--	--	--	--	--	--	--	--	--	--	--	--	--	--	--	--
35	--	--	--	35	--	--	--	--	--	--	--	--	--	--	--	--
36	--	--	--	--	--	--	--	--	--	--	--	--	--	--	--	--

3.4.2. Bias Correction

As previously discussed, raw GCM data generally exhibit biases and therefore must be bias-corrected prior to application to impact studies. Here bias correction is based on the 1961-1990 historical temperature and precipitation data. The correction procedure is summarized below:

$$X'_{i,t} = X_{i,t} - \overline{X}_{i,m} + \overline{X}_{i,o}\,.$$

In the above equation, $X_{i,t}$ is the model prediction for season *i* of year *t*, $\overline{X}_{i,m}$ is the 30-year baseline model mean for season *i*, $\overline{X}_{i,o}$ is the 30-year baseline *observed* seasonal average, and $X'_{i,t}$ is the bias-adjusted model series. X is either temperature or precipitation at the pixel of interest.

The previous adjustment corrects for mean bias. A second adjustment is also made to the model results to conform to the variability of the historical data. This procedure takes the sequence anomalies and scales them consistently with the observed historical variability as follows:

$$\Delta_{i,t} = X'_{i,t} - \overline{X}'_{i,t}$$

$$X''_{i,t} = \Delta_{i,t}\left(\frac{\sigma_{i,o}}{\sigma_{i,m}}\right) + \overline{X}'_{i,t}$$

In the above equations, $\Delta_{i,t}$ is the data anomaly for season *i* of year *t*, $\sigma_{i,o}$ is the historical sequence standard deviation during the baseline period, $\sigma_{i,m}$ is the standard deviation for the model data over the same period, $\overline{X}'_{i,t}$ is the model mean trend in season *i*, and $X''_{i,t}$

is the fully adjusted model data. The final adjusted model sequences exhibit the appropriate baseline mean and variance with respect to the observed data. Unlike the commonly used delta-approach (IPCC, 1999), which imposes the historical variance on the future climate, this approach does not preclude changes in variability.

3.4.3 Indicator Pixels

In some cases, particularly with respect to temperature, all four of the Lake Victoria watershed pixels are found to be significantly represented by the model. In other instances, however, some or all lake pixels are non-significant. In such cases, significant pixels are sought in the general vicinity of the lake watershed to be used as potential indicators of the climate over the target lake pixels. The rationale for this approach is to base future climate assessments on pixels (i.e., geographic areas) where the GCMs exhibit significant prediction skill. As explained below, the climate response over the lake pixels is inferred from the indicator pixels through historically observed spatial relationships.

Two criteria are used in the selection of pixels that may be used as indicators of the future lake watershed climate. As mentioned, the first criterion is significance testing to narrow the field of pixels for which there is some degree of confidence in the model's representation of the climate. Second, historical data for the significant pixels and the target lake pixels are investigated for potentially useful spatial relationships.

Spatial Relationships between Indicator and Target Pixels

Historical data are used in pair-wise comparisons for each indicator-target pixel combination. As with the significance testing, the comparisons are carried out separately for each season because the climate mechanisms often differ from one season to the next, particularly with respect to precipitation. Seasonal data for each potential indicator pixel

are plotted against the seasonal data for a lake pixel over the reference period 1961-2000. A trend is fit to the data with the indicator pixel as the predictor variable and the target pixel as the dependent variable. As shown in Figure 3.4, such relationships may be used to predict the corresponding series for the target lake pixel. The assumption underlying this approach is that the historical spatial relationships between indicator and lake pixels will continue to persist in future climates.

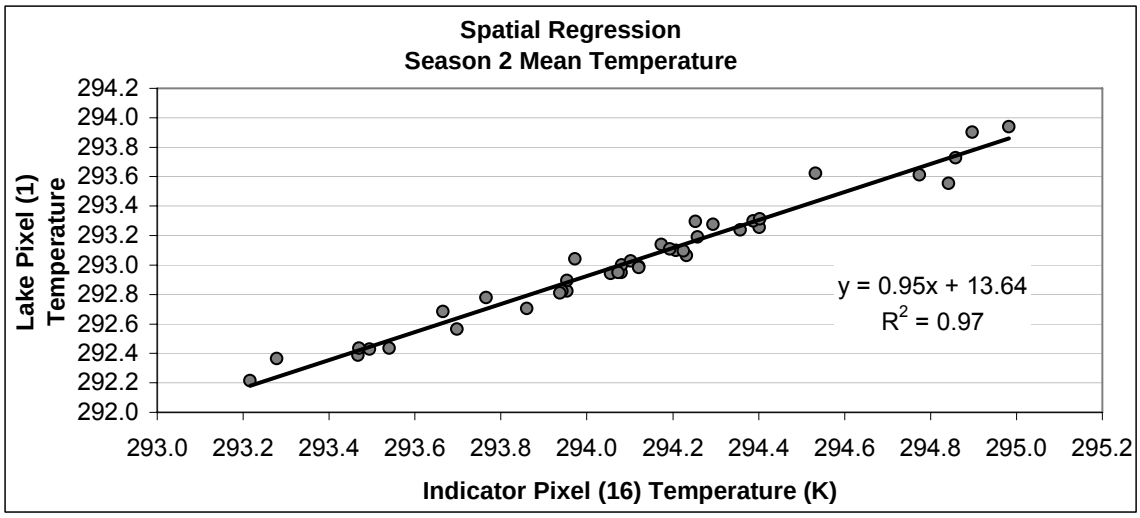

Figure 3.4: Example of the relationship between temperature at regional pixel 16 and one of the Lake Victoria pixels.

Very few indicator pixels were necessary for temperature. Only the ECHAM4 A2 and B2 temperature scenarios require spatial regressions, using two season 1 and three season 2 relationships. The five spatial temperature relationships were very strong, with linear correlation coefficients between 0.88 and 0.97, and slopes ranging from 0.91 to 0.98. Due to the limited number of significant pixels for precipitation, indicator pixels are used more extensively, with all eight model runs requiring indicators to some extent. A total of 16 season 1 and 20 season 2 spatial relationships are applied. The mean correlation

coefficient for the season 1 indicators is 0.64 with a minimum and maximum of 0.48 and 0.77, respectively. In season 2, the mean indicator correlation is 0.60, with a minimum of 0.24 and maximum of 0.82. The range of regression slopes is similar for both seasons and found to be between 0.21 and 1.36. All of these spatial relationships are included in Appendix A. As will be discussed later, the residuals, or unexplained variance, in all relationships are carried forward in the analysis to fully represent the spatial uncertainties.

The underlying assumption that the spatial relationships will persist under a changing climate was tested indirectly as follows: First, all GCMs were verified to exhibit significant spatial relationships similar to those of the real climate during the historical period. Secondly, all GCMs were tested under future climates and indicated that the spatial relationships persist unaltered for all scenarios. Thus, since the GCMs were seen to replicate well the actual climate response in the historical period, it is concluded that, much like the GCMs, the actual climate is most likely to continue to exhibit the same spatial relationships in the future as well.

Once all significant and relevant pixels have been identified, they are bias-corrected, as discussed in the following section, and used to generate complete Lake Victoria watershed coverage. When lake pixels themselves are statistically significant, they are used directly. In cases where one or more lake pixels are not significant the best indicator pixel is used, together with the established spatial relationships, to predict one or more lake pixels. While all three GCMs represent temperature well in general, in some cases, there is no appropriate precipitation indicator pixel for one of the two seasons. In this case an additional step is taken to construct a plausible and consistent sequence for the non-significant season. The procedure is based on observations of season 1 and season 2 trends at pixels demonstrating model significance in both seasons.

The seasons were found to have non-diverging trends under the future climate scenarios. With this in mind, anomalies from the non-significant season are added to the trend of the significant season and further bias-corrected. In this way, the covariance of temperature and precipitation is preserved by maintaining the original season anomalies.

3.4.4 Downscaling

The processed GCM data in its original resolution is too coarse for use in hydrologic modeling. There is thus the need to downscale this data over the lake and watershed areas within each GCM pixel. Downscaling is accomplished by establishing the historical relationships between spatial scales. These relationships are quantified by spatially aggregating the observed CRU data over each sub-area and comparing with the overall scaled-up value at the GCM node. An example of this aggregation process is shown in Figure 3.5.

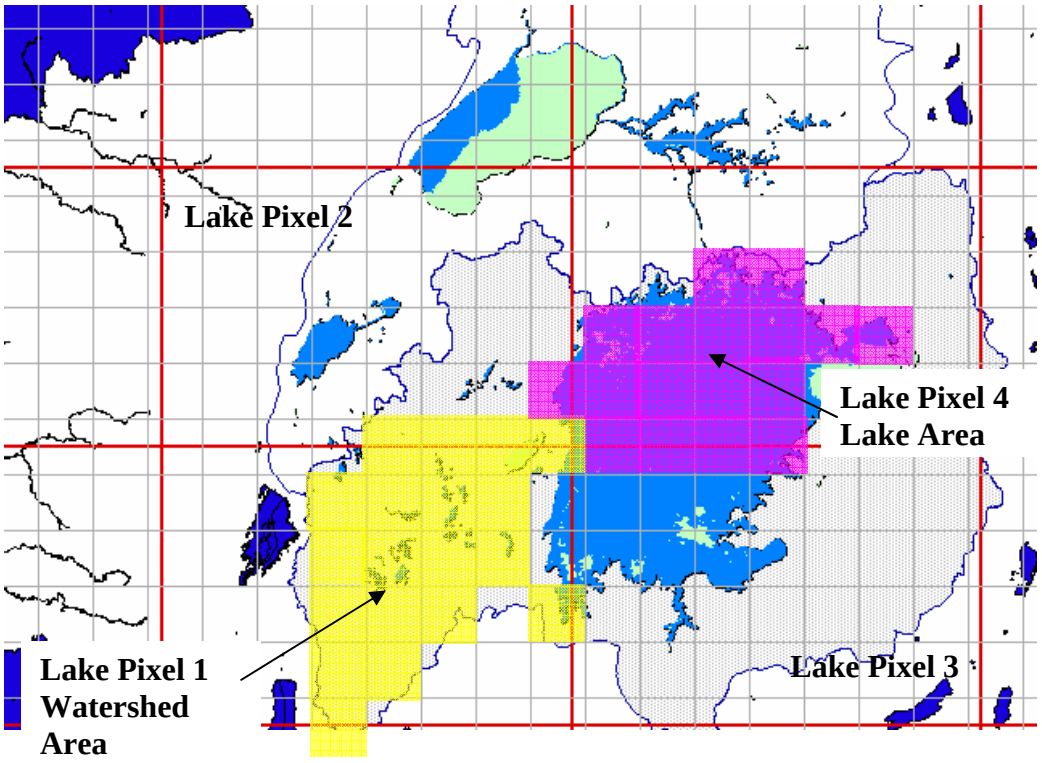

Figure 3.5: Example of spatial aggregation using the CRU data set.

The downscaling procedure employed here establishes a statistical relationship between the large node value and each sub-area of interest. For the Lake Pixel 2 watershed area and Lake Pixel 4 lake area the relationship depends on the season, while for all other sub-areas the relationship is invariant from one season to the next (Figure 3.6). As can be seen in Figure 3.5, the sub-areas generally occupy between one quarter and one half of the large node. As a result, simple linear regressions explain the scaling relationships quite well. The average correlation between the large nodes and sub-areas is 0.99 for temperature and 0.91 for precipitation. While the temperature relationship slopes are all very close to one, the precipitation slopes range from 0.74 to 1.15. Using these relationships, future lake and watershed sequences are generated by applying the downscaling function to GCM data at the larger nodes.

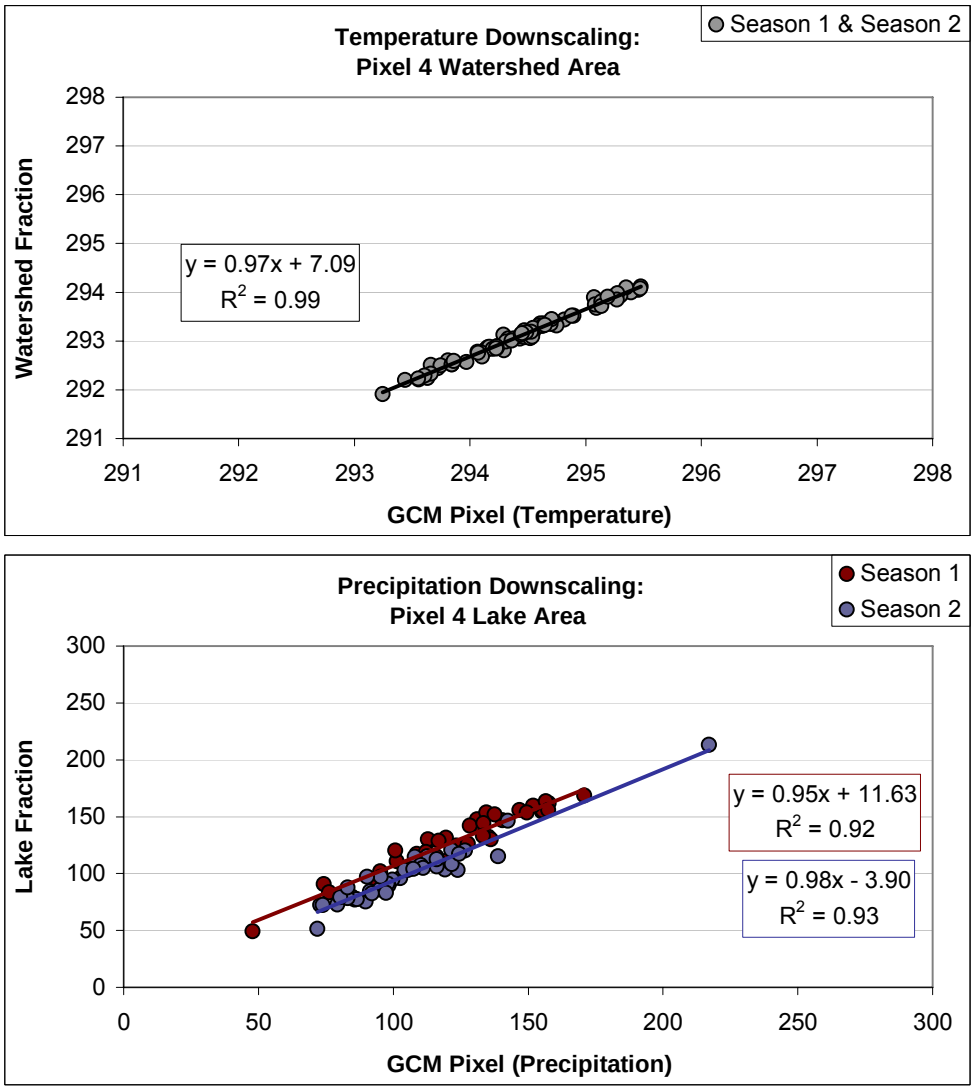

Figure 3.6: Example of season independent (top) and season dependent (bottom) downscaling relationships.

3.4.5 Spatial Variability

Several steps in the GCM processing procedure rely on regression equations, which when used alone do not entirely reflect the underlying variability of the climate. To avoid this artificial variance reduction, the regression residuals from both the spatial and downscaling procedures are recorded and later reintroduced using a bootstrapping method.

Spatial regression residuals are recorded for each indicator pixel, while downscaling residuals are stored for each lake and watershed sub-area within the domain of the four Lake Victoria GCM nodes. The connection between these residuals and the final downscaled sequences is illustrated as follows: Consider an indicator pixel *I*, used to predict lake pixels 2 and 4. Temperature and precipitation values at lake pixel 4 are subsequently downscaled to the watershed area lying within pixel 4 (Figure 3.7).

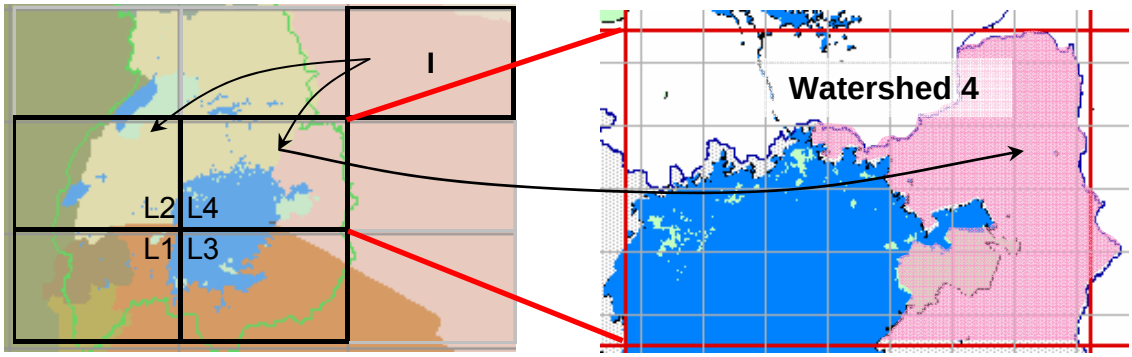

Figure 3.7: Illustration of the regionalization of an indicator pixel and subsequent downscaling.

The spatial regression from indicator pixel *I* to Lake Pixel 4 accounts for the deterministic component as does the downscaling function; however, in reality the value at Lake Pixel 4 includes a residual term, which in turn impacts the downscaling step.

$$Lake_{4,t} = a_0 + a_1 \cdot I_t + e_{4,t}$$

$$Wshed_{4,t} = b_0 + b_1 \cdot Lake_{4,t} + e_{w4,t}$$

$$Wshed_{4,t} = b_0 + b_1 \cdot (a_0 + a_1 \cdot I_t + e_{4,t}) + e_{w4,t}$$

In the above equations, $Lake_{4,t}$ is the estimated temperature or precipitation value for lake pixel 4 at time *t*; I_t is the corresponding value at the neighboring indicator pixel; $Wshed_{4,t}$ is the downscaled value representing the watershed sub-area within lake pixel 4; a_0, a_1, b_0, and b_1 are regression coefficients; $e_{4,t}$ is the spatial regression residual for pixel 4 at time *t*; and $e_{w4,t}$ is the downscaling residual for watershed 4 at time *t*.

This effect is incorporated by bootstrapping residuals from the 40 years used to develop the statistical relationships and later reintroducing them in the sequences. To maintain spatial covariance as well as temperature-precipitation covariance, each model time step uses the same residual year for each lake pixel, sub-area, and variable (temperature or precipitation). The process is repeated multiple times, resulting in an ensemble of potential realizations. While reintroducing the residuals restores variability, the ensemble facilitates an assessment of the uncertainty associated with indicator pixel and downscaling methods.

3.4.6 Final Sequences

Final temperature and precipitation sequences are generated for both watershed and lake surface areas. An ensemble of 20 traces was produced for each pixel area using the bootstrapped residuals, as previously mentioned. Pixels 1 and 2 do not contain appreciable lake area and therefore only have corresponding watershed sequences. Pixels 3 and 4 include considerable lake and watershed areas and thus have both downscaled sequences. The ensemble means for all scenarios are presented below (Figures 3.8-3.11).

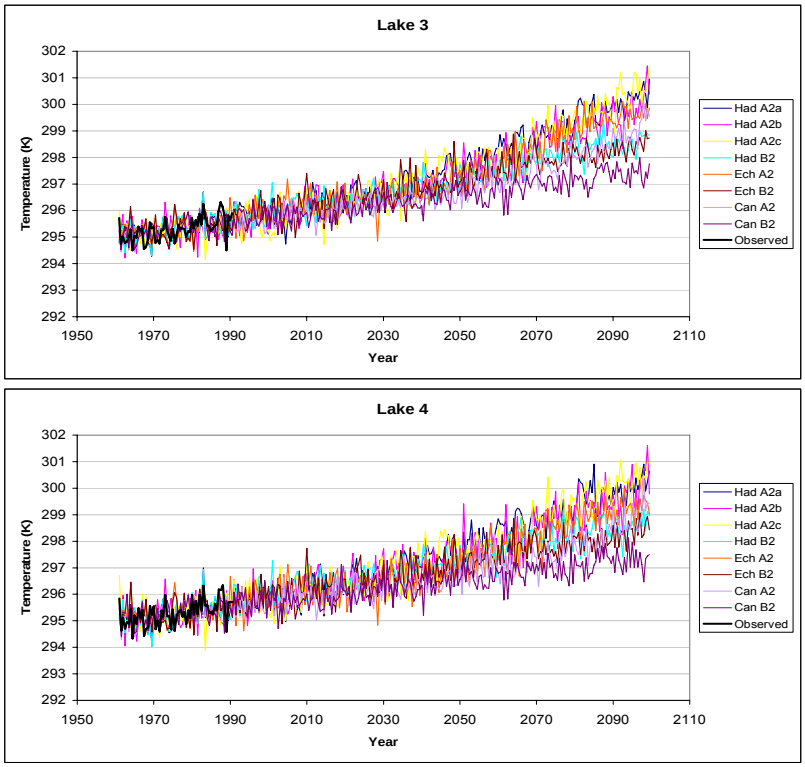

Figure 3.8: Downscaled temperature sequences for the lake sub-areas with observed baseline shown in black.

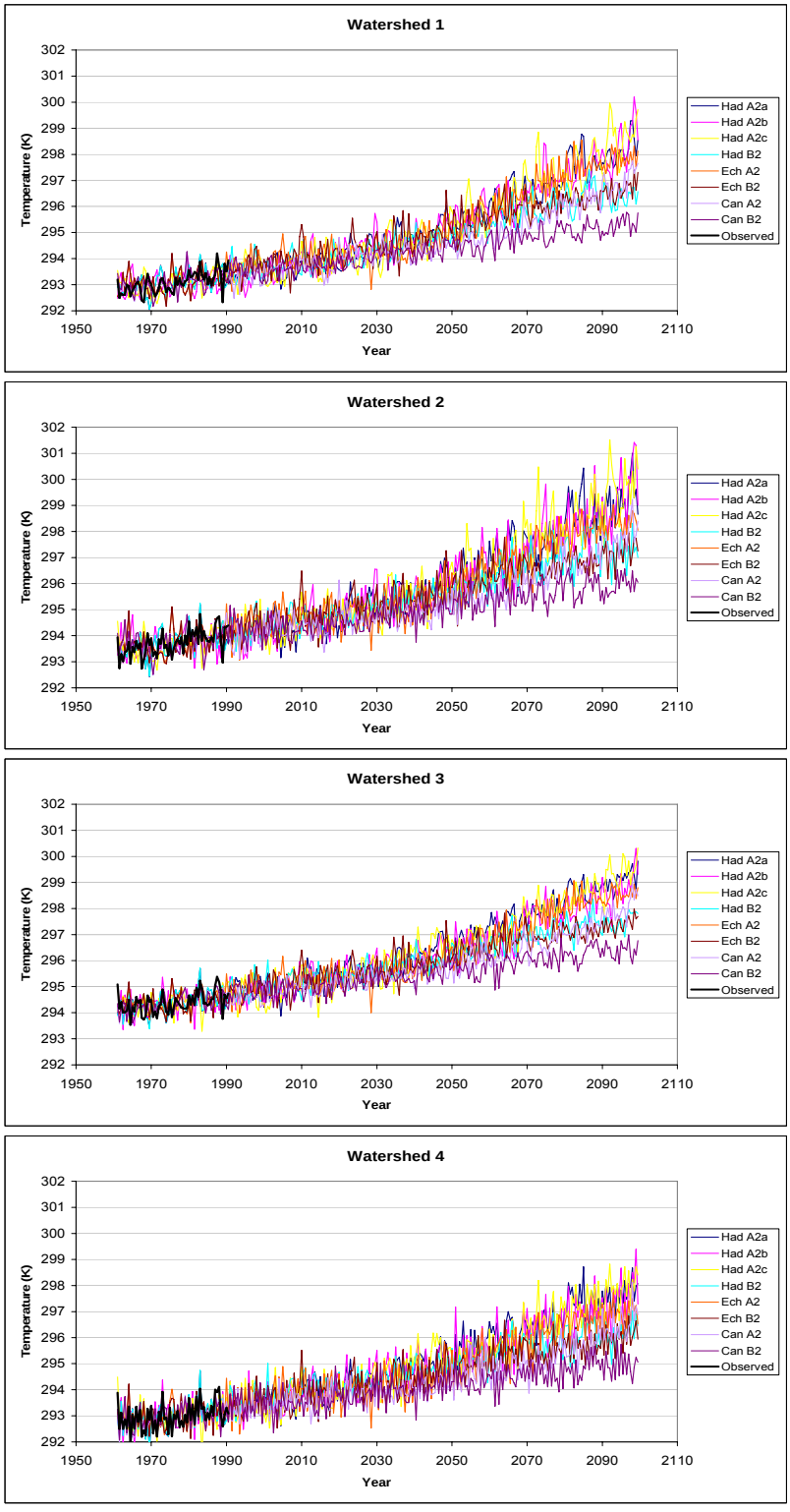

Figure 3.9: Downscaled temperature sequences for the watershed sub-areas with observed baseline shown in black.

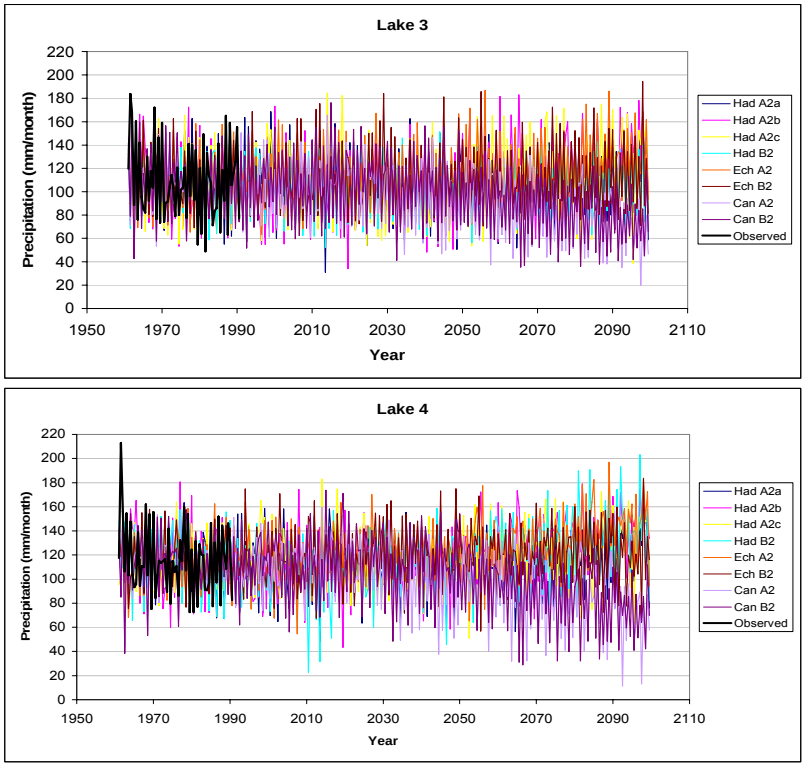

Figure 3.10: Downscaled precipitation sequences for the lake sub-areas with observed baseline shown in black.

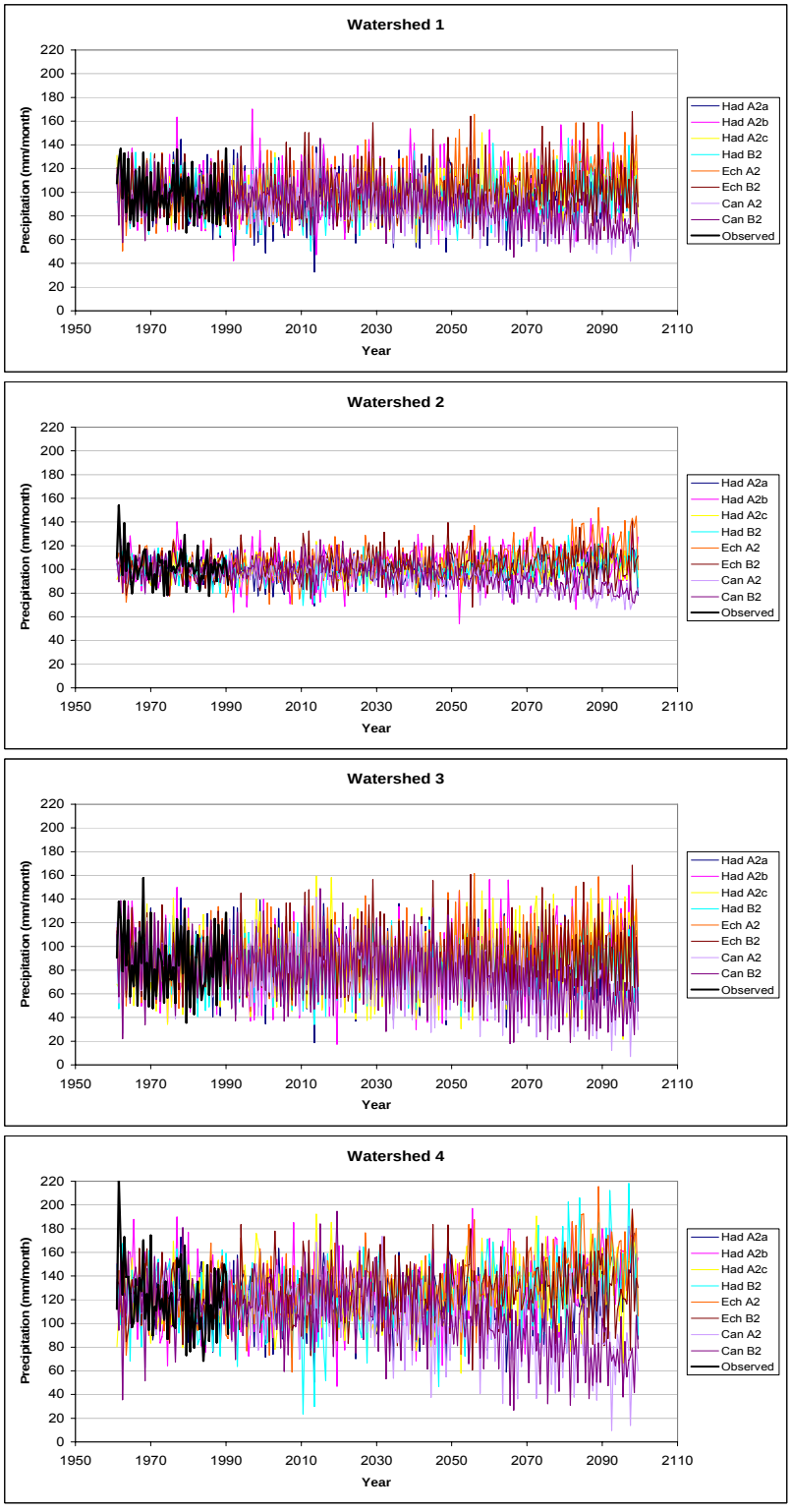

Figure 3.11: Downscaled precipitation sequences for the watershed sub-areas with observed baseline shown in black.

Temperature Assessment

The results show an increasing temperature trend for all models and in both A2 and B2 scenarios. Bias-correction has ensured that all sequences have the appropriate baseline climatology corresponding to the observed historical data; however, the A2 and B2 temperature scenarios begin to diverge from each other around 2030 for HadCM3 and around 2040 for Echam4 and CGCM2. Beyond the point of separation, which is observed in all watershed and lake sequences, both scenario types continue to increase but with the A2 temperatures increasing at considerably greater rates than B2 temperatures. In the final year, 2099, the A2 and B2 ensemble means differ by approximately 2 °C for all models. Note that in the final two decades, 2080s and 2090s, the B2 sequences approach a steady rate of increase as seen in the approximately linear trends, while the A2 sequences indicate a continued acceleration as shown by concave trends. Figure 3.12 illustrates these features for the watershed of pixel 2.

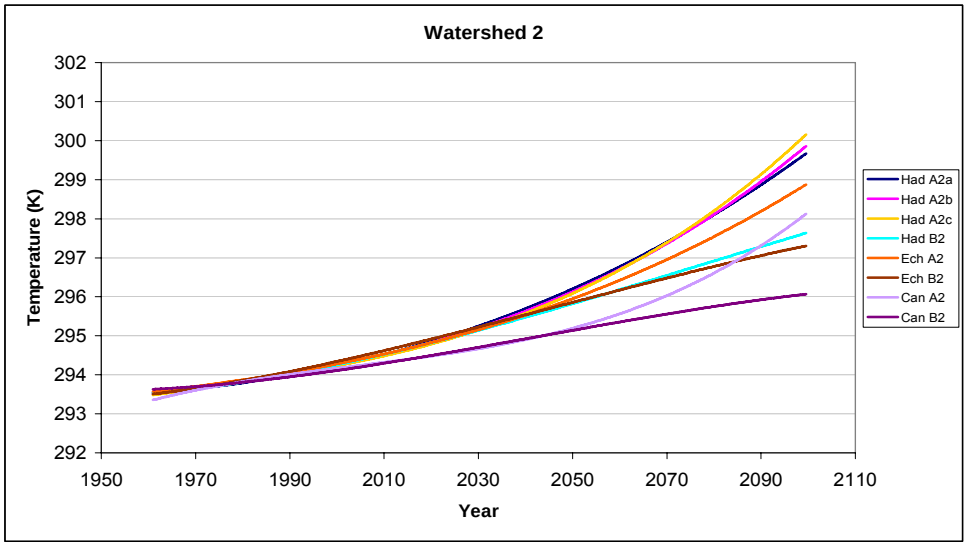

Figure 3.12: Trendlines for the eight projected temperature sequences over the downscaled watershed area of pixel 2.

Table 3.3 summarizes the projected temperature changes between the baseline period (1961-1990) and the final 30 years (2070-2099). Overall, the 30-year average responses range from 1.9 to 5 °C. HADCM3 consistently projects the greatest change among models, with respect to a specific atmospheric forcing scenario, while CGCM2 predicts the smallest change. All three models indicate nearly the same sensitivity to the A2/B2 scnearios, which is found to be between 1.0 to 1.2 °C. It should be noted, however, that over the final 30 years, the CGCM A2 projection indicates a rapidly increasing rate of temperature change (Figure 3.12).

As expected, there are differences among the three HadCM3 A2 traces. While the model characteristics and atmospheric forcing for the three traces are identical, the initial conditions used in the model are not. Therefore, the differences among these traces are attributable to the model climate's sensitivity to initial conditions. This sensitivity is shown in Table 3.3 to be approximately one-fifth to one-fourth of the HadCM3 sensitivity to atmospheric forcing (A2 and B2 scenarios).

Table 3.3: Projected temperature changes between final 30 years (2070-2099) and 30-year baseline (1961-1990).

	Temperature Change (°C)					
Model/SubArea	**WS 1**	**WS 2**	**WS 3**	**WS 4**	**Lake 3**	**Lake 4**
HadA2a	4.4	4.7	4.2	4.2	4.3	4.3
HadA2b	4.5	4.8	3.9	4.0	4.0	4.0
HadA2c	4.6	5.0	4.2	4.3	4.4	4.3
HadB2	3.2	3.4	3.0	3.0	3.1	3.1
EchA2	4.3	4.2	3.7	3.5	3.9	3.6
EchB2	3.2	3.1	2.7	2.7	2.8	2.7
CanA2	3.2	3.2	2.9	2.8	3.0	2.8
CanB2	2.0	2.1	1.9	1.8	1.9	1.9
HadA2 spread/SRES A2-B2 spread	0.19	0.19	0.28	0.25	0.28	0.25

Table 3.4: Projected percentage precipitation changes between final 30 years (2070-2099) and 30-year baseline (1961-1990).

	Precipitation Change (%)					
Model/SubArea	**WS 1**	**WS 2**	**WS 3**	**WS 4**	**Lake 3**	**Lake 4**
HadA2a	2.7	0.8	5.0	3.2	5.1	3.1
HadA2b	11.9	6.5	13.9	18.1	12.3	15.7
HadA2c	8.2	3.7	16.4	12.5	14.1	11.0
HadB2	2.0	7.5	-1.6	16.2	-1.3	14.3
EchA2	17.5	17.4	17.7	25.0	15.1	21.6
EchB2	6.3	6.3	5.9	7.4	4.7	5.7
CanA2	-24.9	-17.9	-35.7	-37.6	-30.6	-32.9
CanB2	-21.9	-15.9	-31.8	-34.1	-27.5	-30.3
HadA2 spread/SRES A2-B2 spread	14.05	0.85	1.74	1.15	1.42	1.13

Precipitation Assessment

Unlike temperature trends, precipitation does not exhibit a distinct climate change signal consistent across models. The most notable characteristic of the results is that CGCM2 projects precipitation decreases across all sub-areas, while the other two models appear to project small to moderate increases.

The 30-year average differences (2070-2099 minus 1961-1990), expressed as percentages of the average baseline precipitation, are presented in Table 3.4. Here it is seen that the projected precipitation changes range from -38% to +25%. In general, irrespective of the projected sign of the trend, B2 results generally show a lower response magnitude than A2.

As with temperature, the HadCM3 traces are used to assess the relative sensitivities of model precipitation to initial conditions and atmospheric forcing. While temperature trends indicate that HadCM3 is approximately four times more sensitive to projected

emissions than initial conditions, precipitation results indicate that the sensitivities are roughly equal, with one notable exception seen for watershed area 1 where the trace spread is 14 times larger than the differences among forcing scenarios.

In light of the sparse and variable results for significance testing, the apparently large impact of initial condition uncertainty on projected changes, and the inconsistencies in the sign of precipitation changes, the precipitation results should be interpreted with caution and are not regarded with nearly the confidence of the temperature results. This may be particularly true with respect to the CGCM2 runs. While this model projects large negative trends in both the A2 and B2 sequences, prior to model processing, this model demonstrated the largest positive precipitation biases of all eight runs.

3.5 Blue Nile

3.5.1 Model Skill

The Blue Nile differs from the Lake Victoria region in a few important ways that have bearing on GCM skill and the availability of potential climate indicator pixels. First, the changes in climatic behavior, such as the modality of precipitation, occur over much shorter distances in the Blue Nile region. Not surprisingly, GCM performance tends to be spotty, particularly in the transitional areas between uni-, bi- and tri-modal precipitation. This can clearly be seen by viewing north-south transects of model climatologies together with observed climatologies, where the GCMs occasionally exhibit transitional regimes displaced by one or more pixels. Secondly, unlike in the Lake Victoria region, the Blue Nile hydrology is best described with a minimum *monthly* time step. Due to the large storage capacity and induced hydrologic time lags, longer seasonal aggregations still produced a reasonable hydrologic model for Lake Victoria. Since the majority of rainfall and the high flow periods for the Blue Nile occur primarily between June and September, a six-monthly aggregation would only serve to mask the

highly seasonal hydrology and could not accurately capture the timing and magnitude of the annual flood.

As a result of the more spatially complex precipitation structure, the regional extent of potential indicator pixels for the Blue Nile basin is much smaller than in the Lake Victoria region, and only eleven GCM pixels were considered relevant to the Blue Nile sub-basins in Ethiopia and Sudan (Figure 3.13). Furthermore, the GCMs demonstrate much lower statistical significance for monthly precipitation data. Consequently, there is insufficient confidence in any of the GCM scenarios to support the exact methods used for Lake Victoria on a monthly basis.

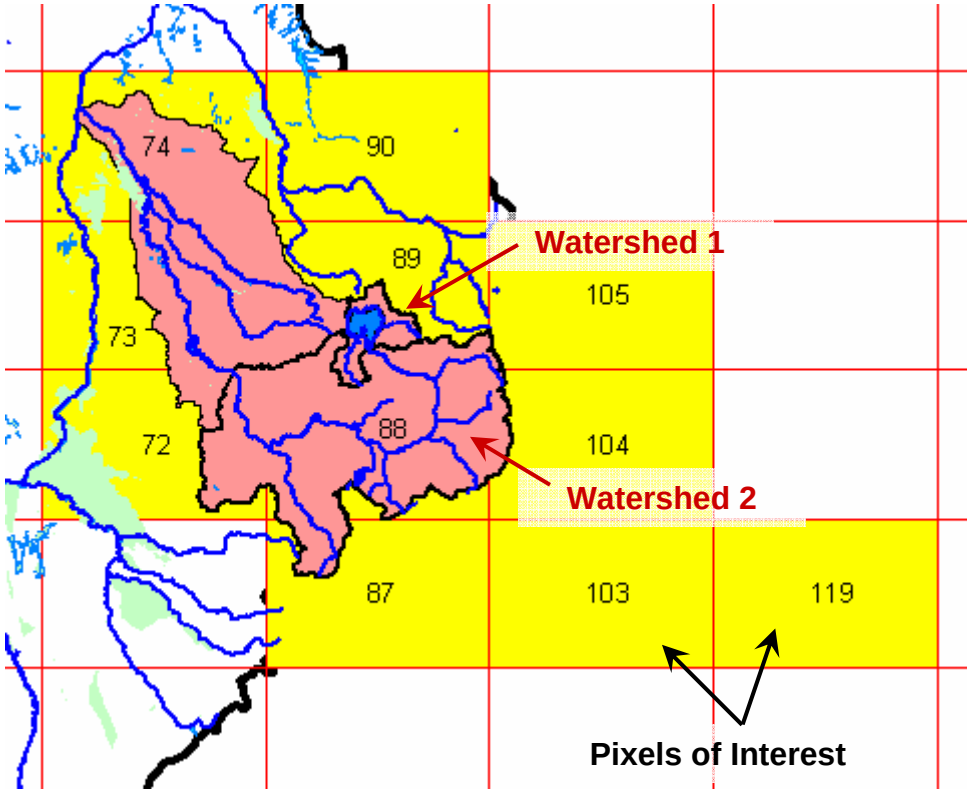

Figure 3.13: Blue Nile region (pixels of interest shown in yellow).

Although the basic statistical procedure is consistent across all regions of the Nile, more extensive seasonal analysis has been carried out in the Blue Nile to better understand model performance for multiple seasonal aggregations. Statistical significance was evaluated at monthly, 2-monthly, 3-monthly, 4-monthly, 6-monthly, and annual aggregations for each of the 11 GCM nodes in the region. In addition, the 3-monthly and 6-monthly data have been aggregated with two different delineations due to the timing of the rainy season(s).

As with Lake Victoria, there is a much more extensive set of statistically significant temperature data than precipitation. Even on a monthly basis, the models perform quite well. However, due to the difficulties of the GCMs to reproduce the baseline precipitation climatologies in some areas, only pixels where the models were able to capture the basic climatology structure were considered for further analysis. The reasoning behind this criterion is that if the models are generating baseline climatologies vastly different from the observed behavior, they are not sufficiently capturing the rainfall mechanisms and therefore may be unreliable predictors of a changing climate. With this in mind, precipitation is the limiting factor and primary focus for selecting indicator pixels. This is further discussed in section 3.4.3.

3.5.2 Bias Correction

The bias and variance adjustments described for Lake Victoria are applied to Blue Nile temperature. Precipitation, however, is treated somewhat differently in this region. Precipitation in the Blue Nile, as well as most of the remaining Nile regions, is highly seasonal with marked dry seasons. The bias and variance correction procedure applied to the 6-monthly data for Lake Victoria has some shortcomings when dealing with periods of extremely low precipitation. For example, the distribution of some precipitation data is best described in two parts, one with a concentrated probability of no precipitation, and

another part that describes the characteristics of the remaining, nonzero data. In the case of temperature, however, the previously described bias and variance adjustments are applied here.

As before, the correction procedure is applied on a season by season basis. The previous method has been expanded as follows. A low precipitation threshold, *d*=5 mm/month*, is used to define the proportion of low versus substantial precipitation. In cases where the baseline precipitation has less than 10% of its values below the threshold, *d**, the standard correction procedure is applied. However, in cases where more than 10% of the observed precipitation is below the threshold, low precipitation (average monthly precipitation $\leq d^*$) and high precipitation are addressed separately.

The goal for adjusting model data in very low precipitation seasons is to reconcile the concentrated probability of the model data with that observed in the historical baseline. If *n* data points fall below *d** in the observed baseline period, then a corresponding model threshold d_{mod} is located such that the same number of baseline model data fall below d_{mod}. Model data $\leq d_{mod}$ are scaled by a factor d^*/ d_{mod}. All model data above d_{mod} are adjusted according to the original method. The difference here is that the adjustment is with respect to the model and historical data that are above their respective thresholds.

$$X'_{i,t} = \begin{cases} \left(X_{i,t} - \overline{X}_{i,m}\right) * \left(\frac{\sigma_{i,o}}{\sigma_{i,m}}\right) + \overline{X}_{i,o} & \text{if } (X_{i,t} > d_{mod}) \\ X_{i,t}\left(\frac{d^*}{d_{mod}}\right) & \text{if } (X_{i,t} \leq d_{mod}) \end{cases}$$

In the above expression, $X'_{i,t}$ is the adjusted model precipitation for season *i* at time *t*, $X_{i,t}$ is the original model precipitation at time *t*, $\overline{X}_{i,m}$ is the mean model precipitation for

the data above d_{mod}, $\overline{X}_{i,o}$ is the mean observed precipitation for the data above d^*, $\sigma_{i,m}$ is the model standard deviation for the data above d_{mod}, and $\sigma_{i,o}$ is the observed standard deviation for data above d^*. Again, if the concentrated probability of very low precipitation is less than 10%, the top expression is applied for all data, with the means and standard deviations being derived from the combined high and low precipitation data. In such a case the method is seen to be exactly the same procedure as applied in Lake Victoria region.

3.5.3 Indicator Pixels

Precipitation

The statistically significant seasonal sets for precipitation were found to be rather disjoint in both space and time for all models. One specific example is for the HadA2c run. This model was found to have statistical significance at pixel 87 for a single 3-monthly aggregation from June to August, which represents a wet season. However, the model demonstrated much different results at neighboring pixels 88 and 103, where again a single 3-monthly aggregation was found to be significant for each, but for both pixels the significance was during a dry season. The conclusion from this example is that at the 3-monthly aggregation, HadA2c captures the rainy season behavior with some skill, while at neighboring pixels it does not. Table 3.5 is a summary of all seasonal sets that pass the two criteria previously mentioned, a) the model climatology resembles the key features of the historically observed 30-year climatology, and b) the set is statistically significant.

Table 3.5: Blue Nile precipitation indicator sets.

Can A2		Can B2		Ech A2		Ech B2	
Pixel	Season	Pixel	Season	Pixel	Season	Pixel	Season
P 73	May	P 72	Nov-Dec	P 74	Mar	P 74	Jan
P 73	Jul-Dec	P 73	May	P 74	Jul	P 74	Feb
P 87	Nov-Apr	P 87	Mar-Apr	P 74	Nov	P 74	Jul
P 88	Apr	P 87	Nov-Apr	P 74	Jul-Aug	P 74	Nov
P 88	Nov	P 88	Apr	P 74	Nov-Dec	P 74	Nov-Dec
P 88	Mar-Apr	P 88	Mar-Apr	P 74	Jan-Mar	P 74	Jan-Mar
P 88	Nov-Dec	P 88	Jan-Apr	P 74	Jul-Sep	P 74	Dec-Feb
P 88	Jan-Apr	P 88	Sep-Dec	P 74	Dec-Feb	P 103	Sep-Nov
P 88	Nov-Apr	P 88	Nov-Apr	P 74	May-Aug	P 104	Jan
P 104	Apr	P 104	Dec-Feb	P 74	Jul-Dec	P 104	Feb
P 104	Dec-Feb	P 104	Sep-Nov	P 74	May-Oct	P 104	Oct
P 104	Nov-Apr	P 104	Nov-Apr	P 74	Jan-Dec	P 104	Jul-Dec
P 105	Sep	P 105	Dec	P 103	Nov-Dec	P 104	Nov-Apr
P 105	Dec	P 105	Dec-Feb	P 103	Sep-Nov	P 119	Dec
P 105	Nov-Dec	P 105	Sep-Nov	P 104	Jan	P 119	Jul-Sep
P 105	Dec-Feb	P 105	Jan-Apr	P 104	Oct	P 119	Jun-Aug
P 105	Nov-Apr	P 105	Nov-Apr	P 104	Oct-Dec		
P 119	Dec-Feb	P 105	Jan-Dec	P 104	Jul-Dec		
				P 119	Oct		
				P 119	Nov		
				P 119	Jul-Sep		
				P 119	Oct-Dec		
				P 119	Sep-Nov		

Had A2a		Had A2b		Had A2c		Had B2	
Pixel	Season	Pixel	Season	Pixel	Season	Pixel	Season
P 87	Sep	P 74	Jan	P 87	Jun-Aug	P 88	Feb
P 88	Oct	P 74	Dec	P 87	Nov-Apr	P 89	Jan
P 89	Jan	P 74	Sep-Nov	P 88	Dec-Feb	P 89	Oct
P 89	Oct	P 87	Oct	P 89	Jul	P 89	Jan-Feb
P 89	Sep-Oct	P 87	Nov-Dec	P 89	Dec-Feb	P 89	Jan-Dec
P 89	Jan-Dec	P 87	Jan-Mar	P 103	Aug	P 103	Jan
P 103	Jul	P 89	Jun	P 103	Sep	P 103	May-Jun
P 103	May-Jun	P 89	May-Jun	P 103	Jan-Mar	P 103	May-Aug
P 103	Apr-Jun	P 89	Nov-Dec	P 104	Nov	P 104	Jan
P 103	Jun-Aug	P 89	Apr-Jun	P 104	Nov-Dec	P 104	Jun
P 103	May-Aug	P 89	Sep-Nov	P 119	May-Jun	P 119	Jan
P 103	May-Oct	P 89	May-Oct	P 119	Sep-Dec	P 119	Feb
P 103	Jan-Dec	P 89	Jan-Dec	P 119	Jul-Dec	P 119	Apr
P 104	Jan	P 103	Jul-Aug	P 119	Nov-Apr	P 119	Dec
P 119	Jan	P 119	Jan			P 119	Jan-Feb
P 119	Feb					P 119	Sep-Oct
P 119	Mar					P 119	Jul-Sep
P 119	Apr					P 119	Dec-Feb
P 119	Sep-Oct					P 119	Jan-Apr
P 119	Jan-Mar					P 119	May-Aug
P 119	Jul-Sep					P 119	May-Oct
P 119	Jun-Aug					P 119	Jan-Dec

Considering the summary of results presented above, a method has been developed with the following properties in mind: 1) it should incorporate as much of the statistically significant model data as possible; 2) it should consider the strength of the spatial correlation between each indicator set and the target pixel; and 3) it should consider the relative importance of the seasonal rainfall for each set. Since the available indicator data generally does not have sufficient spatial and seasonal coverage to be used directly to construct precipitation scenarios, they have instead been used as part of a historical analog method for constructing the scenarios.

The historical analog method is carried out for each of the four Blue Nile target pixels. For each model year defined from 1962 to 2099, all indicator sets are simultaneously compared against the corresponding historical data (defined by pixel and season) from a particular year between 1962 to 2000. The historical year best matching the combined set of indicators is selected to represent the monthly precipitation. The criteria for selecting the historical year is as follows:

$$i : Min\left\{\sum_{k}\left[\left(M_{j,k} - H_{i,k}\right)\rho_k\left(\frac{P_k}{\sum_{k} P_k}\right)L_k\right]^2\right\}$$

In the above expression, i is the historical year index (1962-2000), j is the model year index (1962-2099), k is the indicator set index (defined by pixel and season), $M_{j,k}$ is the model precipitation from indicator k during model year j, $H_{i,k}$ is the historically observed precipitation for the same pixel and season as indicator k but during year i, ρ_k is the correlation between the indicator pixel and the target pixel, $P_k \Big/ \sum_{k} P_k$ is the proportion of

precipitation in set *k* relative to all indicator sets based on historical averages, and L_k is the length of the indicator season in months. The rational behind this objective function is to give greater weight to indicator sets that have higher correlations with the target, account for a larger portion of precipitation, and represent a greater portion of the year. Below is an example of how a model precipitation scenario is constructed from the results of the historical analog procedure; model data are replaced by the historical data selected with the analog method.

$$
\begin{array}{lcl}
\textit{Scenario} & & \textit{AnalogIndex} \\
M_{1962,Jan} & = & H_{1993,Jan} \\
M_{1962,Feb} & = & H_{1993,Feb} \\
\vdots & & \vdots \\
M_{1962,Dec} & = & H_{1993,Dec} \\
\vdots & & \vdots \\
M_{2017,Jan} & = & H_{1968,Jan} \\
M_{2017,Feb} & = & H_{1968,Feb} \\
\vdots & & \vdots
\end{array}
$$

The method implies two assumptions of particular concern. First, since the method attempts to match precipitation from spatially distributed indicators, it assumes that the spatial pattern of precipitation will continue in the future. However, the indicators are not all equally weighted nor will all years of the observed record indicate identical patterns. Therefore, there is flexibility in the method to generate sequences with spatial patterns that vary to some degree. Second, there is the concern of introducing a bias, in particular if the climate becomes much wetter than in the past. Because true future data with which to compare the results are unavailable, this investigation is somewhat limited. Instead, the historical precipitation frequency curves can be compared with the future sequences to see if there are alarming shifts towards the wettest years in the historical record. In doing so, none of these comparisons indicated method-limiting precipitation. Figure 3.14

shows the frequency comparison for one of the Blue Nile sub-basins under the HadA2a scenario, which will ultimately be shown to indicate a 12% precipitation increase.

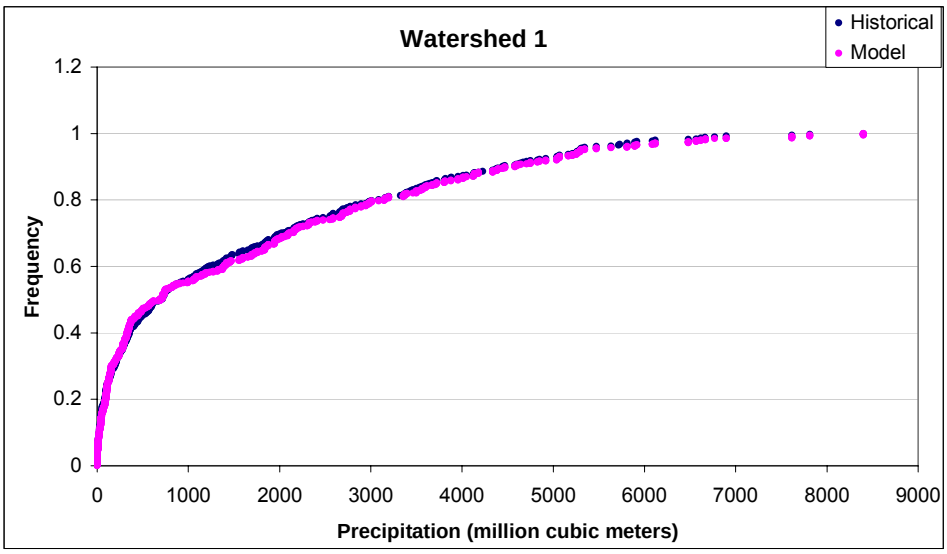

Figure 3.14: Frequency curves of historical precipitation (blue) and future precipitation under the HadA2a scenario.

Temperature

Much like Lake Victoria, the significance results for temperature were more extensive than for precipitation, which indicates considerably greater model skill with respect to temperature. However, since the model data for precipitation is not being used directly, model temperatures will not necessarily exhibit the correct co-variability with the constructed precipitation sequences. This raises a major question for working with temperature data: while it clearly would be incorrect to use the historical analog method for temperature given the expected increasing trend, how can we construct a series that incorporates both model skill and exhibits the correct temperature-precipitation co-variability?

The method developed works as follows. The bias-corrected target data are used in two ways. First, the temperature trend is estimated by a cubic polynomial. Note that all model runs demonstrated at least annual temperature significance over the four target pixels, with most showing considerable monthly significance. Second, the monthly data are used to generate departure sequences, which represent each month's departure from the mean trend.

$$\overline{M}(t) = a_1 t + a_2 t^2 + a_3 t^3 + a_0$$

$$m(t) = M(t) - \overline{M}(t)$$

In the above expressions, $M(t)$ is the original monthly temperature at time *t*, $\overline{M}(t)$ is the mean temperature trend, and $m(t)$ is the monthly departure of temperature from the trend at time *t*. The same procedure, but with a linear trend, is applied to the historical temperature series.

The historical departures are ranked and their frequencies calculated by month (i.e., each month of the year is ranked separately). The frequencies are then compiled into a time-series according to the order of years used in the historical analog method for precipitation (the analog index). Then 39-year blocks of the future departure sequences are processed in the same way, such that for the first 39 years (1962-2000) each month is ranked from 1 to 39 and the frequency calculated. The model departure matching the historical analog frequency is then selected, month by month. The next block of 39 years is processed in the same manner until reaching the end of the model horizon. An example of this method is illustrated in Figure 3.15. Finally, the newly constructed departure sequences are added to the model trends to generate the final monthly temperatures.

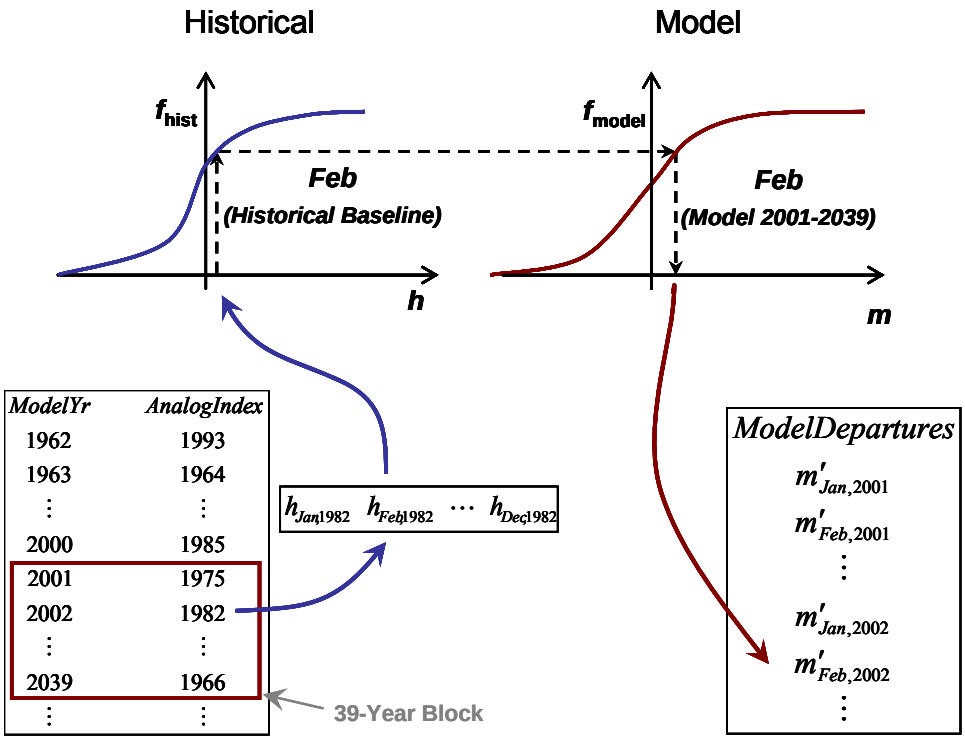

Figure 3.15: An example of using frequency matching to select future model departures (*h* represents historical temperature departures, *m* the model departures, and *m'* the final model departures.)

There are three key points of interest for this method. First, the constructed temperatures will maintain their seasonal structure since the method is applied on a month by month basis. Second, the analog index is used to select historical temperature departures that correspond directly to the precipitation sequences discussed in the previous section. As a result, when relatively low (high) temperatures have accompanied a particular historical monthly precipitation, similarly low (high) temperatures will be selected from the future temperature distribution via the frequency matching, thus forcing the temperature to vary in a consistent way with the precipitation. Finally, because the temperature departures and the trend to which they are added are derived from the original GCM data, they maintain both the projected increases in temperature as well as any changes in variability that the models project.

3.5.4 Downscaling

Coarse resolution climate data are converted to smaller scale basin sequences much the same way as in Lake Victoria. One minor difference in this work is that gridded historical data are projected to the sub-basin areas using a simple area-weighted average. Even with monthly data, the majority of downscaling relationships are sufficiently described for all months of the year together. The R^2 values for temperature are 0.97 and 0.99 for the upper and lower basins, respectively. And the precipitation R^2 values are 0.98 and 0.996 for the same basins.

Table 3.6: Blue Nile downscaling statistics.

Temperature			Precipitation		
Predictor Pixel	Target Basin	R^2	Predictor Pixel	Target Basin	R^2
P 89	L. Tana	0.968	P 89	L. Tana	0.978
P 88	2	0.994	P 88	2	0.996

While charts of all downscaling relationships are included in Appendix A, two cases are presented here for discussion purposes. Out of all precipitation and temperature relationships, only one warranted a seasonal partition. Figure 3.16 shows the relationships between pixel 89 and watershed 1. The season 1 relationships consists of data in months January through April and August through October. Although it does not appear to be an obvious seasonal breakdown, this separation represents the months of increasing temperature in season 1 and decreasing temperature in season 2. While the temperatures seem to overlap to some extent in these seasons, it is seen that the season 2 relationship is mildly nonlinear. This is likely due to the fact that there are two factors leading to decreasing temperature, the seasonal precession of the sun and the onset of the rainy season.

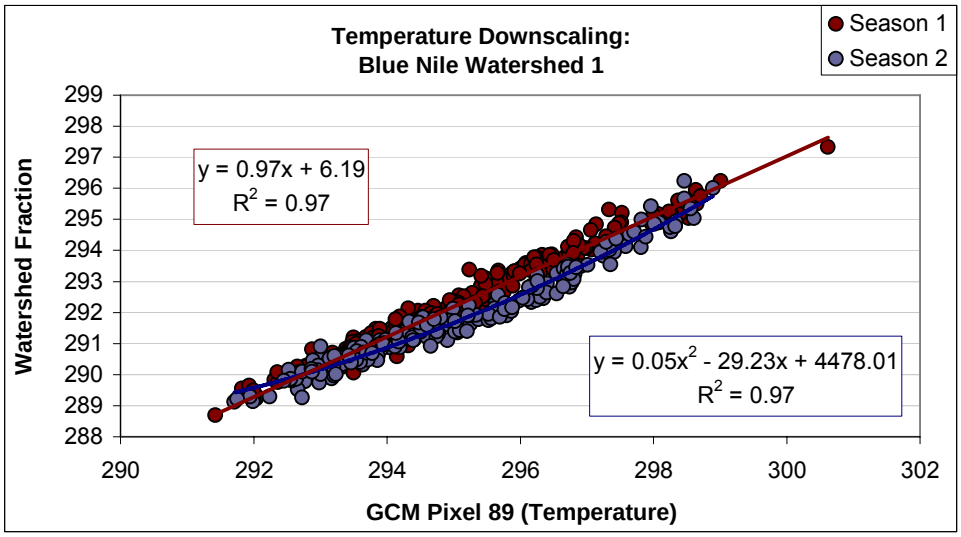

Figure 3.16: Season dependent downscaling from Pixel 89 to watershed 1.

Looking at all other downscaling relationships for the Blue Nile, it is seen that the statistical regressions are remarkably good for both precipitation and temperature (Figure 3.17). Some relationships are expected to be well fit as a result of the target watershed filling a large portion of the upscaled pixel area. However, it is also likely that the fit is artificially high due to the sparse availability of station data in this region, which may have led to gridded data with inflated spatial correlations.

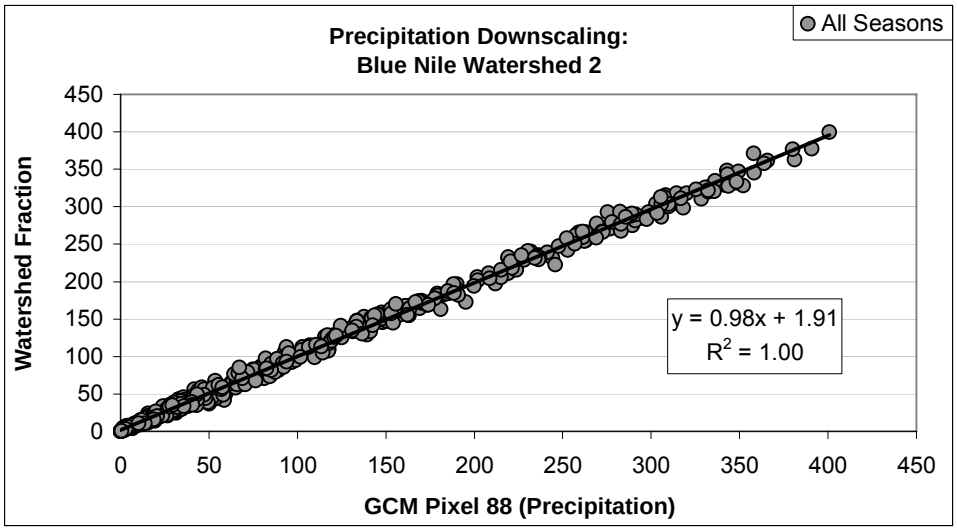

Figure 3.17: An example of very high correlations between large scale pixels and watershed sequences.

3.5.5 Spatial Variability

The Blue Nile methodology uses regional indicators to select historical analog sequences for each target pixel. As a result, spatial regressions between indicators and their neighboring target pixels are unnecessary. However, as with Lake Victoria, the downscaling procedure does employ spatial regressions between the large pixels of the GCM grid and Blue Nile sub-basins. Here we could bootstrap the residuals of these relationships as has been described previously. But this is not necessary, as the analog approach yields additional information that may be incorporated here.

Future climate scenarios are dependent upon historically realized sequences. As such, we can incorporate this information to select residuals that occurred under similar conditions. For example, if precipitation in the year 2015 is represented by the historical analog derived from 1967, then the monthly downscaling residuals that are recorded for the year 1967 are applied to the monthly downscaled sequences in the future. This applies to both temperature and precipitation.

3.5.6 Final Sequences

The final watershed sequences for temperature and precipitation are presented in Figures 3.18 and 3.19, respectively. For visual and analytic clarity, the precipitation results are presented as three-year moving averages. The sequences shown for this and the remaining basins are not derived from 20-member ensembles as was the case for Lake Victoria (p. 45). At this stage, the ensembles are not relevant because indicator pixels have not passed through spatial models, and the downscaling errors have been reconciled with the historically realized relationships (selecting residuals from the year of historical analog.) However, these sequences will eventually be expanded to a similar ensemble during the hydrologic analysis in Chapter 4.

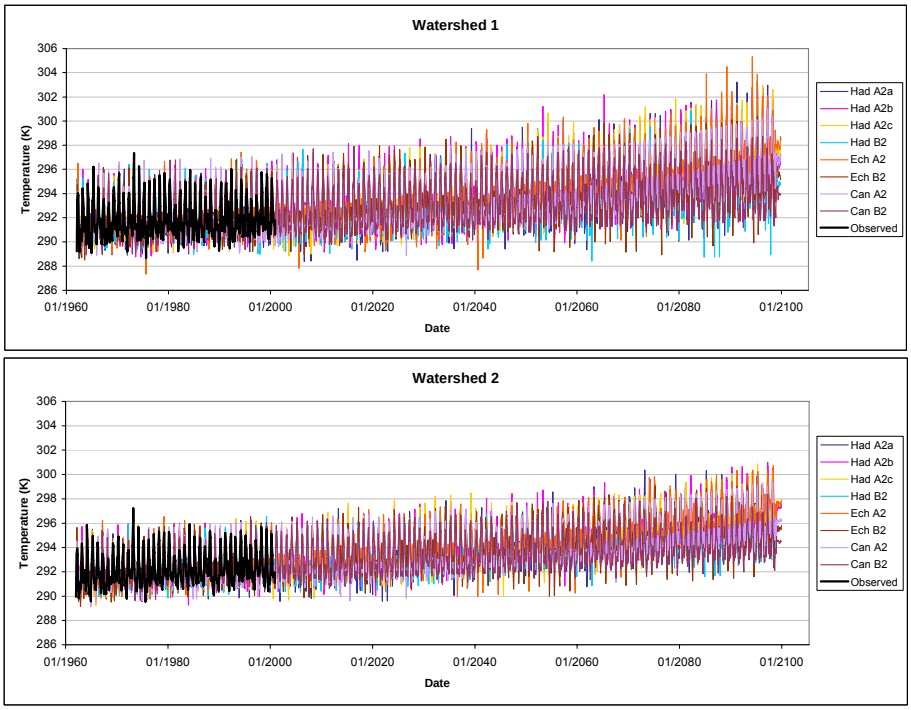

Figure 3.18: Temperature sequences for two sub-basins in the Upper Blue Nile (observed baseline shown in black).

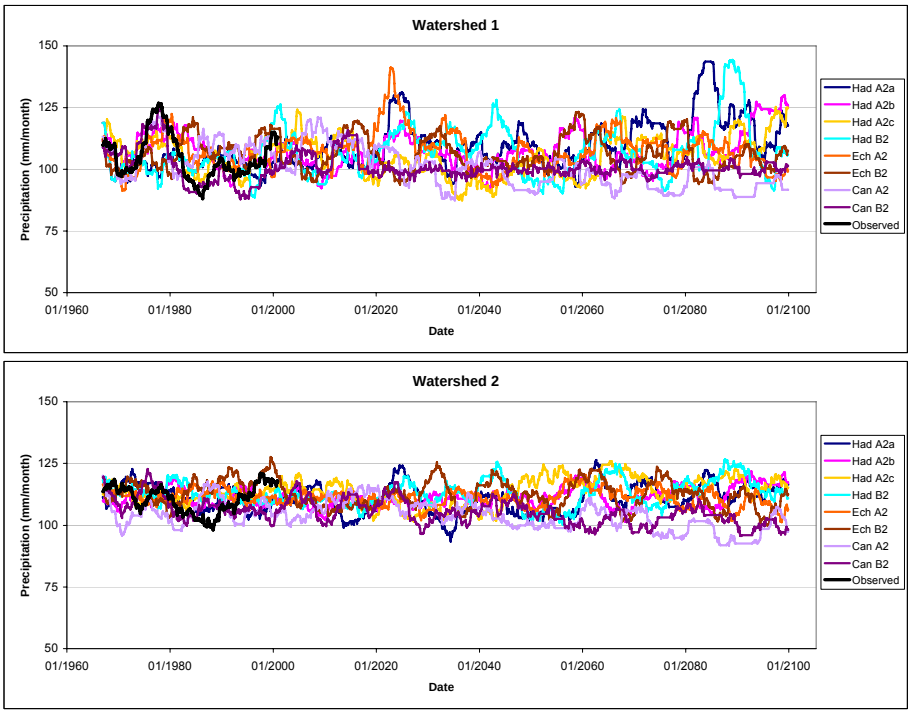

Figure 3.19: Precipitation sequences for two sub-basins in the Upper Blue Nile (observed baseline shown in black).

Temperature Assessment

Again, all eight scenarios project appreciable temperature increases. The historical mean annual temperatures for watersheds 1 and 2 are within 0.3 °C of each other. And, in fact, the projected future temperature increases are seen to be similar as well. The mean annual temperatures from the first 30-years (1962-1991) are compared to the average from the latest 30 years (2070-2099). Table 3.7 summarizes the comparisons. The A2 scenarios project temperature increases between 3.9 and 4.8 °C, with EchA2 reflecting the greatest change and CanA2 the lowest. Temperature increases from the B2 scenarios range from 1.9 to 3.0 °C, or approximately 2 °C less than the more extreme scenario. As with the Lake Victoria results, all B2 scenarios show a linear trend, while the A2 scenarios are nonlinear and imply more rapid temperature change in the future. Compared with the Lake Victoria results, the Blue Nile scenarios appear to be more

sensitive to model initial conditions. The spread of results from the three HadA2 traces is between 1/3 to 1/2 of the difference between the A2 and B2 scenarios; whereas in Lake Victoria, the effect of atmospheric forcing was 4 to 5 times the effect of initial conditions.

Table 3.7: Projected temperature changes between the final 30 years (2070-2099) and the 30-year baseline (1962-1991).

Temperature Change (°C)		
Model/SubArea	**WS 1**	**WS 2**
HadA2a	4.1	3.9
HadA2b	3.9	4.1
HadA2c	4.5	4.4
HadB2	2.8	2.8
EchA2	4.8	4.5
EchB2	3.1	3.0
CanA2	4.0	3.3
CanB2	2.1	1.9
Had A2 spread/SRES A2-B2 spread	0.45	0.37

Precipitation Assessment

The precipitation sequences in both sub-basins show marked wet-dry episodes that recur approximately every 10 to 15 years. The upper basin, or watershed 1, exhibits greater variability than the lower basin; although both watershed are situated within the Ethiopian highlands. The Hadley and Echam scenarios appear to have more pronounced wet-dry episodes than the Canadian scenarios.

Table 3.8 presents a summary comparison of precipitation changes between the last 30 years of the model horizon and the baseline period. The most obvious feature is that the Hadley scenarios indicate precipitation increases for both watersheds, while the Echam

and Canadian models show decreases. HadA2a indicates a 12% increase for watershed 1 precipitation, while CanA2 indicates a 13% reduction. All other scenarios indicate relatively small changes.

Table 3.8: Projected precipitation changes between the final 30 years (2070-2099) and the 30-year baseline (1962-1991).

Precipitation Change (%)		
Model/SubArea	**WS 1**	**WS 2**
HadA2a	12.3	0.8
HadA2b	4.9	3.1
HadA2c	5.8	3.5
HadB2	4.8	0.7
EchA2	-1.5	-2.5
EchB2	-1.7	-2.6
CanA2	-13.3	-9.8
CanB2	-2.2	-7.2
Had A2 spread/SRES A2-B2 spread	0.98	25.05

Given the natural precipitation variability, and obvious persistence, it is difficult to assess the significance of these summary comparisons. For example, beginning around 2045, the HadB2 scenario experiences a prolonged drought that lasts nearly 15 years. Nevertheless, in the final 30-year period HadB2 is exceptionally wet, with a modestly wet episode around 2080 immediately followed by the wettest period in the sequence. The Echam scenarios have less pronounced behavior in the final 30 years and do not seem to reveal any obvious downward trend in spite of a lower 30-year average. The Canadian scenarios are the only sequences that appear to have a steady decline in precipitation.

3.6 Atbara

Model skill in the Atbara and remaining Nile regions was analyzed in the same manner as the Blue Nile. Five pixels were considered in the analysis of the Atbara region and are identified in Figure 3.20.

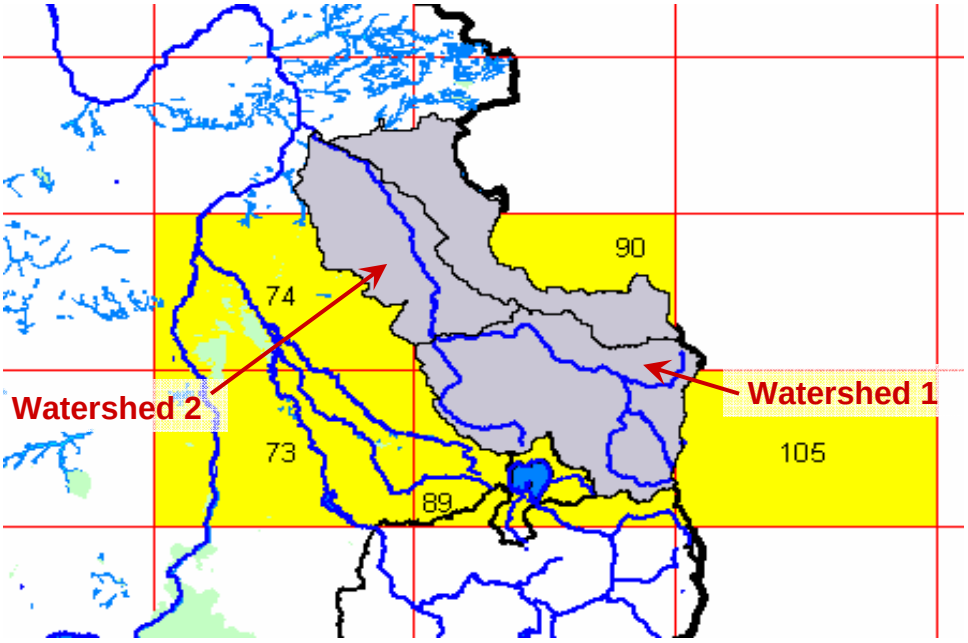

Figure 3.20: Atbara region with pixels of interested highlighted in yellow.

3.6.1 Indicators

Potential indicator data are drawn from the five area pixels based on each model's ability to represent the precipitation climatology. The pixels emerging from this initial filter are very few. Six of the eight model runs generated only a single pixel with reasonable precipitation climatology. The HadA2b and HadA2c runs were found to have two, but only one of the HadA2c pixels resulted in any statistically significant seasonal series. This led to limited indicator sets from which to select the analog sequences. All eight models demonstrated sufficient temperature significance over the target pixels to support

the temperature scenario method. Table 3.9 summarizes the indicator sets identified for each model run.

Table 3.9: Atbara precipitation indicator sets.

Can A2		Can B2		Ech A2		Ech B2	
Pixel	Season	Pixel	Season	Pixel	Season	Pixel	Season
P 105	Sep	P 105	Dec	P 74	Mar	P 74	Jan
P 105	Dec	P 105	Dec-Feb	P 74	Jul	P 74	Feb
P 105	Nov-Dec	P 105	Sep-Nov	P 74	Nov	P 74	Jul
P 105	Dec-Feb	P 105	Jan-Apr	P 74	Jul-Aug	P 74	Nov
P 105	Nov-Apr	P 105	Nov-Apr	P 74	Nov-Dec	P 74	Nov-Dec
		P 105	Jan-Dec	P 74	Jan-Mar	P 74	Jan-Mar
				P 74	Jul-Sep	P 74	Dec-Feb
				P 74	Dec-Feb		
				P 74	May-Aug		
				P 74	Jul-Dec		
				P 74	May-Oct		
				P 74	Jan-Dec		
Had A2a		**Had A2b**		**Had A2c**		**Had B2**	
Pixel	Season	Pixel	Season	Pixel	Season	Pixel	Season
P 89	Jan	P 74	Jan	P 89	Jul	P 89	Jan
P 89	Oct	P 74	Dec	P 89	Dec-Feb	P 89	Oct
P 89	Sep-Oct	P 74	Sep-Nov			P 89	Jan-Feb
P 89	Jan-Dec	P 89	Jun			P 89	Jan-Dec
		P 89	May-Jun				
		P 89	Nov-Dec				
		P 89	Apr-Jun				
		P 89	Sep-Nov				
		P 89	May-Oct				
		P 89	Jan-Dec				

3.6.2 Downscaling and Spatial Variability

Two sub-basins are used in the hydrologic model for the Atbara River. Therefore, a total of 4 downscaling relationships were used. The relationships were developed in the same manner as previously described. The R^2 values for temperature are 0.97 and 0.99 for the upper and lower basins, respectively (Table 3.10). And the precipitation R^2 values are

0.96 and 0.88 for the same basins. The residuals from these relationships are reintroduced in the final sequence based on the year of the historical analog, as described previously.

Table 3.10: Atbara downscaling statistics.

Temperature			Precipitation		
Predictor Pixel	Target Basin	R^2	Predictor Pixel	Target Basin	R^2
P 89	1	0.965	P 89	1	0.963
P 74	2	0.989	P 74	2	0.876

3.6.3 Final Sequences

Temperature and precipitation for the two Atbara sub-basins are presented in Figures 3.21 and 3.22. As with the Blue Nile results, precipitation is presented as three-year moving averages.

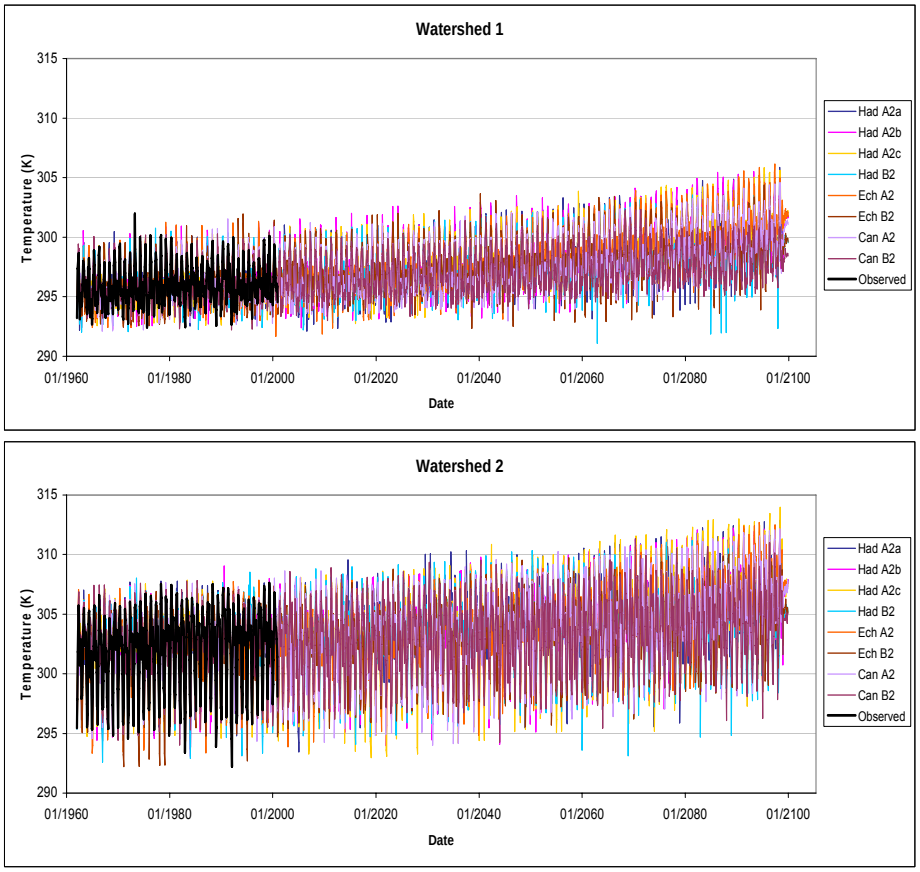

Figure 3.21: Temperature sequences for two Atbara sub-basins (observed baseline shown in black).

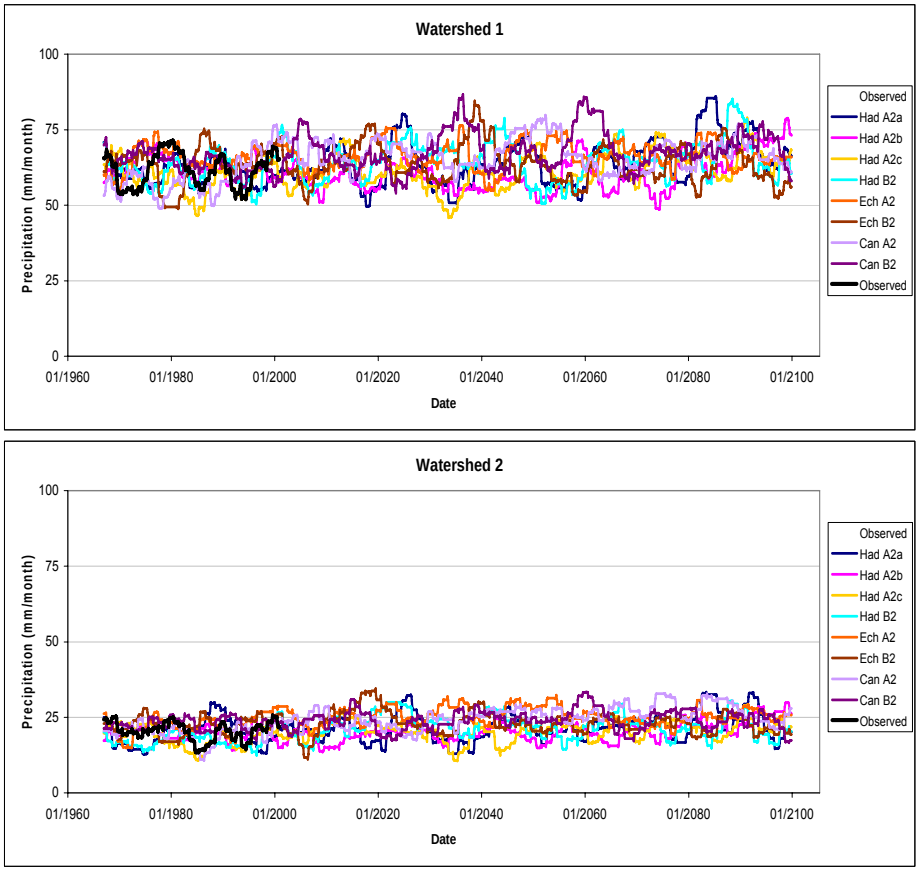

Figure 3.22: Precipitation sequences for two Atbara sub-basins (observed baseline shown in black).

Temperature Assessment

The projected temperature changes for Atbara are comparable to the Blue Nile Results . Across the A2 scenarios, temperatures increase between 3.6 and 4.7 °C, while the B2 scenarios range from 2.0 to 3.3 °C (Table 3.11). Interestingly, the HadA2 traces differ by as much as 0.6 °C in the upper watershed, while the lowland watershed shows little sensitivity to model initial conditions. Finally, consistent with other regions, the Echam and Hadley scenarios project the largest temperature increases.

Table 3.11: Projected temperature changes between the final 30 years (2070-2099) and the 30-year baseline (1962-1991).

Temperature Change (°C)		
Model/SubArea	**WS 1**	**WS 2**
HadA2a	4.0	3.9
HadA2b	3.9	3.9
HadA2c	4.5	4.0
HadB2	2.9	2.7
EchA2	4.7	4.3
EchB2	3.3	3.1
CanA2	3.6	3.9
CanB2	2.0	2.4
Had A2 spread/SRES A2-B2 spread	0.54	0.08

Precipitation Assessment

Overall, precipitation is projected to increase over the Atbara basin. The sole exception is the EchB2. The EchB2 changes shown in the summary table (Table 3.12) are most likely insignificant against the background of interannual variability. The other scenarios, however, do suggest an overall trend of increasing precipitation. In general, the changes in watershed 2 are greater than watershed 1; although, historically, watershed 2 experienced considerably less rainfall than watershed 1- approximately 1/3. The Hadley model continues to show considerable spread among its three A2 traces, suggesting that even in the presence of a stronger climate change signal climate system uncertainty remains relevant.

Table 3.12: Projected precipitation changes between the final 30 years (2070-2099) and the 30-year baseline (1962-1991).

Precipitation Change (%)		
Model/SubArea	**WS 1**	**WS 2**
HadA2a	10.6	11.9
HadA2b	5.4	21.6
HadA2c	13.3	22.0
HadB2	5.6	19.5
EchA2	1.6	16.8
EchB2	-1.1	1.8
CanA2	17.9	41.6
CanB2	4.6	4.0
Had A2 spread/SRES A2-B2 spread	1.60	1.33

3.7 Sobat

Five area pixels were assessed for climatology and statistical significance in the Sobat region. The five potential indicator pixels are identified in Figure 3.23.

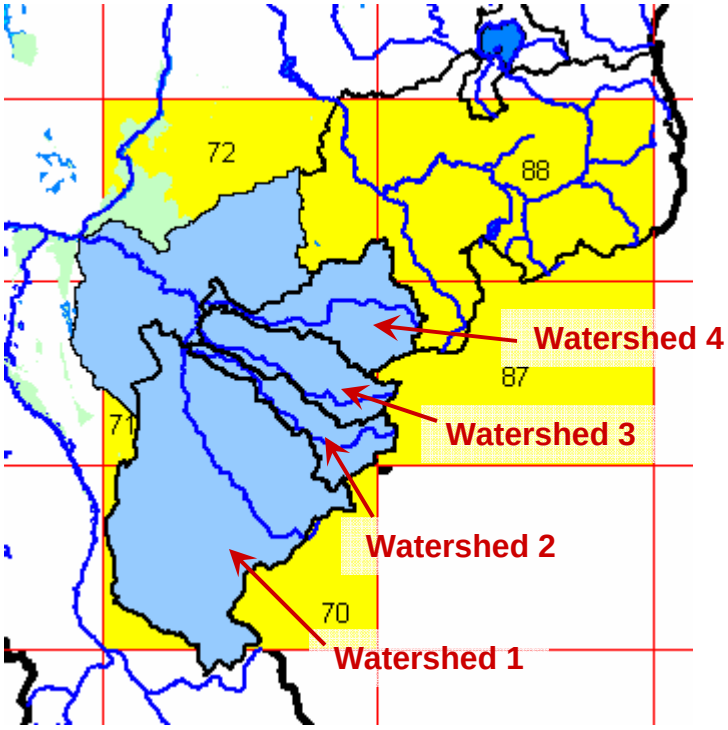

Figure 3.23: Sobat region with pixels of interested highlighted in yellow.

3.7.1 Indicator Pixels

The Sobat basin shares part of its climatic features with the Equatorial Lakes to the southwest, while to the northeast it exhibits similar climatology to the Blue Nile region. Given the transitional nature of this location, it is surprising that both the Hadley and Canadian model runs were able to reasonably represent the precipitation climatologies at 4 to 5 of the pixels being considered. Even so, many of these pixels do not yield many statistically significant seasons. The two Echam runs did not produce reasonable climatologies at *any* of the five pixels, but the statistically significant seasons are ultimately used in the absence of better results. Consequently, the Echam derived scenarios should be held in lower confidence for the Sobat region.

Overall, the Sobat is found to have more precipitation indicators than the Atbara. As in the previous basins, the temperature significance results were sufficient to support the temperature scenarios. The final indicator sets are presented in Table 3.13.

Table 3.13: Sobat precipitation indicator sets.

Can A2		Can B2		Ech A2		Ech B2	
Pixel	Season	Pixel	Season	Pixel	Season	Pixel	Season
P 70	Mar	P 70	Apr	P 70	Jul	P 71	Feb
P 70	Apr	P 70	Jan-Mar	P 71	Jun-Aug	P 71	Jul
P 70	Dec	P 70	Jan-Apr	P 72	Jan	P 71	Aug
P 70	Mar-Apr	P 71	Apr	P 72	Feb	P 71	Jul-Aug
P 70	Jan-Apr	P 71	Nov-Apr	P 72	Aug	P 71	Jul-Sep
P 71	Apr	P 72	Nov-Dec	P 72	Nov	P 71	Jun-Aug
P 71	Mar-Apr	P 87	Mar-Apr	P 72	Jan-Feb	P 72	Jan
P 71	Jan-Apr	P 87	Nov-Apr	P 72	Jul-Aug	P 72	Feb
P 87	Nov-Apr	P 88	Apr	P 72	Sep-Oct	P 72	Aug
P 88	Apr	P 88	Mar-Apr	P 72	Jul-Sep	P 72	Nov
P 88	Nov	P 88	Jan-Apr	P 72	Oct-Dec	P 72	Jan-Feb
P 88	Mar-Apr	P 88	Sep-Dec	P 72	May-Aug	P 72	Jul-Aug
P 88	Nov-Dec	P 88	Nov-Apr	P 72	Sep-Dec	P 72	Nov-Dec
P 88	Jan-Apr			P 72	Jul-Dec	P 72	Jul-Sep
P 88	Nov-Apr			P 87	Jul	P 72	Oct-Dec
				P 88	Jun	P 72	May-Aug
				P 88	Mar-Apr	P 72	Sep-Dec
				P 88	Dec-Feb	P 72	Jul-Dec
				P 88	Jun-Aug	P 72	May-Oct
				P 88	Jan-Apr	P 88	Feb
				P 88	Jan-Jun	P 88	Oct
				P 88	Nov-Apr	P 88	Mar-Apr
				P 88	Jan-Dec	P 88	Dec-Feb
						P 88	Jun-Aug
						P 88	Jan-Apr
						P 88	Nov-Apr
						P 88	Jan-Dec

Had A2a		Had A2b		Had A2c		Had B2	
Pixel	Season	Pixel	Season	Pixel	Season	Pixel	Season
P 70	Jan	P 70	Oct	P 70	May	P 70	Jan
P 70	Sep	P 70	Jul-Aug	P 71	Nov-Dec	P 70	Feb
P 71	Jan	P 70	Nov-Dec	P 71	May-Aug	P 70	Sep
P 71	May	P 70	Oct-Dec	P 87	Jun-Aug	P 71	Jan
P 71	Sep	P 70	Jun-Aug	P 87	Nov-Apr	P 71	Jan-Feb
P 71	Oct	P 70	May-Aug	P 88	Dec-Feb	P 71	Dec-Feb
P 71	May-Jun	P 70	Jul-Dec			P 88	Feb
P 87	Sep	P 70	May-Oct				
P 88	Oct	P 71	Nov-Dec				
		P 87	Oct				
		P 87	Nov-Dec				
		P 87	Jan-Mar				

3.7.2 Downscaling

The hydrologic model developed for the Sobat river uses four sub-basins. The basins are delineated to represent the upper Pibor, the Baro basin, and the basins of two smaller tributaries located between the Pibor and Baro (Figure 3.23). Temperature and precipitation have been downscaled to these four basins using simple regression techniques and with all months included in each relationship.

In some cases more than one large pixel was used as an indicator of the basin series. The predictor pixels and regression R^2 values are summarized in the table below. As with the previous basins, the relationships appear very strong, but this again could be due to limited station data.

Table 3.14: Sobat downscaling statistics.

Temperature			Precipitation		
Predictor Pixel(s)	Target Basin	R^2	Predictor Pixel(s)	Target Basin	R^2
P 70	Pibor	0.979	P (70,71)	Pibor	0.986
P 71	2	0.922	P 71	2	0.877
P 71	3	0.979	P 71	3	0.979
P 71	Baro	0.960	P (71,72,87)	Baro	0.919

3.7.3 Final Sequences

Final temperature and precipitation sequences for the four Sobat sub-basins are shown in Figures 3.24 and 3.25.

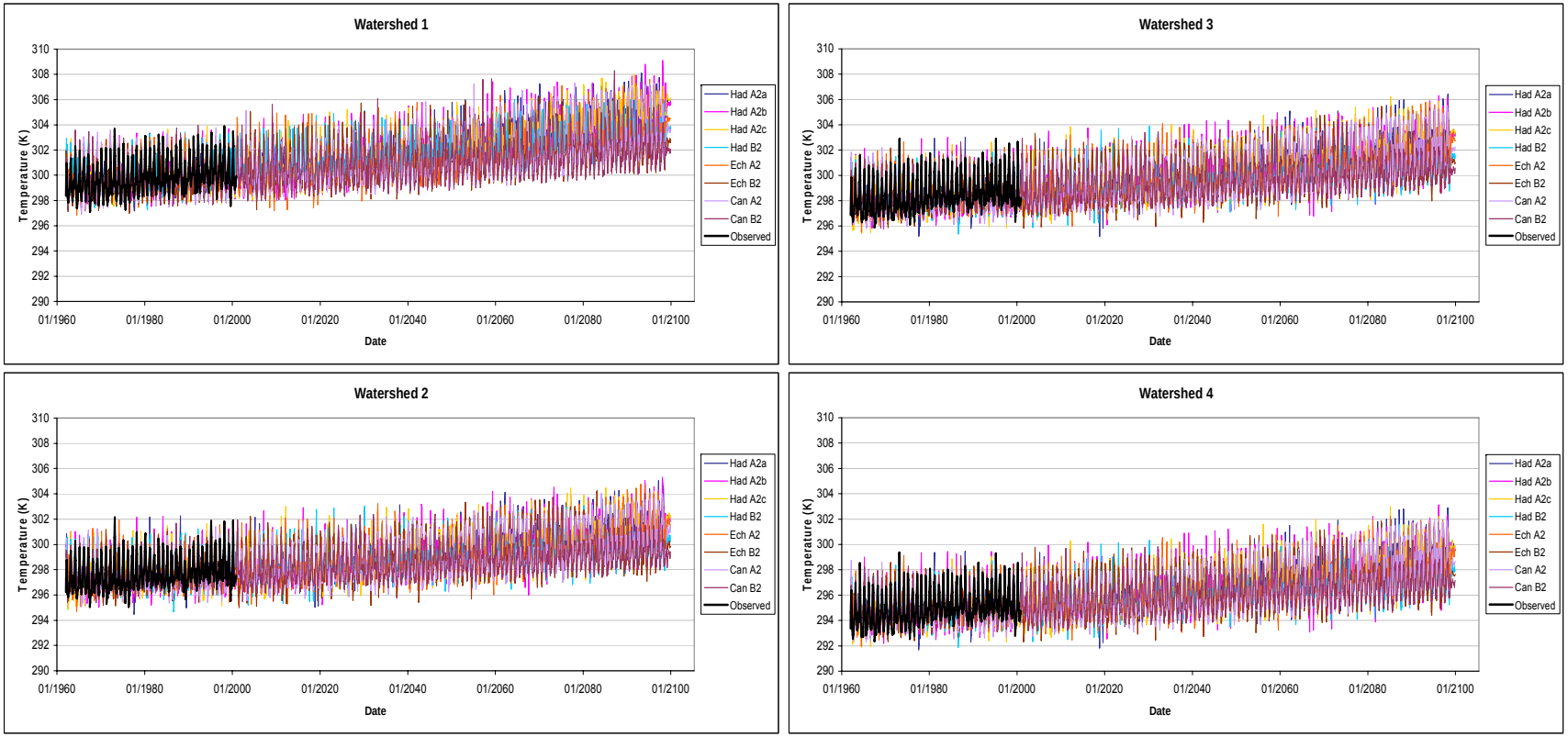

Figure 3.24: Temperature sequences for four Sobat sub-basins (observed baseline shown in black).

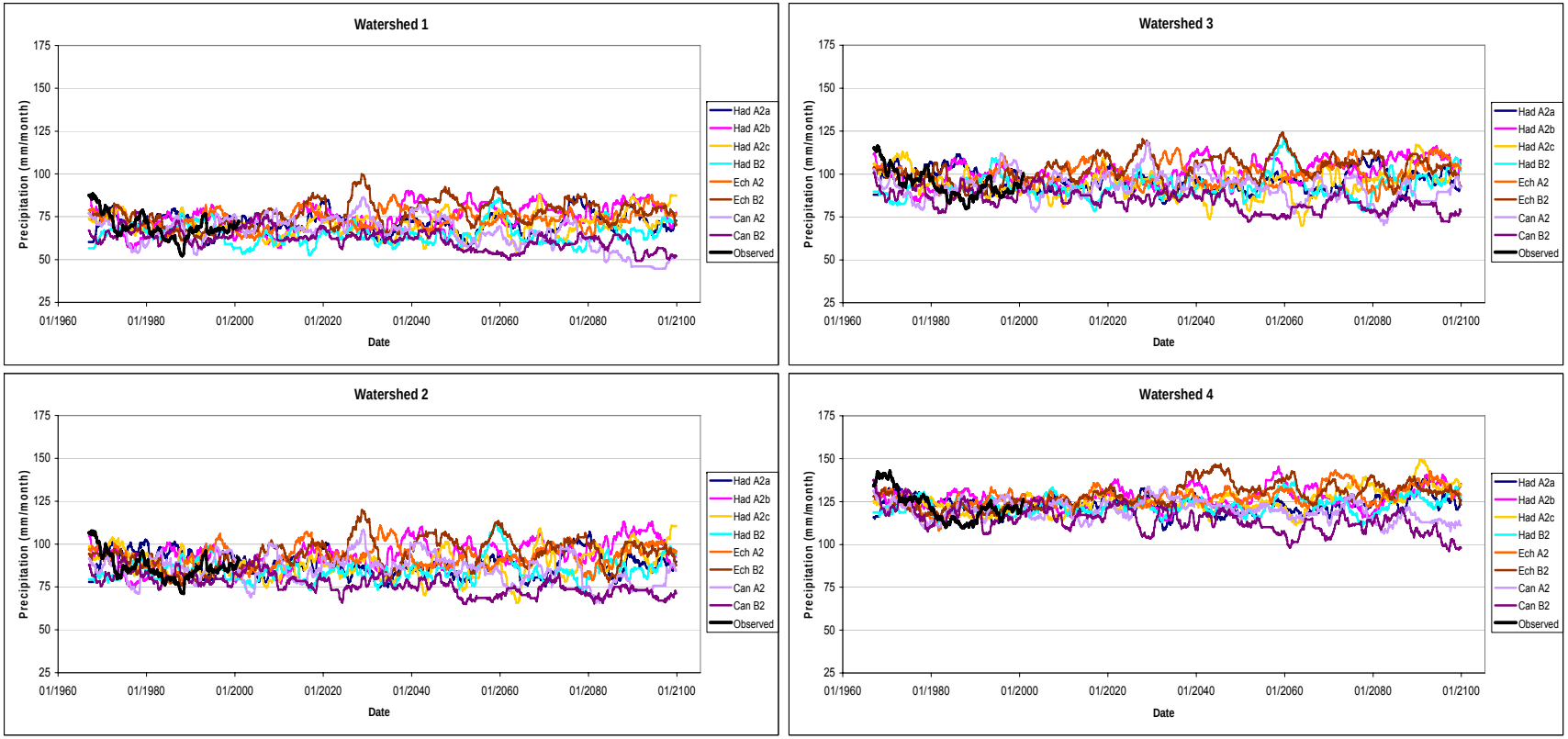

Figure 3.25: Precipitation sequences for four Sobat sub-basins (observed baseline shown in black).

Temperature Assessment

The 30-year average temperature changes are summarized in Table 3.15. Watersheds 2 thru 4, which extend up to parts of the Ethiopian plateau, show somewhat less climate sensitivity than the Blue Nile. On average, the temperature changes are around 0.5 °C less. The Hadley scenarios show surprisingly large temperature increases for watershed 1. The HadA2 traces project between 4.8 and 5.2 °C increases by the 2080s. This particular sub-basin extend up into the Lake Plateau region and may be expected to more closely resemble changes occurring in the eastern portion of the Lake Victoria watershed. Even so, the changes projected here are more than 0.5 °C higher than the corresponding Hadley scenarios for the eastern watersheds of Lake Victoria. The Echam and Canadian scenarios, on the other hand, show similar climate sensitivity over watershed 1 as they do for the eastern half of the Lake Victoria basin.

Table 3.15: Projected temperature changes between the final 30 years (2070-2099) and the 30-year baseline (1962-1991).

	Temperature Change (°C)			
Model/SubArea	**WS 1**	**WS 2**	**WS 3**	**WS 4**
HadA2a	4.9	3.7	4.1	4.0
HadA2b	4.8	3.5	3.8	3.7
HadA2c	5.2	3.8	4.2	4.1
HadB2	3.6	2.5	2.7	2.6
EchA2	3.7	3.1	3.4	3.4
EchB2	2.6	2.2	2.5	2.4
CanA2	3.0	2.6	2.9	2.8
CanB2	2.1	1.6	1.9	1.9
Had A2 spread/SRES A2-B2 spread	0.23	0.24	0.22	0.22

Precipitation Assessment

The precipitation results presented in Table 3.16 may appear inconsistent. The Hadley and Echam scenarios predict small increases in precipitation, and the Canadian predicts moderate decreases. However, a few of the Hadley scenarios actually show negative changes, and most of the Echam and Canadian results imply a larger change for B2 than A2. But, as cautioned previously, the 30-year averaged results should be interpreted together with the sequences shown in Figure 3.25. In doing so, we see that the underlying variability may again be playing a role in the summary statistics.

Even though HadB2 shows a negative change for watershed 1, a linear trend fit to the entire series shows a positive slope, albeit ever so slight. And the Canadian B2 trend does in fact exhibit a milder slope than the A2. Overall, the conclusion is that the results are fairly consistent. The Canadian scenarios indicate decreases similar to other basins, and, in general, the Hadley and Echam changes are minimal.

Table 3.16: Projected precipitation changes between the final 30 years (2070-2099) and the 30-year baseline (1962-1991).

	Precipitation Change (%)			
Model/SubArea	**WS 1**	**WS 2**	**WS 3**	**WS 4**
HadA2a	4.9	0.1	-0.8	2.4
HadA2b	6.3	7.6	7.1	-0.2
HadA2c	6.0	2.9	1.2	10.2
HadB2	-2.1	1.8	3.1	1.8
EchA2	4.4	5.0	6.0	6.8
EchB2	8.8	8.3	5.9	7.1
CanA2	-16.8	-6.4	-4.7	-4.0
CanB2	-11.4	-12.9	-10.3	-9.6
Had A2 spread/SRES A2-B2 spread	0.20	4.19	2.02	17.96

3.8 Equatorial Lakes below Lake Victoria

Four pixels in the area of lakes Kyoga, George and Albert were considered as potential indicators. The equatorial lakes region and indicator pixels are shown in Figure 3.26.

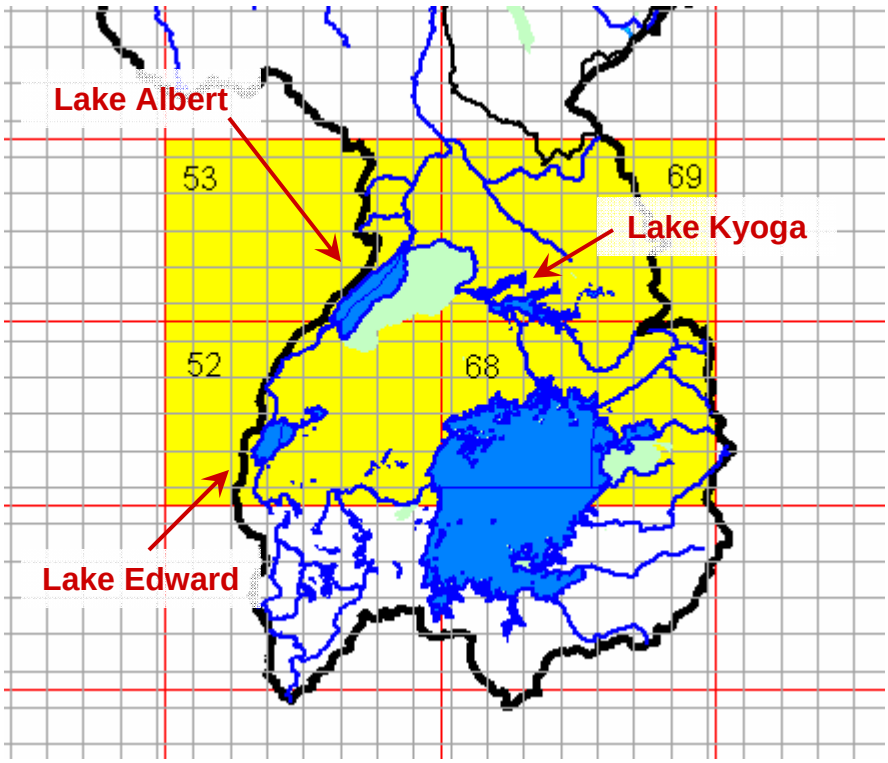

Figure 3.26: Equatorial Lakes region with pixels of interest highlighted in yellow.

3.8.1 Indicator Pixels

The general structure of precipitation climatology is well represented for all four pixels by all eight model runs. In spite of improved model performance in this region, the historical analog method is employed here rather than the method used in Lake Victoria. The lower lakes in this region have much less extensive watershed areas and storage capacity, thus rendering the six-monthly time step of the Lake Victoria analysis inappropriate for this application. The final indicator sets are presented in Table 3.17.

Table 3.17: Equatorial lakes precipitation indicator sets.

Can A2		Can B2		Ech A2		Ech B2	
Pixel	Season	Pixel	Season	Pixel	Season	Pixel	Season
P 52	May	P 53	Mar	P 52	Mar	P 52	Jan
P 52	May-Jun	P 53	Sep-Nov	P 52	Jan-Feb	P 52	Feb
P 53	Sep	P 53	May-Oct	P 52	Jan-Mar	P 52	May
P 53	May-Jun	P 68	Jun	P 52	Jan-Apr	P 52	Jun
P 53	Sep-Oct	P 68	Sep-Nov	P 52	Jan-Jun	P 52	Jan-Feb
P 53	Sep-Nov	P 69	Apr	P 53	Jan	P 52	Jan-Mar
P 53	May-Aug			P 53	May	P 52	Jan-Apr
P 53	May-Oct			P 53	Jan-Feb	P 52	Jan-Jun
P 68	Mar-May			P 53	May-Jun	P 53	Jan
P 68	Sep-Nov			P 53	Jan-Mar	P 53	Feb
P 69	Sep			P 53	Apr-Jun	P 53	May
P 69	May-Jun			P 53	Jan-Jun	P 53	Jun
P 69	Mar-May			P 69	Nov	P 53	Jan-Feb
P 69	May-Oct					P 53	Jan-Mar
						P 53	Apr-Jun
						P 53	Jan-Apr
						P 53	Jan-Jun
						P 53	Jul-Dec
						P 53	Jan-Dec

Had A2a		Had A2b		Had A2c		Had B2	
Pixel	Season	Pixel	Season	Pixel	Season	Pixel	Season
P 52	Aug	P 52	Dec	P 52	Jan	P 52	Dec-Feb
P 52	Sep	P 52	Nov-Dec	P 52	May	P 53	Jan
P 52	Jul-Aug	P 52	Oct-Dec	P 52	Jun	P 53	Jan-Dec
P 52	Jul-Sep	P 52	Jul-Dec	P 52	May-Jun	P 68	Apr
P 52	Dec-Feb	P 53	Jul-Sep	P 52	Mar-May	P 68	Sep
P 52	Jan-Dec	P 68	May	P 53	May	P 68	Sep-Oct
P 53	Jan	P 68	Sep	P 53	Nov	P 69	Sep
P 53	Aug	P 68	Oct	P 53	May-Jun	P 69	Oct
P 53	Oct	P 68	Dec	P 68	May	P 69	Sep-Oct
P 53	Jul-Aug	P 68	Sep-Oct	P 69	Oct	P 69	Jul-Dec
P 53	Sep-Oct	P 68	Nov-Dec			P 69	Jan-Dec
P 68	Sep	P 68	Jul-Sep				
P 68	Sep-Oct	P 68	Oct-Dec				
P 68	Jul-Sep	P 68	Jun-Aug				
P 69	Jul	P 68	Sep-Nov				
P 69	May-Aug	P 68	Sep-Dec				
P 69	Jul-Dec	P 68	Jul-Dec				
P 69	Jan-Dec	P 68	Jan-Dec				
		P 69	Jul				
		P 69	Nov				
		P 69	Jul-Aug				
		P 69	Nov-Dec				
		P 69	Jul-Sep				
		P 69	Oct-Dec				
		P 69	Sep-Dec				
		P 69	Jul-Dec				
		P 69	Jan-Dec				

3.8.2 Downscaling

The historical data for the contributing areas to the lakes are taken as simple averages of the pixels covering these areas. The contributing areas and overlying CRU pixels are shown in Figure 3.27.

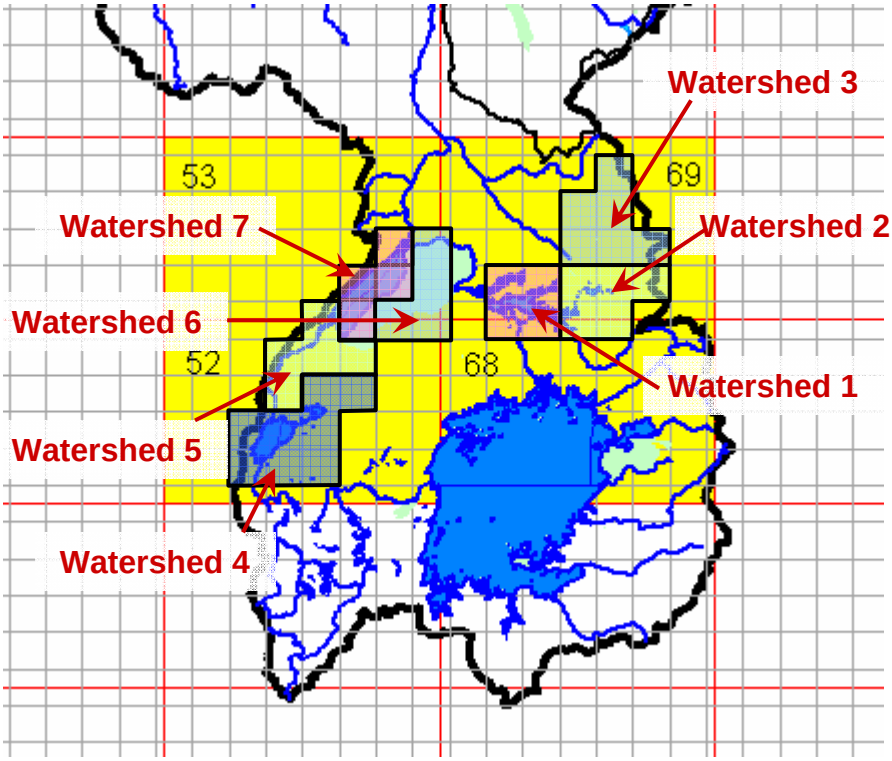

Figure 3.27: CRU pixels over the Equatorial Lakes.

The R^2 values for precipitation range between 0.68 and 0.92 (3.18). Basins 1, 2 and 3 have an alternative set of relationships. While pixel 69 is closest to these basins, the Echam runs do not demonstrate even annual temperature significance for this pixel. Therefore, alternate relationships have been developed using the neighboring pixel 53 at which the Echam runs demonstrate skill. The R^2 values for the temperature relationships ranged from 0.73 to 0.99, with the lowest values associated with the alternate

relationships. Overall, the relationships used here are not as strong as the previous three basins. The primary factor is that the difference in spatial scale between the large pixels and the target areas is much greater for these areas.

Table 3.18: Equatorial Lakes downscaling statistics.

Temperature			Precipitation		
Predictor Pixel	Target Basin	R^2	Predictor Pixel	Target Basin	R^2
P 69	1	0.918	P 69	1	0.749
P 53	1*	0.862	--	--	
P 69	2	0.959	P 69	2	0.885
P 53	2*	0.766	--	--	
P 69	3	0.986	P 69	3	0.918
P 53	3*	0.734	--	--	
P 52	4	0.975	P 52	4	0.922
P 52	5	0.980	P 52	5	0.736
P 53	6	0.951	P 53	6	0.682
P 53	7	0.962	P 53	7	0.735
* Indicates relationship used for Echam A2 and B2 scenarios.					

3.8.3 Final Sequences

Final temperature and precipitation sequences for the three Lake Kyoga and four Lake Albert watersheds are presented in Figures 3.28 – 3.31.

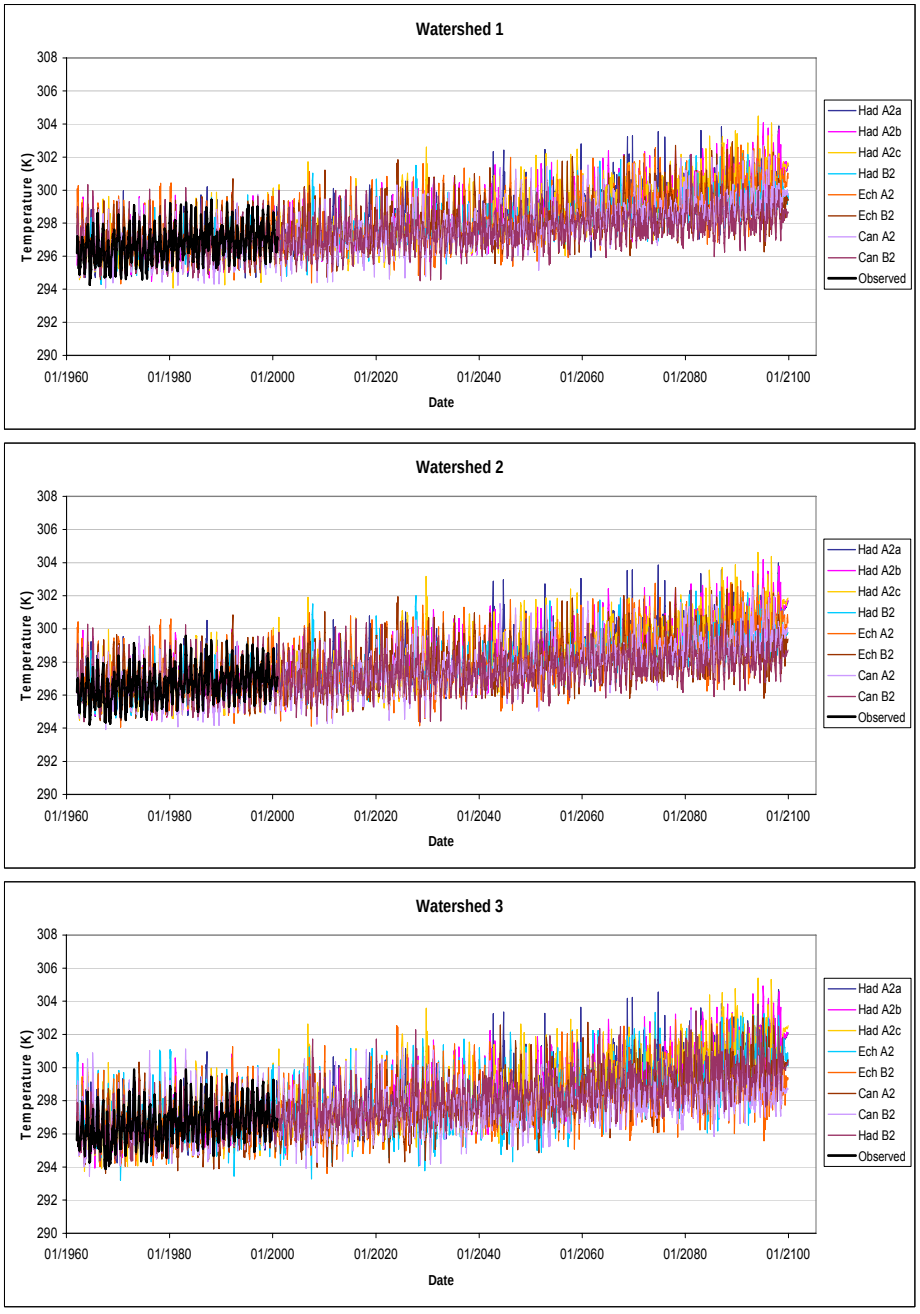

Figure 3.28: Temperature sequences for the Lake Kyoga sub-basins (observed baseline shown in black).

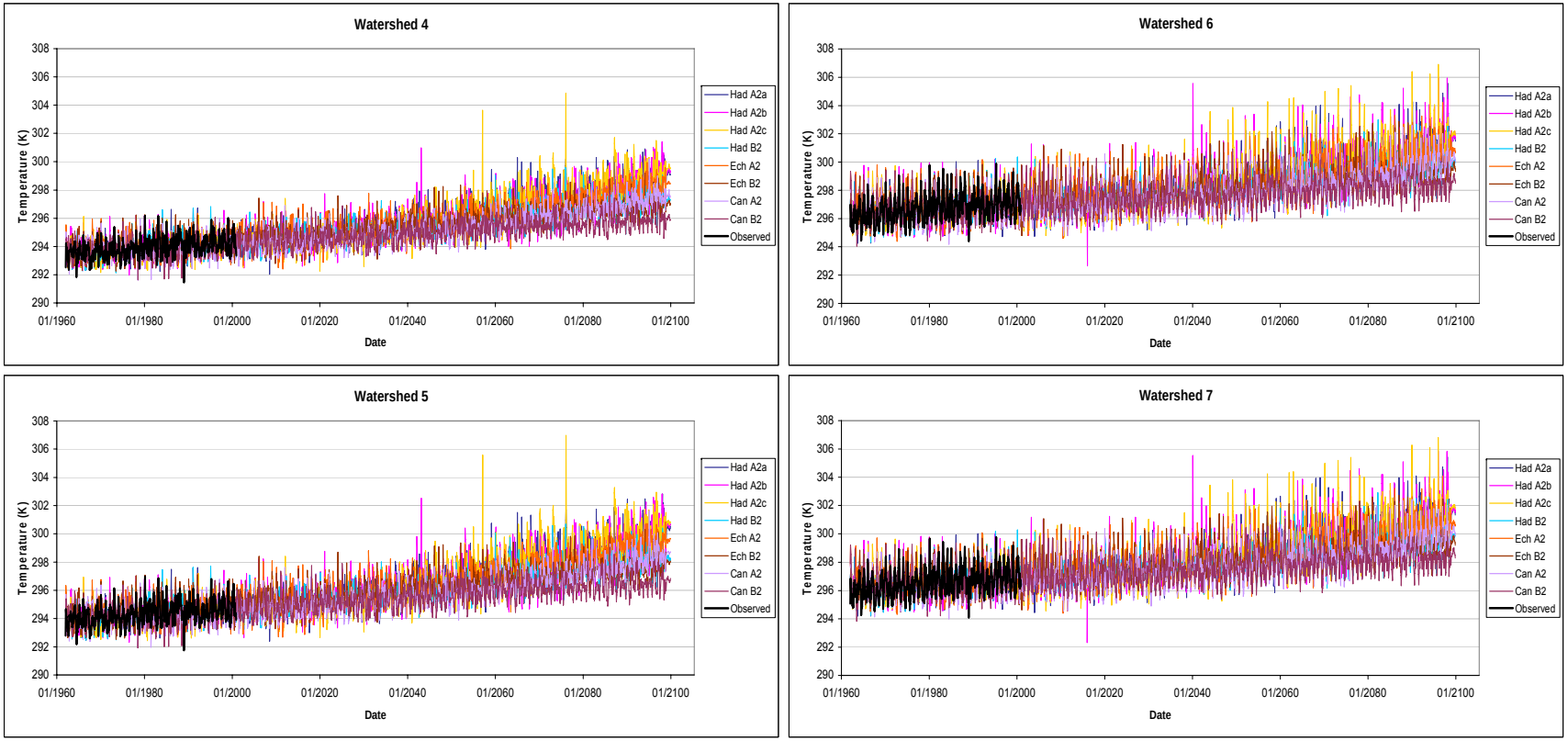

Figure 3.29: Temperature sequences for the Lake Albert sub-basins (observed baseline shown in black).

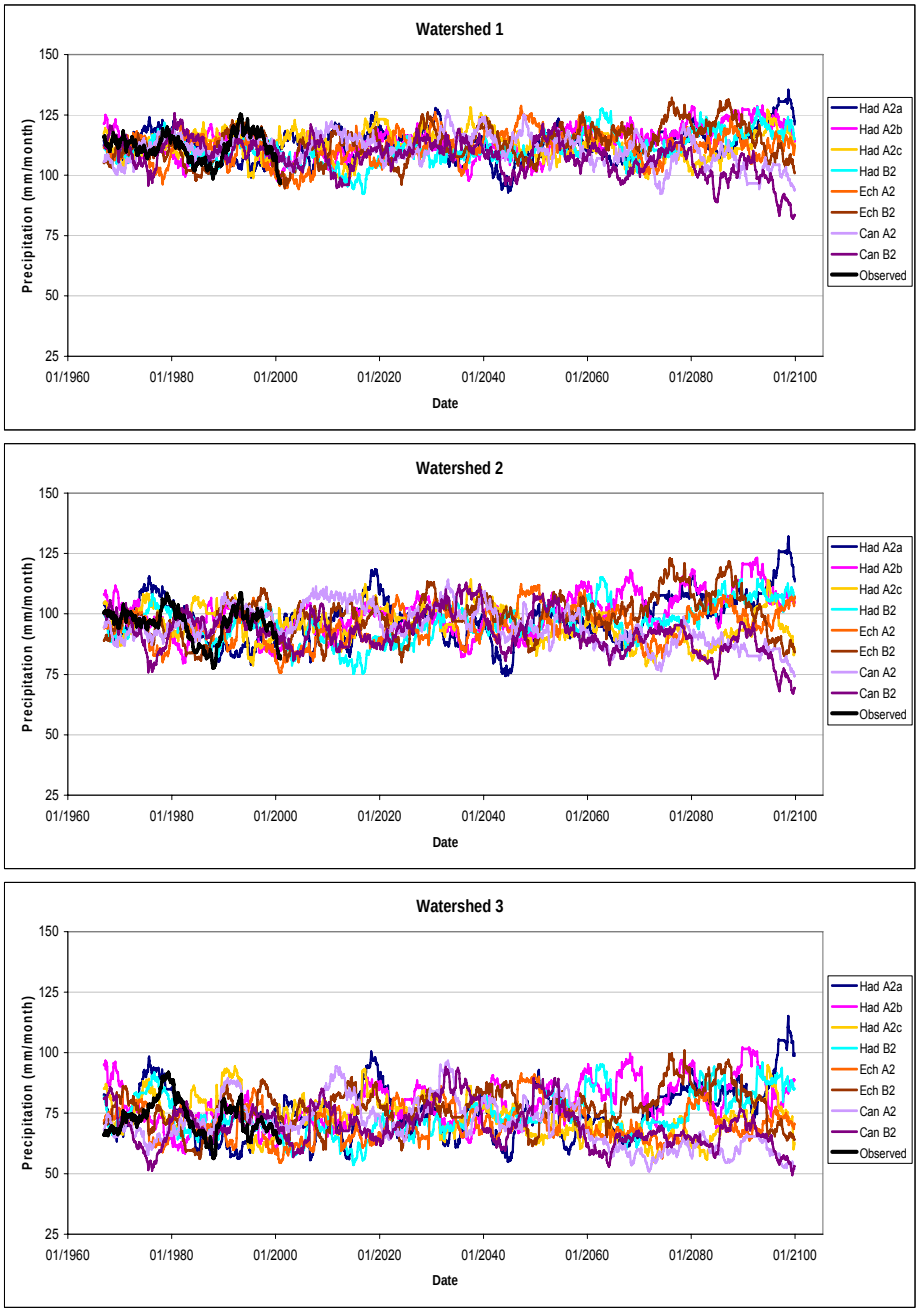

Figure 3.30: Precipitation sequences for the Lake Kyoga sub-basins (observed baseline shown in black).

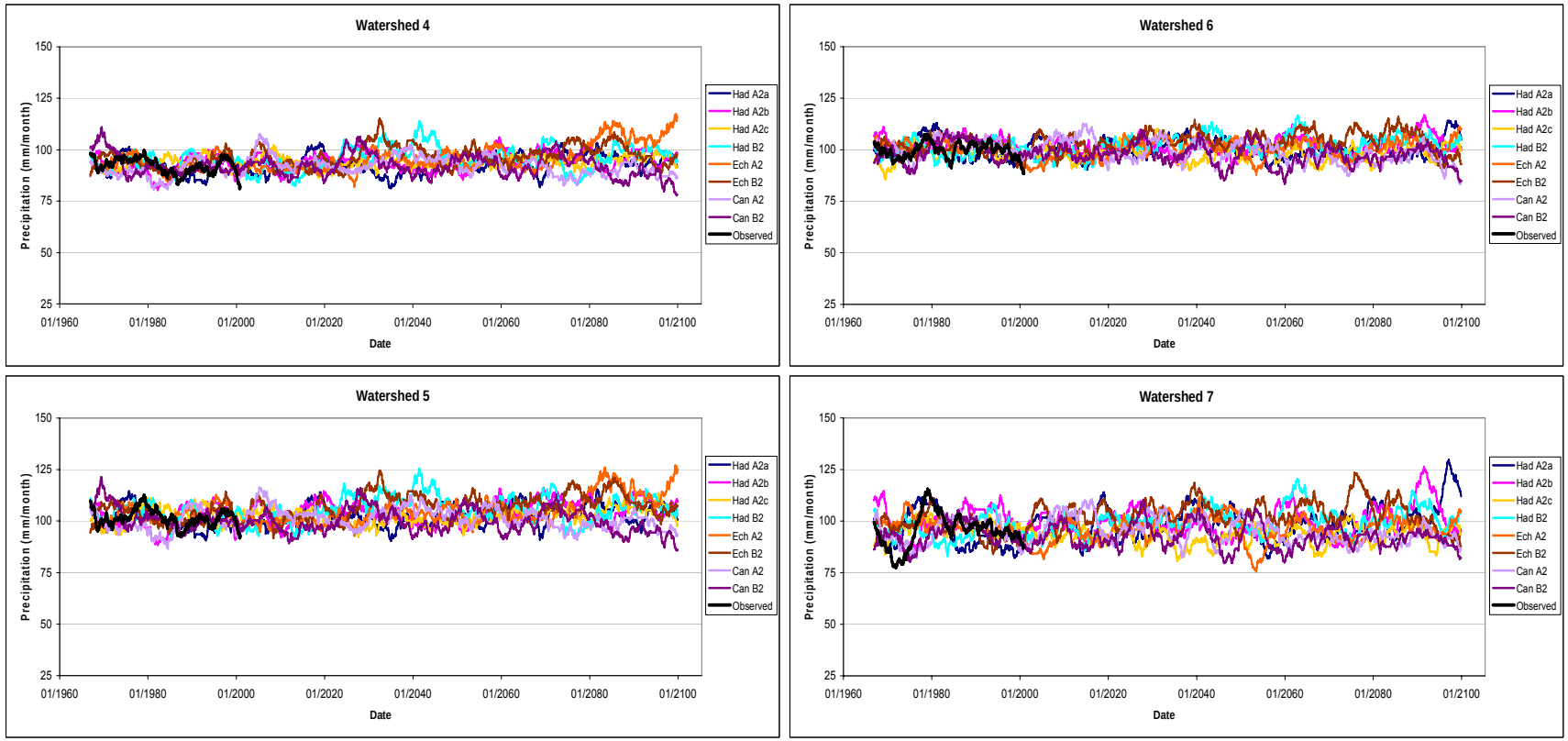

Figure 3.31: Precipitation sequences for the Lake Albert sub-basins (observed baseline shown in black).

Temperature Assessment

Watersheds 4 through 7 have similar changes to the those projected over the western half of the Lake Victoria watershed, as would be expected. Overall, the Canadian scenarios yield milder temperature increases, with the Hadley scenarios projecting the greatest temperature increases. Interestingly, the western watersheds appear less sensitive to model initial conditions than in the east.

Projected temperature changes for all scenarios are summarized in Table 3.19. Increases over the Lake Kyoga watersheds range between 2.6-4.6 °C under A2 forcing, and 1.6-3.2 °C under B2 forcing. Similarly, ranges for the Lake Albert watersheds are 2.7-5.0 °C and 1.7-3.5 °C for A2 and B2 forcing, respectively.

The Hadley scenarios indicate a greater temperature increase over watershed 3 compared to the lower lying watersheds near Lake Kyoga. This is consistent with the Hadley results in Sobat watershed 1, which extends into the same region near Mt. Elgon in western Kenya. The results are also consistent with projected changes in the northeastern Lake Victoria watershed.

Table 3.19: Projected temperature changes between the final 30 years (2070-2099) and the 30-year baseline (1962-1991).

	Temperature Change (°C)						
Model/SubArea	**WS 1**	**WS 2**	**WS 3**	**WS 4**	**WS 5**	**WS 6**	**WS 7**
HadA2a	3.7	3.8	4.3	4.2	4.9	4.0	4.1
HadA2b	3.6	3.8	4.3	4.2	4.8	4.0	4.1
HadA2c	3.9	4.1	4.6	4.4	5.0	4.1	4.1
HadB2	2.7	2.8	3.2	3.0	3.5	2.8	2.9
EchA2	3.1	2.9	3.2	3.8	4.4	3.5	3.6
EchB2	2.1	2.0	2.1	2.8	3.2	2.5	2.5
CanA2	2.6	2.7	3.1	3.0	3.5	2.7	2.8
CanB2	1.6	1.6	1.8	1.8	2.1	1.7	1.7
Had A2 spread/SRES A2-B2 spread	0.29	0.34	0.34	0.18	0.16	0.07	0.07

Precipitation Assessment

The Hadley and Echam scenarios primarily indicate precipitation increases by the end of the century (Table 3.20). Most of these increases are very small and likely insignificant against the underlying variability. While the Hadley A2 traces project precipitation changes as high as +18%, they also indicate reductions by as much as -12%.

The primary concern with the historical analog method is the possibility of truncating scenarios of increasing precipitation. Because Lake Victoria and the lower equatorial lakes are situated in the same region and share similar climates, it is constructive to compare the differences in projected precipitation under the two indicator methods described in this chapter. The Lake Victoria method uses the bias-corrected model sequences directly, rather than selecting similar sequences from the historical record. The maximum precipitation increase seen in the Lake Victoria Echam scenarios is 25%, while in the lower equatorial lakes it is 14.7%. Taken alone this might be interpreted as an artificial underestimate associated with the analog method. However, looking at the Hadley scenarios, it is seen that the maximum increase is 18% both over Lake Victoria

and the lower lakes. This seems to suggest that the smaller change in Echam is due to spatially varying Echam projections rather than an inability of the historical record to produce greater precipitation.

Table 3.20: Projected precipitation changes between the final 30 years (2070-2099) and the 30-year baseline (1962-1991).

	Precipitation Change (%)						
Model/SubArea	**WS 1**	**WS 2**	**WS 3**	**WS 4**	**WS 5**	**WS 6**	**WS 7**
HadA2a	4.6	12.4	18.2	3.7	3.3	-0.2	7.4
HadA2b	6.1	8.3	11.8	4.1	5.5	-1.0	1.3
HadA2c	-1.7	-8.1	-11.9	0.6	1.2	0.9	-2.0
HadB2	4.9	7.9	8.6	1.1	-0.2	3.6	5.4
EchA2	2.0	6.8	0.6	14.7	12.8	-0.1	-1.1
EchB2	6.0	10.2	12.7	8.1	9.2	2.0	4.9
CanA2	-6.6	-11.3	-17.5	-1.5	-2.1	-7.9	-5.5
CanB2	-10.4	-11.8	-8.8	-6.1	-6.5	-5.5	-3.9
Had A2 spread/SRES A2-B2 spread	25.38	4.57	3.15	1.35	1.24	0.48	4.82

3.9 GCM Scenario Field Significance

The previous sections have presented the GCM skill results for the Nile sub-basins. The statistical tests evaluate climate model skill at individual pixels within an area of interest. Because the climate data are actually a field, conducting multiple hypothesis tests on the pixels within the field may lead to a number of coincidentally significant results. This is known as the problem of multiplicity or field significance. The question remains: how many significant pixels are needed to represent a significant field? Another statistical procedure has been designed to answer this question and is described below.

First, paired data are generated that conform to the null hypothesis that the model and historical data are not related. Using a bootstrapping procedure, the model-historical data are repeatedly sampled. However, in this case the model data are selected randomly, while the historical data remain in their original order. The resulting bootstrap samples have the same spatio-temporal structure as the original sample because the random sequences used to shuffle the data are consistent across all pixels and involve the moving blocks technique as before. The bootstrap samples are used to generate the null distribution for $\hat{\theta}$ at each pixel and to define distribution critical values. The critical value represents the minimum value of $\hat{\theta}$ required to pass the statistical significance test at a predefined level α. Values of $\hat{\theta}$ above the critical value are considered unlikely to occur purely by chance.

Next, an additional 1000 bootstrap samples are generated. Each bootstrap replicate yields a field of $\hat{\theta}^*$. The number of pixels with $\hat{\theta}^*$ greater than their respective critical values are counted and recorded. Finally, a distribution of the *number of significant pixels* is generated from the 1000 pixel counts. The distribution describes the number of pixels that may be expected to show significance under the null hypothesis. That is, it describes how many pixels are expected to show significance purely by chance. At this point, it is possible to define the critical number of pixels required to designate the field as significant.

This field significance test has been applied to two fields in the Nile basin, the Equatorial Lakes region (Figure 3.32) and the Eastern Nile (Figure 3.33). Tables 3.21 through 3.24 show the results of these tests for the annual and bi-annual cases using a significance level of $\alpha = 10\%$. GCM runs that pass the field significance test are indicated with a

"Pass" followed by the number of pixels that actually showed significance and the minimum number required for field significance (critical value).

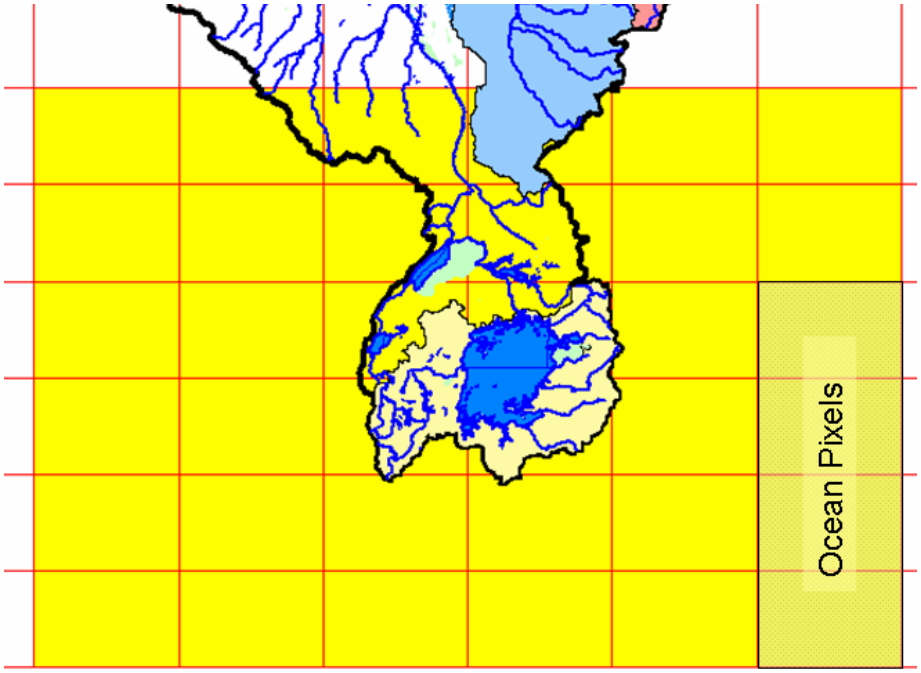

Figure 3.32: Equatorial Lakes field with thirty-two pixels (yellow).

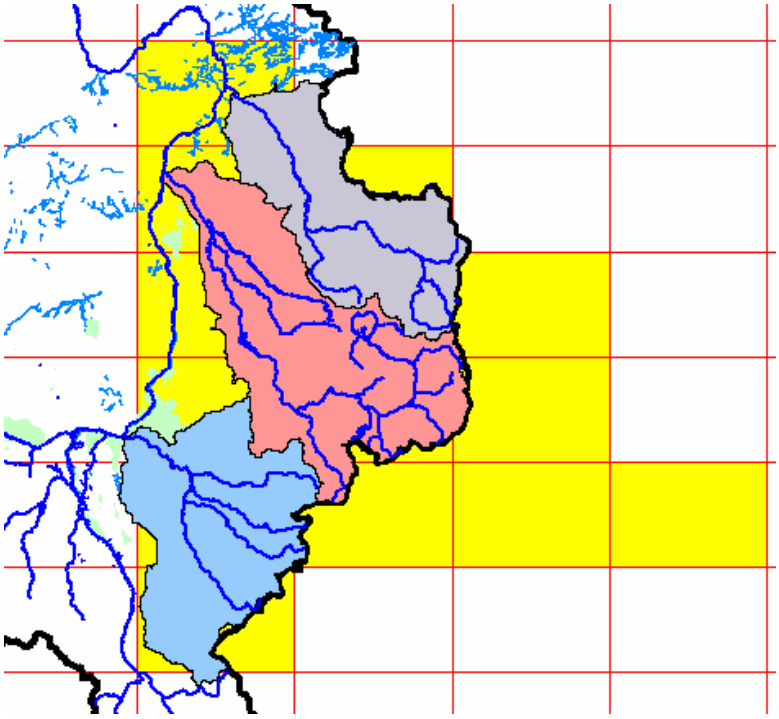

Figure 3.33: Eastern Nile field with fourteen pixels (yellow).

Table 3.21: Equatorial Lakes field significance results for temperature shown with the number of significant pixels over the critical number of significant pixels.

Model/Season	Annual	6-Monthly	
	Jan-Dec	Jan-Jun	Jul-Dec
Had_A2a	Pass (29/12)	Pass (29/12)	Pass (28/11)
Had_A2b	Pass (26/10)	Pass (27/12)	Pass (19/9)
Had_A2c	Pass (25/11)	Pass (26/12)	Pass (24/10)
Had_B2	Pass (30/12)	Pass (24/12)	Pass (29/10)
Ech_A2	Pass (24/11)	Pass (19/12)	Pass (21/10)
Ech_B2	Pass (24/12)	Pass (19/12)	Pass (22/9)
Can_A2	Pass (27/11)	Pass (24/11)	Pass (24/11)
Can_B2	Pass (28/12)	Pass (26/12)	Pass (31/10)

Table 3.22: Equatorial Lakes field significance results for precipitation shown with the number of significant pixels over the critical number of significant pixels.

Model/Season	Annual	6-Monthly	
	Jan-Dec	Jan-Jun	Jul-Dec
Had_A2a	--	--	--
Had_A2b	Pass (9/8)	--	Pass (11/8)
Had_A2c	Pass (10/7)	--	--
Had_B2	--	--	--
Ech_A2	--	--	--
Ech_B2	--	--	--
Can_A2	--	--	--
Can_B2	--	--	--

Table 3.23: Eastern Nile field significance results for temperature shown with the number of significant pixels over the critical number of significant pixels.

Model/Season	Annual	6-Monthly	
	Jan-Dec	Jan-Jun	Jul-Dec
Had_A2a	Pass (13/5)	Pass (6/5)	Pass (13/5)
Had_A2b	Pass (13/4)	Pass (4/4)	Pass (11/4)
Had_A2c	Pass (12/5)	Pass (7/5)	Pass (10/5)
Had_B2	Pass (12/5)	Pass (5/4)	Pass (11/5)
Ech_A2	Pass (10/6)	--	Pass (12/5)
Ech_B2	Pass (10/5)	--	Pass (12/5)
Can_A2	Pass (13/5)	Pass (7/5)	Pass (7/5)
Can_B2	Pass (14/5)	Pass (8/4)	Pass (9/5)

Table 3.24: Eastern Nile field significance results for precipitation shown with the number of significant pixels over the critical number of significant pixels.

Model/Season	Annual	6-Monthly	
	Jan-Dec	Jan-Jun	Jul-Dec
Had_A2a	--	--	--
Had_A2b	--	--	--
Had_A2c	--	--	--
Had_B2	--	--	--
Ech_A2	Pass (4/4)	--	Pass (6/4)
Ech_B2	--	--	--
Can_A2	--	--	--
Can_B2	--	--	--

The results represent the overall regional performance of the models with respect to temperature and precipitation. Temperature is shown to be very well represented as a field both in the Equatorial Lakes region and in the Eastern Nile region. These results instill further confidence in the model simulated temperatures. Precipitation results, on the other hand, do not indicate overall regional skill. This is not surprising given the sparse statistical significance results previously presented for each sub-basin. What is seen here, however, is that the HadA2b and HadA2c runs appear to perform better in the Equatorial Lakes region than the other models. In the Eastern Nile, the EchA2 run shows the best overall performance. Such information may be useful in establishing the relative importance of each climate scenario.

3.10 Summary Remarks on Climate Scenarios

This chapter develops new methods for generating plausible future climate scenarios. Aspects of this work that make it unique and beneficial are: the ability to objectively assess the value of GCM output and use their strengths as the basis for constructing complete scenarios; maintain the internal consistency of the original model data; enable

future changes in variability; and the use of a statistical basis for assessing the relative value of different scenarios. The methods do not apply the delta approach, as is currently common place in climate change assessments. In fact, from the discussion of climate scenario results presented here, it becomes evident that 30-year mean changes are not always as meaningful as they might seem. Therefore using these changes as the basis for applying a bulk adjustment to the historical climate (delta approach) may lead to crude and misleading results. Whereas, allowing the changes to vary continuously throughout the horizon enables a full assessment of the potential changes in the context of past and future variability and trends. Furthermore, the persistence seen in many of the basin precipitation sequences may have important implications for the hydrologic changes in their respective basins. But perhaps even more so for the potential mitigation or exacerbation of changes via correlations across basins.

The new methods have been successfully applied to five major regions of the Nile River basin. Eight temperature and precipitation scenarios have been developed over each basin and are summarized as follows.

Basin wide, the temperature scenarios consistently range between 2.8 and 5.2 °C under the more extreme A2 forcing, and 2-3.5 °C under the B2 forcing. The Canadian model is consistently at the lower end of the scenario range, while the Hadley generally represents the more extreme projections.

Precipitation changes are not as straightforward as temperature. The Hadley scenarios generally project very little to moderate precipitation increases over all basins. The Echam scenarios indicate substantial precipitation increase over Lake Victoria, moderate increase over the lower equatorial lakes, and negligible to minor reductions in the Sobat, Blue Nile and Atbara basins. The Canadian scenarios show large reductions over Lake

Victoria, substantial reductions over the lower equatorial lakes, Sobat and Blue Nile, and increases over the Atbara basin.

Chapter 4: Hydrologic Modeling

The next step towards understanding the potential impacts of climate change is to translate climate scenarios into hydrologic output. This chapter describes the basic hydrologic features of the primary Nile sub-basins, hydrologic model development, and simulation of future lake and river responses to future climate scenarios. The basins are discussed in the order presented in Chapter 3: Lake Victoria, Blue Nile, Atbara, Sobat, and the lower equatorial lakes. The chapter concludes with a discussion of hydrologic uncertainties and a summary of basin-wide results.

4.1 Lake Victoria

The climatic and hydrologic features of the Lake Victoria region were presented in Chapter 2. This very large lake is especially important to Main Nile flows and has unique features that may have implications for long term changes in Lake outflow. First, due to the historical balance between precipitation and evaporation over the lake surface, the long term outflow from the lake has been roughly equal to the inflow from the surrounding watersheds. The relative magnitude of this inflow has been estimated at approximately one-third of the total water input to the lake system. Furthermore, given the large surface area and precarious balance between precipitation and evaporation, the lake water balance is especially susceptible to changes in either or both of these terms. Consequently, any investigation into lake response to climate change must begin with an appropriate hydrologic model that captures the relative importance and sensitivity to climate forcing of each water balance term- watershed runoff, lake precipitation, and lake evaporation.

4.1.1 Lake Water Balance

The purpose of the hydrologic modeling is to relate atmospheric forcing (precipitation and temperature) to watershed outflow into Lake Victoria. Watershed outflow is an important component of lake water balance, which determines the changes that lake storage undergoes in response to precipitation, evaporation, and watershed outflow sequences:

$$S(k+1) = S(k) + P(k) - E(k) - O(k) + Q(k),$$

where S(k) represents lake storage at the beginning of time period k, P(k) represents lake precipitation, E(k) lake evaporation, O(k) lake outflow, and Q(k) watershed outflow into the lake.

The previous section described the development of precipitation and mean temperature sequences for lake and watershed areas consistent with 8 runs from 3 different GCMs and 2 future emissions scenarios. Here we describe the development of a hydrologic model for the lake watershed that is later run under future climate scenarios to quantify the hydrologic response of the lake and its watershed.

Lake Evaporation

Lake evaporation is assumed to take place at the climatic potential rate and can be estimated from the Malmstrom potential evapotranspiration formula (Dingman, 2002):

$$PET(k) = 40.9 * \exp\left[\frac{17.3(T_{mean}(k) - 273.15)}{T_{mean}(k) - 273.15 + 237.3}\right].$$

In the above expression, $T_{mean}(k)$ is the monthly mean air temperature over the lake in Kelvin, and PET(k) is the potential evapotranspiration rate in millimeters per month. The constant 273.15 serves to convert Kelvin into degrees Celsius.

A more elaborate method, proposed by Linacre (1993), was also applied in this study. The method is a simplification of Penman's evaporation formula that may be applied when insufficient data is available to support the Penman calculations. The Linacre formula requires monthly data for mean temperature, dew point temperature, and wind speed as well as latitude and elevation. Lake irradiance is estimated as a function of latitude and percent departure of temperature from the annual mean. When used on a biannual time step, the Linacre equation demonstrated two obvious inconsistencies. First, use of six-monthly data essentially renders the radiation term as a step function that only distinguishes the relative temperature of two seasons without regard to the absolute difference in average temperatures. Consequently, the seasonal differences in potential evaporation appear too large given the small seasonal variation of temperature in the region. Second, even on an annual basis, lake evaporation estimates approached nearly two times the long term mean for Lake Victoria, thus distorting hydrologic calculations.

Even though it is an air temperature based method, the Malmstrom formula performs well at the six-monthly scale in this region. The main reasons for this can be attributed to the following factors: *(1)* Lake Victoria inflows and other advective processes have a marginal thermodynamic effect relative to its storage; *(2)* the seasonal variability of water temperature is mild, due to the equatorial lake location, thus minimizing potential temperature-evaporation phase shifts; and *(3)* the six-monthly time resolution further enhances the importance of air temperature on the evaporation process. However, given the exponential shape of this PET formula, the question remains as to whether it will continue to be valid under a changing climate with significant temperature increases.

One approach to test its validity is to apply it in an area where present day temperatures are comparable to projected future temperatures for Lake Victoria. To this end, the Malmstrom PET formula is also applied to Lake Nasser in Egypt. Over the period 1960-2000, Lake Victoria temperatures average 21.9° C and Lake Nasser temperatures average 25.9° C, approximately 4° higher.

Shahin (1985) cites a range of Lake Victoria evaporation estimates between 3.1 and 4.5 mm/day, while the HydroMet project estimated approximately 4 mm/day in a typical year (WMO, 1974). The average annual estimate from the Malmstrom formula is 3.6 mm/day over the 1960 – 2000 period. This is approximately 10% lower than the HydroMet estimate and lower than the mid range given by Shahin.

Sadek et al (1997) revisit historical estimates of Lake Nasser evaporation, citing a range of 4.65 – 7.95 mm/d; although, in updated calculations they narrow the range to 5.7-6.3 mm/day. Applying the Malmstrom formula to the Lake Nasser monthly temperature means yields an estimate of 4.78 mm/day. This estimate is at the low end of earlier evaporation estimates and approximately 15% less than the low end of the more recently published range. This analysis indicates that the Malmstrom formula produces conservative estimates of evaporative losses over the range of temperatures projected for Lake Victoria.

Watershed Evapotranspiration

For hydrologic modeling purposes, the Lake Victoria watershed is distinguished in three sub-watersheds: one corresponding to the western two GCM pixels (lake pixels 1 and 2), one representing the southeastern corner of the lake region (lake pixel 3), and a third representing the northeastern quadrant (lake pixel 4). Specifically, the southwest and northwest pixels include the Kagera River watershed and is referred to as Watershed 1;

the southeast pixel mainly includes lake watersheds in northern Tanzania (Watershed 2); and the northeast pixel includes Nzoia, Nyando, Nyala, and other watersheds in northwest Kenya (Watershed 3).

As part of the climate model scenario analysis of the previous section, bias adjusted precipitation and mean temperature sequences have already been developed for the three lake sub-watersheds. The temperature sequences can be converted into watershed evapotranspiration using the Pike evapotranspiration equation (Dingman, 2002; Pike, 1964):

$$ET = \frac{P}{\sqrt{1 + [P/PET]^2}},$$

where ET is the annual evaporation, P is the annual precipitation, and PET is the annual potential evapotranspiration.

Pike (1964) expanded on earlier work by Turc, which was based on the concept that actual evapotranspiration depends on both the availability of water to moisten the soil (precipitation) and the availability of energy to drive evapotranspiration. While Turc used a simple function of mean temperature to estimate the available energy, Pike argued that the Penman estimate of potential evapotranspiration provides a more realistic energy estimate. Using this modification, Pike tested his formula on 4 catchments in Malawi, East-Central Africa. The average error in actual evapotranspiration was 2.5%, with none of the four catchments exceeding 10% error.

There are three important points about the application of the Pike formula in this study. First, the equation uses annual quantities. In this study, however, consistent with the

aggregation of the climate scenarios and hydrologic model calibration, the equation is used to estimate watershed evapotranspiration over six month intervals. In light of the relatively small seasonal temperature variation in the Lake Victoria region, this application is not expected to introduce significant errors. The validity of this assumption will be assessed by the ability of the model to replicate field observations.

Second, while Pike's work employed the Penman estimate of PET, here PET was estimated from the Malmstrom formula. The Malmstrom estimate of PET for the lake was compared against lake evaporation data from the HydroMet project in East Africa (WMO, 1974) and found to be more consistent with the lake water balance than both the published Penman estimates and the six-monthly Linacre PET estimates. Therefore, Malmstrom PET appears to be a justified substitution.

Finally, the Lake Victoria region shares several key similarities with Pike's experimental sites in East-Central Africa. As in Malawi, Lake Victoria exists in a humid climate. In addition, it experiences distinct rainy seasons during which actual evapotranspiration is energy rather than water limited. While Malawi has a single annual rainy season, the equatorial East African area has two rainy seasons (long and short rains), each of which are entirely bounded by the biannual seasons used in this study.

4.1.2 Lake Victoria Hydrologic Model

The choice of the watershed model depends on the data available for its calibration. Generally, three data categories are necessary in developing watershed models: precipitation, evapotranspiration, and stream flow. As discussed earlier, historical precipitation and evapotranspiration data are indeed available for each sub-watershed. However, with the exception of a few individual rivers (such as the Nzoia and partially the Kagera), complete and consistent stream flow data are lacking for the three sub-

watershed areas. Unfortunately, this situation rules out the calibration of hydrologic models for each sub-watershed. Consequently, watershed outflow is only observable in an aggregate sense (from all three sub-watersheds) through its impact on lake levels after the effects of lake precipitation and evaporation are subtracted. Thus, the only plausible modeling approach is to relate rainfall and evapotranspiration of the individual sub-watersheds to total watershed outflow.

Let Q(k) denote total watershed outflow into Lake Victoria over a six-month period k; P(k) lake precipitation volume during period k; PET(k) lake evaporation volume during period k; O(k) lake outflow; $\Delta S(k)$ change in lake storage during period k (i.e., $\Delta S(k) = [S(k+1) - S(k)]$); $P_i(k)$ precipitation volume over sub-watershed i during period k; and $ET_i(k)$ evapotranspiration volume over sub-watershed i during period k. Then, Q(k) can be estimated from

$$\Delta S(k) = P(k) - PET(k) - O(k) + Q(k) \Leftrightarrow Q(k) = \Delta S(k) - P(k) + PET(k) + O(k).$$

Then, the development of the watershed model amounts to identifying an analytical relationship between Q(k) and $\{P_i(k), ET_i(k), i=1,2,3\}$ that satisfactorily explains the historical observations.

After the comparative evaluation of several analytical forms, the following model was shown to exhibit the best overall performance:

$$\frac{Q(k)}{\sum_{i=1}^{3} P_i(k)} = \alpha_o + \sum_{i=1}^{3} \alpha_i \frac{ET_i(k)}{P_i(k)} \text{ , } i= 1, 2, 3,$$

where $\{\alpha_o, \alpha_1, \alpha_2, \text{ and } \alpha_3\}$ are constant coefficients (independent of period k). Using data from the 1961 to 2000 time period, these coefficients were estimated (via linear regression) to have the following values:

Table 4.1: Lake Victoria hydrologic model coefficients.

Coefficient	Value
α_o	0.653194
α_1	-0.309308
α_2	-0.195156
α_3	-0.209716

The coefficient values assume that all quantities are expressed in billion cubic meters per six months.

Figures 4.1 and 4.2 compare observed and predicted (modeled) results over the calibration period (1961 to 2000). It is noted that clearly erroneous data were excluded from the calibration exercise as a result of a quality control measure. Because watershed outflow was estimated based on the lake water balance and using data solely from the lake, it is possible to cross check the results with the mean areal precipitation measured over the watersheds. The ranks of watershed precipitation minus evapotranspiration were compared to the ranks of watershed outflow, and data showing significant deviations from any physically plausible relationship were excluded. The data inconsistencies stem from unreliable precipitation estimates over the vast lake area (nearly 70,000 square kilometers), most of which was and remains ungaged.

The figures illustrate good correspondence between observed and predicted results over a wide range of outflows, and support the conclusion that the model is unbiased and

represents the watershed outflow process well. Specifically, the standard error of the watershed outflow is 2.410 billion cubic meters per six months, which is less than 12% of the mean outflow. It is noted that the aggregation of six months plays a significant role in the performance of the model. Finer time aggregations (i.e., monthly and tri-monthly) were also used, but the results were unsatisfactory. The reason for this is attributed to the long time lags between rainfall and outflow for some lake basins (e.g., the Kagera). The six month resolution appears to be longer than these time lags and can represent the basin hydrologic response more reliably.

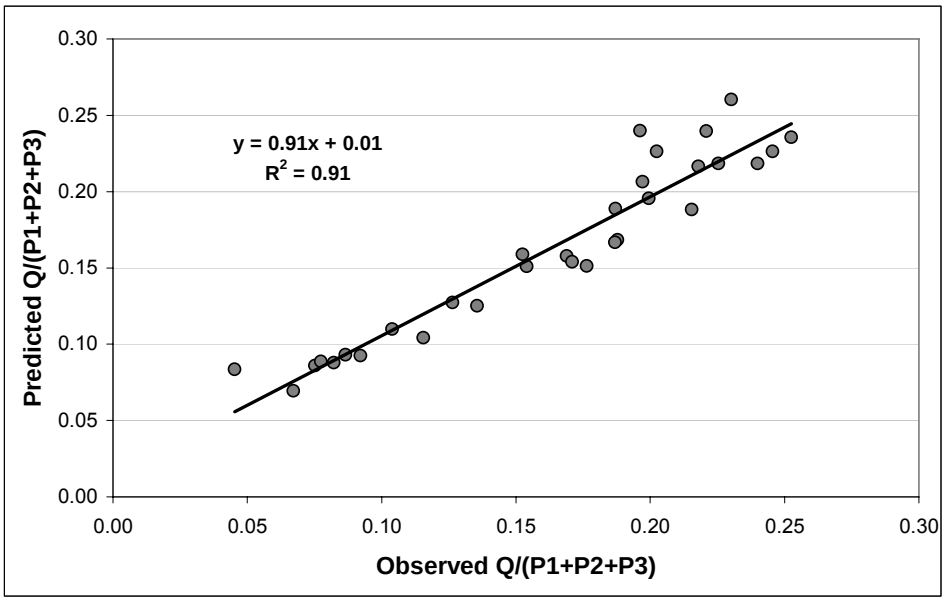

Figure 4.1: Predicted (Q/P) versus observations.

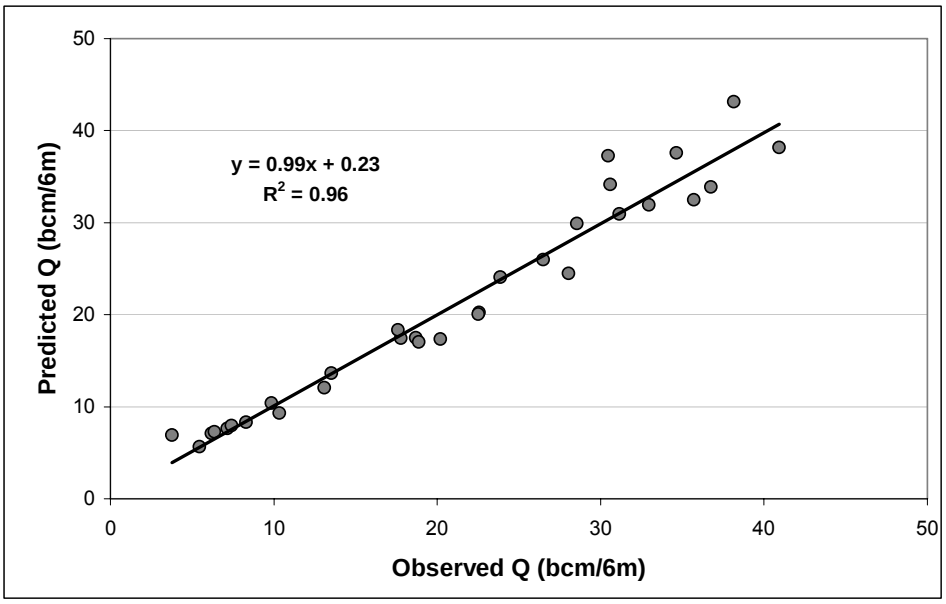

Figure 4.2: Predicted (Q) versus observations.

4.1.3. Retrospective Climate and Hydrology Study

In this section, the hydrologic model is used to investigate the relative significance of the lake water balance terms: What is the magnitude of the average lake precipitation? How does lake precipitation compare with watershed precipitation? What are the relative magnitudes of watershed outflow, lake precipitation, and lake evaporation?

Such questions have been the focus of several previous studies, but although they could ordinarily be answered through a straightforward analysis of field data, past conclusions vary. For example, long term mean lake precipitation estimates range from 1100 to nearly 1600 millimeters per year, the main reason being the lack of precipitation measurements over most of the lake surface. The present study takes a different approach in that it *estimates* lake precipitation based on (1) land (watershed) precipitation and temperature measurements, (2) the hydrologic model, (3) measurements of lake levels and outflows, and (4) lake water balance. The underlying concept is to only use

quantities that can be measured reliably (such as land measurements) and estimate lake precipitation from hydrologic relationships. The estimates thus derived are expected to be more accurate and consistent with the natural lake and watershed response.

This assessment was carried out for the 1960 to 2000 time horizon and led to the results shown on Figures 4.3, 4.4 and 4.5. Several conclusions are noted:

- The mean annual lake precipitation over the 1960-2000 time period is 1330 mm/yr;
- The mean annual precipitation over the three sub-watersheds in the 1960-2000 period are as follows:
    - Watershed 1: 1166 mm/yr (Kagera Basin and southwestern Uganda);
    - Watershed 2: 1020 mm/yr (northern Tanzania);
    - Watershed 3: 1436 mm/yr (western Kenya).

  Thus, lake precipitation exceeds watershed precipitation in two of the three sub-watersheds in a mean annual sense. The highest mean annual precipitation is experienced in Watershed 3 (western Kenya).
- Over the 1960-2000 time horizon, mean annual lake precipitation was nearly equal to mean annual lake evaporation, each amounting to approximately 92 billion cubic meters per year. Thus, long term lake outflow was equal to watershed outflow, the latter estimated at 36.6 billion cubic meters per year or 40% of the mean annual lake precipitation.
- The most variable annual precipitation over the 1960 – 2000 time frame was exhibited by Watersheds 2 and 3 (northeastern and southeastern lake watersheds),each with with a coefficient of variation (CV) equal to 0.17. Lake precipitation exhibited the next highest variability (CV = 0.16), and was followed by Watershed 1 (Kagera Basin and southwestern Uganda; CV = 0.11). Watershed outflow was more variable than precipitation with a CV of 0.34.

In the last six months of 1961, watershed runoff reached 50.8 bcm, nearly 180% higher than its average value, while lake precipitation amounted to 66.5 bcm, or 44% higher than its average value. The first halves of 1962 through 1964 continued to receive very high precipitation, leading to watershed runoff between 31.9 to 43.1 bcm/6-months (75% to 136% higher than average) and lake precipitation between 60.8 and 61.9 bcm/6-months (32% to 34% higher than average). As a result, the lake rose by 2.5 meters during the 1961 to 1964 time frame. This rise is clearly due to excessive regional rainfall that impacted the lake as well as the lake watersheds (Figures 4.3 and 4.4).

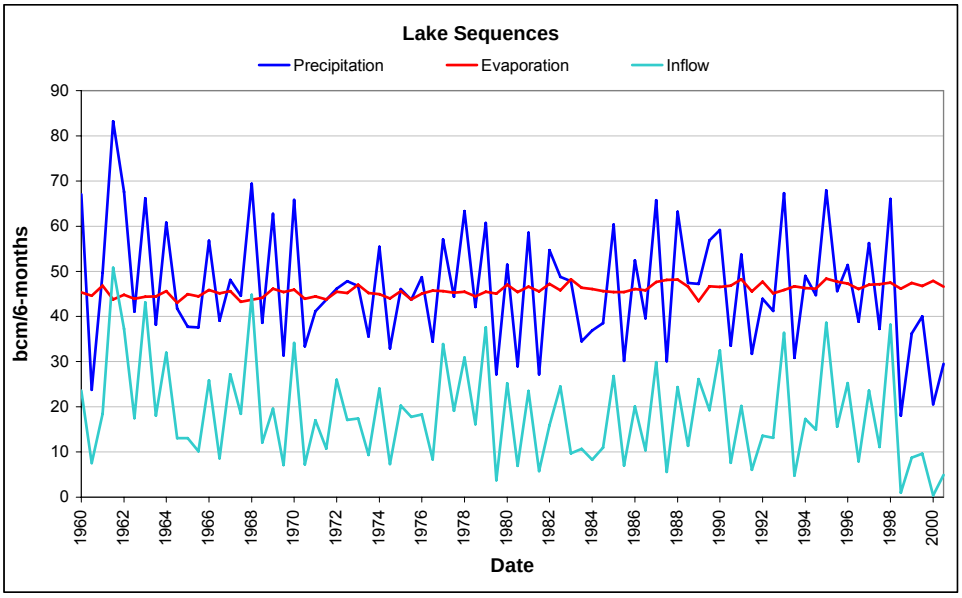

Figure 4.3: Lake sequences.

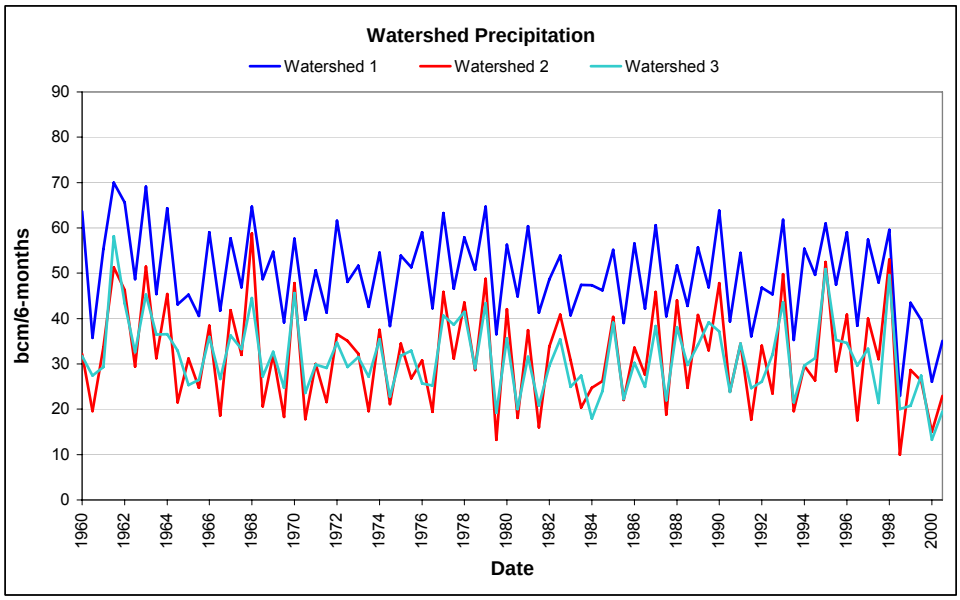

Figure 4.4: Watershed precipitation sequences.

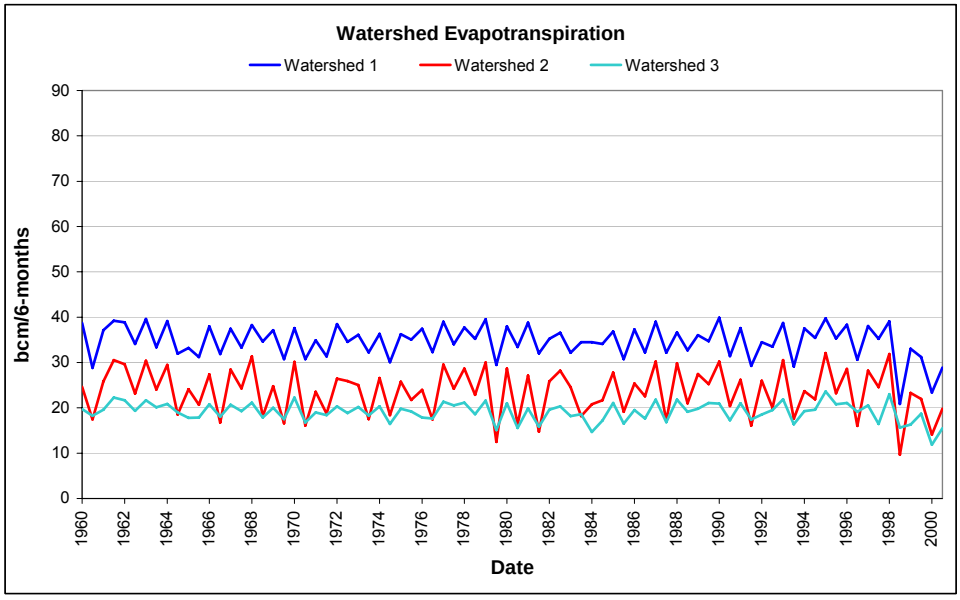

Figure 4.5: Watershed evapotranspiration sequences.

4.1.4 Hydrologic Impact Assessment

The downscaled sequences of temperature and precipitation are used as input to the hydrologic model to simulate the hydrologic changes that are expected as a result of the projected climate scenarios.

The simulated lake water balance sequences for each of the eight model scenarios are shown in Figures 4.6 and 4.7. As estimated in the literature, the historical period exhibits approximate balance between precipitation and evaporation directly over the lake, which results in a similar balance between watershed outflow and net basin supply. There are two main factors determining the future lake response: first is the potential change in water flux at the lake surface; and, second, is the extent to which concurrent changes in watershed runoff either exacerbate or mitigate lake surface imbalance.

The HadCM3 sequences generally show an emerging gap between lake evaporation and precipitation, leading to a net loss over the lake. At the same time, watershed runoff shows a mildly decreasing trend. ECHAM4 indicates a similar response, but to a lesser extent due to somewhat lower temperature increases and higher precipitation projections than HadCM3. CGCM2, on the other hand, while showing a much smaller lake evaporation trend than both of the other two models, projects dramatic decreases in both lake and watershed precipitation, which appears to be the dominant effect in the rapidly decreasing net basin supply. The eight net basin supply sequences are presented together in Figure 4.8.

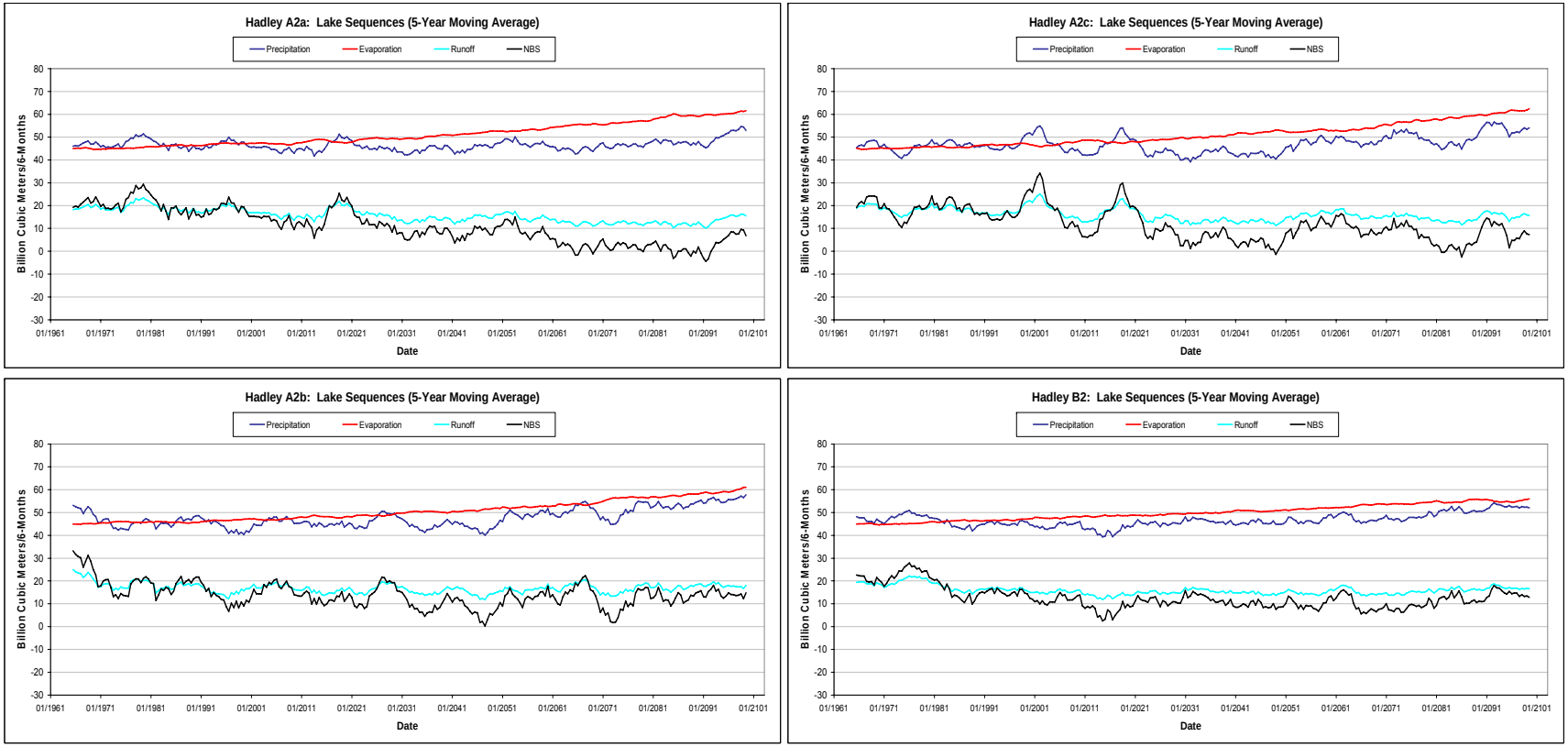

Figure 4.6: Lake Victoria hydrologic sequences (lake precipitation, lake evaporation, watershed runoff, and net basin supply) for Hadley scenarios.

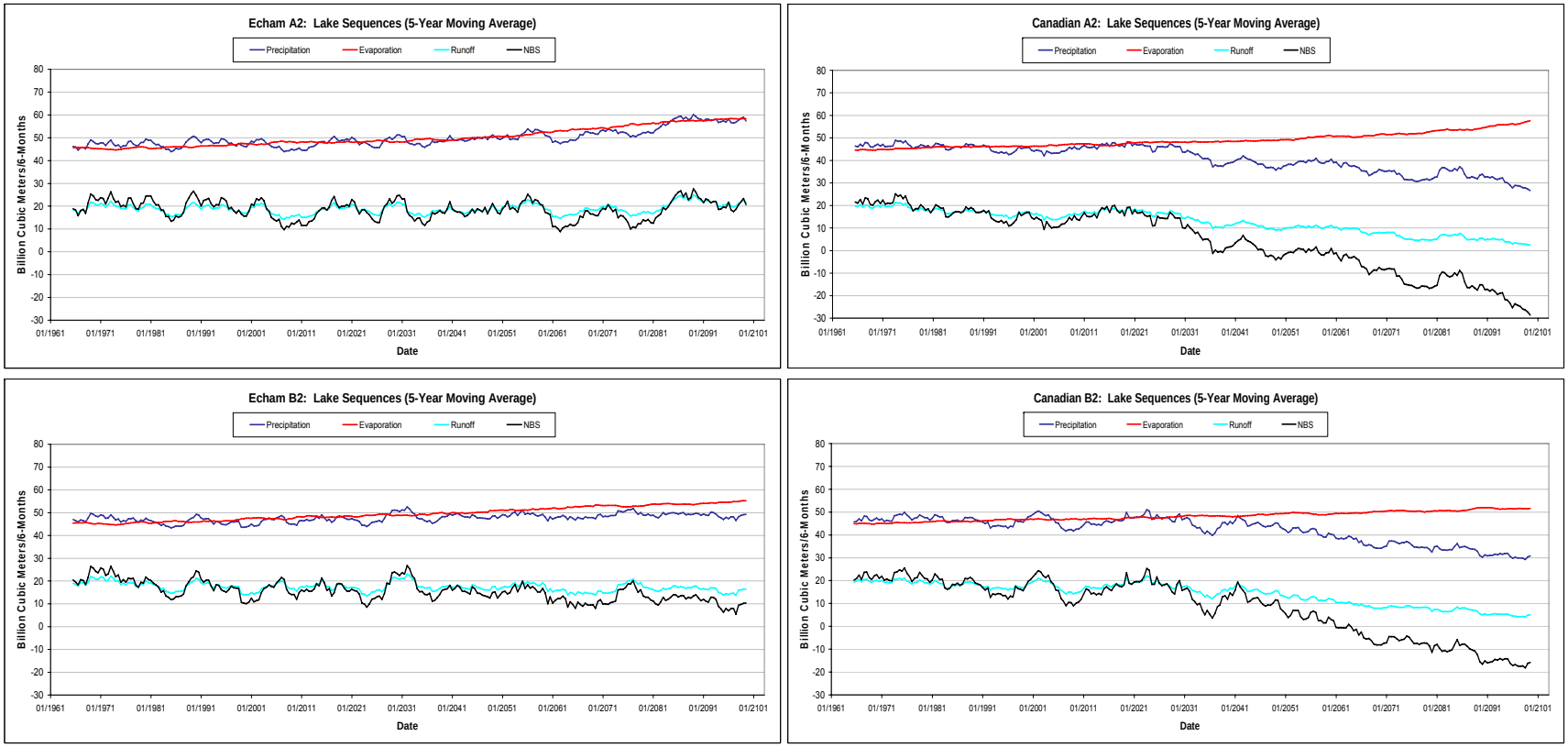

Figure 4.7: Lake Victoria hydrologic sequences (lake precipitation, lake evaporation, watershed runoff, and net basin supply) for Echam and Canadian scenarios.

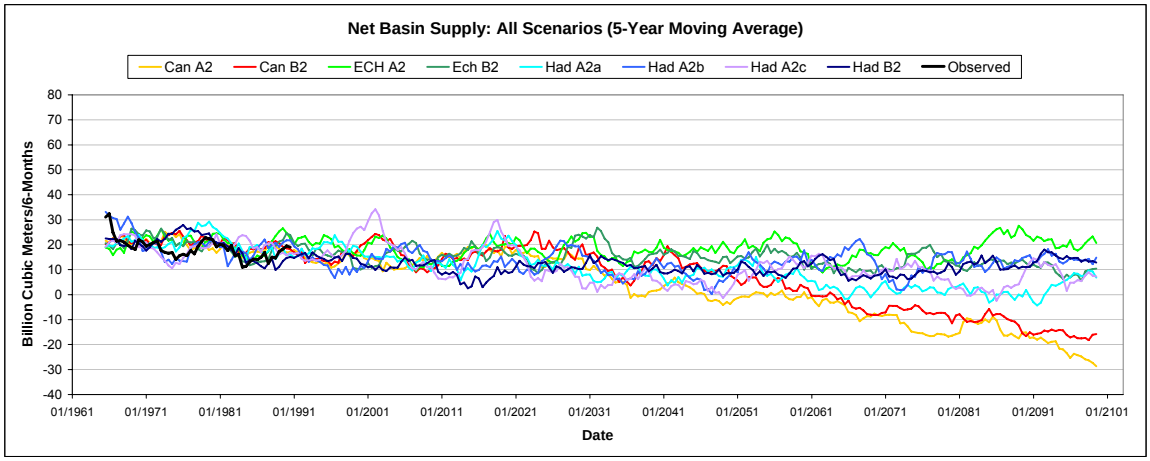

Figure 4.8: Eight-member ensemble of Lake Victoria net basin supply with observed baseline shown in black.

The relative impacts of the two driving factors of lake response are summarized in Table 4.2, where NBS is the net basin supply, Q_w is watershed runoff, and Lake(P-E) is precipitation minus evaporation for the lake surface. Here, all changes are presented as a percentage of the baseline net basin supply. It is clear that in all models the lake surface flux becomes largely negative. At the same time, all but one scenario project decreases in watershed runoff. The A2 scenario of ECHAM4 is the only model that projects an increase in watershed outflow. Even so, the increased precipitation in this scenario is not enough to overcome the total evaporative losses. Again, CGCM2, with its projected precipitation losses, indicates very large net losses due to both the lake surface imbalance and reduced runoff.

Table 4.2: Changes in lake water balance terms between 2070 to 2099 and baseline period, expressed as percentage of net basin supply.

	Lake Balance Change (%)		
Model/Variable	**NBS**	**Qw**	**Lake (P-E)**
HadA2a	-87	-29	-57
HadA2b	-37	-9	-28
HadA2c	-61	-17	-44
HadB2	-41	-12	-28
EchA2	-5	7	-12
EchB2	-39	-10	-29
CanA2	-191	-70	-121
CanB2	-155	-61	-94
HadA2 spread/SRES A2-B2 spread	1.07	1.21	0.99

The most striking observation is that while the model runs represent a wide range of projections for precipitation they all indicate a decrease in the Lake Victoria net basin supply. Even if the CGCM2 projections are discounted due to a lack of confidence in the modeled precipitation, the remaining six scenarios range from 5% to 87% decrease in the NBS with a mean decrease of 45%. If the CGCM2 scenarios are included, the result is a 77% average decrease. In either case, the projected reductions in net lake supply have serious implications for future development in East Africa as well for downstream countries who rely heavily on the Nile flows.

4.2 Blue Nile

The Blue Nile originates from Lake Tana in the Ethiopian highlands. The Upper Blue Nile is known for its steep terrain and remarkably deep gorges that wind through the Ethiopian Plateau. In some places the gorges are as deep as 1200 meters. The river drops nearly 1300 meters along its 900 kilometer course from Lake Tana to the Ethiopia-Sudan border. Below the border, the river travels through the mildly sloping and semi-

arid Sudan Plain for approximately 800 kilometers. The Upper Blue Nile, defined above the Ethiopia-Sudan border, is the most productive portion of the Blue Nile basin. However, there are also two seasonal tributaries, Dinder and Rahad, in the lower reach that also originate deep in the Ethiopian highlands, very near Lake Tana. Flow measurements are available for the Upper Blue Nile at Border, for Dinder and Rahad, and at Khartoum where the full Blue Nile flow is concentrated.

4.2.1 Upper Blue Nile Hydrologic Model

It is appropriate to begin with a brief discussion regarding data quality in the basin. As with many of the basins in East Africa, it is likely that the CRU datasets are derived from minimally available station data. Therefore, spatial and temporal gaps in the data may result in insufficient information to explain some hydrologic events. At the same time, this dependence on only a small set of stations may lead to overly correlated sub-basin sequences. Thus, data quality control should be exercised both in developing statistical models, which may yield unexpected calibration results given interdependent predictors, as well as in the evaluation of overall model performance.

The hydrologic modeling approach employed here aims to allow for seasonally varying flow behavior, emulate lagged response to climate input due to storage and river routing effects, represent potential non-linearities in flow response, and achieve a level of predictive accuracy comparable to and consistent with the other Nile sub-basins.

Contemporaneous precipitation, temperature and flow data (at Border) are available on a monthly basis for the years 1950 through 1977. Flows were initially regressed against precipitation (P), potential evapotranspiration (PET), and P minus PET over six sub-basins. There was little difference in model performance between regressing precipitation and PET separately versus lumping the variables as (P-PET). Therefore, the

latter was selected to improve model efficiency. Model skill improved considerably, however, by modeling the rising versus falling hydrograph limbs. Although the simple linear models were able to capture a significant portion of the flow variability using (P-PET) over the sub-basins as predictors, residual analysis actually suggested a non-linear relationship. Therefore, the linear models were transformed using the logistics equation, resulting in the following model form:

$$Q = \frac{c}{1 + \exp\left(\alpha_0 + \sum_i \alpha_i X_i\right)},$$

where Q is modeled flow at Border, α's are calibrated model coefficients, X_i is (P-PET) over basin *i*, and *c* is a user defined constant.

Working with this model form, various combinations and aggregations of the original six sub-basins were considered along with the addition of lagged predictors. While models that treated all basins as separate predictors tended to achieve slightly better model performance, multi-collinearity of these predictors led to ambiguous statistical results with respect to predictor significance and the meaning of fitted coefficients. Given the highly correlated nature of the precipitation and temperature data developed in this data-sparse region, the sub-basins were aggregated into larger watersheds with little loss of predictive value. Figure 4.9 depicts the final sub-basins used for generating (P-PET) input sequences to the model.

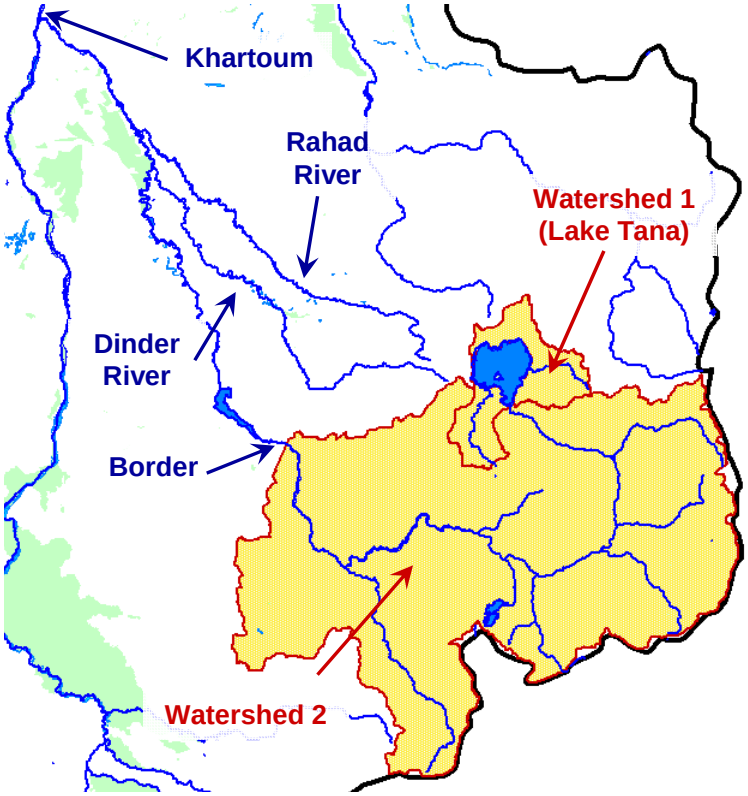

Figure 4.9: Upper Blue Nile hydrologic units.

The final rising and falling hydrograph limb models happened to have identical forms; although the parameters are calibrated separately.

$$Q(k) = \frac{c}{1 + \exp\left(\alpha_0 + \alpha_1 WS_1(k-2) + \alpha_2 WS_2(k) + \alpha_3 WS_2(k-1)\right)},$$

where Q is the flow at Border, k is the time step in months, WS_1 represents (P-PET) in million cubic meters for the Lake Tana watershed, and WS_2 is (P-PET) over the lower basin from the outlet of Lake Tana downstream to Border. The rising (Apr-Aug) and falling (Sep-Mar) limb coefficients are presented in Table 4.3.

Table 4.3: Upper Blue Nile hydrologic model coefficients.

Rising Limb (Apr-Aug)		Falling Limb (Sep-Mar)	
Predictor Variable	Coeff.	Predictor Variable	Coeff.
$WS_1(k\text{-}2)$	-2.30E-04	$WS_1(k\text{-}2)$	-2.31E-04
$WS_2(k)$	-3.84E-05	$WS_2(k)$	-2.20E-05
$WS_2(k\text{-}1)$	-5.93E-05	$WS_2(k\text{-}1)$	-3.61E-05
α_0	2.87E+00	α_0	2.28E+00
c	20905	c	20905
* $c = (1.1*Q_{max})$			

Taking the limits of the model expression reveals that the model is capable of producing flows very near zero but with an upper limit of *c*. If *c* is set arbitrarily high then the model's ability to conform to the non-linear flow response is diminished. Alternatively, if *c* is set too low, the model may not accurately reflect potentially increasing flows under a changing climate. The final value was selected based on knowledge of the projected scenarios of future (P-PET) obtained as part of the climate model analysis. Balancing changes in climate forcing with hydrologic model performance, *c* was established as 110% of the historical maximum Border flow.

The overall model performance is illustrated in Figures 4.10 and 4.11. The model appears to perform quite well, predicting the majority of flood peaks within reasonable limits and generally capturing the interannual variability. A portion of the lower basin contains wetlands that act to delay portions of runoff (Conway, 2000). Including the lag-1 predictor for this basin in both seasons may help to reproduce this effect.

Conway and Hulme (1996) applied a gridded water balance approach to model the same portion of the Blue Nile. Their model uses estimates of monthly precipitation and PET

over 10 minute by 10 minute pixels and estimates monthly runoff for each pixel. They report simulated mean annual flows within 3% of observations over the period 1967 to 1986. However some monthly peak flows were in disagreement by nearly 10 billion cubic meters. Using the same measures, the statistical model developed here is found to simulate mean annual flow within approximately 1% of observations (1950-1977) with a maximum monthly peak flow error of 6.3 km^3. Therefore, it appears that, indeed, the available data do not warrant the use of more elaborate methods.

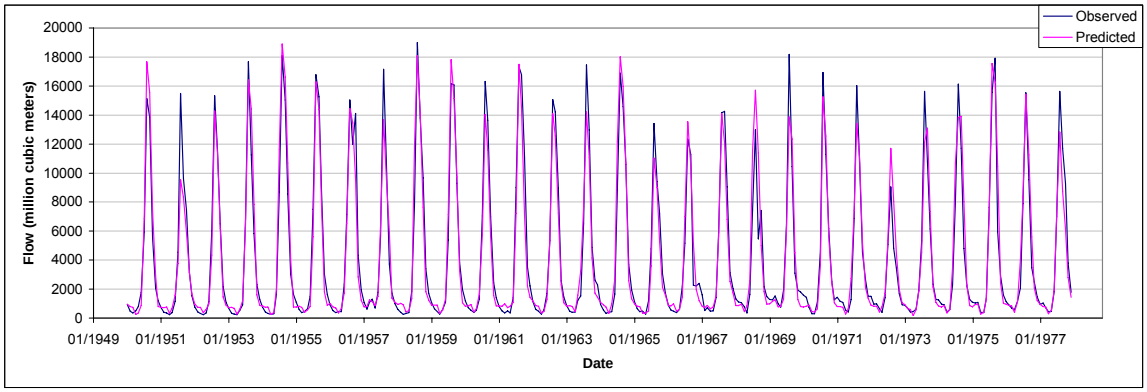

Figure 4.10: Observed (blue) and simulated (pink) Upper Blue Nile flows.

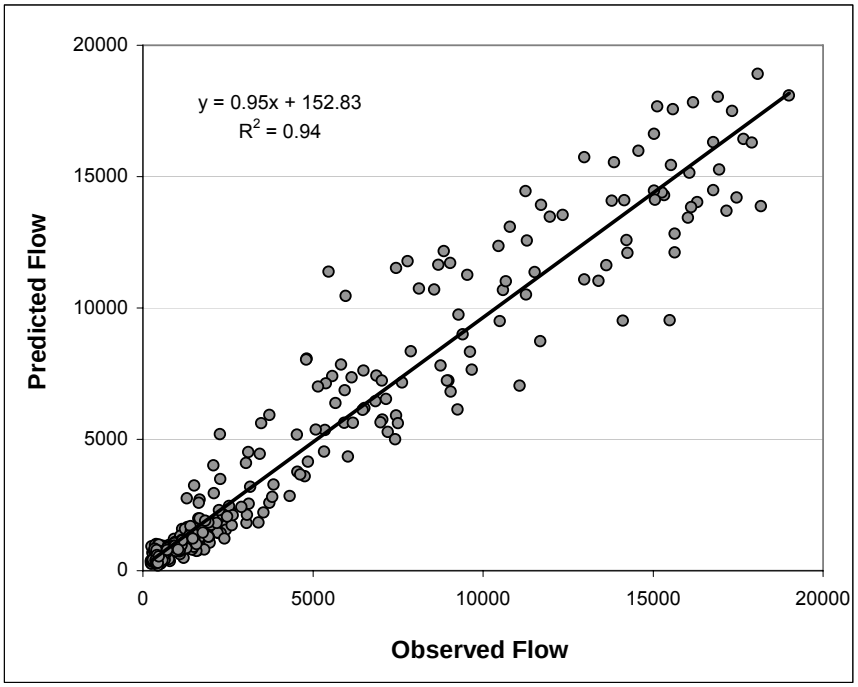

Figure 4.11: Scatter plot of observed versus predicted Upper Blue Nile flows.

4.2.2 Rivers Dinder and Rahad

There are two significant tributaries that join the Blue Nile below the Border station, rivers Dinder and Rahad. While both rivers converge with the Blue Nile well into the Sudan Plain (Figure 4.9), their headwaters are actually located in the same Ethiopian mountain region as the Upper Blue Nile and consequently produce flows that are well correlated with measurements at Border. Given the limitations of climate data in this region and the strength of the relationships with Border, the river flows will be inferred from those simulated for the Upper Blue Nile. The relationship between the Upper Blue Nile and the Dinder and Rahad flows are shown in Figures 4.12 and 4.13, respectively.

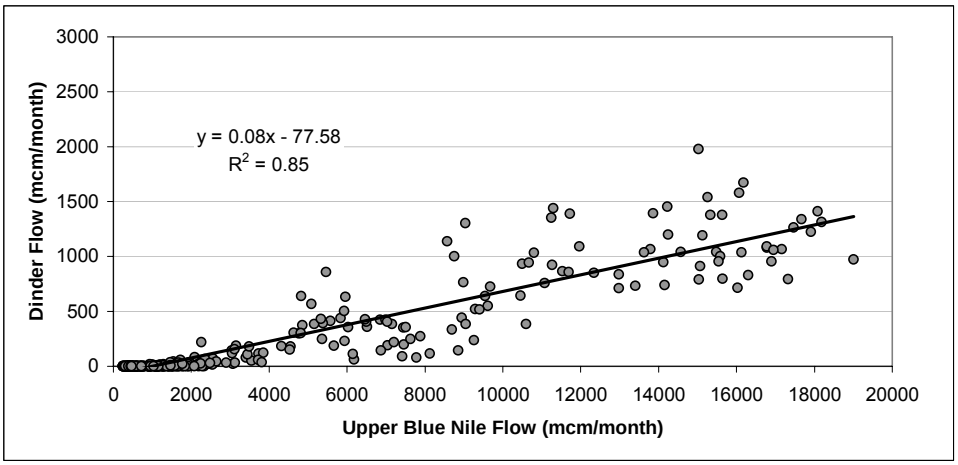

Figure 4.12: Relationship between monthly Border and Dinder flow.

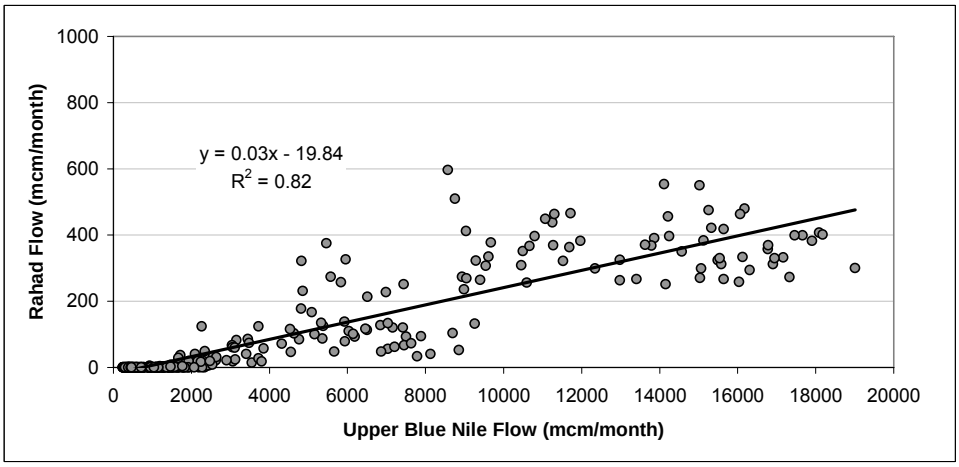

Figure 4.13: Relationship between monthly Border and Rahad flow.

4.2.3 Hydrologic Impact Assessment

Historical and future temperature and precipitation sequences for the two Upper Blue Nile basins have been passed into the Blue Nile hydrologic model. The resulting monthly flow sequences for Blue Nile at Border scenarios are shown in Figure 4.14. Figure 4.15 shows the five-year moving averages for clarity.

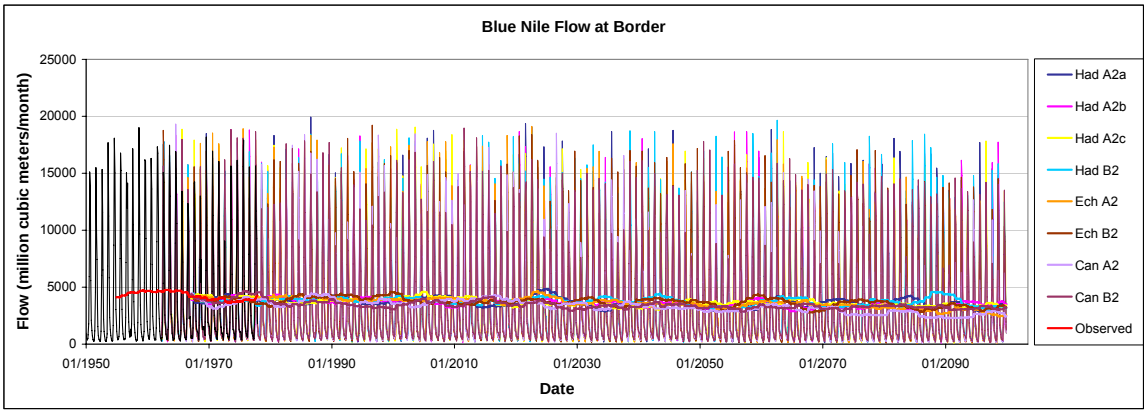

Figure 4.14: Monthly Blue Nile flow sequences for eight climate scenarios.

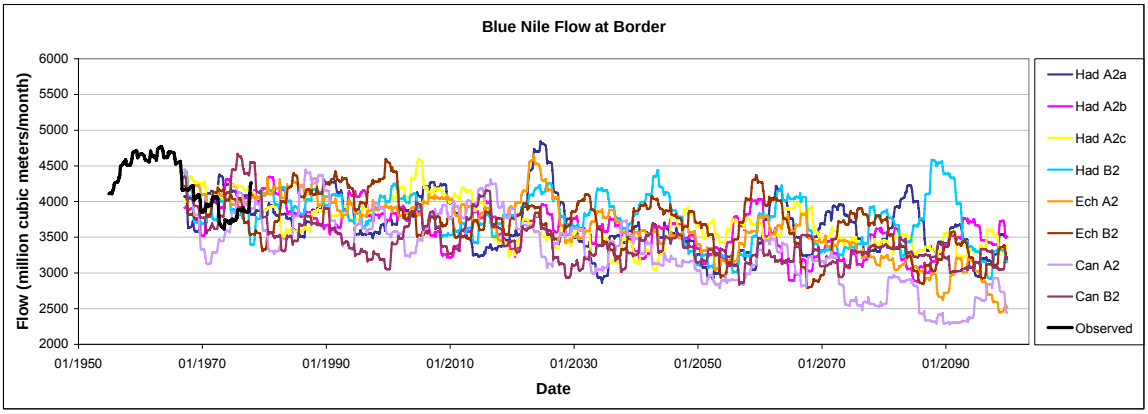

Figure 4.15: Five-year moving average flows at Border.

Climate scenario analysis for the Blue Nile indicated small precipitation increases in all four Hadley scenarios and moderate decreases in the Echam and Canadian scenarios. In spite of their differences in precipitation, all eight river flow sequences indicate marked decline. The HadB2 scenario indicates some recovery in the final decades resulting from two back-to-back wet episodes noted in the previous chapter. However, even this notable rise in the flow scenario appears to be part of a longer term downward trend.

The thirty-year average monthly flows for the baseline period (1962-1991) and final three decades (1970-2099) are shown in Figure 4.16. The eight trace means are bolded, while the minimum and maximum monthly values are indicated with dashed lines. The low flows are impacted the least, and the duration of base flow appears unchanged. Instead, the bulk of the impact appears to be occurring through a delayed and reduced accumulation of effective precipitation (runoff producing) during the rising limb season. The falling limb is necessarily impacted by the lower peak, at least in the initial months of recession.

The future spread of model results is roughly 5,000 million cubic meters, compared with the mean peak of 12,000. The EchA2 and CanA2 scenarios project the greatest changes, with -26.5% and -32.1% reductions in annual average flow, respectively. HadB2 projects the least change at -8.3%.

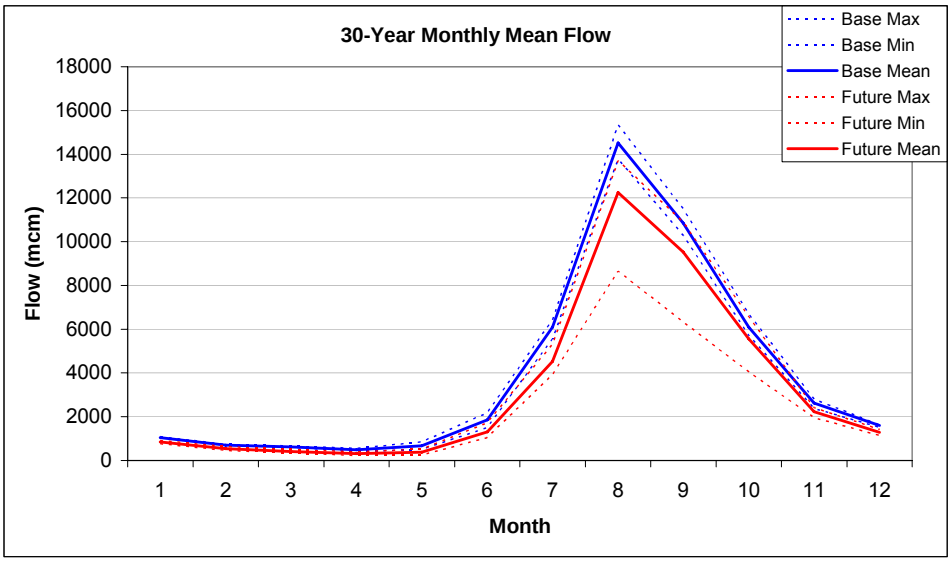

Figure 4.16: Thirty-year mean monthly flows at Border.

The Dinder and Rahad river flows are generated from the modeled flows at Border. As such they experience similar changes with respect to their own hydrographs (Figures 4.17 and 4.18)

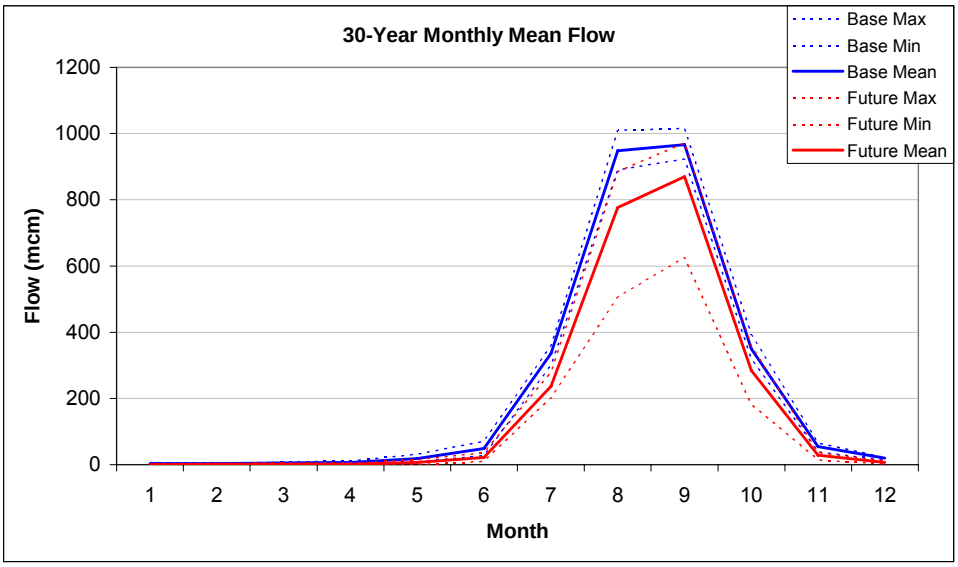

Figure 4.17: Thirty-year mean monthly flows for the Dinder River.

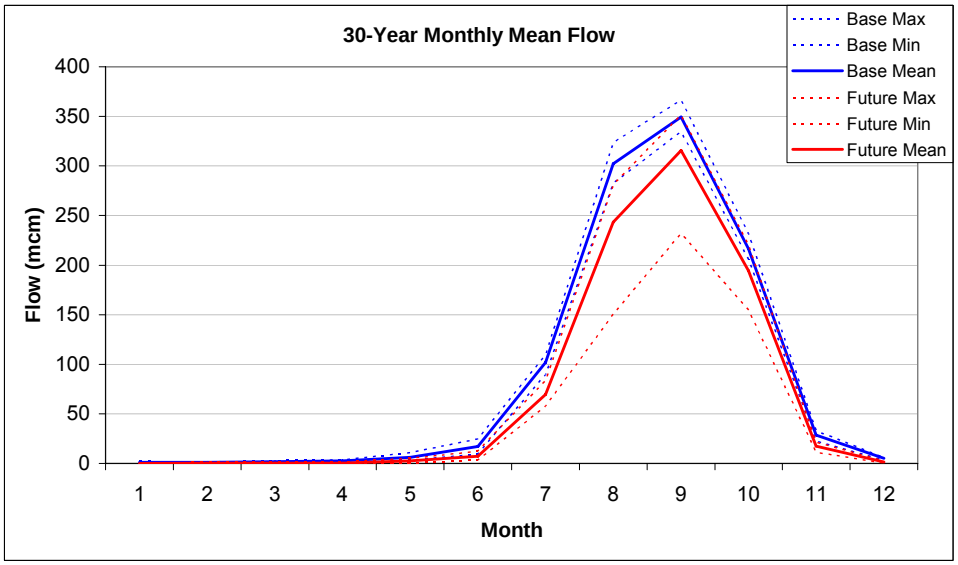

Figure 4.18: Thirty-year mean monthly flows for the Rahad River.

4.3 Atbara

The Atbara basin, located north of and adjoining the Blue Nile basin, drains areas of Ethiopia and Eritrea equaling approximately 68,800 km^2. The headwaters originate in the same mountainous region as Lake Tana and the Dinder and Rahad rivers. The upper reaches of the basin are very steep with a slope more than twice that of the Upper Blue Nile. One small reservoir exists roughly in the middle of the river's 880 kilometer course at Khashm el Girba.

4.3.1 Atbara Hydrologic Model

The Atbara basin is also simulated with a statistical hydrologic model. As with the Blue Nile, contemporaneous temperature, precipitation and flow data are available on a monthly basis from 1950 thru 1977. The process of model development closely followed the experience gained with the Blue Nile model.

The Atbara basin was ultimately delineated into upper and lower watersheds for the purposes of model calibration (Figure 4.19). The Khashm el Girba reservoir is located a short distance (approx. 20 km) below the delineation line of the two basins. The rising limb season is from July thru September, with the remaining months representing the hydrograph recession.

Figure 4.19: Atbara hydrologic units.

The rising limb model incorporates (P-PET) from both the upper and lower watersheds, resulting in a seasonal model R^2 of 0.64. The flow in this season is insensitive to an autoregressive term, which is expected for this highly seasonal and steep basin. On the other hand, the season of flow recession is dominated by the influence of the flow at the previous time step. In fact, the previous month's flow explains 85% of the falling limb variance. Adding (P-PET) terms from watershed 1 explains an additional 4% of the variance for a total model R^2 of 0.89. Combining the two seasonal models yields an overall R^2 of 0.88. Unlike the upper Blue Nile, the Atbara model does not improve with a non-linear transformation. The final model formulations and calibrated coefficients are presented below.

$$Q(k) = \alpha_1 WS_1(k) + \alpha_2 WS_1(k-1) + \alpha_3 WS_2(k) + \alpha_4 WS_2(k-1) + \alpha_0 \quad \text{(July – September)}$$

$$Q(k) = \alpha_1 WS_1(k) + \alpha_2 WS_1(k-1) + \alpha_3 Q(k-1) + \alpha_0 \quad \text{(October – June)}$$

Table 4.4: Atbara hydrologic model coefficients.

Rising Limb (Jul-Sep)		**Falling Limb (Oct-Jun)**	
Predictor Variable	Coeff.	Predictor Variable	Coeff.
$WS_1(k)$	0.04	$WS_1(k)$	0.0052
$WS_1(k\text{-}1)$	0.11	$WS_1(k\text{-}1)$	0.0088
$WS_2(k)$	0.18	$Q(k\text{-}1)$	0.21
$WS_2(k\text{-}1)$	0.11	α_0	143.30
α_0	3874.73		

The falling limb model depends solely on watershed 1 and the previous flow. In fact, adding watershed 2 as a predictor leads to less physically meaningful model coefficients. This suggests that the 2-month accumulated volume in the reservoir and the resulting outflow, as expressed by the autoregressive flow term, effectively describe the recession and low flow months.

A few important differences between the Blue Nile and Atbara basins contribute to the differences in model form: while the headwaters of the Atbara drain similar mountainous terrain as the upper Blue Nile basin, the river slope is more than twice that of the corresponding Blue Nile reach; the Atbara does not originate from a lake; and its flow is more strongly seasonal. With these differences in mind, it is not surprising that the Atbara behaves in a more linear fashion than the Blue Nile.

Model results are shown if Figures 4.20 and 4.21. Overall the model appears to capture the multi-year pattern of high and low flows. Strangely, the model manages to capture many of the peaks extremely well over a significant range of peak magnitudes (e.g., 1950-54 and 1962-69), while other peaks appear to be surprisingly disparate (e.g., 1959-61.) It is difficult to know the extent to which data quality plays into this behavior.

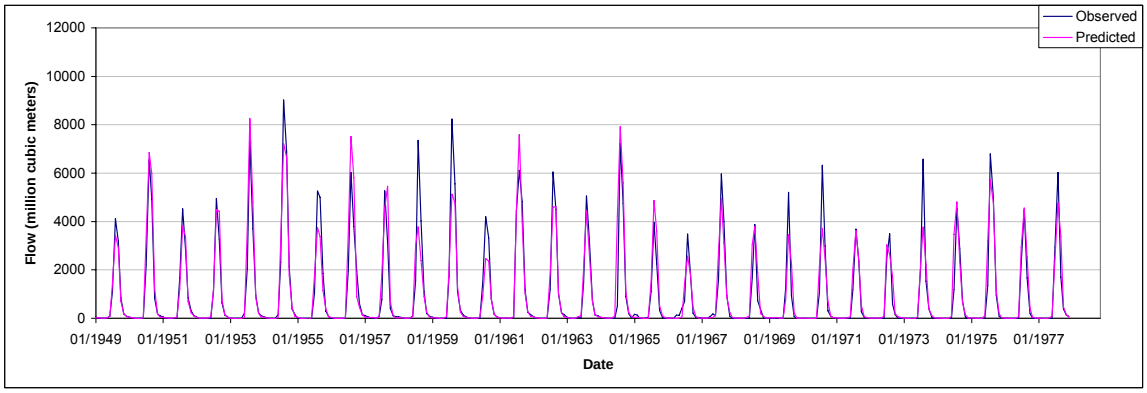

Figure 4.20: Observed (blue) and simulated (pink) Atbara flows.

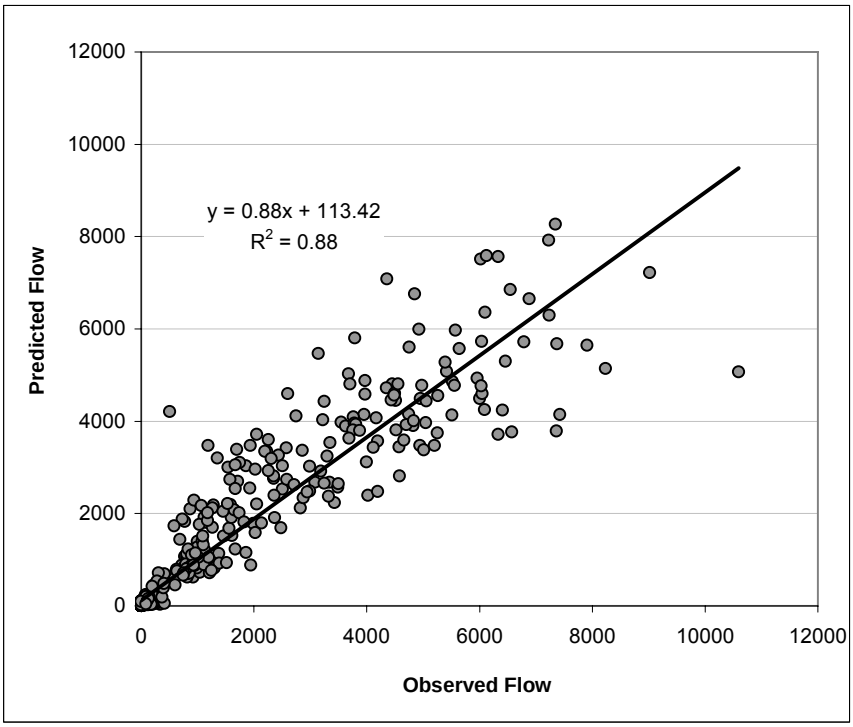

Figure 4.21: Scatter plot of observed versus predicted Atbara flows.

4.3.2 Hydrologic Impact Assessments

The eight temperature and precipitation sequences from the Atbara future climate assessment are used with the basin hydrologic model to generate projected river flows. The simulated monthly Atbara flows are presented in Figure 4.22, while the five-year moving average sequences are shown in Figure 4.23.

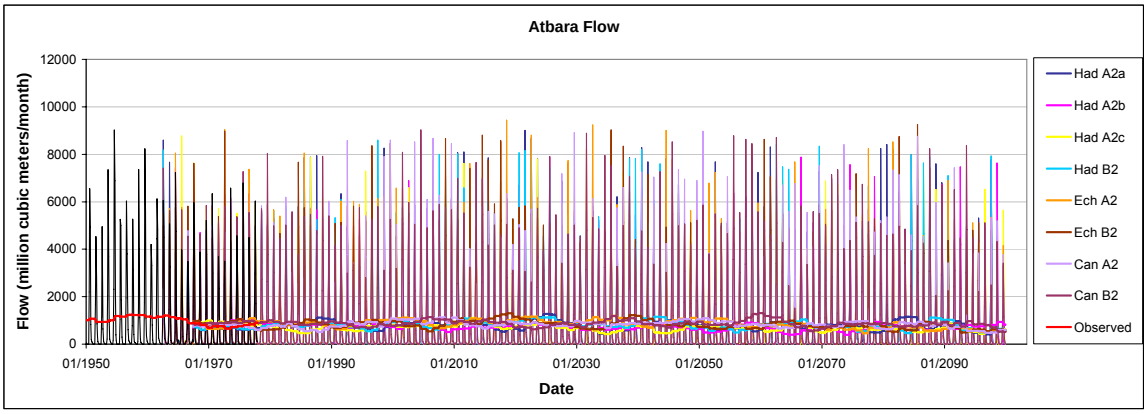

Figure 4.22: Monthly Atbara flow sequences for eight climate scenarios.

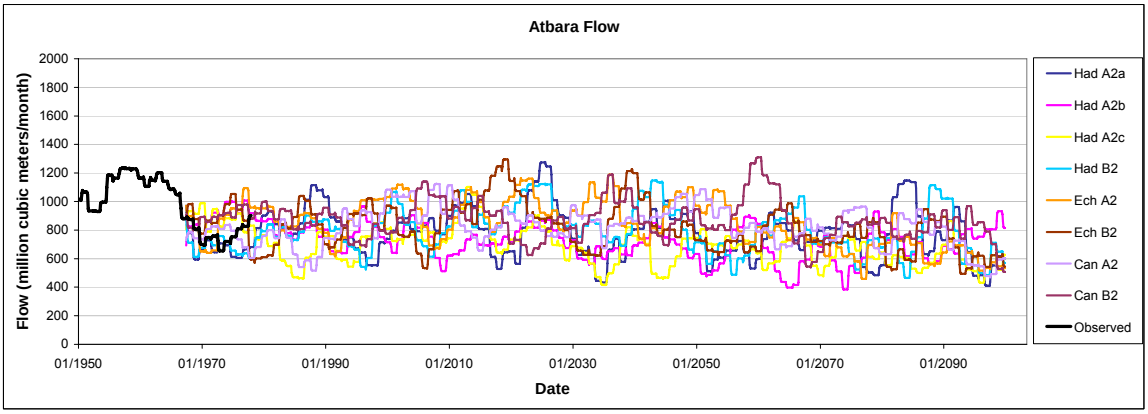

Figure 4.23: Five-year moving average flows for the Atbara River.

As with the Blue Nile flows, all eight scenarios indicate significant flow reductions. The Hadley and Echam scenarios have nearly identical hydrologic impact, which is not surprising since their precipitation and temperature scenarios are consistent across the two neighboring basins. The Canadian scenarios, on the other hand, indicate increasing precipitation of the Atbara basin. This appears to mitigate to some small extent the drying effects of the increasing temperature trend.

Thirty-year mean hydrographs for the Atbara over the baseline and final 30-years are depicted in Figure 4.24. In the Blue Nile, the most striking observation was the reduced peak flow. For the Atbara, however, the peak flows are little impacted. The eight-scenario mean reduction is little more than 2% below the baseline peak flow. The majority of change appears to occur in the early months of the rising limb season. In June and July, the mean change is -44% and -34%, respectively.

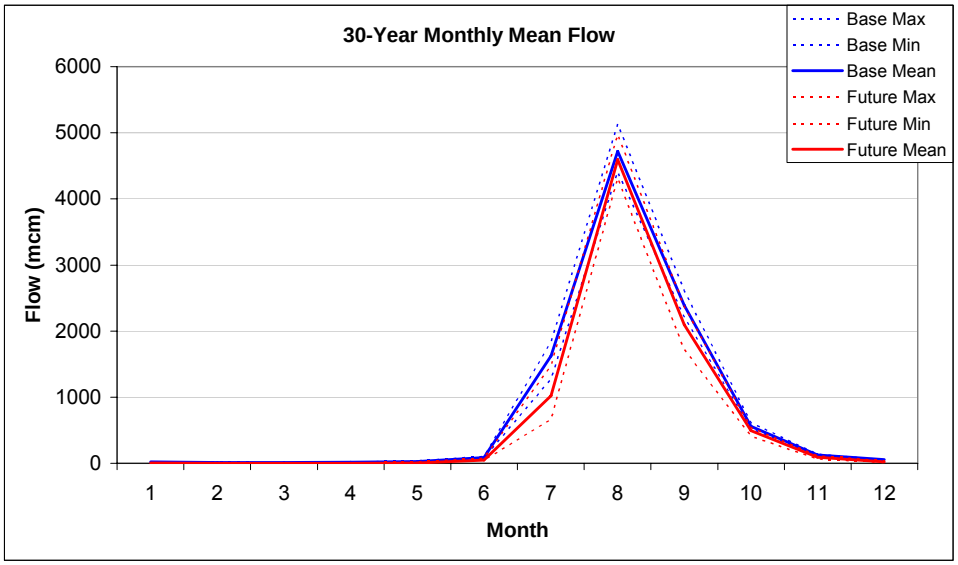

Figure 4.24: Thirty-year mean monthly flows for the Atbara River.

4.4 Sobat

The Sobat is characterized by highly seasonal flow and two distinct contributing watershed areas, the Baro in the northeast and Pibor to the south. The Baro adjoins parts of the Blue Nile basin in the Ethiopian highlands and is the dominate contributor to Sobat flow. The Baro loses flow through small channels that spill into the Machar marshes, but also by overflowing its own banks and spilling into the floodplain. While connectivity

with the marshes implies ever-present losses to flow, the tendency to overflow its banks effectively limits the peak flow emerging from the Baro.

The Pibor basin, though more than twice the area of the Baro, is a secondary contributor to Sobat flow. Although it drains parts of the Ethiopian Plateau as well as the equatorial lake plateau to the south, much of the basin is flat and prone to forming swamps. Two tributaries that join the Pibor (the Gabila and Akobo) approximately 80 kilometers before its confluence with the Baro may actually account for the majority of outflow from this region.

4.4.1 Sobat Hydrologic Model

Contemporaneous temperature, precipitation and flow data are available on a monthly basis for the Sobat basin from 1912 thru 1977. However, upon viewing the early temperature series, much of the data appears repetitive, suggesting that sparse data have been augmented with long term average values. As a result, the statistical hydrologic model has been calibrated with the 1920 to 1977 period. The four hydrologic units defined for model calibration are illustrated in Figure 4.25:

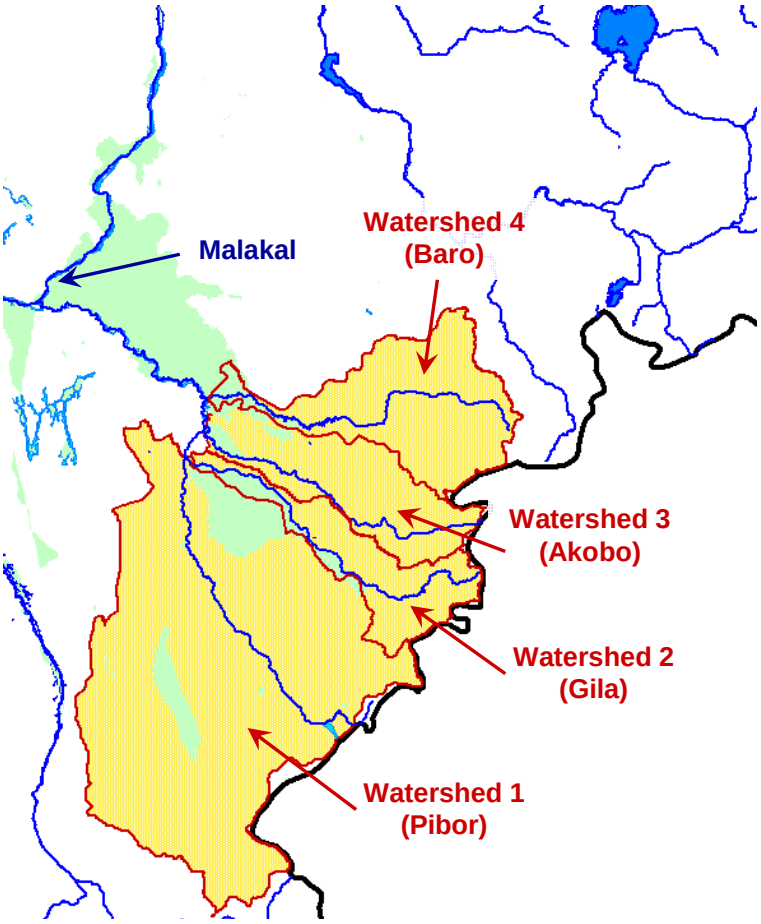

Figure 4.25: Sobat hydrologic units.

The existence of extensive marshes, over bank spillage and two distinct headwater regions cause the Sobat basin to have a somewhat more complicated flow character than both the Blue Nile and Atbara basins. As with the previous basins, models are developed for the rising and falling limbs; although the seasonal delineation is not as straightforward in this case. While the Baro basin typically peaks in August-September, the flow downstream of the Baro-Pibor junction typically peaks in November. Both hydrographs, however, begin to rise around May. Several seasonal delineations were used before settling on the final seasons of May through November and December through April. The advantage of this definition is that both of the main flow regions are in recession

during the December to April season. The final models are shown below with model coefficients given in Table 4.5.

$$Q(k) = \alpha_1 WS_1(k-3) + \alpha_2 WS_2(k-1) + \alpha_3 WS_2(k-2) + \alpha_4 WS_3(k-1) + \alpha_5 WS_3(k-2) + \alpha_6 WS_4(k-2) + \alpha_7 WS_4(k-3) + \alpha_0 \quad (\text{July} - \text{September}),$$

$$Q(k) = \frac{c}{1+\exp(Arg)} \quad (\text{May} - \text{November}),$$

where the argument in the above equation is defined as follows:

$$Arg = \alpha_1 WS_1(k-3) + \alpha_2 WS_2(k-2) + \alpha_3 WS_2(k-3) + \alpha_4 WS_3(k-2) + \alpha_5 WS_3(k-3) + \alpha_6 WS_4(k-2) + \alpha_7 Q(k-1) + \alpha_0 \quad .$$

Table 4.5: Sobat hydrologic model coefficients.

Rising Limb (May-Nov)		**Falling Limb (Dec-Apr)**	
Predictor Variable	Coeff.	Predictor Variable	Coeff.
$WS_1(k-3)$	0.008	$WS_1(k-3)$	5.80E-06
$WS_2(k-1)$	-0.060	$WS_2(k-2)$	6.87E-05
$WS_2(k-2)$	-0.078	$WS_2(k-3)$	-1.31E-05
$WS_3(k-1)$	0.073	$WS_3(k-2)$	-1.32E-04
$WS_3(k-2)$	0.137	$WS_3(k-3)$	-2.20E-04
$WS_4(k-2)$	0.024	$WS_4(k-2)$	-8.63E-05
$WS_4(k-3)$	0.087	$Q(k-1)$	-1.09E-03
α_0	1205.8	α_0	2.31
		c	3238.29
* $c = (1.1*Q_{max})$			

The recession season drains in a typical non-linear fashion, while the rising flow season was better described with a linear model. It is possible that the Baro over bank flow and additional wetland areas elsewhere in the basin act to dampen what otherwise may have been a non-linear response during the upswing of the rainy season. The combined model performance is illustrated in Figures 4.26 and 4.27.

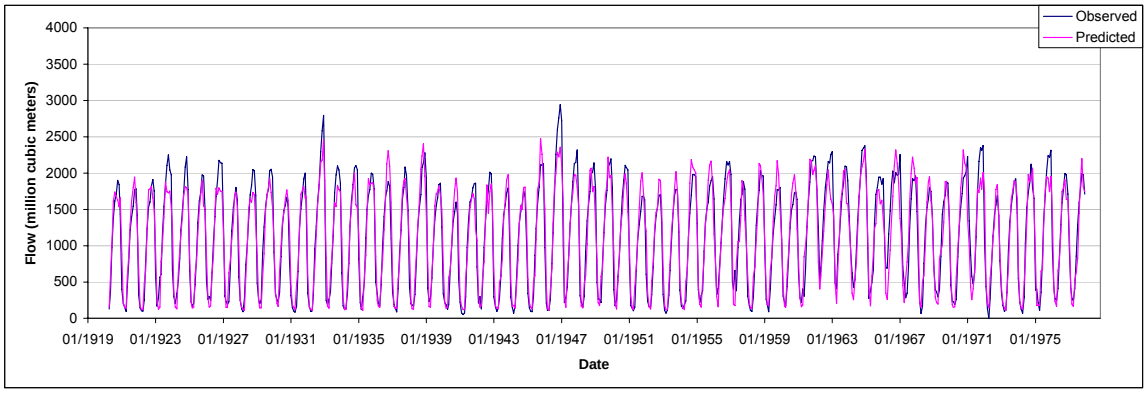

Figure 4.26: Observed (blue) and simulated (pink) Sobat flows.

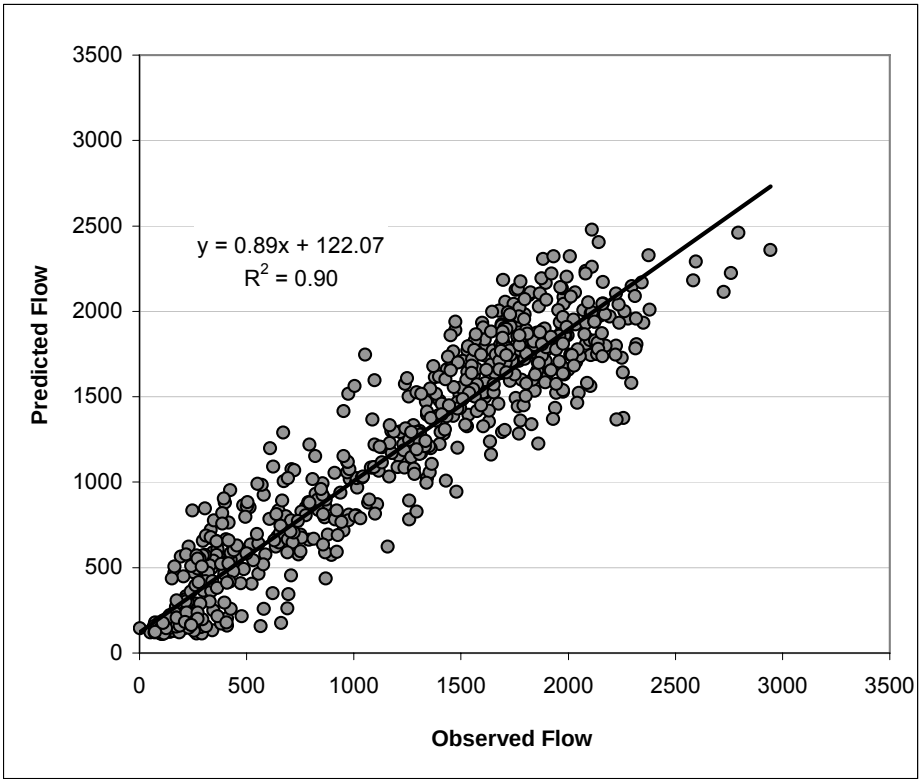

Figure 4.27: Scatter plot of observed versus predicted Sobat flows.

In light of the complicated nature of the Sobat basin, the model performs surprisingly well. The Sobat exhibits more low flow variability than the Blue Nile and Atbara rivers, and the model appears to capture these flows extremely well. Across all months, the model explains 90% of the observed variance.

4.4.2 Hydrologic Impact Assessment

The eight Sobat basin climate scenarios have been used as input to the flow simulation model. The resultant monthly flow sequences are shown in Figure 4.28. The five-year moving average flows are presented in Figure 4.29.

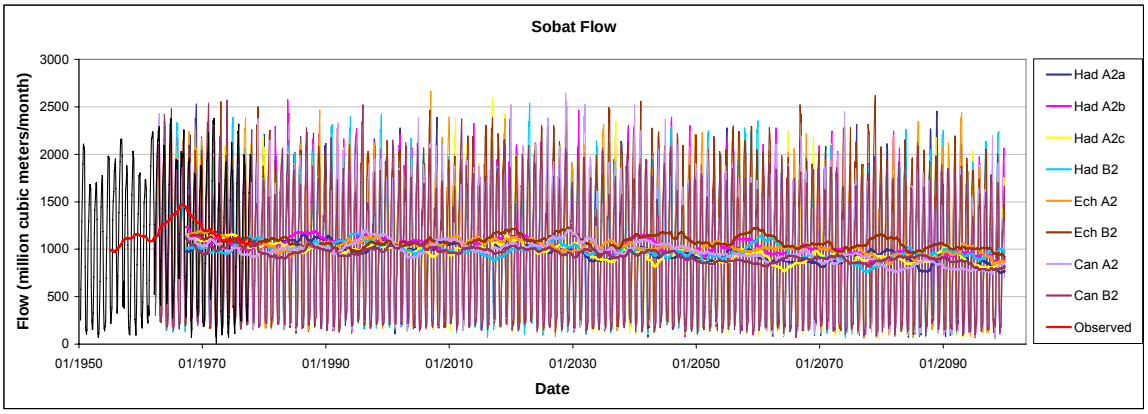

Figure 4.28: Monthly Sobat flow sequences for eight climate scenarios.

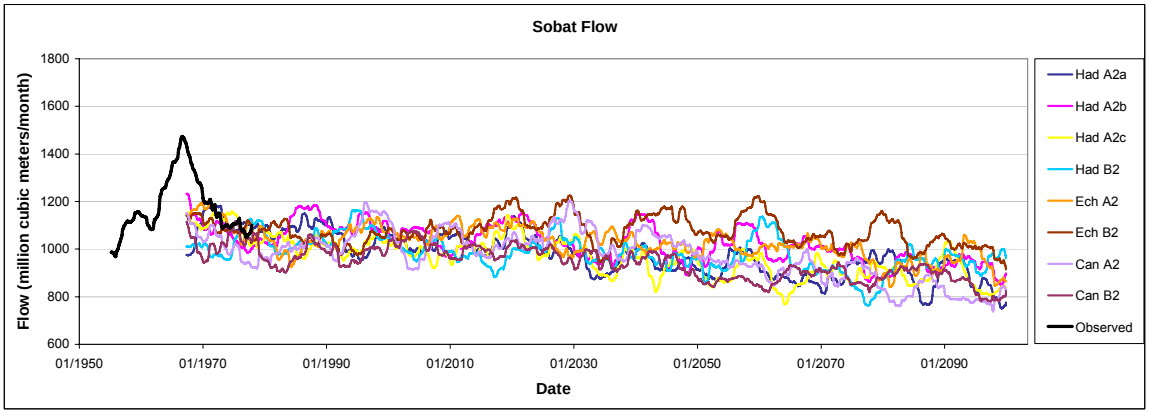

Figure 4.29: Five-year moving average flows for the Sobat River.

The simulated Sobat flows portend the same dramatic flow decreases as the preceding basins. Here, only the Canadian scenarios predict substantially reduced precipitation, but even the Hadley and Echam scenarios, which show precipitation increase, have very small and possibly non-significant precipitation changes. The final 30-years of flow indicate between -5% to -18.4% flow changes from the baseline period.

The mean hydrograph for the Sobat is affected a little differently from the other basins. As seen in Figure 4.30, the low flow season is essentially extend by two months, with the remainder of the hydrograph affected in a relatively uniform manner.

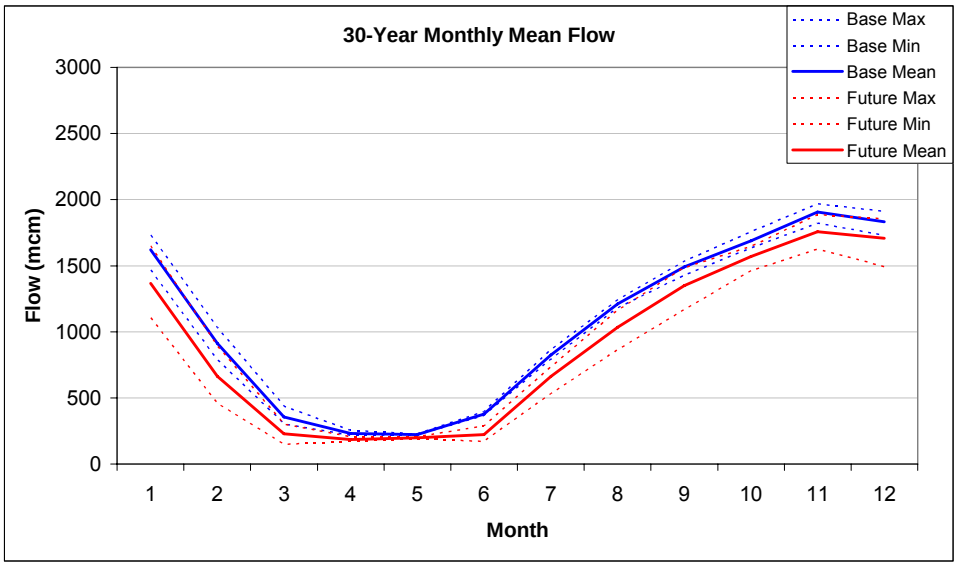

Figure 4.30: Thirty-year mean monthly flows for the Sobat River.

4.5 Equatorial Lakes below Lake Victoria

Outflow from Lake Victoria travels along the Upper Victoria Nile, passing through a series of falls, and enters Lake Kyoga about 130 kilometers downstream. The lake itself is a shallow depression of only 3 to 5 meters depth. The drainage area is primarily low hill country and flat valleys; though to the northeast it drains a steeper portion of the Kenyan highlands. Historically, Lake Kyoga is believed to be a sink rather than a source of water since much of the river inflow is lost to evaporation in swampy areas and over the lake itself.

The outflow from Lake Kyoga travels along the Lower Victoria Nile and enters Lake Albert. Lake Albert is a deep lake, reaching 50 meters in some places, with a surface area of approximately 5,300 km^2. As with Lake Kyoga, evaporation over the lake is high and offsets inflow from its immediate watershed (17,000 km^2) and direct lake precipitation. But Lake Albert has an additional source of inflow via the River Semliki, which connects Lake Albert to Lakes Edward and George to the southwest. These lakes contribute an additional drainage area of 30,500 km^2. Consequently, Lake Albert has historically been a positive contributor to the equatorial lake water balance.

4.5.1 Lake Kyoga and Lake Albert Hydrologic Models

The Lake Kyoga and Lake Albert models have been developed with monthly precipitation, temperature and NBS data for the period 1950 to 1977. Mean areal precipitation and temperature data were developed over three watershed areas for Lake Kyoga, while four areas were used as input to the Lake Albert model (Figure 4.31). As with the previous hydrologic models, precipitation minus PET was found to be the best performing predictor variable.

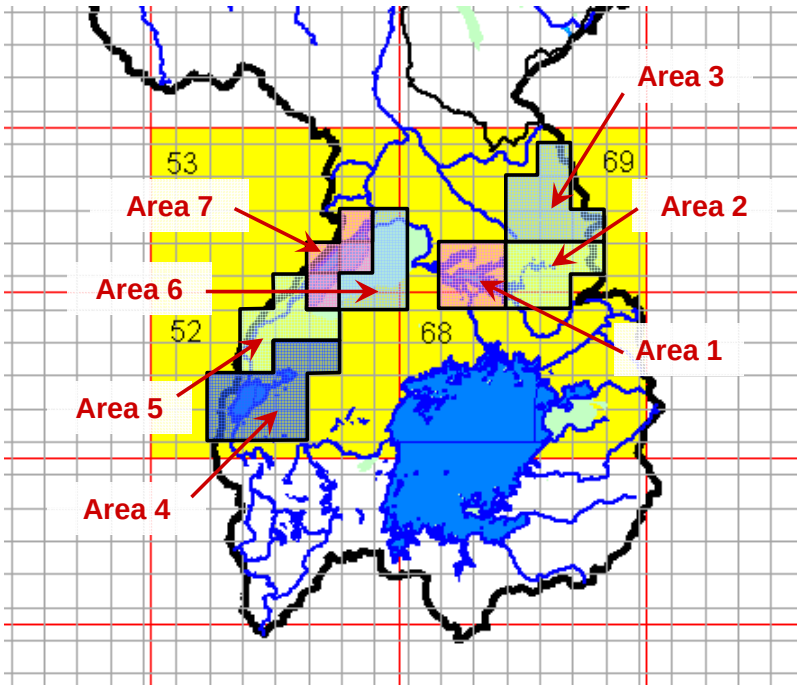

Figure 4.31: Lake Kyoga and Lake Albert hydrologic units.

The historical record of Lake Kyoga NBS is not independent of the Lake Victoria net basin supply. In fact, errors in estimating the Lake Victoria NBS are propagated to lakes Kyoga and Albert through its influence on the assumed lake inflows. As a result, current and previous Lake Victoria NBS tend to improve the model performance for both lakes. Similarly, Lake Kyoga NBS plays a role in the Lake Albert model. The final models are shown below, with model coefficients presented in Table 4.6.

$$\begin{aligned} NBS_{Kyoga}(k) = {} & \alpha_1 A_1(k) + \alpha_2 A_2(k-1) + \alpha_3 A_3(k-1) + \alpha_4 NBS_{Kyoga}(k-1) \\ & + \alpha_5 NBS_{LVic}(k) + \alpha_6 NBS_{LVic}(k-1) + \alpha_7 NBS_{LVic}(k-2) + \alpha_0 \quad , \end{aligned}$$

$$\begin{aligned} NBS_{Albert}(k) = {} & \alpha_1 A_4(k-2) + \alpha_2 A_5(k-1) + \alpha_3 A_6(k-1) + \alpha_4 A_7(k) + \alpha_5 NBS_{Albert}(k-1) \\ & + \alpha_6 NBS_{LVic}(k) + \alpha_7 NBS_{LVic}(k-1) + \alpha_8 NBS_{Kyoga}(k) + \alpha_9 NBS_{Kyoga}(k-1) + \alpha_0 \quad , \end{aligned}$$

where k is the time step in months, α's are model coefficients, A_i is P-PET in millimeters averaged over area i, and NBS is net basin supply in million cubic meters for the specified lake.

Table 4.6: Lake Kyoga and Lake Albert hydrologic model coefficients.

Lake Kyoga		Lake Albert	
Predictor Variable	Coeff.	Predictor Variable	Coeff.
$A_1(k)$	2.324	$A_4(k\text{-}2)$	-2.84E-01
$A_2(k\text{-}1)$	1.128	$A_5(k\text{-}1)$	-1.20E+00
$A_3(k\text{-}1)$	0.775	$A_6(k\text{-}1)$	1.25E+00
$NBS_{Kyoga}(k\text{-}1)$	0.447	$A_7(k)$	3.82E+00
$NBS_{LVic}(k)$	0.020	$NBS_{Albert}(k\text{-}1)$	4.89E-01
$NBS_{LVic}(k\text{-}1)$	-0.007	$NBS_{LVic}(k)$	2.33E-02
$NBS_{LVic}(k\text{-}2)$	0.001	$NBS_{LVic}(k\text{-}1)$	-1.48E-02
α_0	77.1	$NBS_{Kyoga}(k)$	0.14
		$NBS_{Kyoga}(k\text{-}1)$	-0.05
		α_0	174.80712

Model generated versus observed NBS for Lake Kyoga and Lake Albert are shown in Figures 4.32 and 4.33, respectively. The Lake Albert model performs better than the Lake Kyoga model, with an R^2 of 0.71 versus 0.56 for Lake Kyoga. Both models, however, are able to capture the overall interannual variability, though monthly values may differ considerably. The monthly errors are not so large as to be of great concern. Outflow from the equatorial lakes region enters the extensive wetlands of the Sudd, where flow persistence becomes the overriding factor for downstream impacts.

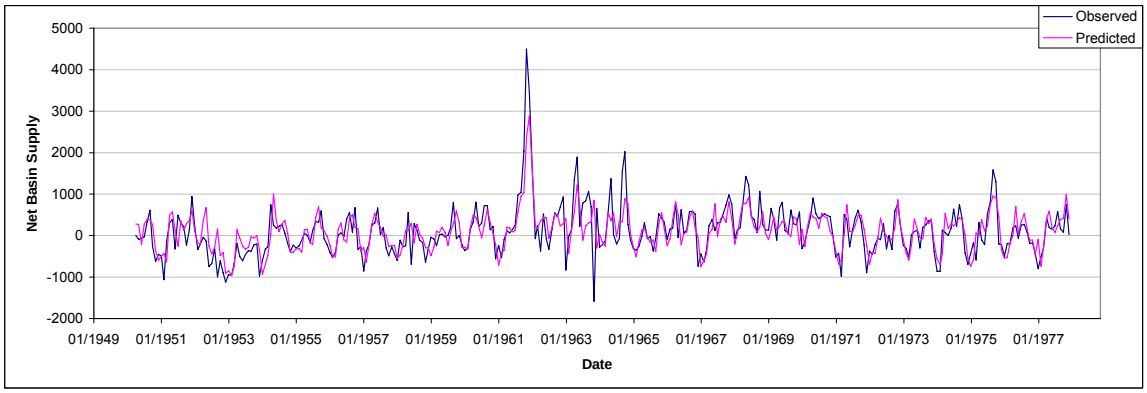

Figure 4.32: Observed (blue) and simulated (pink) Lake Kyoga net basin supply.

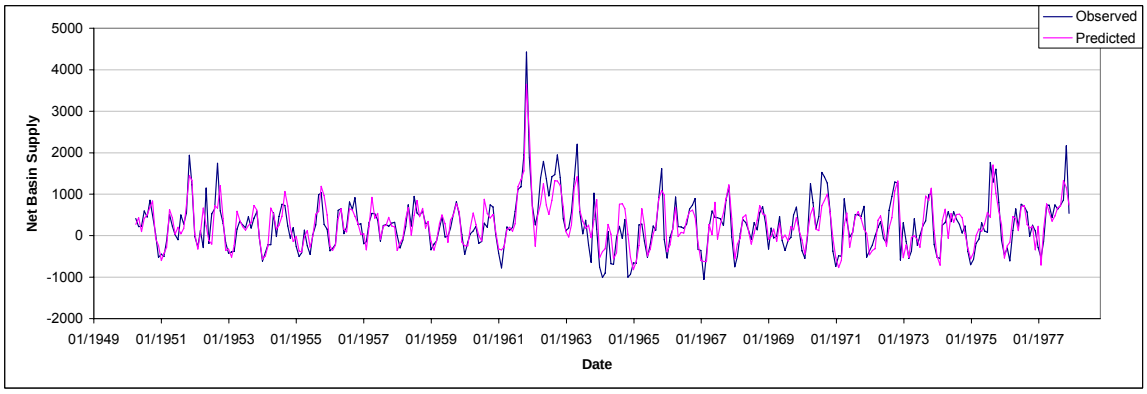

Figure 4.33: Observed (blue) and simulated (pink) Lake Albert net basin supply.

4.5.3 Hydrologic Impact Assessment

The Lake Kyoga and Albert hydrologic models have been driven with the eight future climate scenarios. The simulated net basin supply sequences are presented in Figures 4.34 and 4.35 (five-year moving averages.)

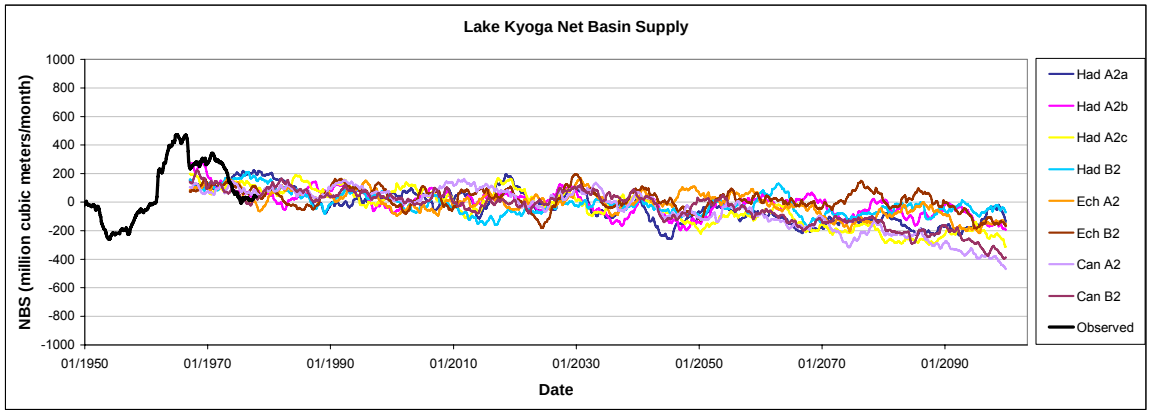

Figure 4.34: Five-year moving average net basin supply for the Lake Kyoga.

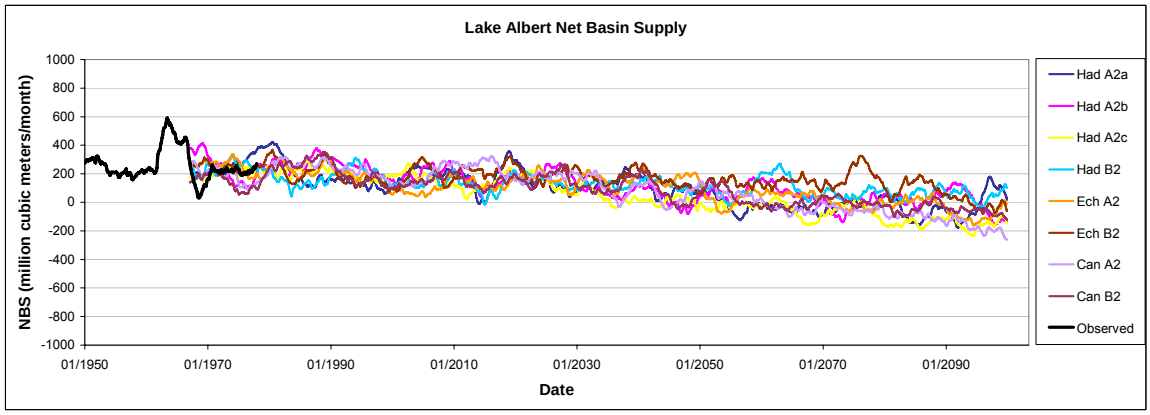

Figure 4.35: Five-year moving average net basin supply for the Lake Albert.

The 1912 to 1977 mean NBS for Lake Kyoga is -46 million cubic meters per month. The projected change over the 2070-2099 period between -100 (HadB2) and -397 mcm per month (HadA2a). For Lake Albert the baseline mean NBS is 313 mcm per month. The projected future change is between -145 (HadB2 and CanB2) and -364 mcm per month (HadA2a). Clearly, all eight scenarios project substantial reductions to the NBS of each lake.

The seasonal changes are reflected in the mean monthly lake NBS charts (Figures 4.36 and 4.37). The impacts appear to occur fairly uniformly across the year; although, Lake Albert shows slightly greater losses during Jul-Aug-Sep.

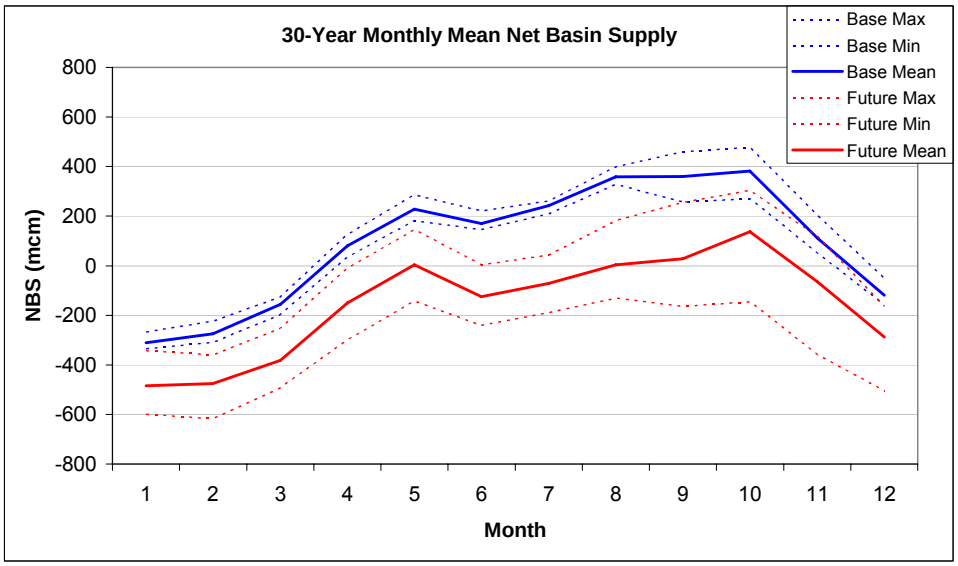

Figure 4.36: Thirty-year mean monthly NBS for Lake Kyoga.

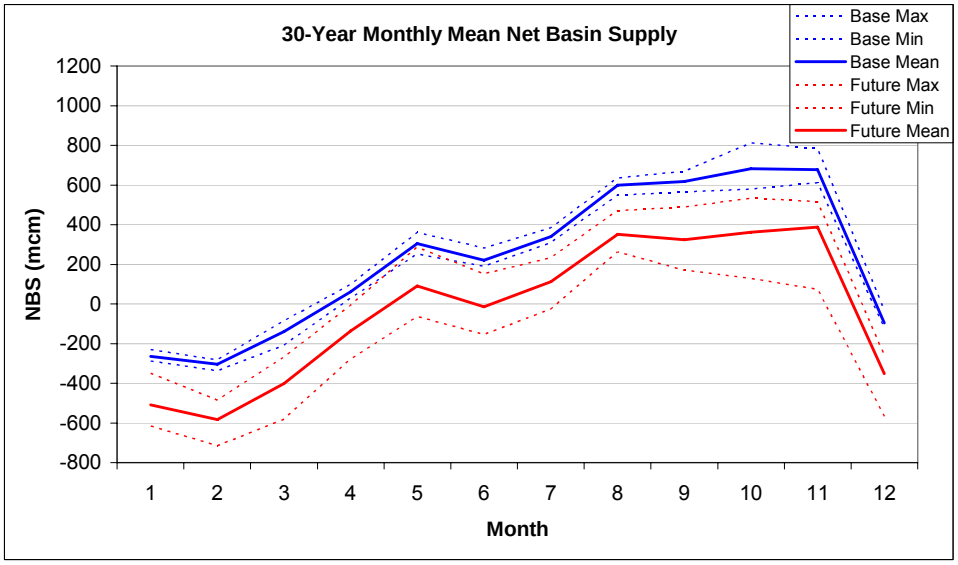

Figure 4.37: Thirty-year mean monthly NBS for Lake Albert.

4.6 Uncertainty in Hydrologic Scenarios

The previous sections have focused on the differences among all eight climate and hydrologic scenarios as well as differences among the three HadCM3-derived scenarios. These differences highlight some of the uncertainty associated with (a) the original climate models and (b) the effect of model initial conditions on the resulting temperature, precipitation, and flow sequences. The new methods discussed in this work introduce additional uncertainty to the final flow sequences. The sources of this additional contribution stem from the spatial relationships employed between indicator and target pixels, downscaling relationships, and hydrologic model errors.

Chapter 3 described the bootstrapping procedure used to generate 20-member ensembles of potential temperature and precipitation, based on historically determined regression errors. The same concept has been applied to hydrologic model errors. For each year of the simulation horizon (1962 to 2099), an historical year from the model calibration period (1950-1977 in most cases) is randomly selected. The monthly model residuals from the randomly selected historical years are then applied to the corresponding simulated monthly flows. The resulting sequence represents one possible realization given the uncertainties of the hydrologic model. This process is repeated 20 times and results in an ensemble of potential realizations. Note also that the scenarios of precipitation and temperature are themselves 20-member ensembles. Each climate trace is carried forward individually as input to the hydrologic models. This ensures that the final hydrologic traces reflect the cumulative climate and hydrologic methods uncertainty. The 20-member ensembles for each basin are included in Appendix B.

The following examples illustrate how this information may be interpreted. Figure 4.38 shows the 20 HadA2a traces of Lake Kyoga net basin supply. The trace mean is indicated with a bold black line, while the 10-year moving average is shown in red. The

Lake Kyoga hydrologic analysis shows that HadA2a projects a 397 mcm/year decrease in the net basin supply by the final 30 years. There are two observations. First, this projected change appears small compared to the previous 100 year variability. Second, the change is rather small compared with the underlying uncertainty, as shown in the trace spread about the mean. These observations apply to all Lake Kyoga Scenarios.

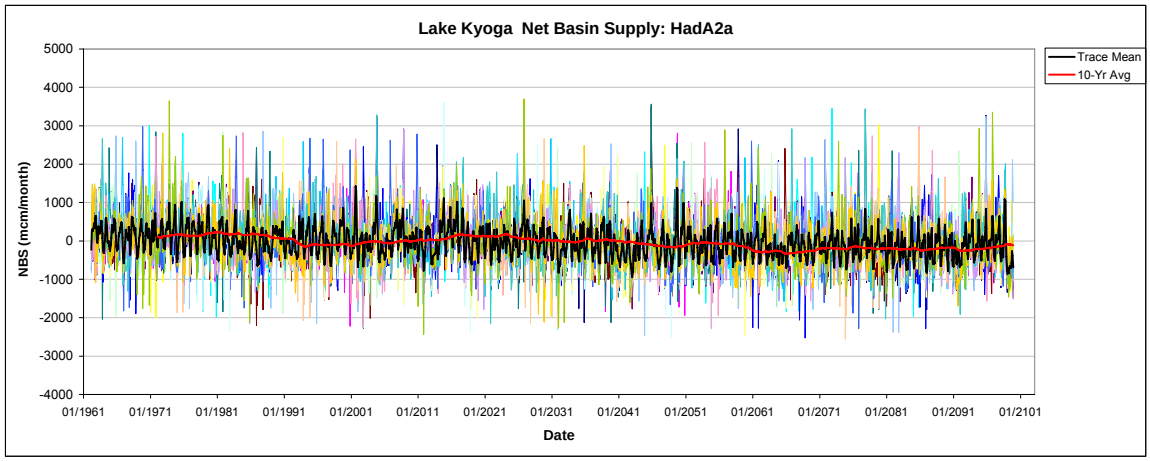

Figure 4.38: Had A2a Lake Kyoga net basin supply ensemble.

Figures 4.39 and 4.40 show Blue Nile flows as projected by the EchA2 and HadB2 scenarios. Necessarily, both scenarios show similar uncertainty in simulated peak flows. In the EchA2 scenario, the final 30 year decline in peak flows appears to be substantial, even in light of the trace spread. The HadB2 scenario, on the hand, does not indicate the same trend strength.

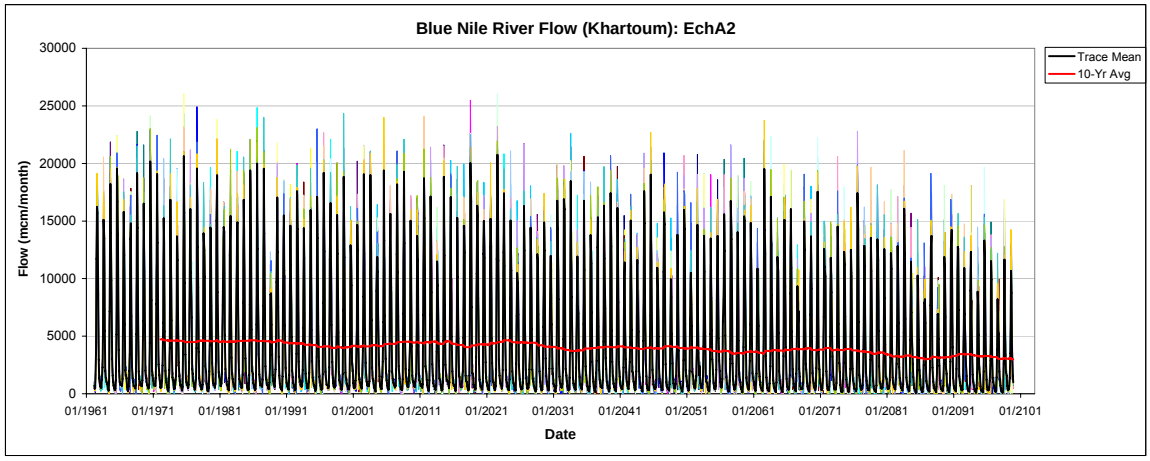

Figure 4.39: EchA2 Blue Nile flow ensemble.

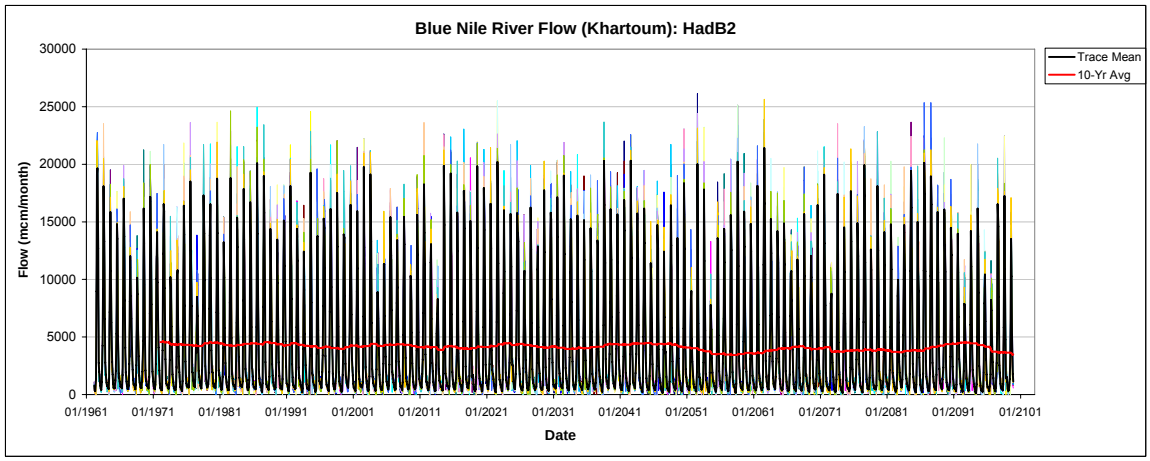

Figure 4.40: HadB2 Blue Nile flow ensemble.

The mean trace flow, or NBS, for each basin is the basis for the scenario comparisons of the previous sections. They also serve as the input sequences to the water resources assessments described in Chapter 5.

4.7 Summary Remarks on Hydrology

Taken alone, the climate scenario assessments of the previous chapter are difficult to interpret in terms of potential climate change impacts. While temperature results show

consistent increases across all study basins, the precipitation scenarios are sometimes ambiguous due to small signal to noise ratios as well as differences in the sign of precipitation across models and across basins. In this chapter the analysis is taken to the next critical step of understanding the basin scale hydrologic implications.

Hydrologic models have been developed for each individual study region. These models assimilate the projected climate scenarios and produce results to which we can better relate impacts. And, as has been shown in the preceding sections, the hydrologic results are far from ambiguous. Indeed, all of the hydrologically converted scenarios portend significant reductions in stream flow (and NBS) sequences. Tables 4.7 and 4.8 summarize the eight hydrologic scenarios across all basins.

Table 4.7: Summary of flow scenarios for the Blue Nile, Atbara and Sobat river basins.

	Flow Change (%)				
Model/River	**Border**	**Dinder**	**Rahad**	**Atbara**	**Sobat**
Had A2a	-10.2	-9.7	-8.7	-10.1	-17.5
Had A2b	-14.4	-15.8	-14.4	-14.6	-15.7
Had A2c	-14.2	-15.3	-13.8	-14.9	-16.5
Had B2	-8.3	-9.4	-8.5	-6.9	-10.7
Ech A2	-26.5	-30.1	-27.7	-25.9	-12.2
Ech B2	-15.0	-17.0	-15.5	-18.0	-5.1
Can A2	-32.1	-38.5	-35.8	-3.0	-18.4
Can B2	-14.6	-17.8	-16.4	-9.4	-13.6
Model Mean	-16.9	-19.2	-17.6	-13.1	-13.7

Table 4.8: Summary of NBS scenarios for the Equatorial Lakes.

NBS Change (mcm)			
Model/Basin	**Lake Victoria**	**Lake Kyoga**	**Lake Albert**
Had A2a	-2922 (-87%)	-397	-364
Had A2b	-1268 (-37%)	-323	-250
Had A2c	-1849 (-61%)	-190	-267
Had B2	-1335 (-41%)	-100	-145
Ech A2	-168 (-5%)	-242	-253
Ech B2	-1314 (-39%)	-206	-284
Can A2	-6241 (-191%)	-350	-335
Can B2	-5272 (-155%)	-156	-145
Model Mean		-245	-255
		Historical Mean	
1912-1977:	2274	-46	313
1950-1977:	2946	99	262

* Lake Victoria % change with respect to model baseline.

The hydrologic impacts of the basins are summarized as follows: the equatorial lakes experience a general year round reduction in their net basin supplies; the Sobat basin experiences an additional month of low flows at the beginning and at the end of the historically defined base flow period; the Blue Nile flows have a less rapid increase in the rising limb of the hydrograph and markedly lower peak flows; the Atbara experiences very little change in peak flows but with a slowing of the accumulation of effective rainfall. The coordinated response of the Main Nile flows to the hydrologic changes of these basins will be explored in the next chapter.

Chapter 5: Water Resources Assessments

5.1 Background

The primary hydrologic features of the Nile sub-basins have been previously discussed. This section provides an overview of existing and proposed developments within the Nile system. The locations of the referenced facilities are indicated on Figure 5.1.

Equatorial Lakes

The total storage capacity in the equatorial lakes is 260 bcm, with 215 provided by Lake Victoria and the remainder from lakes Kyoga and Albert. The outflow from Lake Victoria is regulated by the Owen Falls Dam, but this is operated according to the so called Agreed Curve, which dictates that releases follow the natural stage-outflow relationship. The hydroelectric capacity of the dam is 380 Megawatts (MW). The upper and lower Victoria Niles, with their steep slopes, have considerable capacity for further hydroelectric development. Plans exist for a total of five additional hydroelectric facilities that would bring the combined equatorial lakes hydroelectric capacity to 2300 MW (Georgakakos and Yao, 2000).

Sudd, Bahr el Ghazal, and Machar Marshes

There are several significant water sinks in the contributing basins between Bor and Malakal. The long term inflow to the Sudd swamps from the Victoria Nile is 33.3 bcm (estimated from 1905-1983). Roughly half of this volume, 16 bcm, remains at the Sudd exit. The tributaries of the Bahr el Ghazal to the west are estimated to produce some 11.3 bcm, yet only 0.3 bcm actually make it through the swamps in that basin and join the White Nile. And, as previously mentioned, the Machar Marshes in the Sobat basin claim

portions of the Baro runoff. The Sobat does contribute, on average, 13.5 bcm to the White Nile in spite of the losses.

Given the magnitude of evaporative losses, several water conservation projects have been proposed for these regions. The most notable is the Jonglei Canal, which would divert part of the Victoria Nile flow around the Sudd. The proposed canal would accept up to 43 mcm per day at Bor and discharge within the Sobat basin just prior to the junction with the White Nile. Additional projects propose to reclaim water via channels in the Bahr el Ghazal and Machar Marshes. There is an important point regarding the proposed wetland bypasses. The local populations rely heavily on the seasonal wetlands in both the Sudd and Bahr el Ghazal to provide grazing for their cattle in the dry season. Therefore, there are concerns about the ecological and economic consequences of modifying the hydrology of these basins (Sutcliffe and Parks 1999).

White Nile

From Malakal, the White Nile flows 840 km to Khartoum. The Gebel el Aulia Dam is located approximately 40 km upstream of Khartoum and exerts backwater effects as far upstream as 600 km. The reservoir storage capacity is 3.5 bcm and its primary purpose is to raise the river stage for irrigation pumping.

Blue Nile

The Upper Blue Nile drops 1300 m along its 900 km decent from Lake Tana to the Ethiopia-Sudan border. The average annual outflow at the border is approximately 48.7 bcm. Presently, a hydroelectric weir at the Lake Tana outlet and two small reservoirs below the border in Sudan are the only developments on the Blue Nile. Lake Tana has storage and hydroelectric capacities of 13.8 bcm and 200 MW, respectively. The Roseires reservoir can hold up to 2.7 bcm and has a hydroelectric capacity of 250 MW.

And the Sennar reservoir can hold approximately 1 bcm and has a hydroelectric capacity of 15 MW. Due to the tremendous topographic relief in this basin, future development on the Upper Blue Nile includes plans for four additional hydroelectric reservoirs that would bring the total basin storage 75.8 bcm and yield a hydroelectric capacity of 5,576 MW.

The Atbara river has one existing reservoir at Khashm el Girba. This facility has a maximum storage capacity of 1.4 bcm and hydroelectric capacity of 13 MW.

Main Nile

The Main Nile extends from Khartoum, Sudan to Aswan, Egypt. Lake Nasser is formed behind the High Aswan dam and extends upstream 400 km. Average annual inflow to Lake Nassar is 84 bcm. The High Aswan dam was built above the original Aswan dam (Old Aswan) in 1964, and the combined storage and hydroelectric capacities are 137.6 bcm and 2700 MW, respectively.

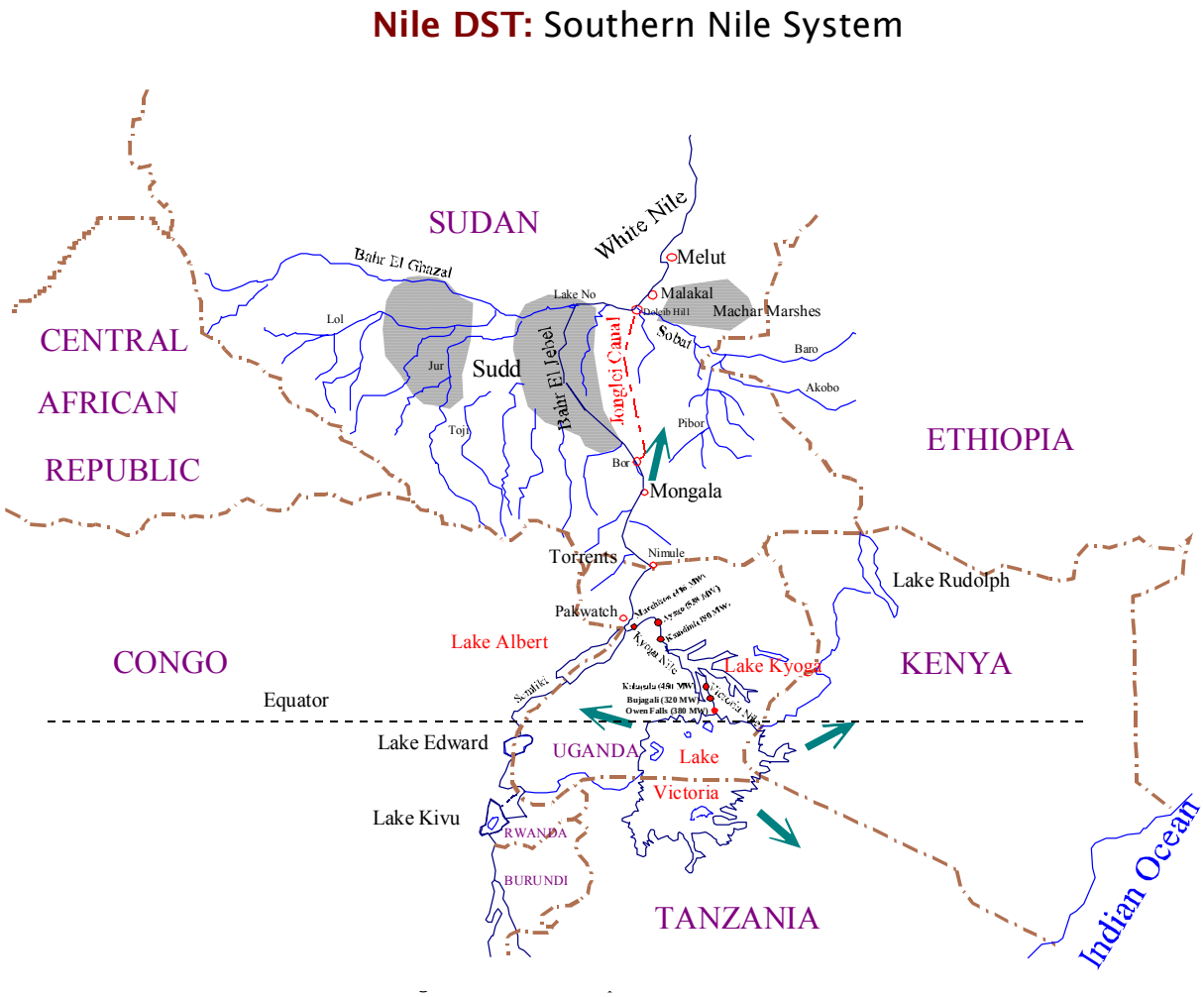

Figure 5.1(a): The Nile system with existing and planned development. *From Georgakakos and Yao, 2000*

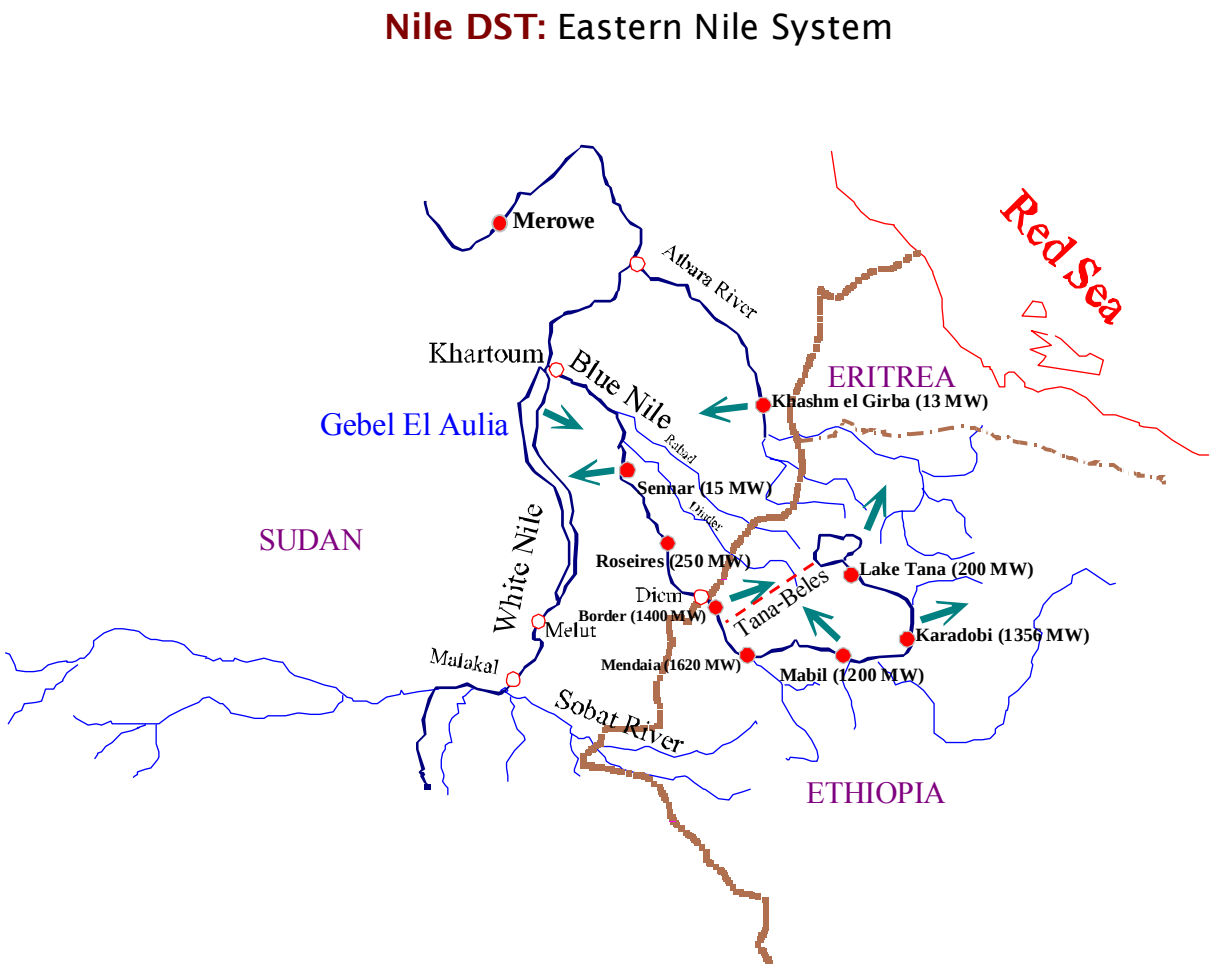

Figure 5.1(b): The Nile system with existing and planned development. *From Georgakakos and Yao, 2000*

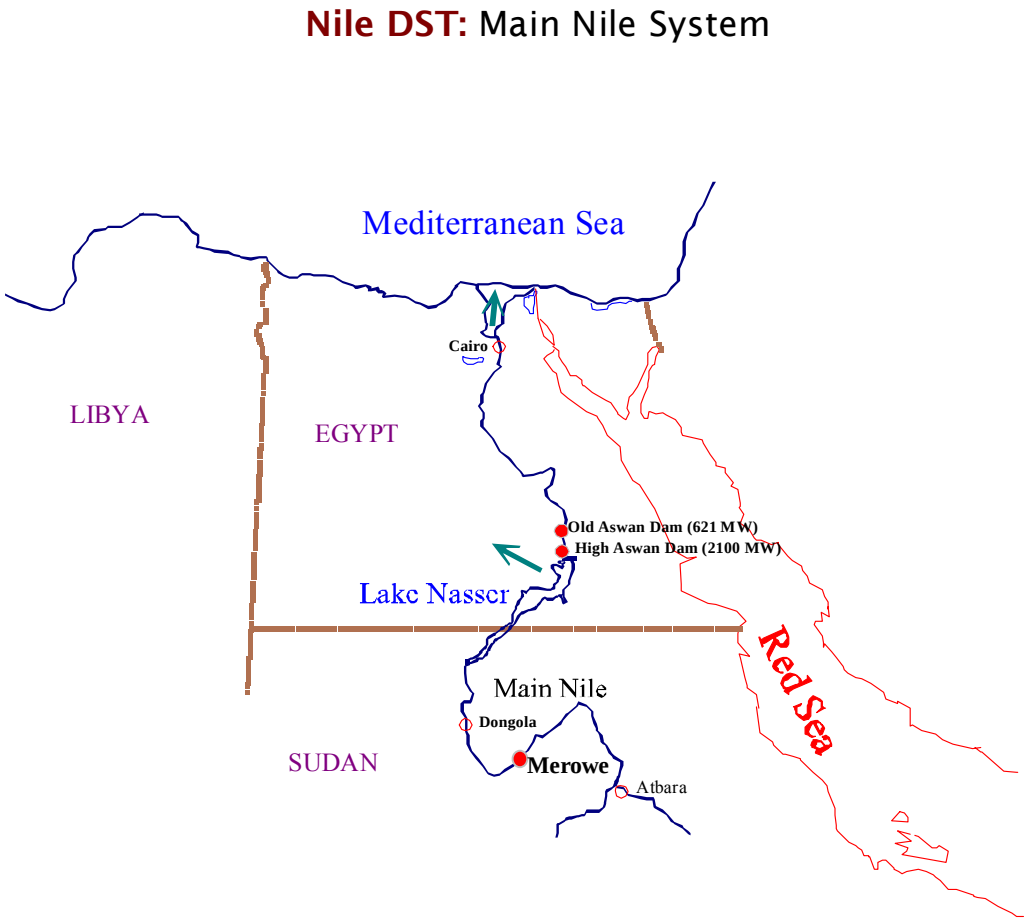

Figure 5.1(c): The Nile system with existing and planned development. *From Georgakakos and Yao, 2000*

5.2 Basin Development Scenarios

The baseline scenario for assessments represents the existing state of basin development. The lower equatorial lakes are unregulated and there are no sizeable reservoirs along the Upper Blue Nile in Ethiopia. Existing reservoirs include the Owen Falls Dam in Uganda; the Gebel el Aulia, Sennar, Roseires, and Khasm el Girba in Sudan; and the Old Aswan and High Aswan Dams in Egypt.

An alternate scenario is also explored that assumes full implementation of planned projects along several reaches of the Nile system. Potential future developments along the Victoria Nile include the full regulation of the Equatorial Lakes, and several hydropower facilities along the Victoria and Kyoga Nile reaches. White Nile development may involve several water conservation projects in the Sudd, the Bahr el Ghazal, and Machar Marshes (Sobat basin). Ethiopia, with its dramatic topographic relief, could potentially develop four additional reservoirs along the Upper Blue Nile at Karadobi, Mabil, Mendaia, and Border (Figure 5.1). The Equatorial Lakes are assumed to be regulated according to local water needs, and the characteristics of the existing and planned reservoirs are included in Appendix C.

Several modeling assumptions are made with respect to the wetland projects. The Bahr el Ghazal and Machar Marshes water contributions are assumed to follow the historically observed seasonality of their respective regions and have a maximum combined benefit of 4.75 bcm per year. There is considerable uncertainty in previous water balance studies in these areas due to limited hydrologic information. The 4.75 bcm benefit used here is conservative with respect to previous studies of these sites (Chan and Eagleson, 1980, El-Hemry and Eagleson, 1980, UNDP, 1981, Fahmy and Fahmy, 1981, Sutcliffe and Parks, 1999). The Jonglei canal is assumed to operate whenever the flow at Bor is greater than 30 mcm per day, with a maximum conveyance of 43 mcm per day. Flows in excess of 73

mcm per day are returned to the Bahr el Jebel. This policy aims at maximizing the water gains from the Sudd and is estimated to reduce evaporative losses by up to 7 bcm per year (Georgakakos and Yao, 2000).

5.3 Assessment Methodology

5.3.1 Data Base *(from Georgakakos and Yao, 2000)*

The data used for this assessment fall into three major categories: hydrologic data, reservoir and other project data, and demand data. Hydrologic data include rainfall, temperature, evaporation, and streamflow for different climate scenarios. Reservoir and other project data include capacity-elevation-area curves, tailwater curves, spillway and other hydraulic outlet features, hydropower plant characteristics (number and type of turbines, turbine power-net head-discharge curves, and hydraulic losses), and diversion canal capacities. Demand data include current and future agricultural water use requirements, flood stage thresholds, and typical daily/seasonal power demands.

This extensive database has been assembled from many sources, the most important of which are Nile Basin governmental agencies with which the authors have collaborated for several years. Among these agencies are departments of water development, ministries of water, hydrometeorological services, agricultural experiment stations, and power utilities in Tanzania, Uganda, Kenya, Ethiopia, Sudan, and Egypt. This interaction has taken place directly or through international organizations such as the Food and Agriculture Organization of the United Nations (FAO), international aid organizations, and the World Bank. Data and relevant information have also been obtained from a variety of other sources including the Nile Basin Volumes and Supplements (Hurst and associates, 1931, 1938, 1946, 1950, 1966), United States Bureau of Reclamation Study (1964), the Proceedings of the Nile 2002 Conference Series, and numerous published books and journal articles.

5.3.2 Water Resources Models *(from Georgakakos and Yao, 2000)*

The Nile Decision Support Tool

The assessments described here utilize the Nile Decision Support Tool (Nile-DST), which integrates several sub-basin models currently used by Nile Basin agencies for operational and planning purposes. The model and its applications are discussed in a series of published and forthcoming articles (1996, 1997a, 1998a,b,c, 1999a,b,c). What follows is a brief description of the modeling components.

The Nile-DST is designed to reproduce the Nile Basin response to various hydrologic conditions, development scenarios, and operational strategies. The primary model functions include inflow forecasting, river and reservoir routing, and reservoir control.

The purpose of the inflow forecasting component is to predict 10-day inflows several months into the future. The forecasted inflows are presented as equally likely realizations reflecting historical (and future climate) inflow characteristics such as seasonal and long-term variability. Such forecasts play an integral role in reservoir management since the optimal management policy at any given time is dependent not only on the current system state, but also on the evolution of future inflow sequences. For example, the optimal release policy for a known reservoir elevation may be different in the case of anticipated high future inflows versus low inflows. Therefore, forecasts are generated for all entry nodes of the river network including Lakes Victoria, Kyoga, and Albert, Torrents, Bahr el Ghazal, Sobat, Lake Tana, Karadobi, Mabil, Mendaia, Border, Roseires, Sennar, Dinder, Rahad, and Khasm el Girba.

The river and reservoir routing components simulate the movement of water through the river reaches and quantify transmission losses and time lags. The routing models are based on statistical or physically-based relationships (depending on available

information) and incorporate model error characterizations. Reservoir and lake outflow through hydropower facilities and spillways is modeled with sufficient detail for use in operational applications.

The purpose of reservoir control is to determine release sequences from each system reservoir such that sub-basin and basin-wide objectives are met as best as possible. System objectives include meeting water supply targets and avoiding water shortages, minimizing losses, maintaining land use patterns (Sudd), regulating river flows, avoiding spillage, and generating as much firm and average energy as possible. The task of the reservoir control module is complicated by the system size, non-linear response, and intrinsic uncertainties. The Nile-DST can be operated based on simple local control policies or in an optimization mode that considers varying degrees of coordinated regional or basin wide operation. The optimization operations are carried out by the Extended Linear Quadratic Gaussian (ELQG) control method (developed by Georgakakos and associates, 1987, 1989, 1993, 1997b,c,d , a trajectory iteration optimization algorithm suitable for multidimensional, dynamic, and uncertain systems.

Nile-DST Assessment Module

The Nile-DST models are designed for operational system management. Namely, given a particular system configuration, the Nile Basin authorities can use them to determine and implement desirable ten-day reservoir operation policies. Operational models, however, cannot assess the long term implications of management policies, nor can they determine the relative merits of different system configurations. To carry out these investigations, an assessment module was developed and added to the Nile-DSS.

The assessment process begins with the selection of a target demand level, a specified system configuration (i.e., a project combination to be considered in the current run), and

a project coordination policy (such as no cooperation, sub-basin level cooperation, or basin-wide cooperation). Then, for each ten-day interval of the assessment periods (baseline, "2030," and "2080"), the assessment module activates the Nile-DST models to (a) generate inflow forecasts (assuming knowledge of only current and past hydrologic conditions), (b) determine reservoir releases, (c) simulate the water movement through all system reaches using actually observed inflows, and (d) record reservoir levels, energy generation, water shortages, flow discharges, spills, wetland areas, and other quantities of interest. The process is repeated at the next and all subsequent ten-day intervals until the end of the assessment horizon. At the completion of the forecast-control-simulation process, the Nile-DSS generates statistics of all recorded sequences and develops a comprehensive database for comparative scenario analysis.

The following are unique features of the Nile decision support system:

- Explicit treatment of hydrologic and model uncertainty;
- Detailed representation of system dynamics and water uses;
- Ability to develop and test sub-basin and basin-wide management strategies; and
- High computational efficiency combined with user-friendly features (running on personal computers).

5.4 Scenario Assessments

The future hydrologic scenarios developed in chapters 3 and 4 have been used in conjunction with the Nile Decisions Support Tool to assess the expected Nile Basin response to potential climate change and development scenarios. In the following discussion, the assessment results are summarized relative to the following criteria:

- Water supply deficits by country (or region);
- Energy generation at the major hydropower facilities; and
- River flow availability and reservoir levels at representative locations throughout the basin.

The following sections detail the findings of the two previously defined development scenarios: 1) current basin configuration, and 2) fully developed infrastructure in the Equatorial Lakes, White Nile, and Blue Nile regions. For purposes of comparison, each chart presented in this assessment features a baseline. The baseline series represent simulated basin response under the baseline climate but for a given development scenario. This allows direct comparison of the system sensitivity to both climate change and basin development. Graphical results are presented by *(1)* sub-region/location, *(2)* climate scenario (baseline, 2030, and 2080), and *(3)* development scenario.

5.4.1 Sensitivity of Water Supply Deficits to Climate Change

Each chart in Figure 5.2 presents the average annual water supply deficits with respect to the Blue Nile basin (Sennar) and Egypt (High Aswan Dam). Currently, the only water supply demands on the Blue Nile occur at Sennar and total 15.62 bcm, annually. The current demand at Aswan, Egypt is 55.5 bcm. Additional demands exist at Gebel el Aulia (1.5 bcm) and Khashm el Girba (1.38 bcm). The results at Sennar and Aswan are highlighted here. Since upstream demands are met by the model first, the Egyptian deficit is considered representative of basin-wide water shortages.

Scenario I: Current Development

Deficits along the Blue Nile are negligible by 2030, and the maximum projected deficit by 2080 is merely 0.13 bcm, or less than 1% of the target demand. In Egypt, however, the majority of scenarios show significant deficits by the 2030s. The Echam scenarios

project the least impact, with just under 2 bcm. The Hadley and Canadian scenarios, though, project deficits from 2.6 to 9.3 bcm, or 5 -17% of Egypt's allocated share. By the 2080s the range of projected deficits grows to 8.4-24.7 bcm (15-45%).

The annual deficit frequency curves for Sennar and High Aswan are shown in Figure 5.3. For clarity, the eight-scenario average is shown for the baseline, 2030s, and 2080s periods. Although the Sennar deficits are low, there is a clear increase in the fraction of years when water supply falls short of the target. Under the baseline climate, small annual deficits occur in approximately 65% of years. In the 2030s and 2080s, the frequency of deficit increases to 80% and 95%, respectively. Under current climate, demand, and development conditions Egypt falls short of its target supply in approximately 10% of years. In contrast, the 2030 mean suggests that deficits will occur in almost all years.

Scenario II: Basin -wide Development

The right side of Figures 5.2 and 5.3 present the water supply deficits projected to occur if full basin-wide development is implemented. As with development scenario I, minimal deficits are projected to occur at Sennar. The frequency curves show deficit improvements under the baseline and 2030 climate, but, unexpectedly, this benefit is not reflected in the 2080 climate. One possible explanation for this is that the rising limb of the Blue Nile hydrograph is only minimally affected by 2030, but by 2080 the rising limb is shown to decrease considerably. Under the full development scenario several reservoirs have been included upstream of Sennar. The delayed flow accumulation may be affecting releases from the upstream reservoirs and subsequently impacting the Sennar supply. Under current development, the flows are directly conveyed downstream.

In Egypt, upstream development offsets much of the climate induced deficits. At 2030, half of the eight climate scenarios lead to no deficits at Aswan. Of the four remaining climate scenarios, potential deficits range from 0.6-3.7 bcm, compared with as much as 9.3 bcm that might occur in the case of present-day development. At 2080, the effect of basin development translates into an average deficit reduction of 5 bcm across the eight climate scenarios. This essentially means that in an average year, Egypt can maintain access to 9% of its allocation that would have been lost under current development conditions.

Not surprisingly, this development scenario also improves the frequency of annual deficits at Aswan. The bottom two charts in Figure 5.3 show that under the baseline climate, this development scenario would eliminate annual deficits completely. Under the 2030 climate, the frequency of annual deficits is reduced from more than 90% to approximately 50%. However, by 2080 the climate change effects overwhelm the system, and again Egypt shows consistent annual deficits.

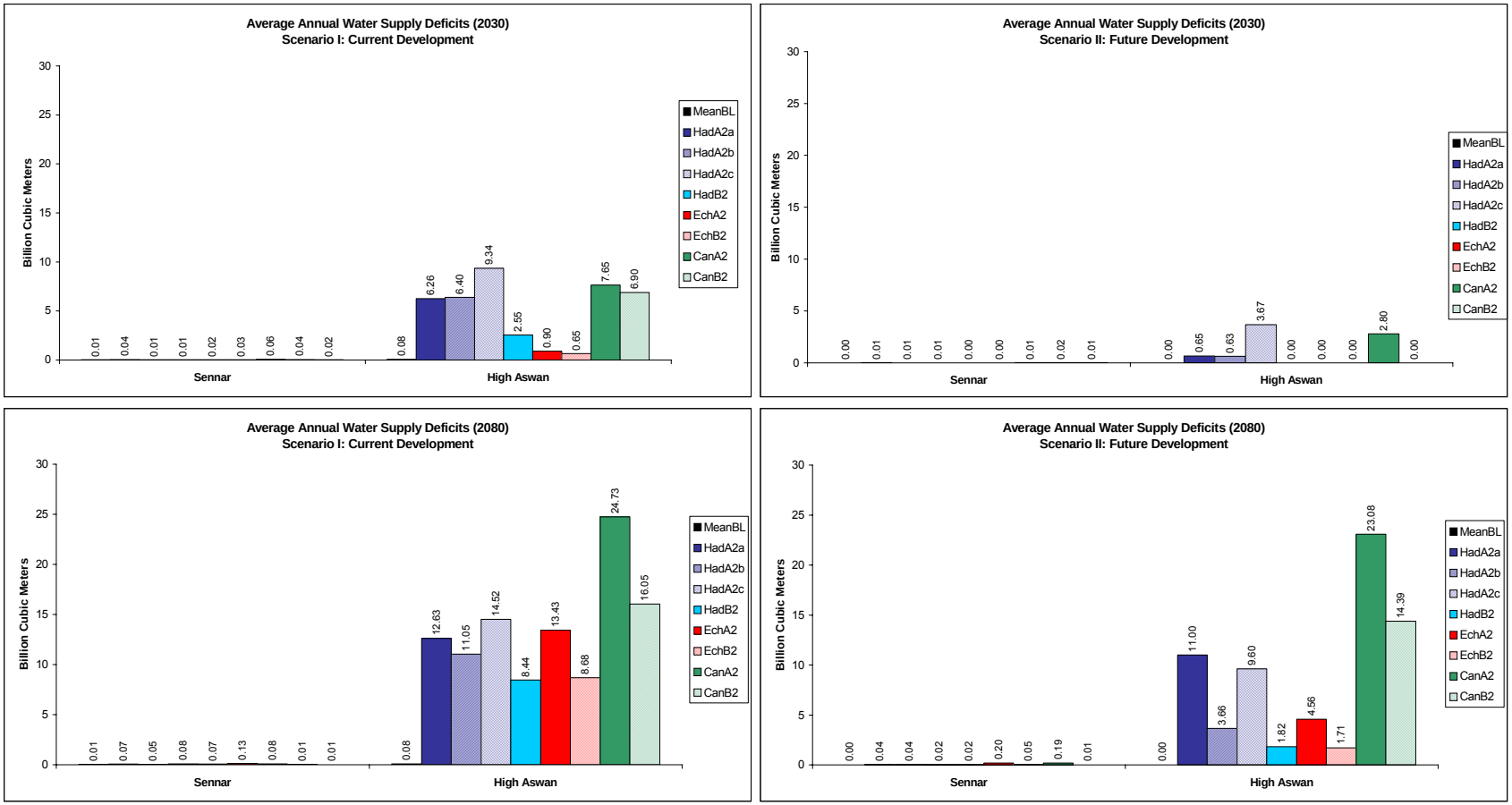

Figure 5.2: Mean annual water supply deficit.

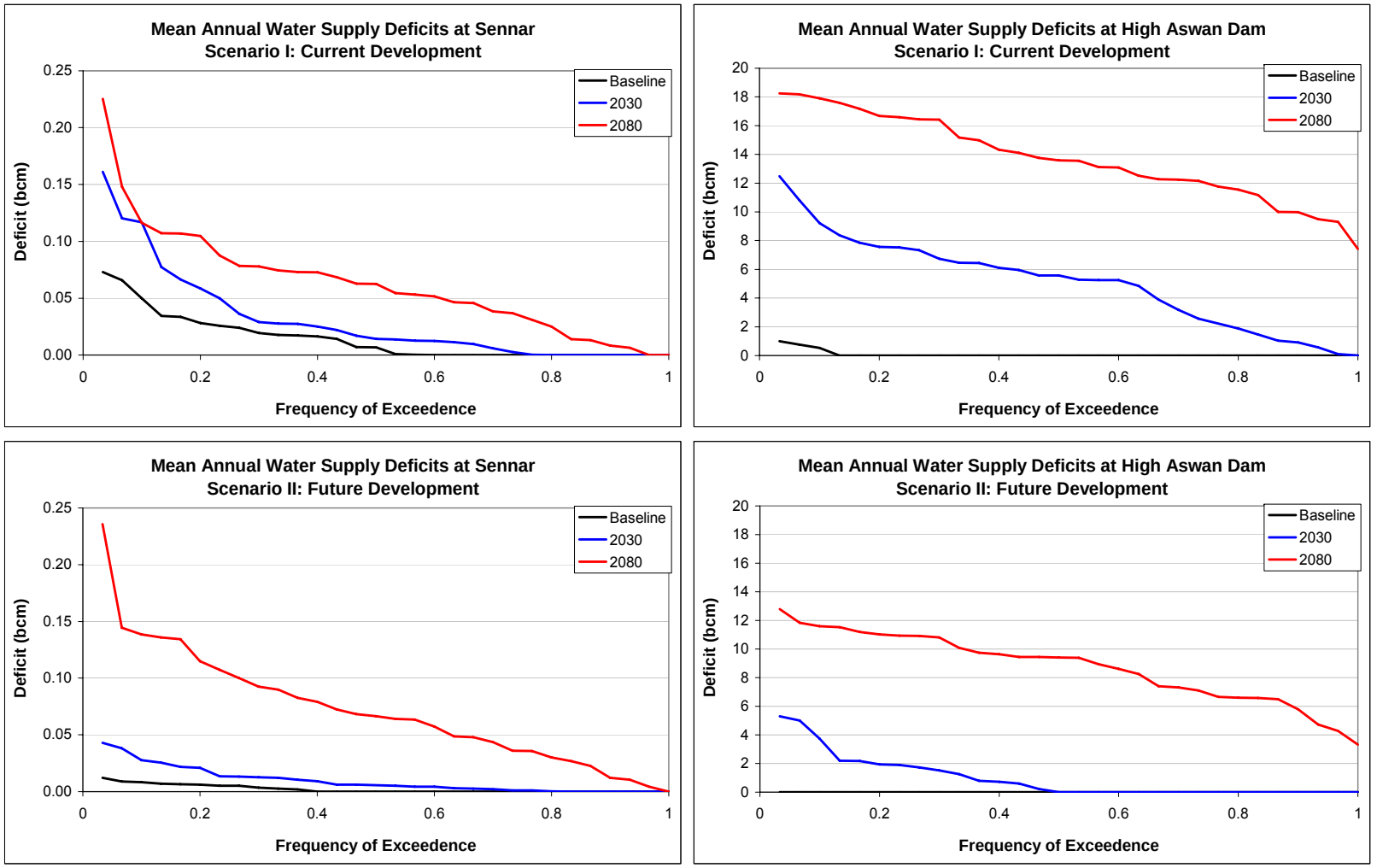

Figure 5.3: Mean annual water supply deficit frequency curves.

5.4.2 Sensitivity of Energy Generation to Climate Change

Figures 5.4 through 5.6 show energy generation for the Victoria Nile, Blue Nile, and Egypt. As before, the baseline values in each chart represent the simulated energy generation under baseline climate conditions but for the development scenario specified.

Scenario I: Current Development

Given the existing hydropower infrastructure, all areas of the Nile Basin show appreciable decreases in energy generation by the 2030s. The projected energy losses range from 11-62% for Lake Victoria, 3.3-6.8% for Ethiopia and Sudan, and 16.6-42.1% for Egypt. The climate scenario average for these regions is 40%, 5%, and 31%, respectively. By the 2080s the corresponding average losses grow to 61%, 10%, and 48%. Basin-wide, the average 2030 energy reductions translate into 9,224 GWH (13.2%), and the 2080 reduction amounts to 21,084 GWH (30.0%).

Scenario II: Basin -wide Development

Hydropower generation increases dramatically with basin development. The effect is most notable in the Equatorial Lakes and in Ethiopia where several new hydroelectric dams are implemented. While no new hydropower facilities are assumed in Egypt, the increased river flow due to the upstream wetland projects and greater temporal flow distribution stemming from additional reservoirs promote higher power production with respect to the current basin development. The key findings for the future development scenario are summarized as follows:

- Under the baseline climate, energy generation from the Equatorial Lakes increases nearly 8 fold, Ethiopia and Sudan more than 25 fold, and Egypt's production increases 17%;

- By 2030, production decreases, with respect to the scenario baseline, for the Equatorial Lakes, Ethiopia/Sudan, and Egypt by 23%, 8%, and 19%, respectively;
- By 2080 the Equatorial Lakes power production is reduced to 50%, Ethiopia/Sudan drops by 17%, and Egypt's production is reduced by 49%;
- Projected 2080 hydropower generation under full basin development compares to the baseline development and climate as follows: For the Equatorial Lakes, energy generation remains 4 times greater; for Ethiopia/Sudan 21 times greater, and for Egypt loses 40% of its present day production.

There are a few aspects of the frequency distributions that are also notable. Climate change is shown to affect all portions of the energy frequency distribution; however, under the full basin development scenario the top 10 to 30% of annual energy generation throughout the basin is maintained considerably higher at 2030 than under present day development conditions. The effect is somewhat smaller for Ethiopia/Sudan than it is for the Equatorial Lakes. As will be shown in the following section, full basin development allows for more adaptable reservoir management and ultimately leads to reservoir levels remaining high for a longer period before the climate change effects begin to deplete water stores.

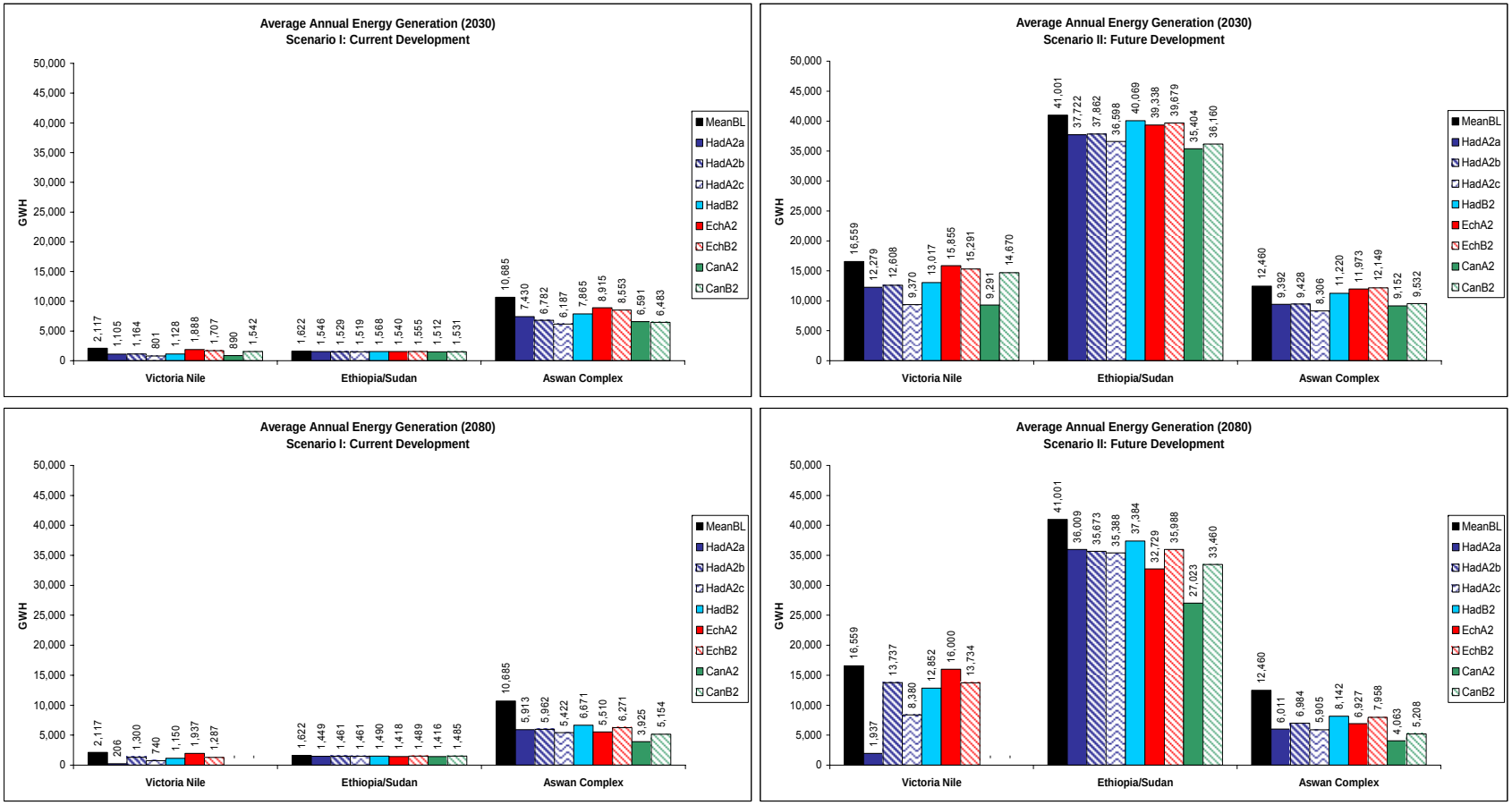

Figure 5.4: Average annual energy generation.

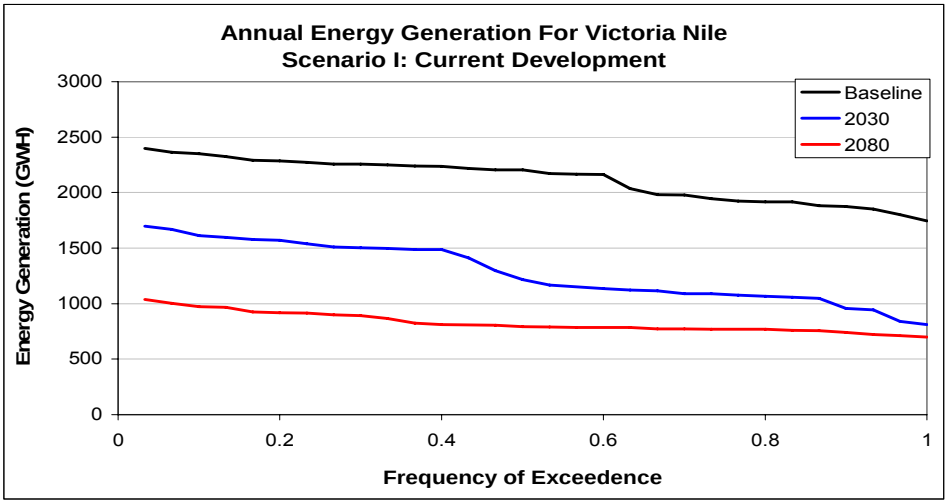

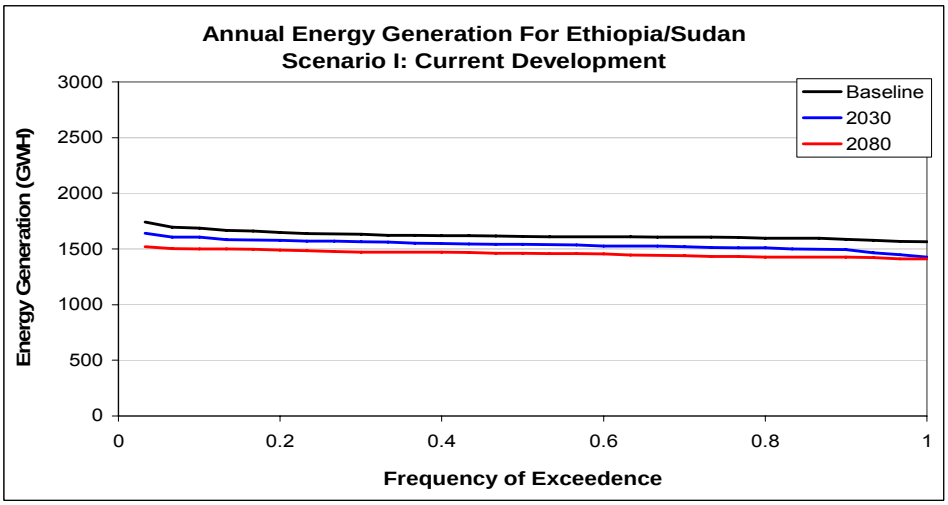

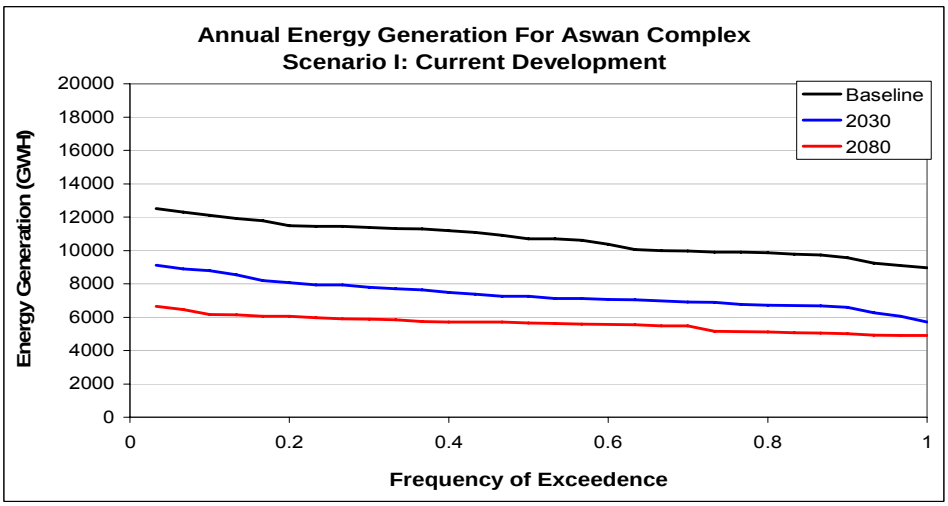

Figure 5.5: Annual energy generation frequency curves (Scenario I).

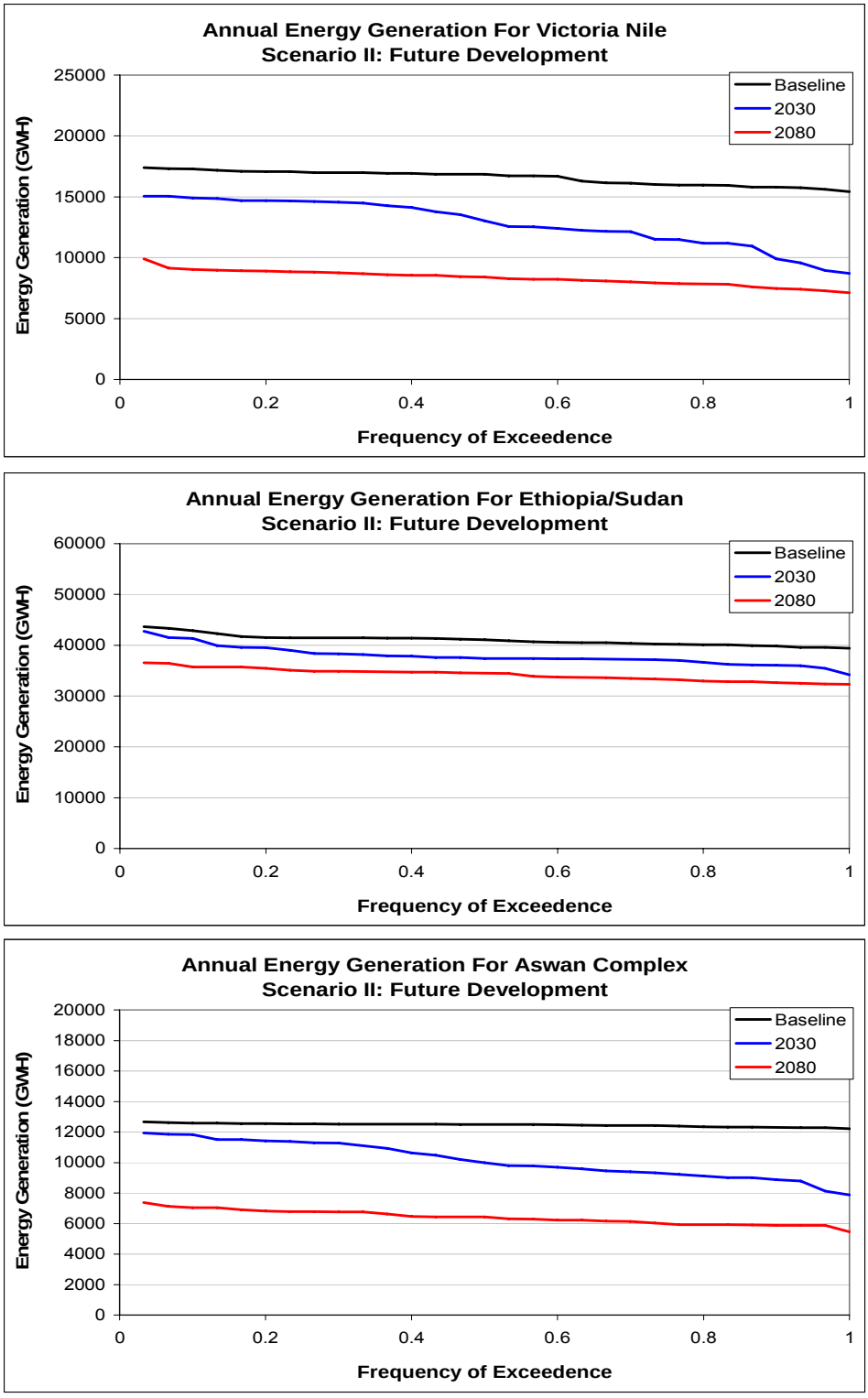

Figure 5.6: Annual energy generation frequency curves (Scenario II).

5.4.3 Sensitivity of River Flow and Reservoir Levels to Climate Change

Figure 5.7 shows the average annual flows at key points in the system: Pakwatch represents the outflow from the Equatorial Lakes; Malakal is on the White Nile below the Sudd swamps and the confluence with the Sobat River; Khartoum measures the total Blue Nile flow prior to the junction with the Main Nile; and Dongola is on the Main Nile between the outlet of the Atbara River and prior to Aswan. Monthly flow frequency curves for the same nodes are presented in Figure 5.8(a) and (b). Finally, monthly reservoir elevations for Lake Victoria and the High Aswan Dam are presented in Figures 5.9 and 5.10, respectively.

Scenario I: Current Development

Taken as an average, the climate scenarios project a 42% reduction in the annual outflow from the Equatorial Lakes by 2030. By 2080 the flows are reduced by 67%. The remaining nodes, Malakal, Khartoum, and Dongola, indicate relative reductions of 12-13% by 2030 and 25-30% by 2080.

The time series of Lake Victoria elevations indicates a steady decline in the lake storage. Over the 30 years from 2020-2049 (2030 climate) the lake remains in decline, while during the final 30 years (2080 climate) the lake has stabilized near the historical lake minimum. As a result, the lake elevation and downstream river flow frequency curves reflect a uniform shift in their distributions from the baseline to 2030 and an overall flattening at 2080. Farther downstream, at Malakal, the stream flows show fairly uniform downward shifts for both periods, which reflects the continued seasonal influence of the Sobat basin during the high flows. The outflow from the Blue Nile (Khartoum) and the downstream Main Nile node (Dongola) indicate greater stream flow reductions during peak flows than low flows. This is expected in light of the Chapter 3 hydrologic assessment, which showed dramatic decreases in the Blue Nile peak discharge.

The High Aswan dam is subject to the effects of both the reduced base flow originating in the Equatorial Lakes and the reduced annual floods associated with Blue Nile discharge. This cumulative effect is seen in Figure 5.9, where Lake Victoria is shown to stabilize at its lowest levels around 2070, but the High Aswan dam declines much more rapidly and reaches its lowest levels by 2030.

Scenario II: Basin -wide Development

The effect of basin wide development can be assessed by comparing the results of Scenarios I and II under the baseline climate. Doing so reveals the following results: average annual flows from the Equatorial Lakes are unaffected; flow below the Sudd swamps and after the Sobat junction is increased by 11 bcm per year; the Blue Nile loses 1 bcm per year; and Dongola gains an additional 8 bcm per year; and minimum flows are increased, while maximum flows decreased at Khartoum and Dongola. Since there is no change within the Equatorial Lakes, the annual gains at Malakal are attributable to the operation of the Jonglei Canal and the wetland projects in the Bahr el Ghazal and Machar Marshes. Recall that the combined maximum benefits from these projects is 11.75 bcm per year, and, under the baseline climate, 94% of the maximum benefit is realized (11 bcm). The Blue Nile, on the other hand, loses 1 bcm per year due to evaporative losses over multiple reservoirs. The cumulative effect of all projects is reflected in the 8 bcm gain at Dongola. It is notable that this analysis ignores the detrimental effects that the Jonglei Canal might have for the Sudd environment and economy. Such analysis will be carried out as part of future assessments.

The relative benefit of basin development diminishes over time due to the impact of climate change. This can be assessed by comparing the charts in Figure 5.7 from left (current development) to right (future development). For 2030, it is seen that the original 11 bcm per year benefit at Malakal is slightly reduced to 10.1 bcm. By 2080, though, the

benefit from these projects drops to 7.4 bcm. In an absolute sense, however, there is an overwhelming benefit to basin development. Under the baseline climate and current development conditions, the average annual flow at Malakal is 32 bcm. Maintaining the status quo results in an average annual flow of 28 bcm at 2030, or a net loss of 4 bcm per year. Under full development the expected yield is 38 bcm, or a net gain of 6 bcm per year. At 2080, the net loss under current development is 10 bcm, while under full development the loss is merely 2 bcm. Therefore, full implementation of the Jonglei Canal and the wetland projects could potentially mitigate the adverse impacts of climate change on downstream water supply to a large extent. However, the cost of the Sudd itself remains to be assessed.

In addition to increased annual flows along the White Nile, the full development scenario leads to greater flow management throughout the system. This is most evident in the elevation sequences for the High Aswan Dam (Figure 5.10). Under current development conditions, the reservoir is rapidly depleted, reaching its lower storage limit around the 2050s. With upstream development, however, the reservoir can be maintained near the top of its range until the 2030s, after which it begins a steady decline reaching the lower storage limit in the 2080s. The extended period of high reservoir levels not only reflects better system adaptability to climate change, but leads to increased power production for each unit release through the turbines.

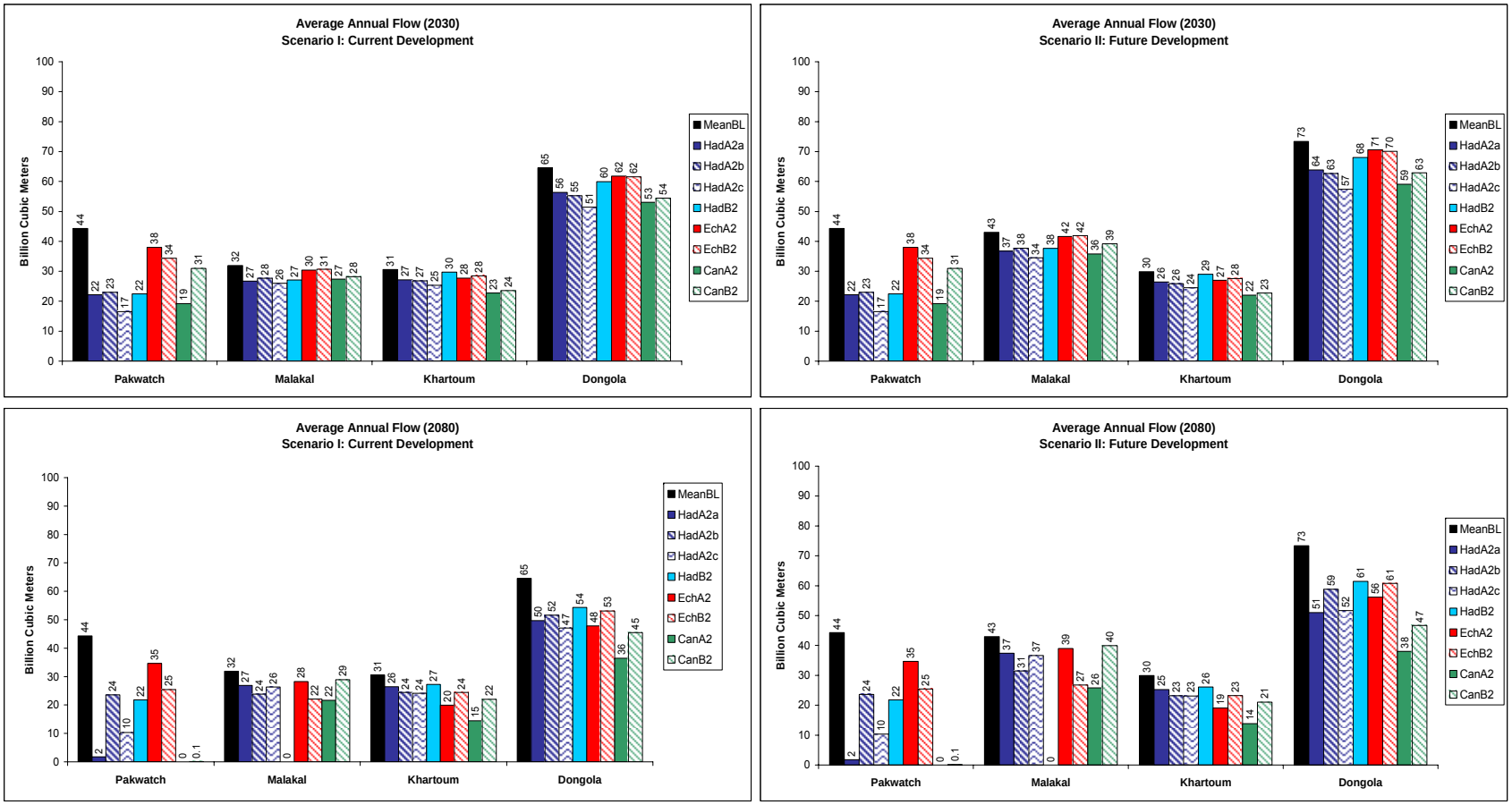

Figure 5.7: Average annual river flow.

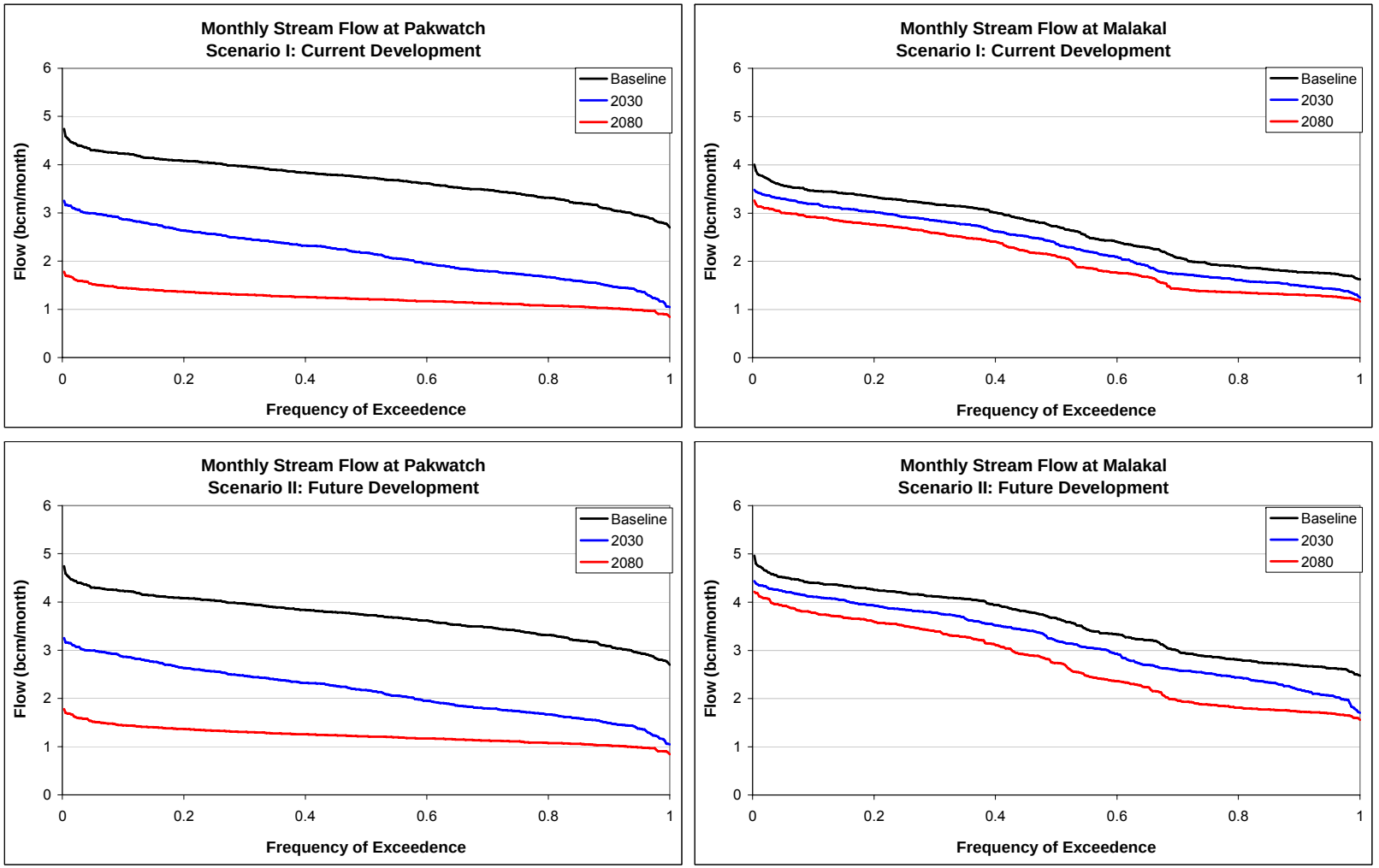

Figure 5.8(a): Monthly river flow frequency curves.

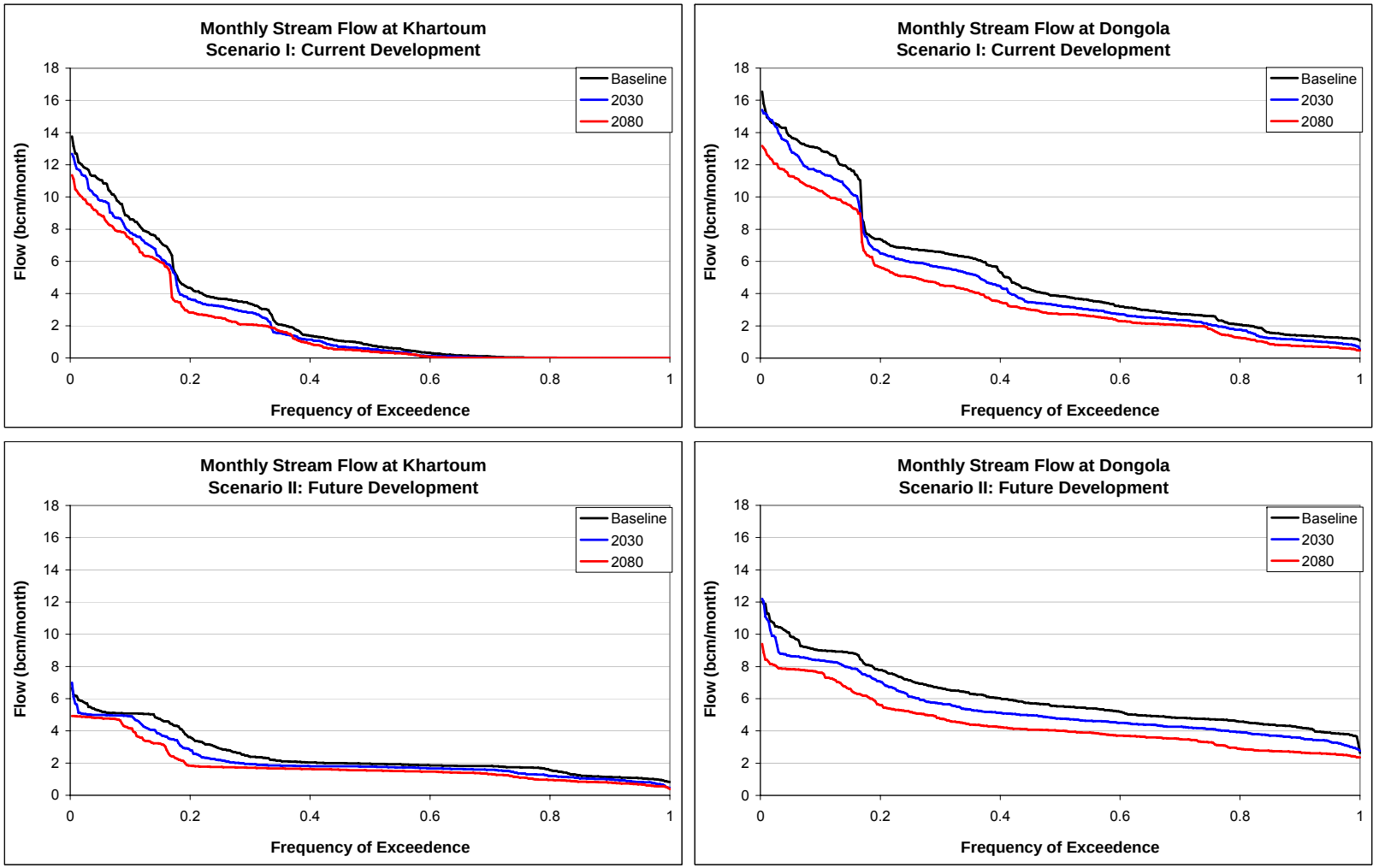

Figure 5.8(b): Monthly river flow frequency curves.

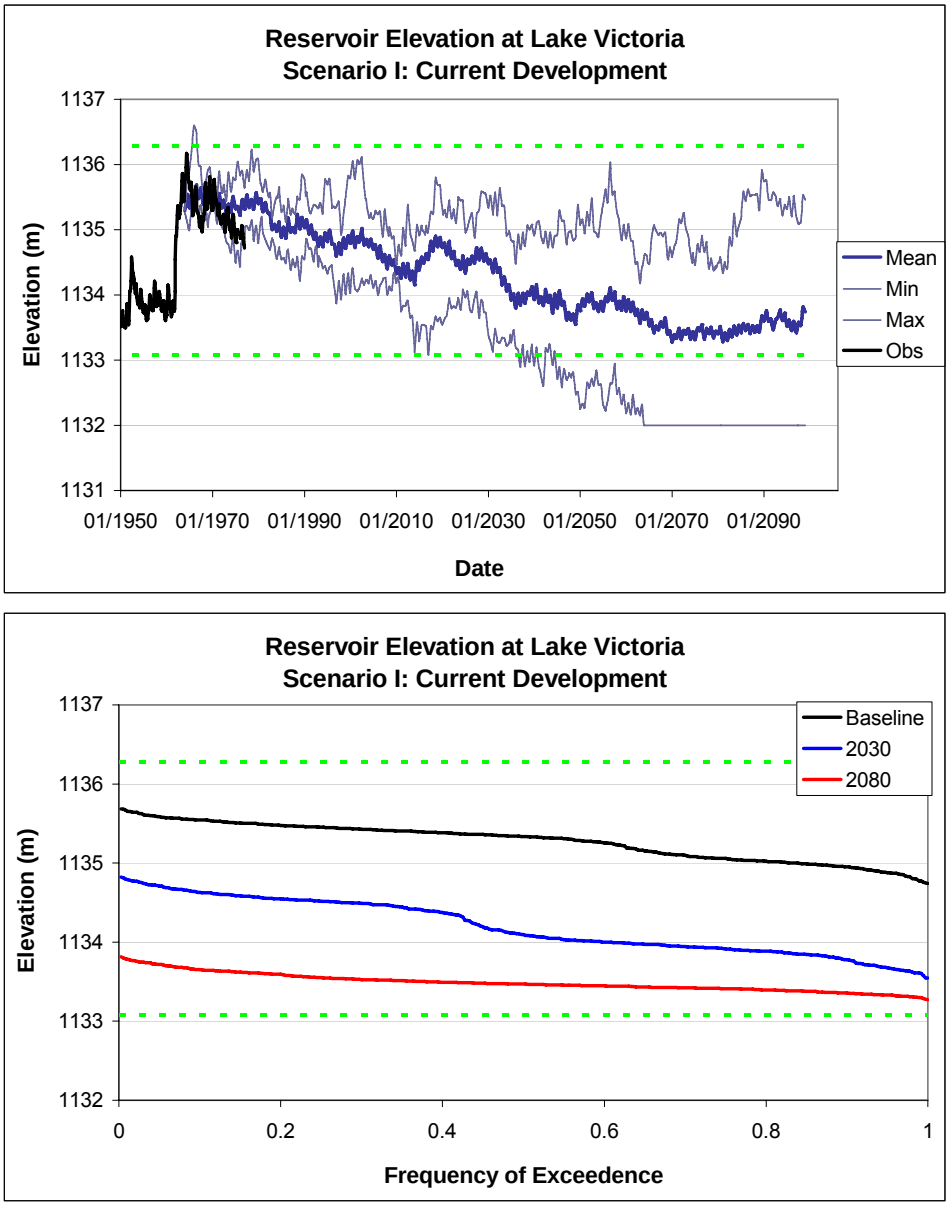

Figure 5.9: Monthly lake level at Lake Victoria.

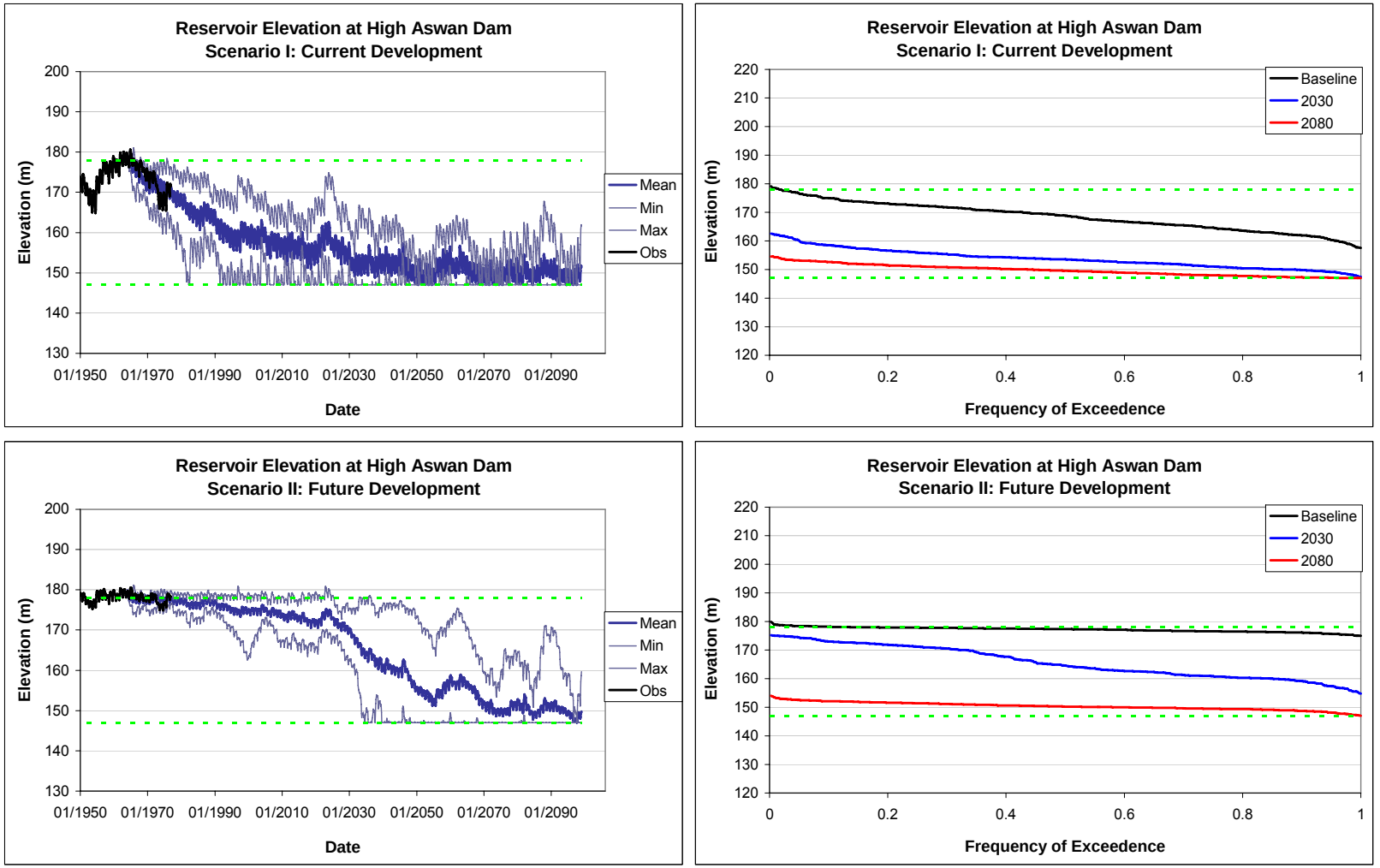

Figure 5.10: Monthly reservoir elevation at High Aswan Dam.

5.5 Summary Remarks on Water Resources Assessments

Climate and hydrologic assessments have been combined with a comprehensive water resources modeling and management tool (Nile-DST) to effectively translate projected climate change into meaningful implications for water resources planning and management in the Nile Basin. In doing so, regional and basin-wide sensitivity to climate change and basin development has been quantified with respect to water supply, energy generation, and river flows. What follows is a summary of the findings.

Southern Nile

Future climate scenarios drive significant reductions to the outflow of the Equatorial Lakes region. Outflows are projected to decrease by 18 and 30 bcm per year by 2030 and 2080, respectively. Accordingly, hydropower drops from more than 2100 GWH to less than 1300 and 850 GWH by 2030 and 2080, respectively.

Development options assessed for the Equatorial Lakes region involve hydropower expansion along the Victoria and Kyoga Niles. Downstream development included water conservation measures in the regions of the Sudd swamps and Machar Marshes. Under the future development scenario, baseline hydropower increases to as much as 16,500 GWH. Under the most adverse climate conditions (2080) the increased hydropower remains nearly 4 times greater than current output.

Water gains through the wetlands projects help to mitigate climate induced flow reductions. Under the baseline, the projects augment flow by 11 bcm; by 2030 the gain is 2 bcm, while at 2080 climate effects force a 2 bcm per year loss. In the absence of these projects, 2080 flow reductions are estimated at 10 bcm.

Eastern Nile

Hydropower generation on the Blue Nile and Atbara Rivers is presently around 1,600 GWH per year. The future development scenario for the Blue Nile involves implementation of five hydropower facilities within the Ethiopian portion of the basin. These facilities are shown to increase the Ethiopia/Sudan energy generation to as much as 41,000 GWH with baseline climate. Climate change effects may reduce the production to approximately 38,000 and 34,000 GWH by 2030 and 2080, respectively. Even under the projected 2080 climate, hydropower production for Ethiopian and Sudan remains at nearly 21 times the current output.

Water supply remains largely adequate along the Blue Nile, with both present and future development scenarios. However, the introduction of new reservoirs on the Upper Blue Nile acts to significantly decrease flood risks at Khartoum and augment the dry period low flows. As a result, Sudan water supply reliability is increased and the seasonal fluctuation range of the High Aswan reservoir level is reduced. The latter implies higher energy generation and drought protection.

Main Nile

In the absence of further basin development, climate change impacts on the Main Nile are projected to include significantly reduced river flow, decreased energy generation, and water supply deficits. By 2030, Egypt's water supply is projected to fall short of demand by 5 bcm per year. This is accompanied by a 30% drop in hydropower from 10,700 to 7,350 GWH.

The upstream development considered in this assessment benefits Main Nile water uses in two ways. First, as previously discussed, water conservation projects on the Southern Nile increase overall flow to downstream reaches. Second, additional reservoir storage

helps to protect against drought, increase minimum flows, and provides overall greater management flexibility. Average annual flows at Dongola increase by 8 bcm at 2030 and 5 bcm at 2080. Minimum monthly flows increase from 1 to 1.5 bcm per month across all time periods. At Aswan, Egypt the upstream development effectively increases near term hydropower by as much as 17% and delays water supply deficits and severe reservoir depletion by approximately 40 years.

The assessment scenarios considered here assume no changes in water demands. However, basin development will most certainly be accompanied by demand increases. Given scenarios of future demand throughout the basin, the assessment approach demonstrated here can be expanded into a broader platform to aide planning for development, assessing potential adaptive management strategies, and as a basis for future trans-boundary cooperation.

Chapter 6: Conclusions and Recommendations

6.1 Scientific Contributions

A comprehensive new approach for assessing the hydrologic and water resources implications of potential climate change was developed. This culminated in several significant contributions:

- A new statistically based method to identify geographic regions where GCM scenarios exhibit significant simulation skill;
- A method to adjust global climate model (GCM) temperature and precipitation that preserves the internal consistency of GCMs while capturing the observed climatology;
- Development and calibration of regional hydrologic models that are temporally and spatially consistent with downscaled GCM scenarios and water resources models;
- Characterization and representation of climate and hydrologic model uncertainties through ensemble generation;
- Developed an integrated approach to climate, hydrologic, and water resources modeling that confers a realistic view of system wide river response;
- Demonstrated the relevance and importance of climate impact assessments to water resources, including the implications for future water policy and management strategies.

It is shown that skillful aspects of GCMs can be leveraged to construct historically consistent regional climates while maintaining internal model consistency. Thus, future climate changes evolve in time rather than being lumped as multi-decadal means. In

addition, future climates are not confined to the historical climate variability. Therefore, this technique overcomes many of the shortcomings of the typical delta approach, which reduces climate change scenarios to discontinuous blocks of 30-year average changes.

In the case study, major river sub-basins were modeled separately, whereas some previous studies have inferred basin-wide changes from stream flow simulations in only a few sub-basins. Moreover, individual basin climates are allowed to evolve separately in time, but subject to regional dynamics as represented by GCMs. It was shown in Chapter 4 that, in fact, the Nile sub-basins are affected differently under the climate change scenarios. A range of changes are observed, including prolonged base flow period in the Sobat River, reduced peak flow in the Blue Nile, and delayed flow accumulation during the onset of the rainy season in the Atbara basin. Taken alone, each basin plays a unique role in supplementing Main Nile flow, affecting both volume and flow distribution.

Viewed individually, it is not possible to understand the combined effects of changes in each basin. Therefore, engaging detailed water resources models has enabled a realistic view of the coordinated sub-basin responses and their impact on the entire river system. In doing so, these climate impact assessments have produced meaningful results that can now be incorporated in water management and policy-making considerations. This is demonstrated with the water resources assessments of Chapter 6, where results are presented in terms of water supply, hydropower generation, river flows, and reservoir level responses. The impacts are not only presented as average differences between future and baseline periods but also as complete time series. Thus, we have also been able to assess changes in frequency and variability. Together, the timing, duration, and magnitude of changes have bearing on flood and drought mitigation, water supply reliability, and system vulnerability.

6.2 Application to the River Nile

The Nile River case study is very important in its own right. Questions about sustainable growth and equitable water sharing agreements are at the center of such landmark initiatives as the Nile Basin Initiative (NBI). Several previous studies have attempted to quantify potential climate change impacts on the Nile, though the conclusions were inconclusive. The assessments carried out in this work have resulted in a number of improvements that lead to more definitive conclusions. First, the detailed climate assessments not only result in a wide range of plausible future climates, but they are accompanied by information about the underlying GCM skill and modeling uncertainties. This information provides an objective basis for end users to weight scenario outcomes. Second, each of the major sub-basins were modeled separately, avoiding tentative generalizations about runoff response across basins from only a few hydrologic simulations. Most importantly, the impacts of climate change have been effectively translated into implications for water resources. The assessments are carried one step further to demonstrate that climate scenarios can be used in conjunction with management models to assess the potential benefits of future development and management strategies that might mitigate adverse climate effects. It is hoped that the results of these assessments will lead to more informed Nile Basin strategies for future development, benefit and cost sharing, adaptive management, and risk assessment.

Summary of Assessment Findings

Detailed assessment findings have been presented in Chapters 3, 4, and 5 for each geographic sub region of the Nile Basin. This section serves to compile these findings but also to provide an inter-comparison of the relative sub-regional responses.

Temperature and precipitation:

- Projected temperature changes are consistent across the sub-basins, ranging from 2.6 to 5.2 °C by 2080 under the A2 emissions scenarios and 1.6 to 3.5 °C under the B2 scenarios.
- Precipitation scenarios indicate both increases and decreases by 2080. The range of projected changes appears to decrease moving northeast from Lake Victoria towards the Atbara basin.
- Equatorial lakes show the widest range of projected precipitation changes, with between -38% and +25% by 2080. However, only the Canadian scenarios show consistently lower precipitation across all watersheds.
- The Sobat basin shows similar response patterns, again with the Canadian scenarios having the only consistently lower precipitation. The range is -17% to +10%.
- Blue Nile precipitation changes by between -13 and +12%, with Hadley scenarios yielding the only projections of increased precipitation.
- While the Atbara range in precipitation is -1% to +41%, the more productive watershed 1 indicates precipitation changes between -1% and +18%.
- In spite of the widely varying precipitation projections, all scenarios result in reduced basin outflows across the region.

There is much more confidence in the temperature projections than precipitation. Significance testing indicates that temperature is represented quite well throughout the Nile basin and in all models. Furthermore, all scenarios agree that temperatures will increase substantially during the 21st century. Conversely, all models have very limited skill with respect to precipitation, and scenarios disagree as to the sign and magnitude of projected changes.

Stream flow and Net basin supply:

- Average annual reduction to net basin supplies for the equatorial lakes cumulatively range from 0.67 billion cubic meters (bcm) to 6.9 bcm (0.67 to 2.3 bcm neglecting Canadian scenarios). This is the most significant hydrologic response in the Nile.
- The second most significant flow reduction occurs in the Blue Nile, where annual flows are projected to decrease by 0.3 to 1.2 bcm.
- Additional flow reductions occur in the Sobat and Atbara basins and account for as much as 0.5 bcm of loss.

Water resources assessments:

- By 2030 annual flows are projected to decrease by 18 bcm below the equatorial lakes, 4 bcm on the Blue Nile, and 8 bcm along the Main Nile.
- By 2080, the flow reductions below the lakes, Blue Nile and Main Nile are expected to reach 30, 8, and 16 bcm, respectively.
- Lake Victoria levels decline steadily and approach the historical low level near 2070.
- The High Aswan Dam declines more rapidly and reaches the lower reservoir limit near 2030.
- Reduced river flows and storage lead to annual water supply deficits at Aswan of 5 bcm by 2030 and 13.7 bcm by 2080.
- Lake Victoria is projected to lose approximately 800 GWH of its current power production by 2030, with losses amounting to 1250 GWH by 2080.
- Aswan Complex hydropower is expected to decrease by 3350 GWH and 5100 GWH by 2030 and 2080, respectively.
- Reservoir development and water conservation projects

- Basin development helps to delay the onset of water shortages and reservoir depletion at Aswan by 40 years or longer.
- Additional hydropower facilities along the Victoria Nile and Blue Nile will maintain basin power generation at 3.5 to 4 times the current production beyond 2080.

6.3 Recommendations for Future Work

This work can be expanded in various ways that involve the climate, hydrology, and water resources components as outlined below:

1. ***Generate a broader range climate scenarios to include additional GCM experiments, provided that they are more easily accessible.*** The current study incorporates eight GCM experiments from three climate models. Experiments from additional climate models would help to improve characterization of model uncertainty through comparison of inter-model differences.

2. ***Incorporate multiple traces per GCM scenario to assess the uncertainty of initial conditions across several models.*** Multiple model traces come from the same model and atmospheric forcing scenarios and differ only with respect to the initial climate model conditions. However, the projected climates are not identical due to the sensitive dependence of the climate on initial conditions. Presently, HadCM3 is the only model with multiple traces available through the IPCC data distribution center. If multiple traces can be obtained for additional models, the climate system unpredictability can be better characterized.

3. ***Apply relative weights to the GCM-derived climate scenarios based on the model skill analysis.*** This work included a detailed analysis of GCM skill, both at individual nodes

as well as overall regional performance through field significance tests. This information can be used to expand the eight climate scenarios into a weighted ensemble based on the skill associated with each GCM experiment. An example of how this could be done is a follows. Determine the p-value, or confidence level, for each GCM run from the field significance test (Chapter 3). Assign a weight to each model run as the ratio of the individual confidence level to the summation of all model runs. Previously, 20 traces have been generated for each climate scenario that reflect the climate scenario uncertainty. Now, the number of traces generated from each scenario could be determined according to the assigned weights. For example, out of 100 total climate scenario traces, the number stemming from each GCM experiment would be 100*weight. The result is an ensemble of potential future climates that are weighted according to the confidence in a range of climate projections.

4. ***A study of the relative accuracy of statistical and dynamic downscaling methods might help to define the most suitable methods for each spatial scale of interest.*** In the Nile Basin, the relative sizes of the hydrologic units and the GCM nodes were similar enough that simple linear regression produced reasonable results. However, this will not necessarily be the case for other basins or for finer scale hydrologic models.

5. ***While various methods were used to develop conservative evaporation and evapotranspiration estimates, a more comprehensive application of Penman based methods would be useful.*** These methods require additional inputs such as net radiation, cloudiness, humidity, and wind speed. Such variables are generated by GCMs, but need to be assessed with respect to model skill and, if necessary, adjusted to conform with real measurements.

6. ***Expand the water resources assessments to include more demand, development, and water management scenarios.*** More water resources assessments would serve to highlight the socio-economic impacts of climate change for the Nile Basin, as well as the development and management strategies that would best mitigate adverse impacts.

Appendix A

Temperature and Precipitation Spatial Relationships

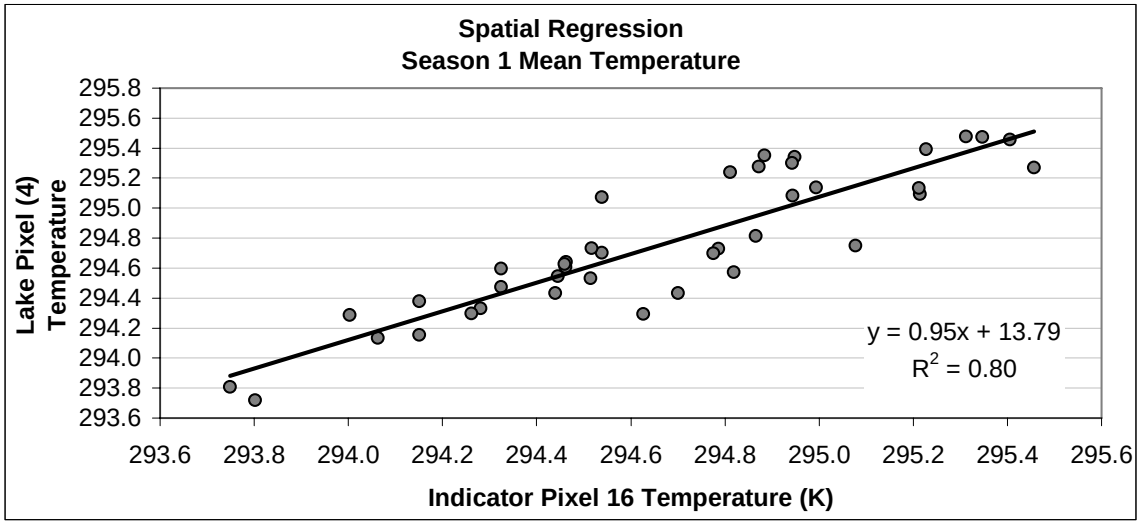

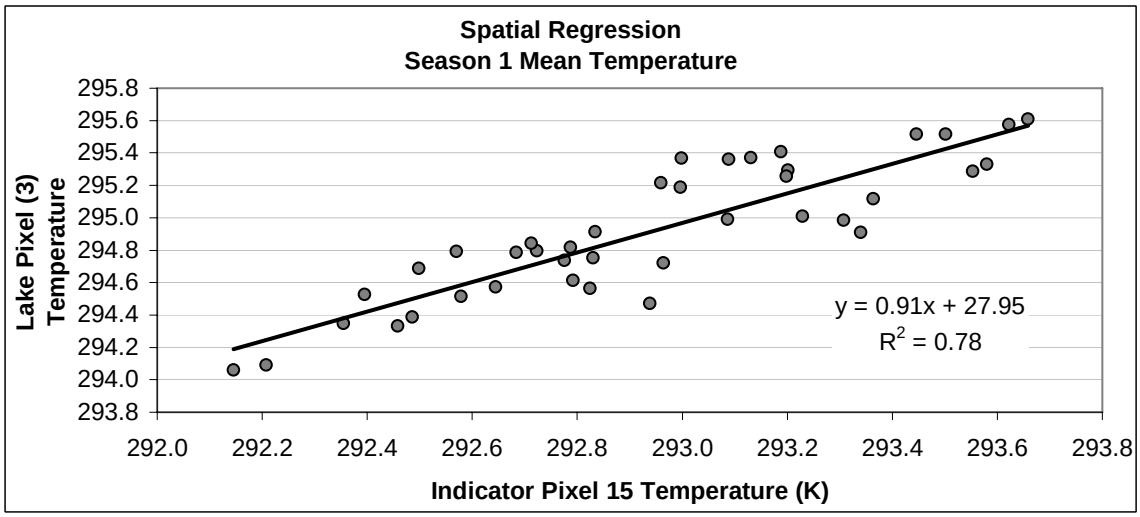

Figure A.1(a-b): Lake Victoria Indicator-Target pixel temperature relationships (S 1).

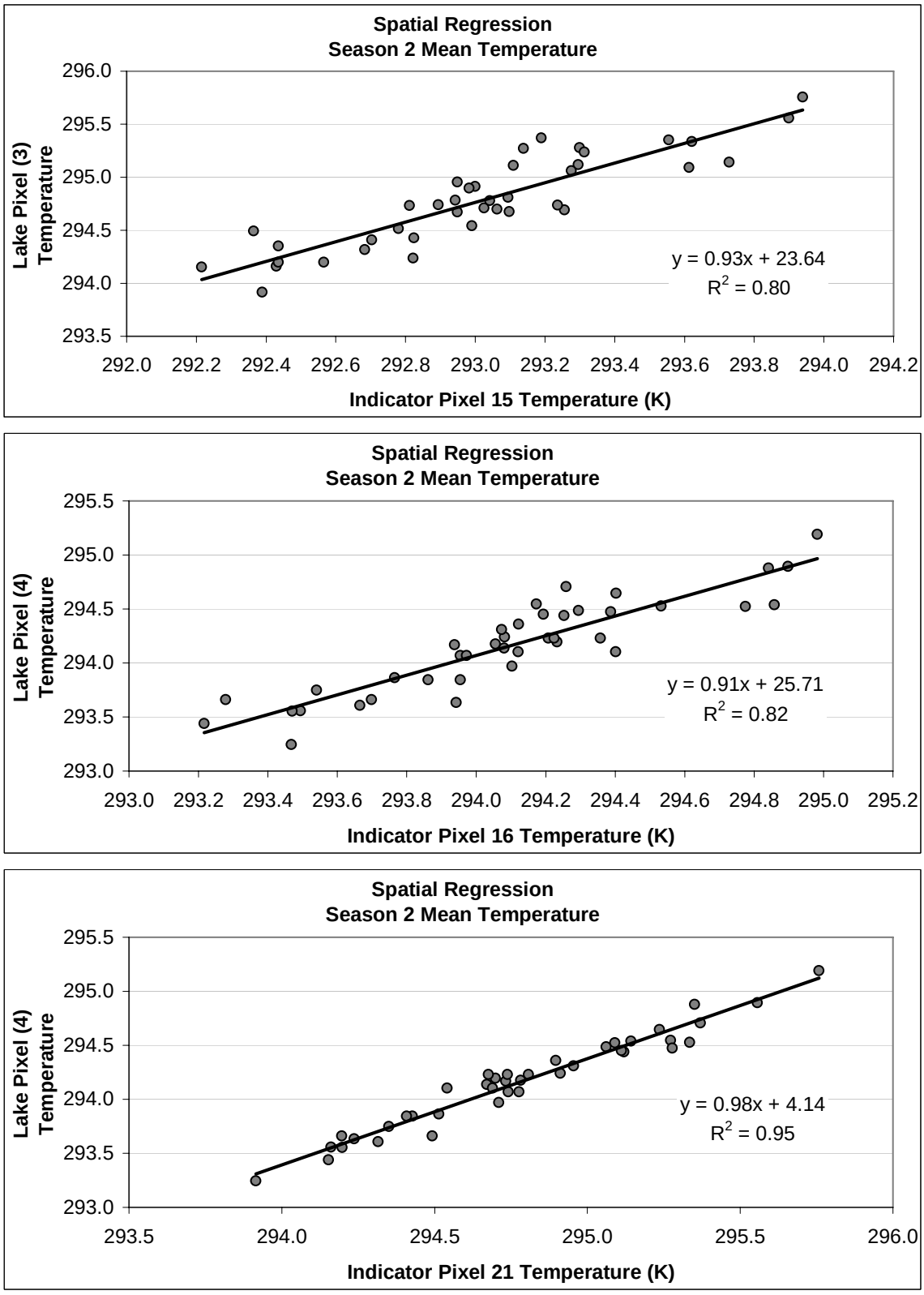

Figure A.2(a-c): Lake Victoria Indicator-Target pixel temperature relationships (S 2).

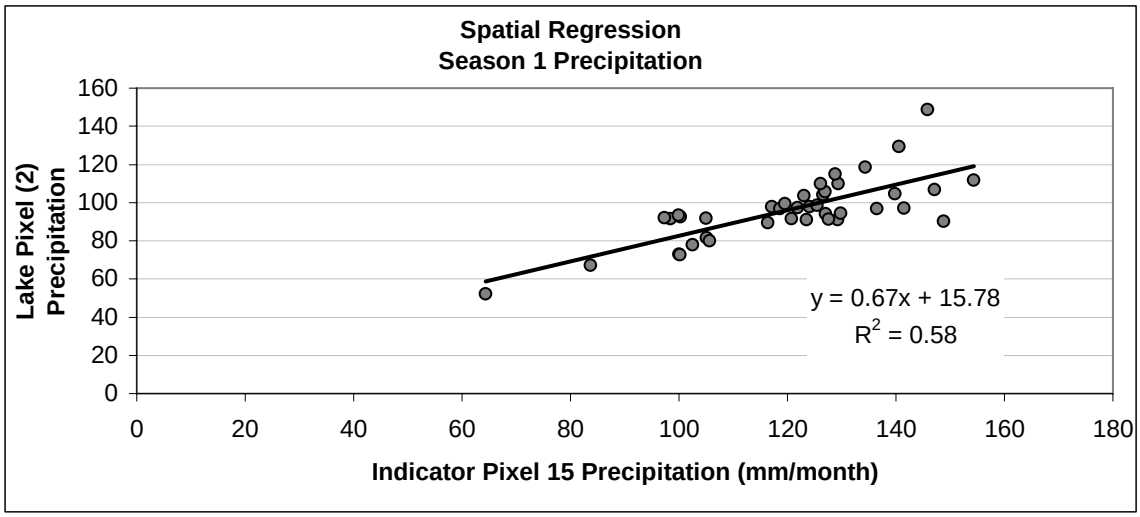

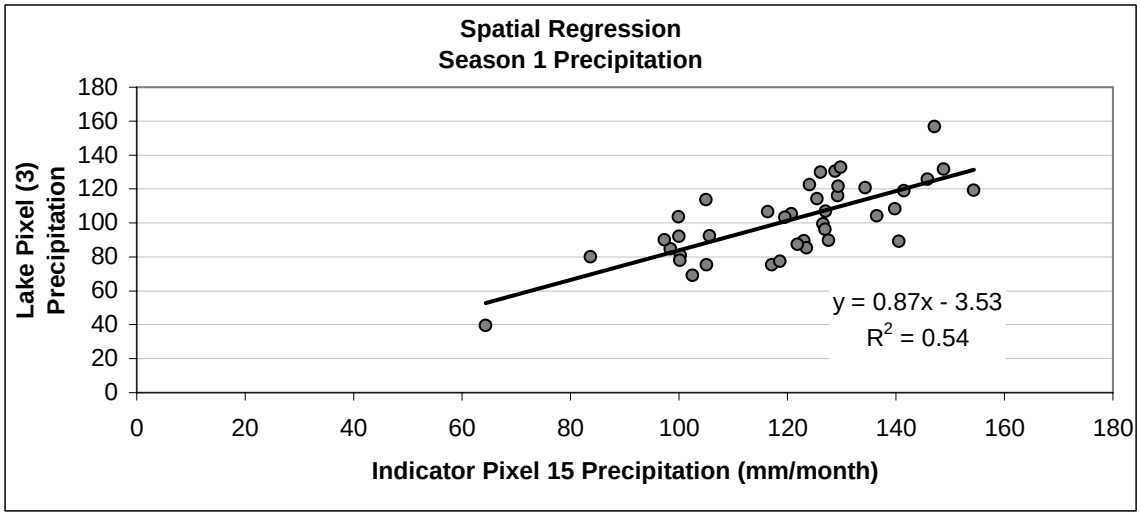

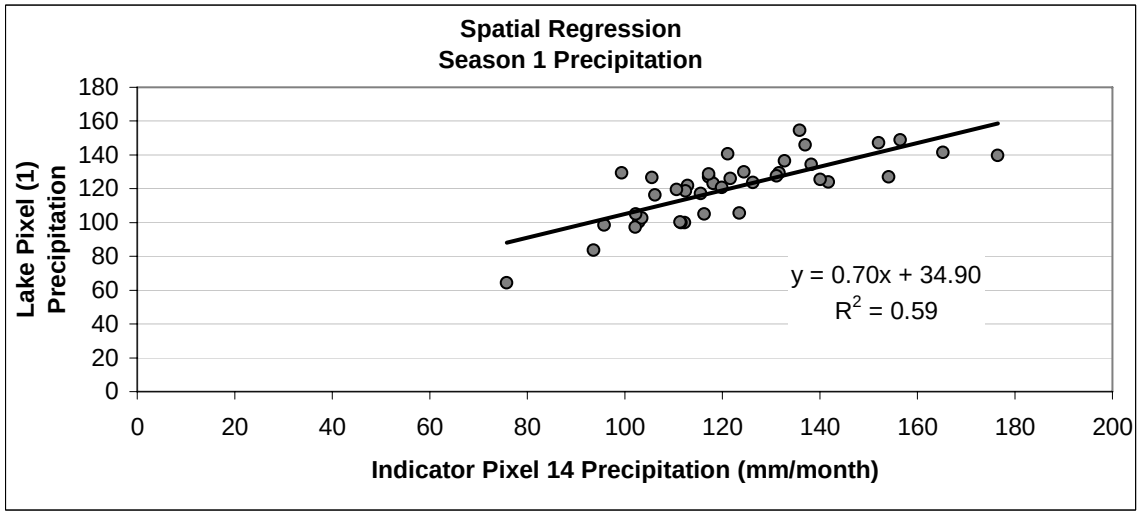

Figure A.3(a-c): Lake Victoria Indicator-Target pixel precipitation relationships (S 1).

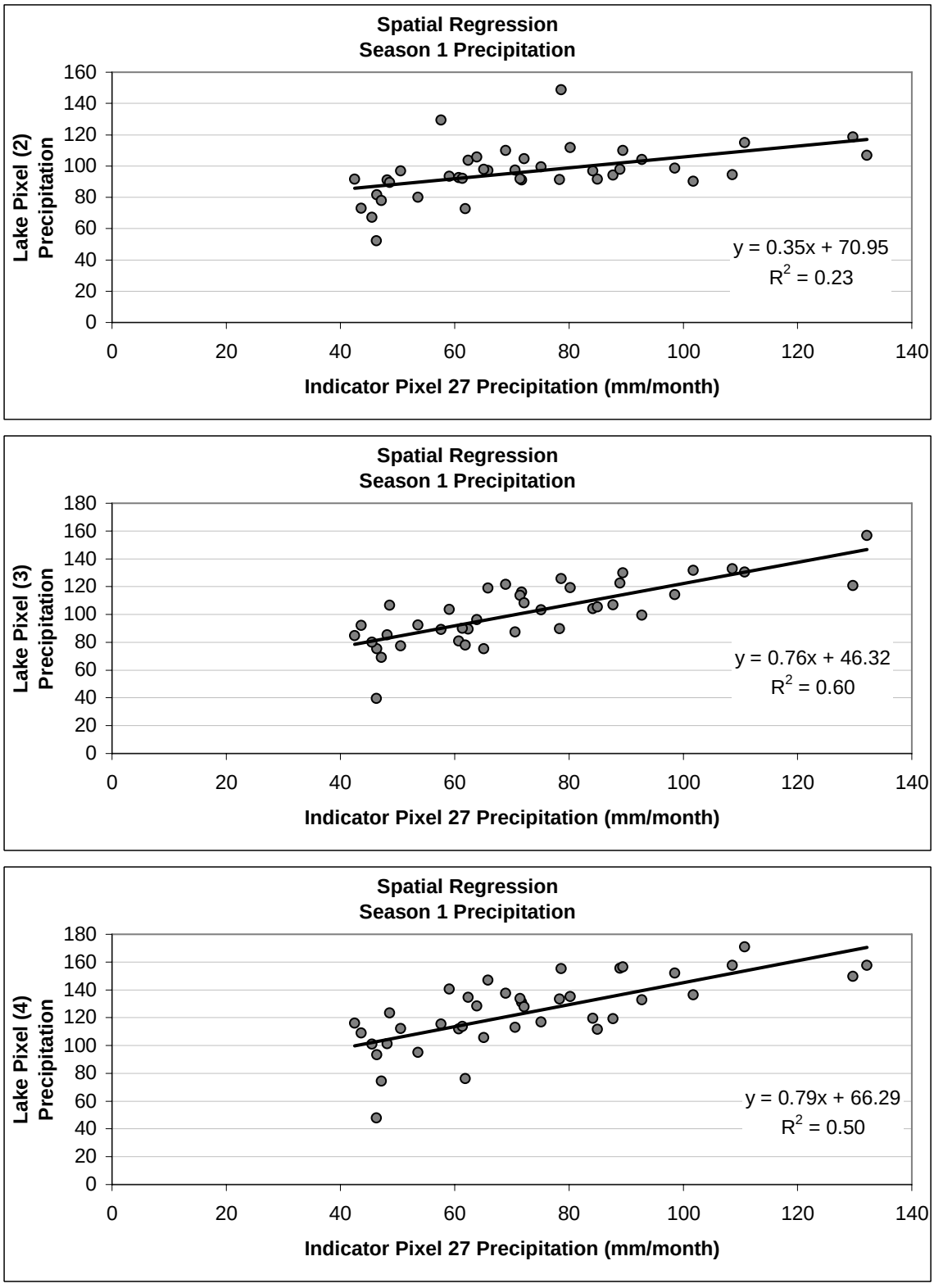

Figure A.3(d-f): Lake Victoria Indicator-Target pixel precipitation relationships (S 1).

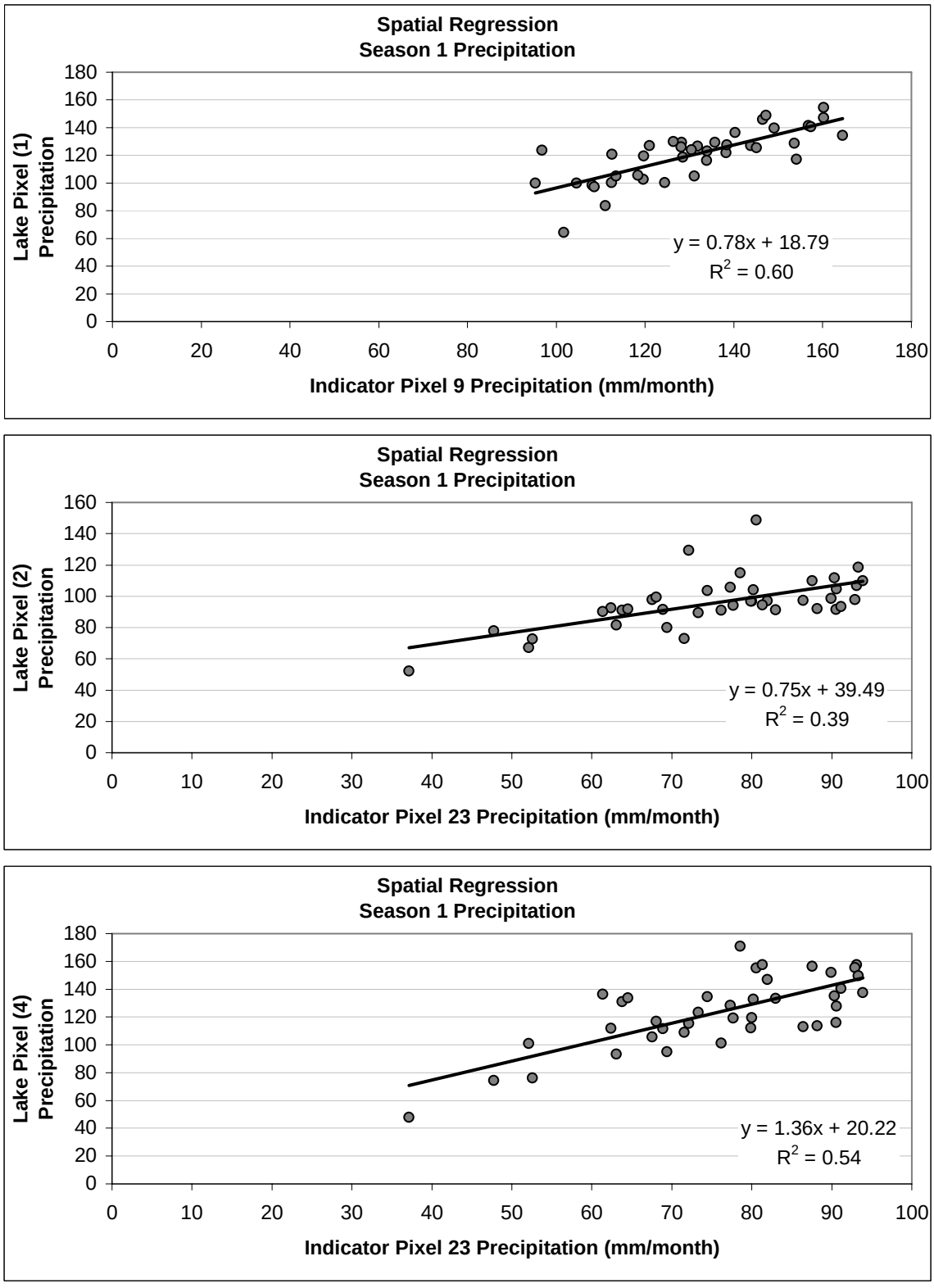

Figure A.3(g-i): Lake Victoria Indicator-Target pixel precipitation relationships (S 1).

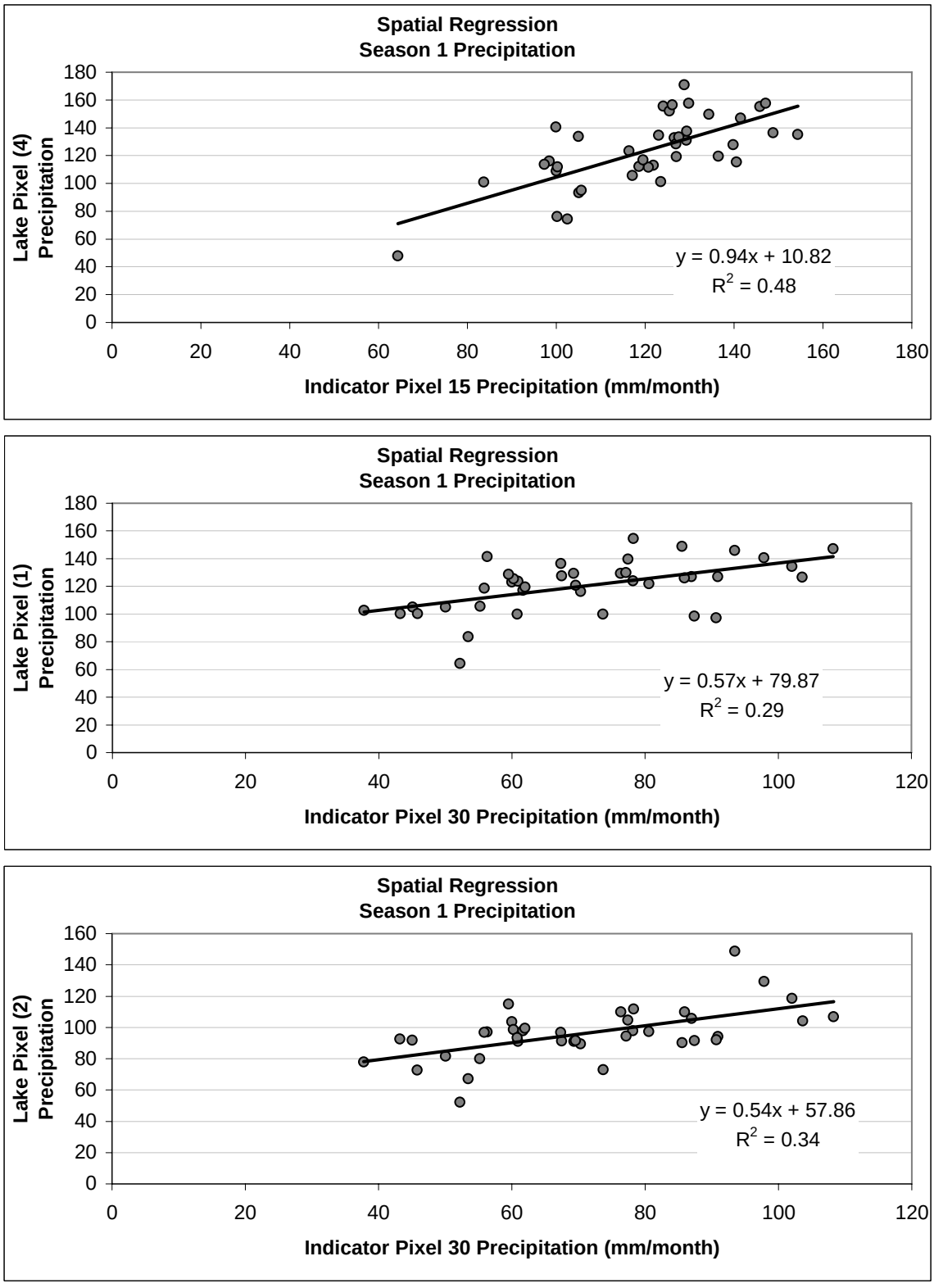

Figure A.3(j-l): Lake Victoria Indicator-Target pixel precipitation relationships (S 1).

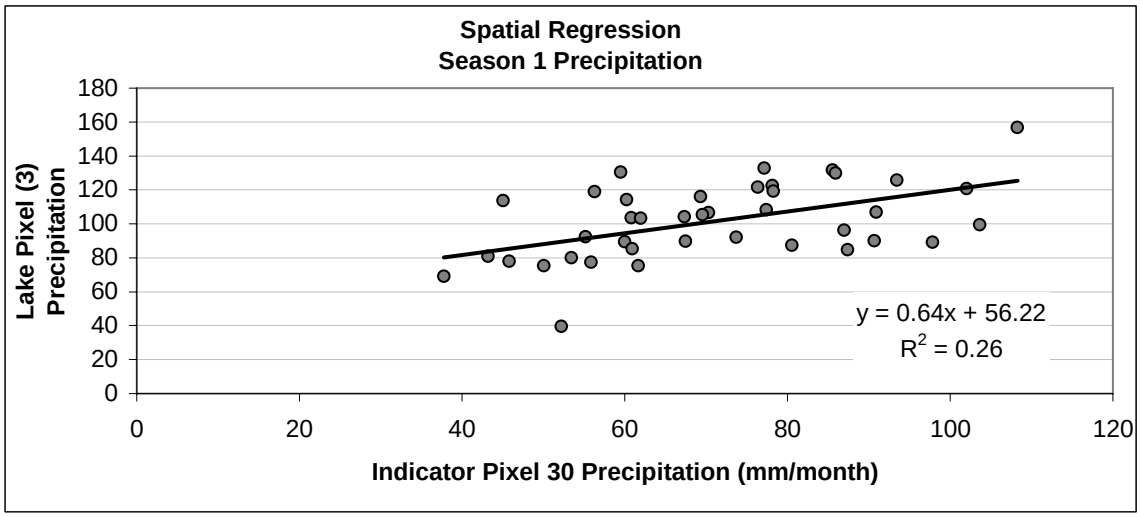

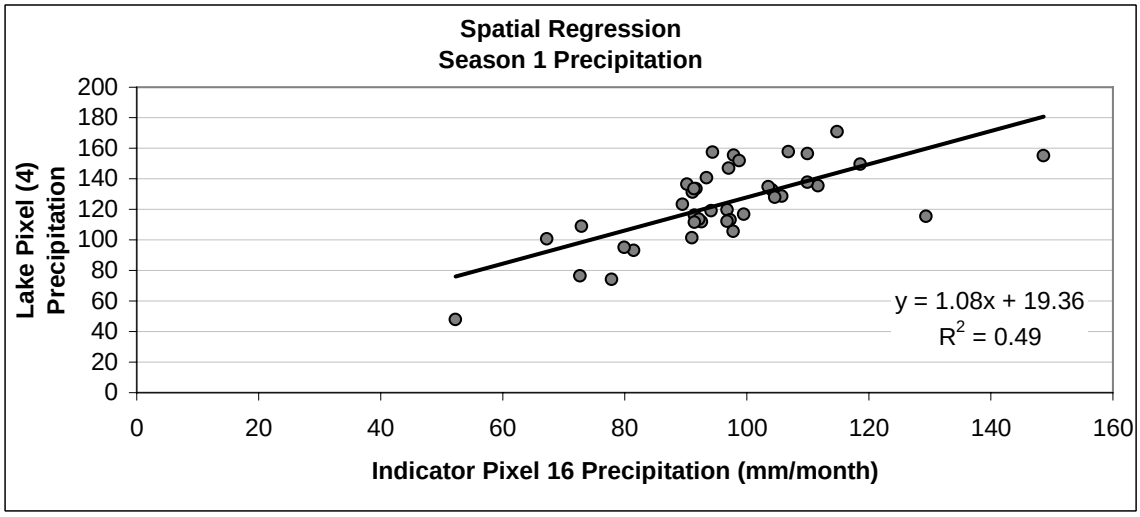

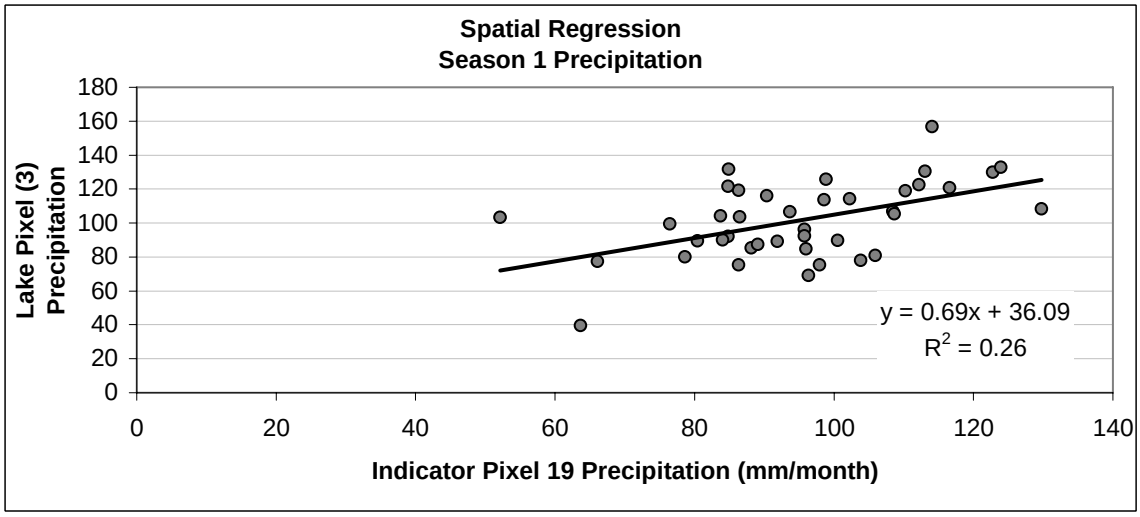

Figure A.3(m-o): Lake Victoria Indicator-Target pixel precipitation relationships (S 1).

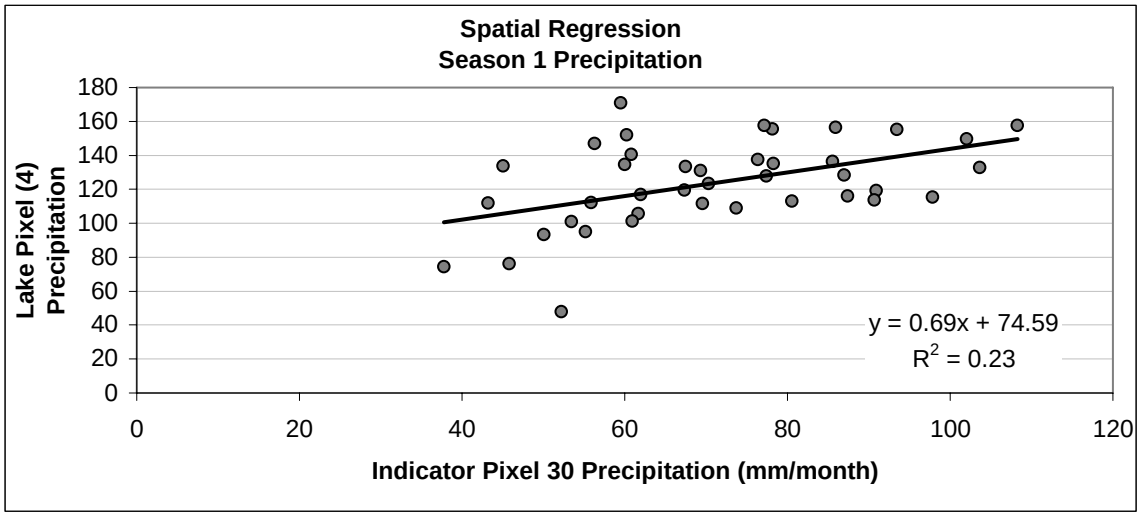

Figure A.3(p): Lake Victoria Indicator-Target pixel precipitation relationships (S 1).

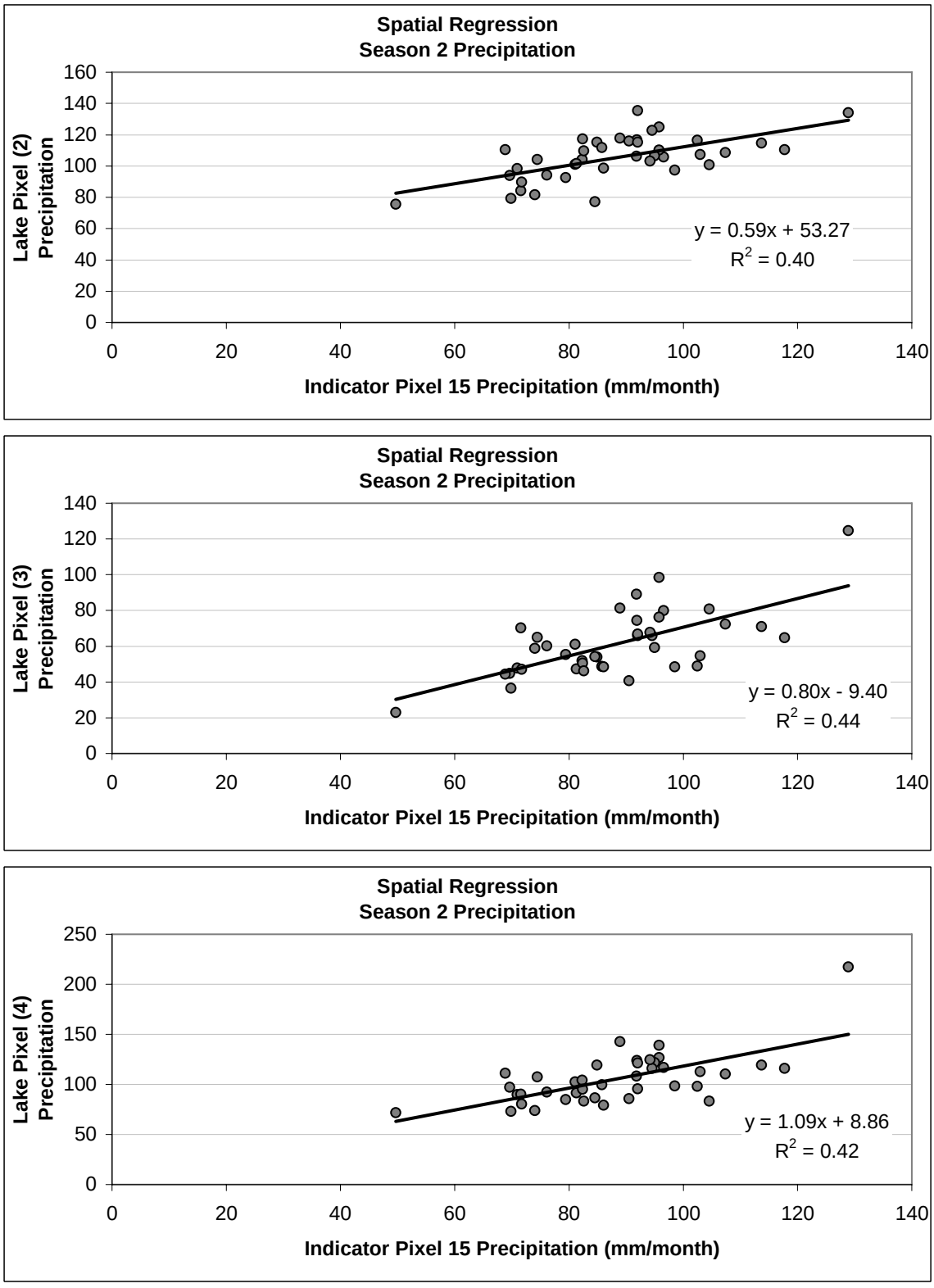

Figure A.4(a-c): Lake Victoria Indicator-Target pixel precipitation relationships (S 2).

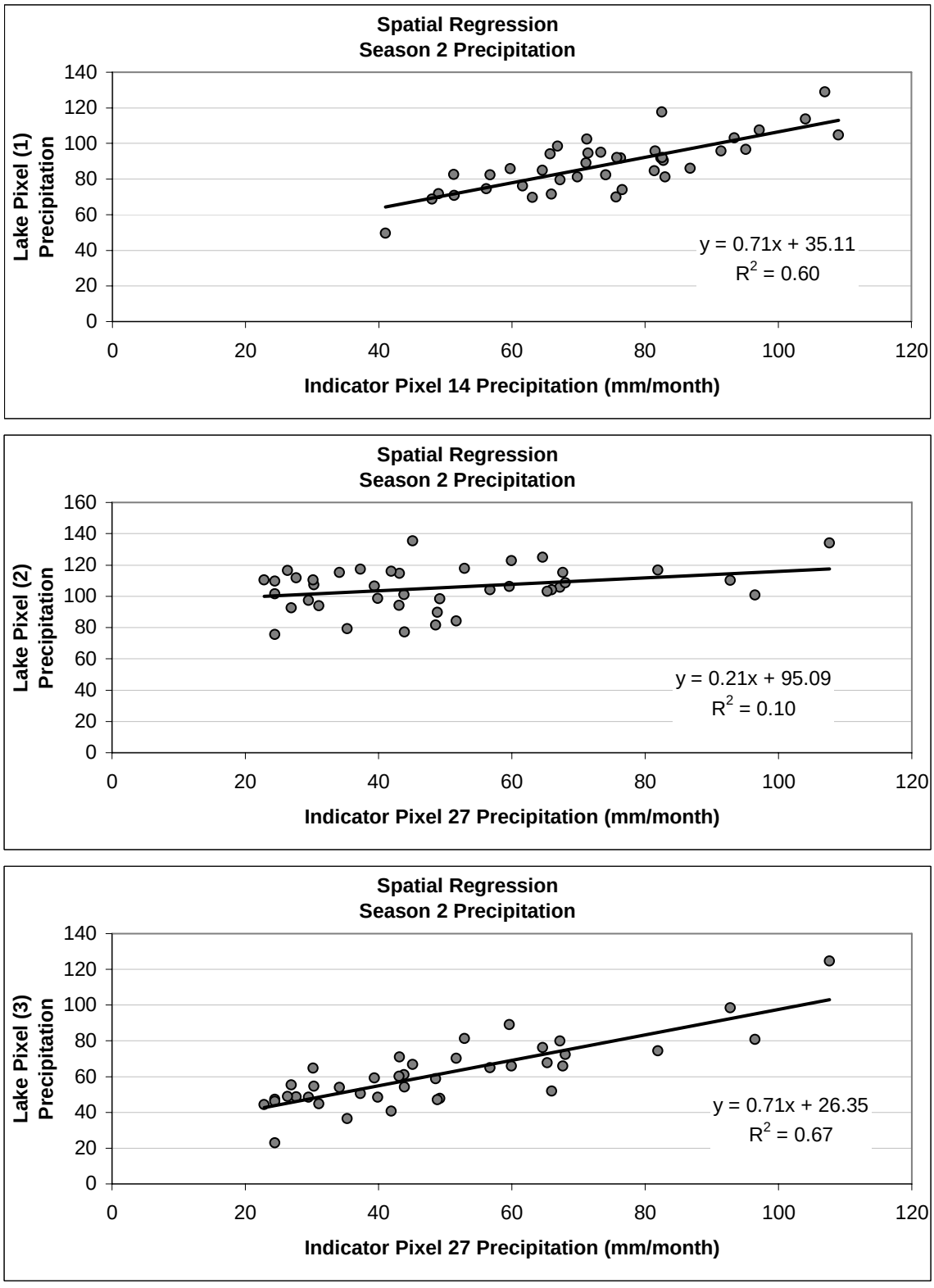

Figure A.4(d-f): Lake Victoria Indicator-Target pixel precipitation relationships (S 2).

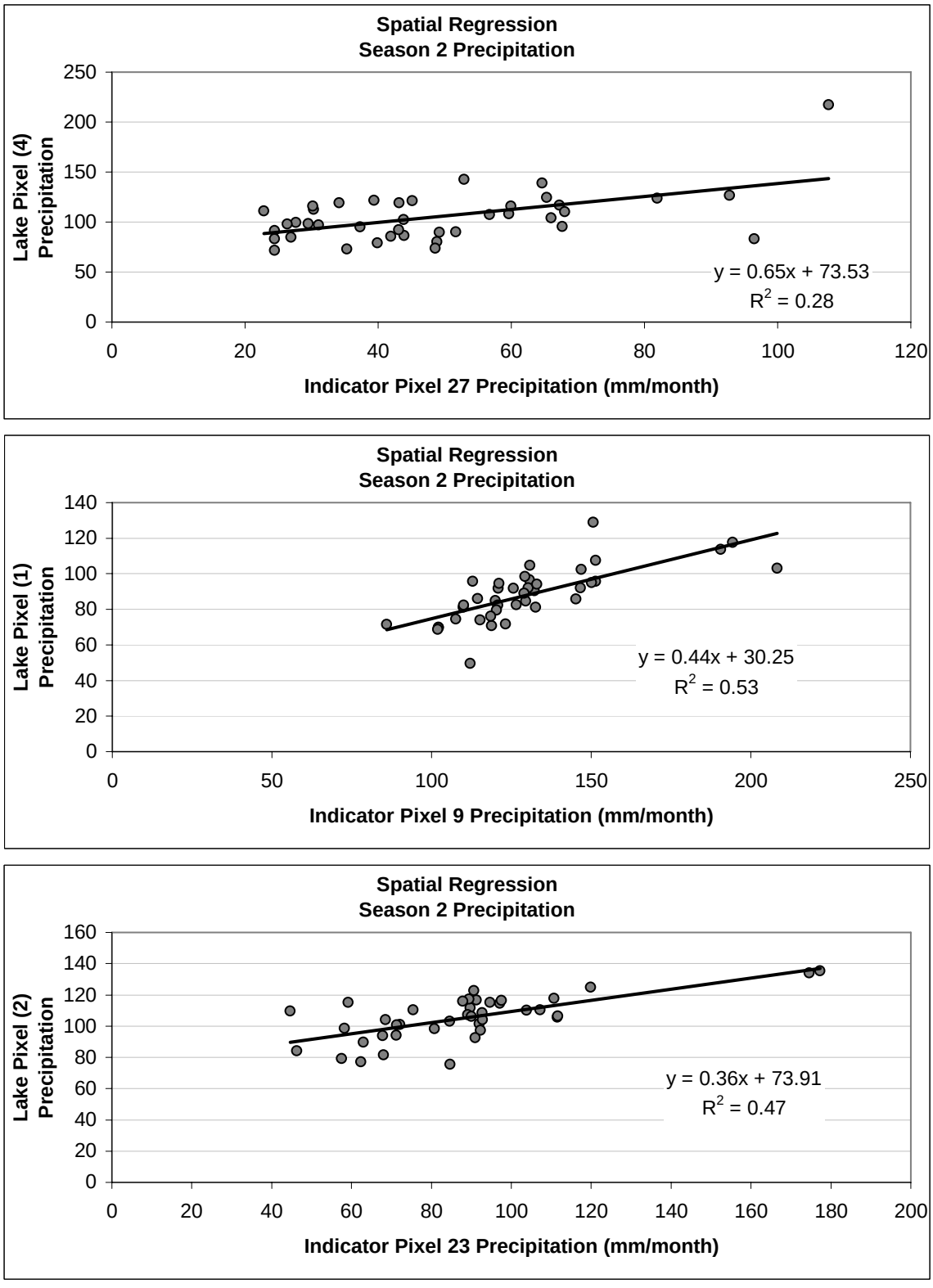

Figure A.4(g-i): Lake Victoria Indicator-Target pixel precipitation relationships (S 2).

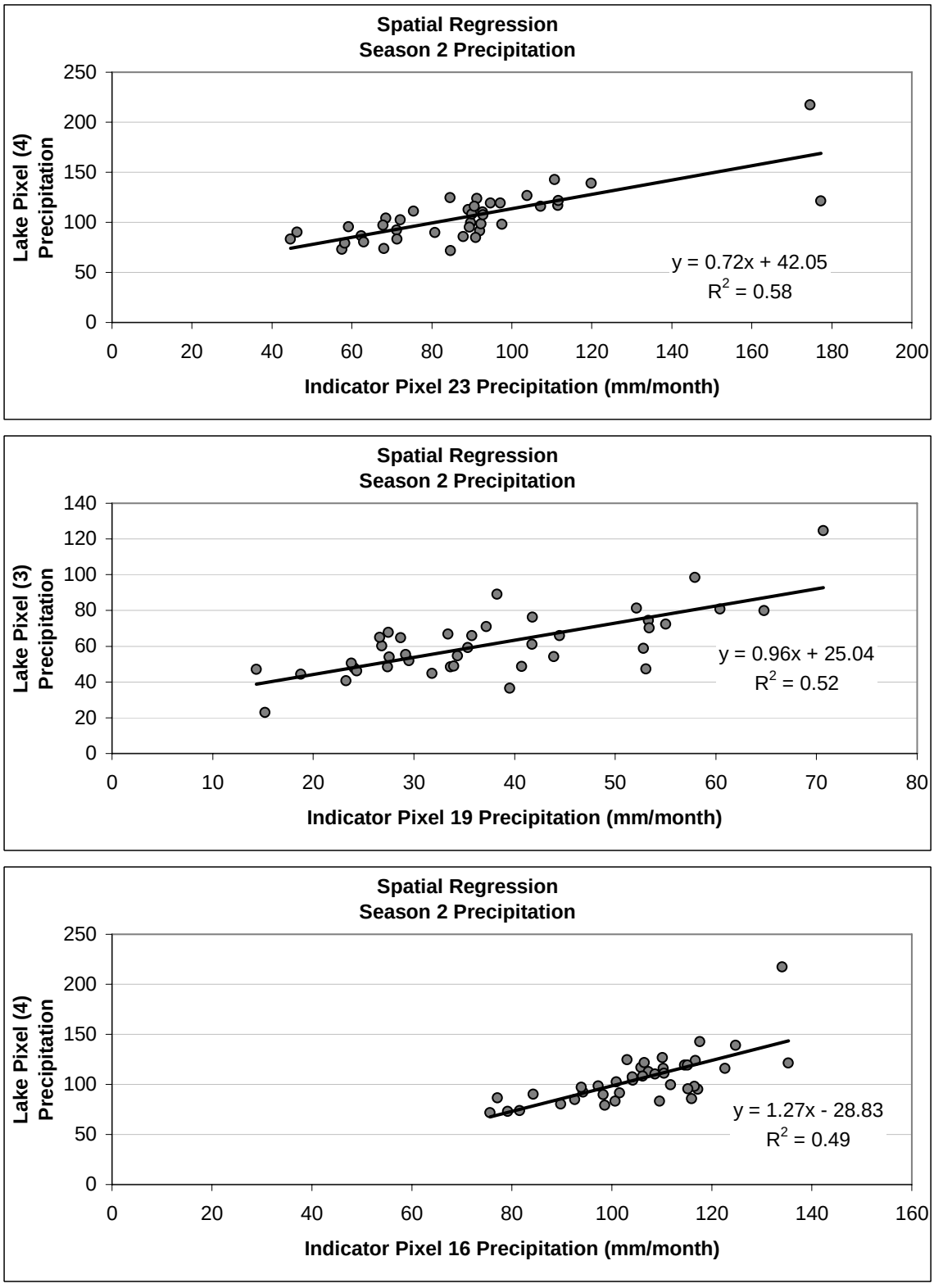

Figure A.4(j-l): Lake Victoria Indicator-Target pixel precipitation relationships (S 2).

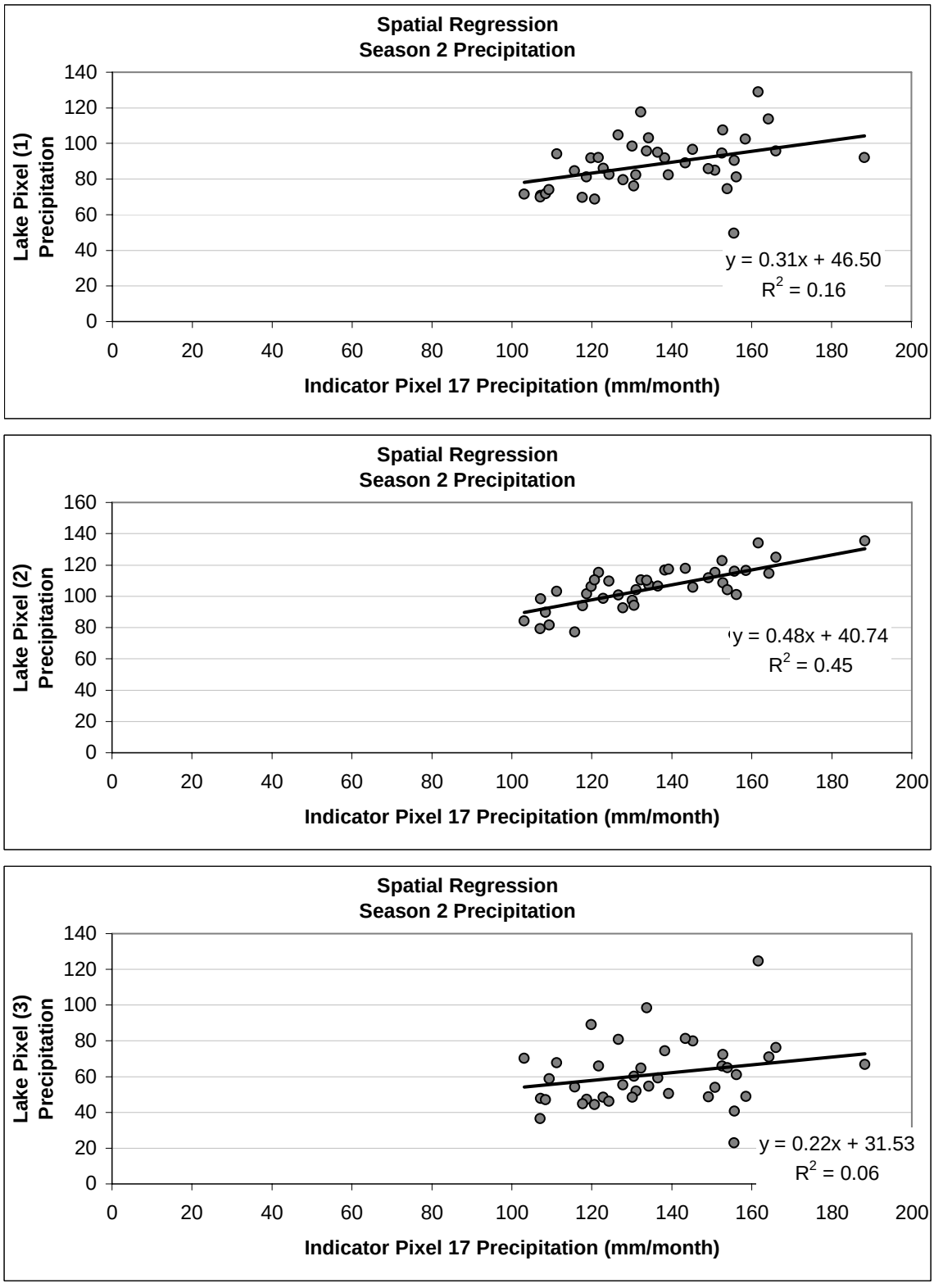

Figure A.4(m-o): Lake Victoria Indicator-Target pixel precipitation relationships (S 2).

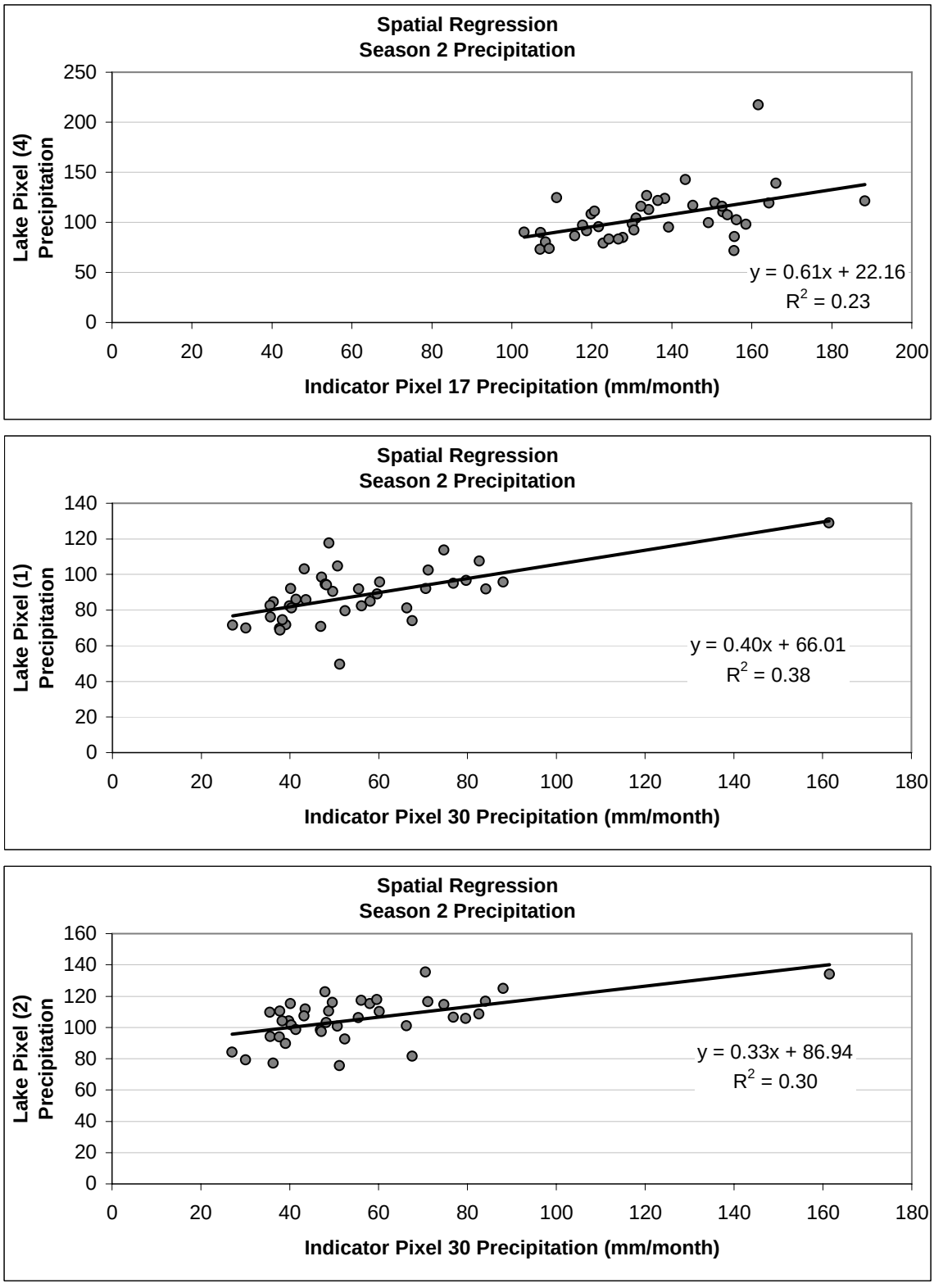

Figure A.4(p-r): Lake Victoria Indicator-Target pixel precipitation relationships (S 2).

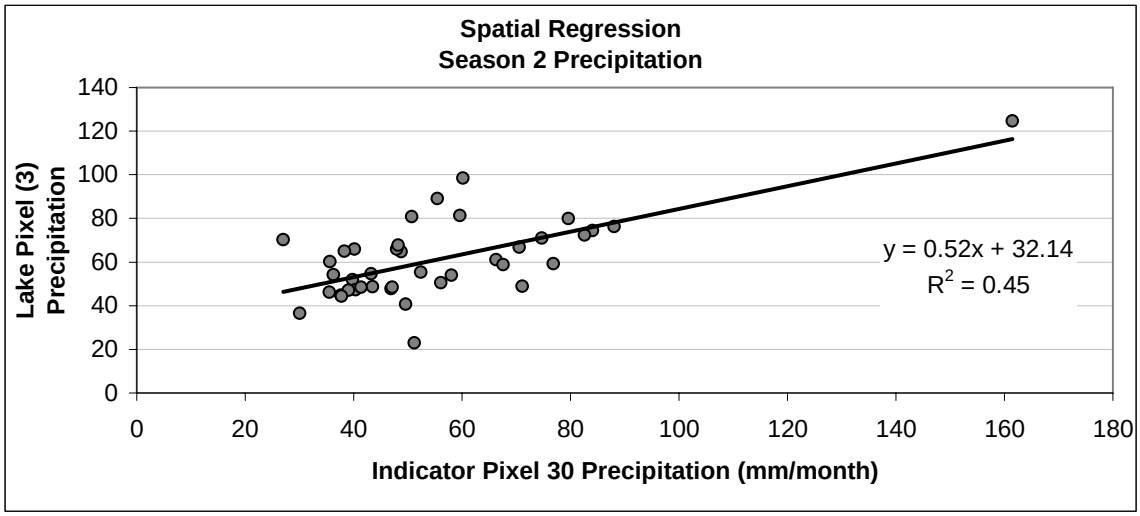

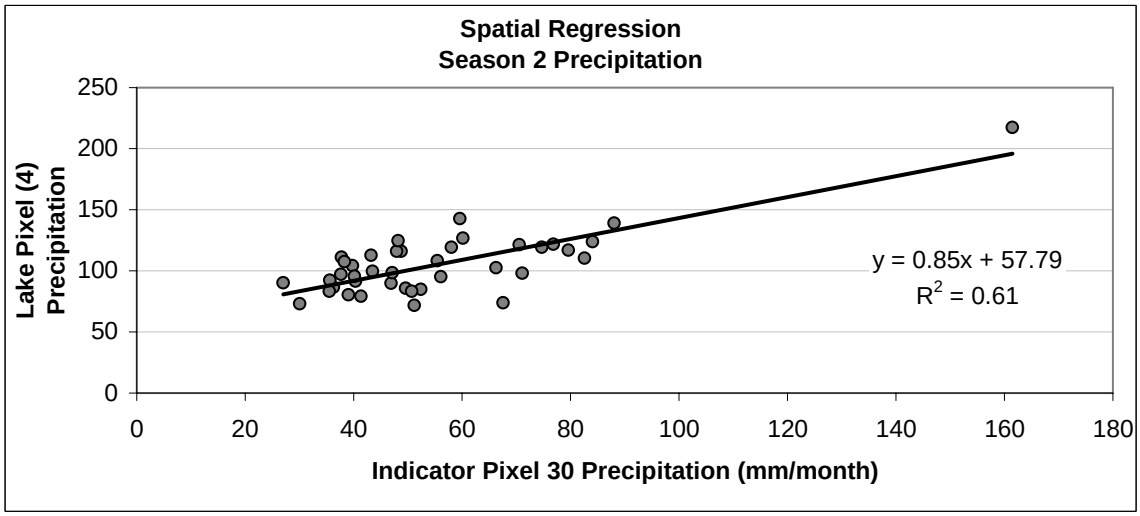

Figure A.4(s-t): Lake Victoria Indicator-Target pixel precipitation relationships (S 2).

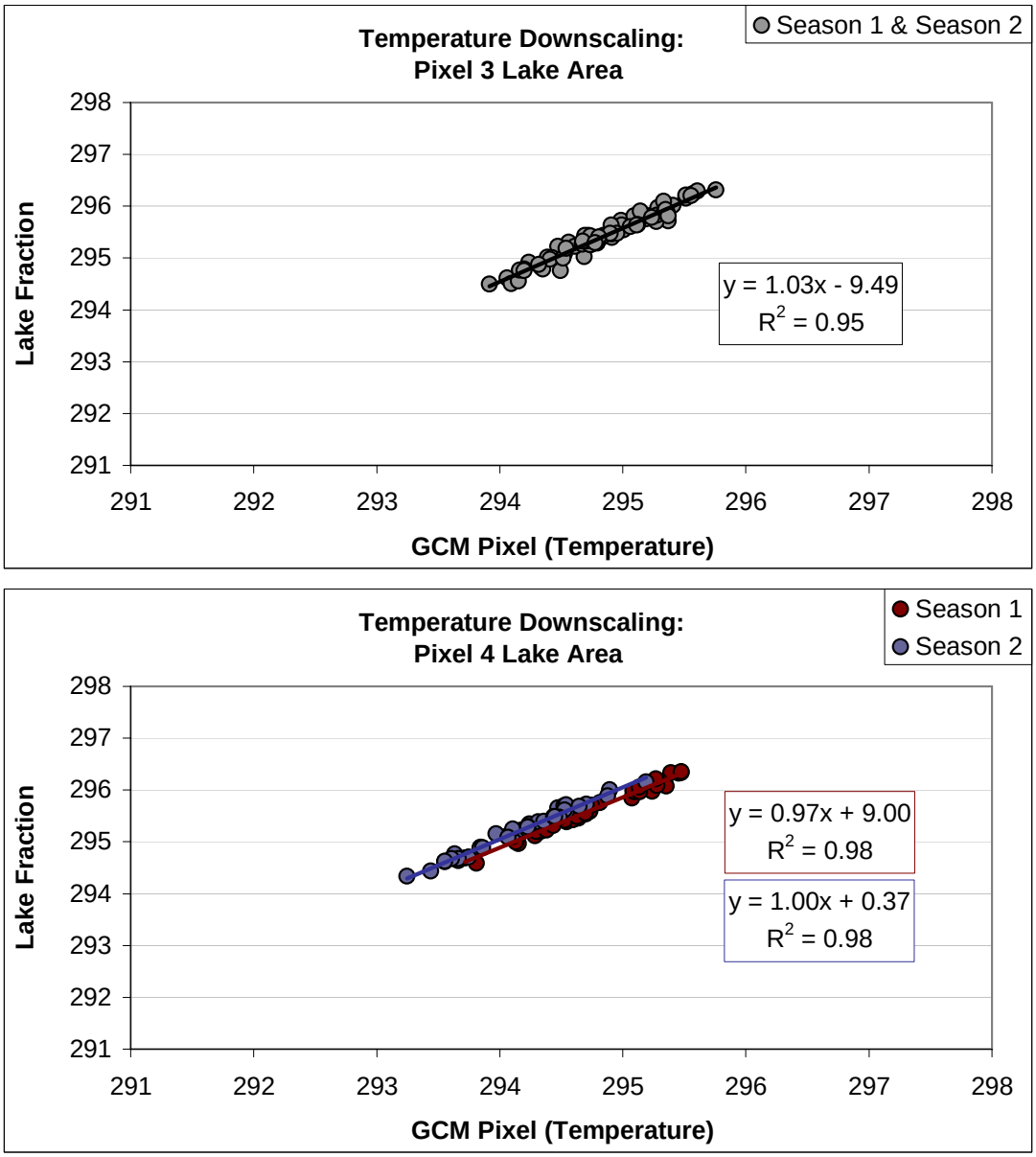

Figure A.5(a-b): Lake Victoria temperature downscaling relationships.

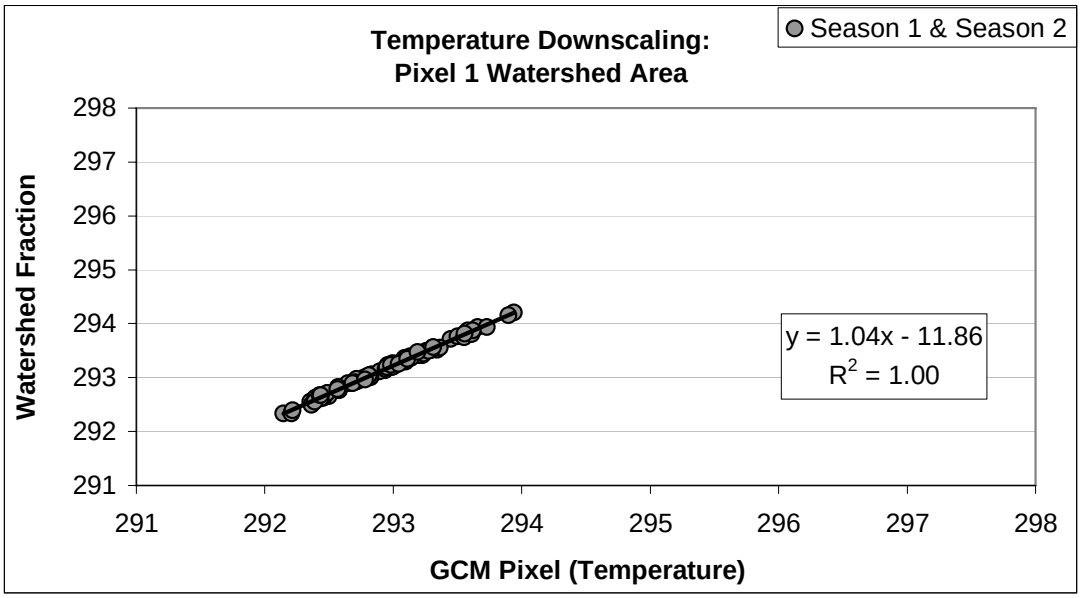

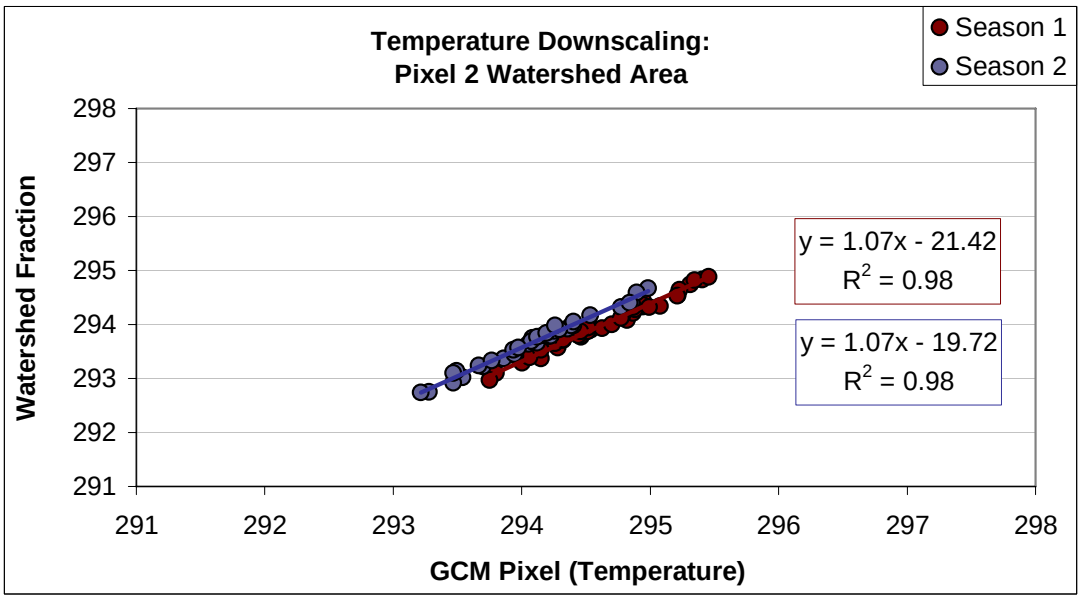

Figure A.5(c-d): Lake Victoria temperature downscaling relationships.

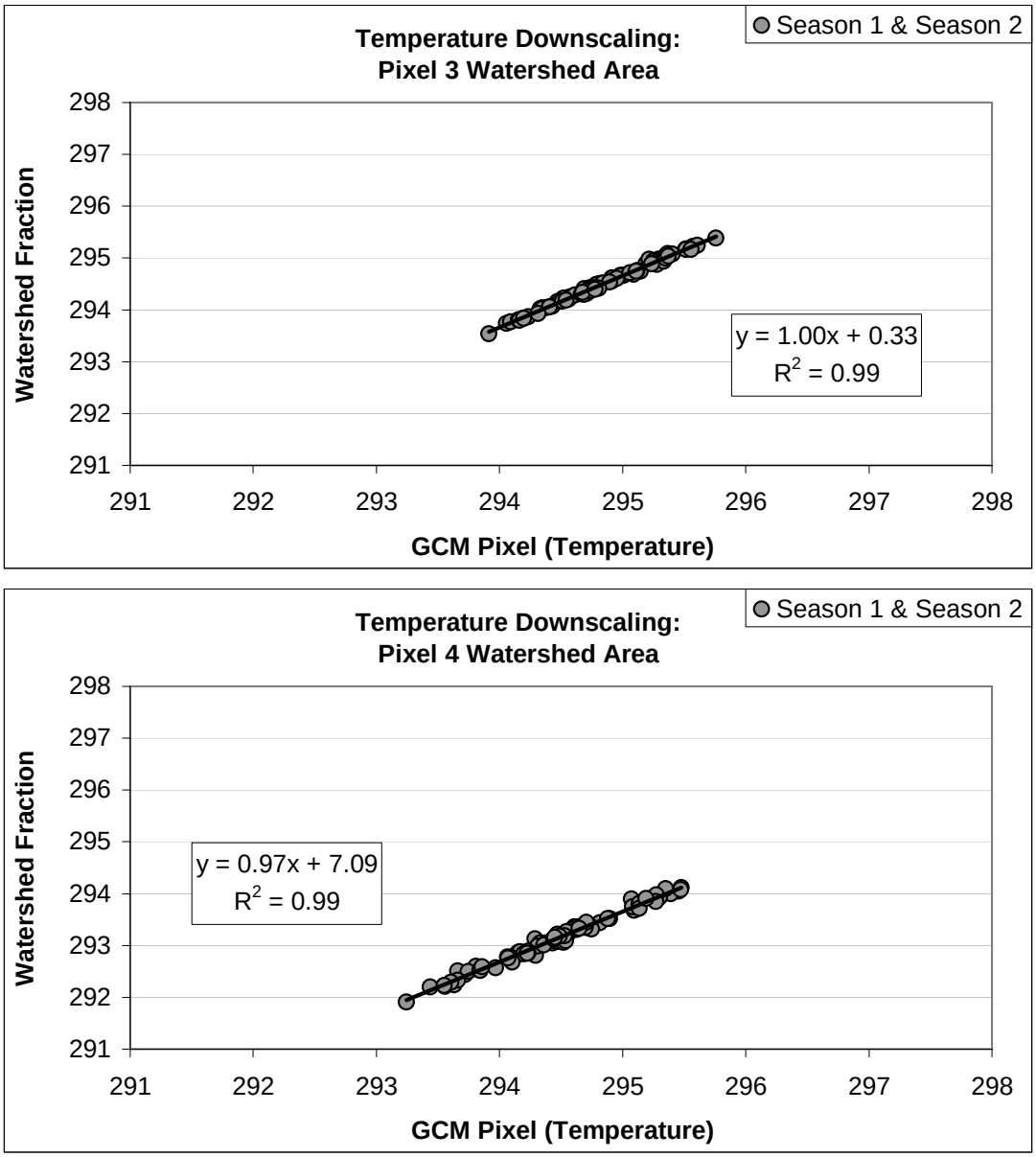

Figure A.5(e-f): Lake Victoria temperature downscaling relationships.

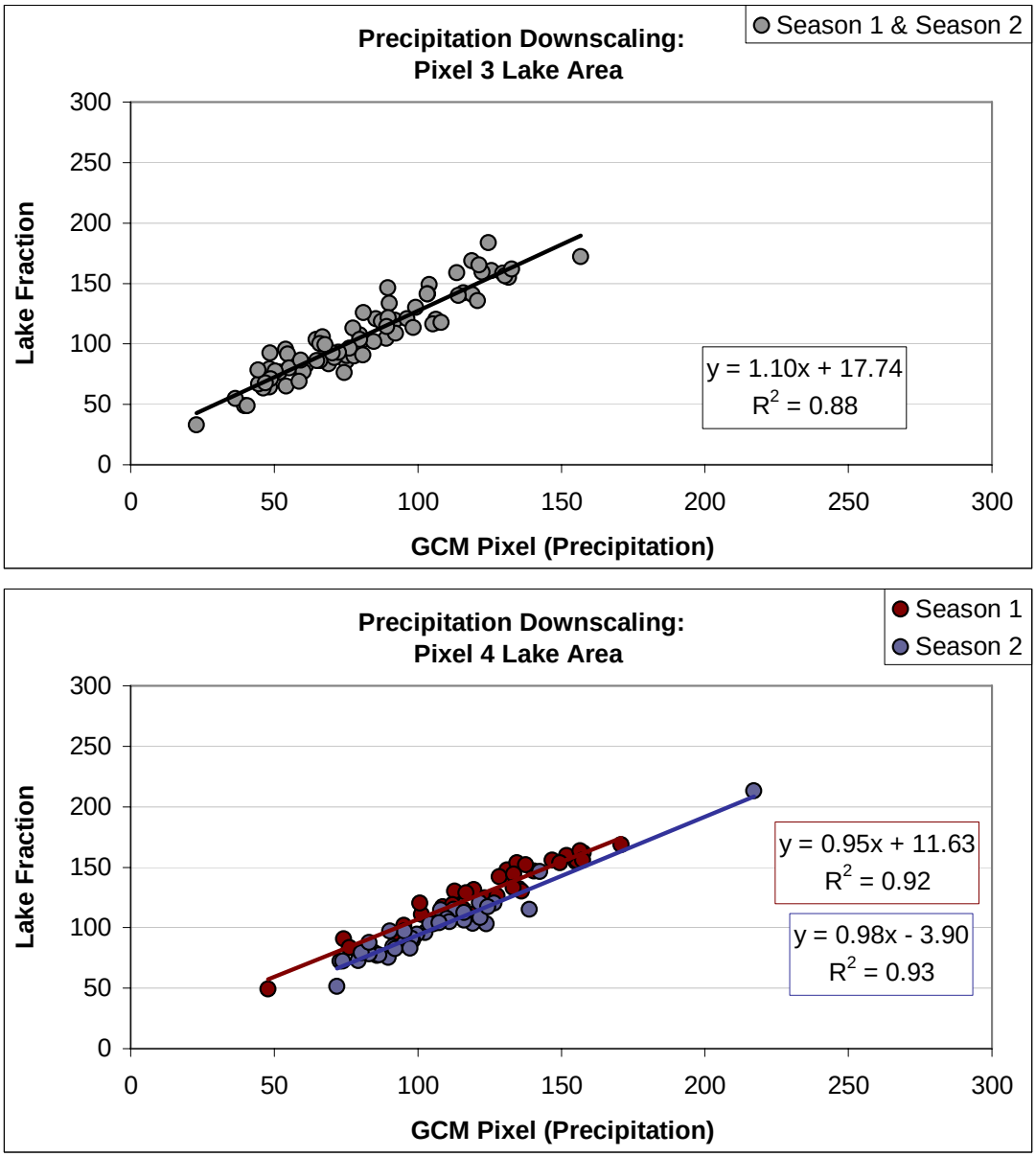

Figure A.6(a-b): Lake Victoria precipitation downscaling relationships.

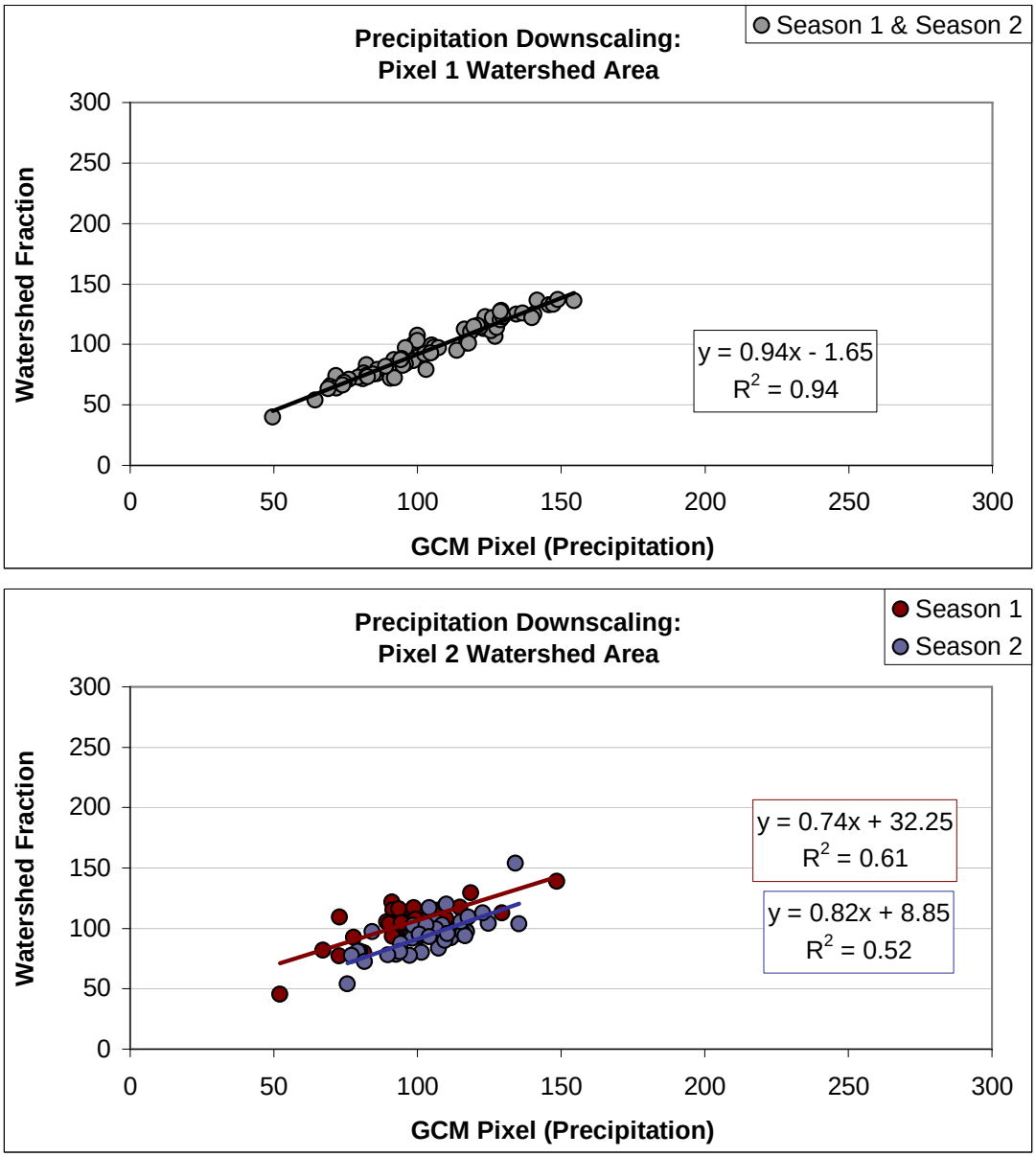

Figure A.6(c-d): Lake Victoria precipitation downscaling relationships.

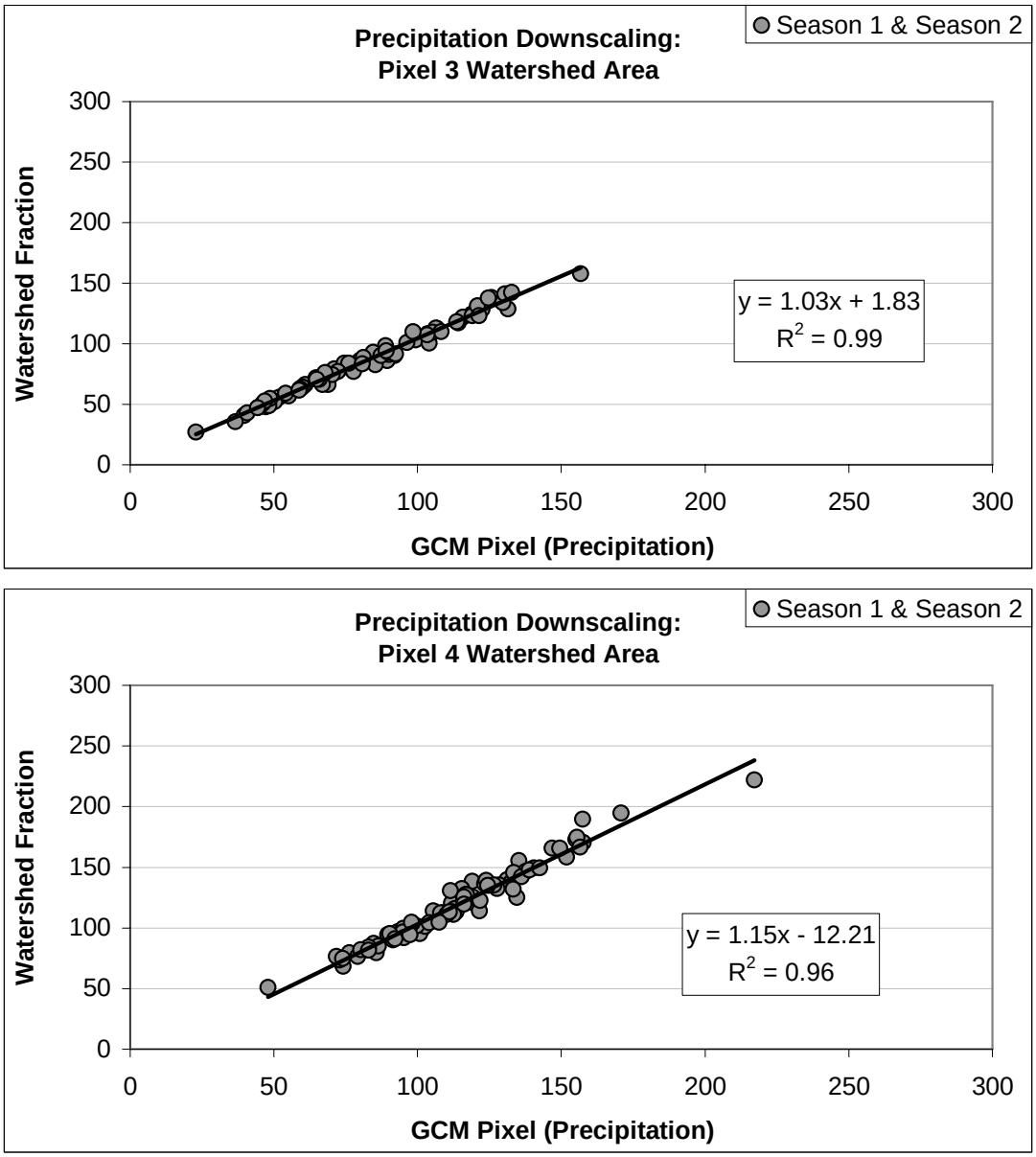

Figure A.6(e-f): Lake Victoria precipitation downscaling relationships.

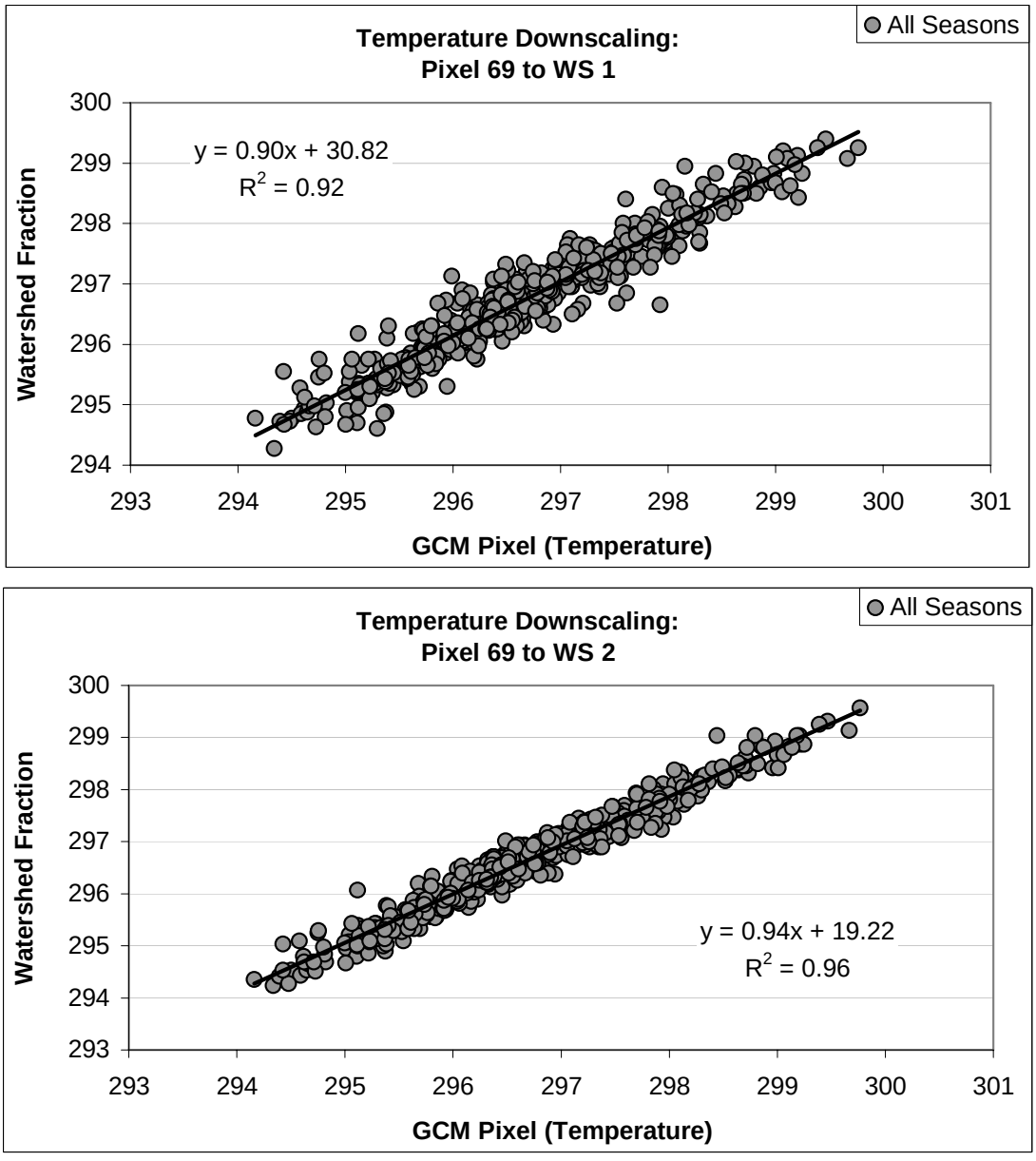

Figure A.7(a-b): Equatorial Lakes temperature downscaling relationships.

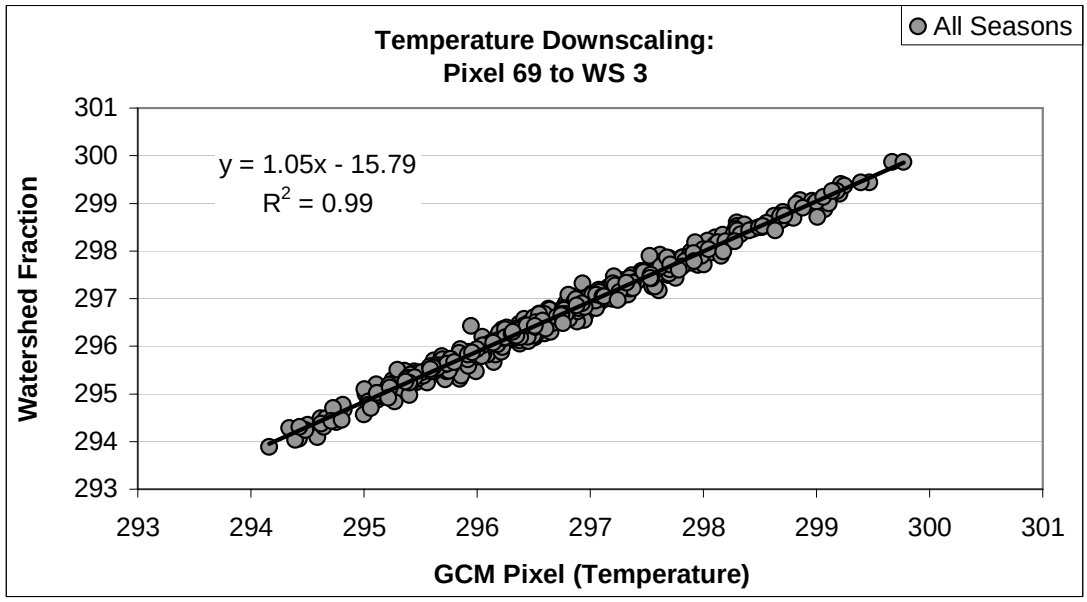

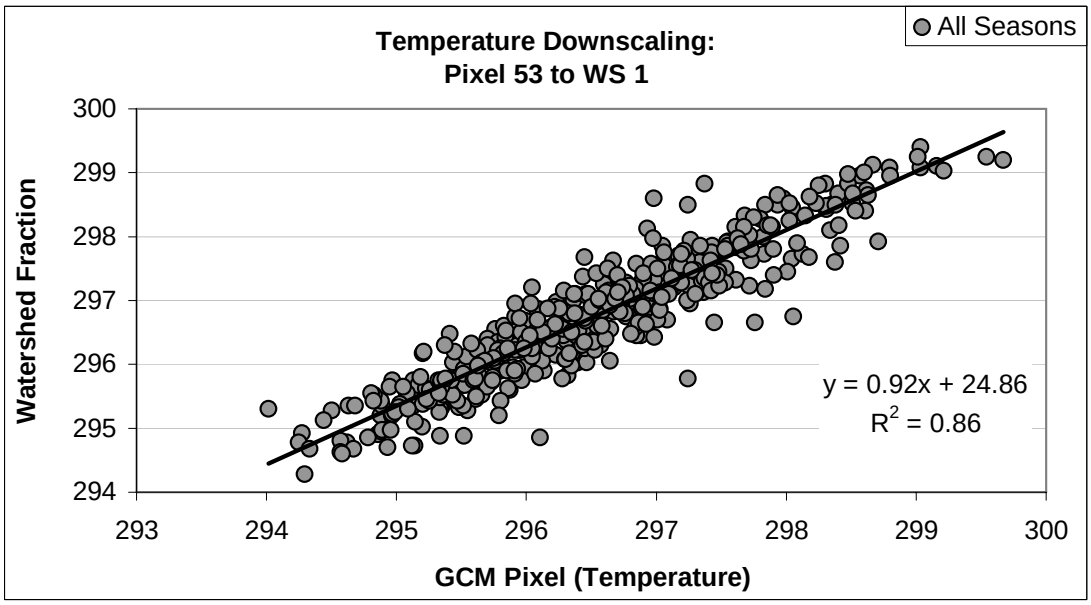

Figure A.7(c-d): Equatorial Lakes temperature downscaling relationships.

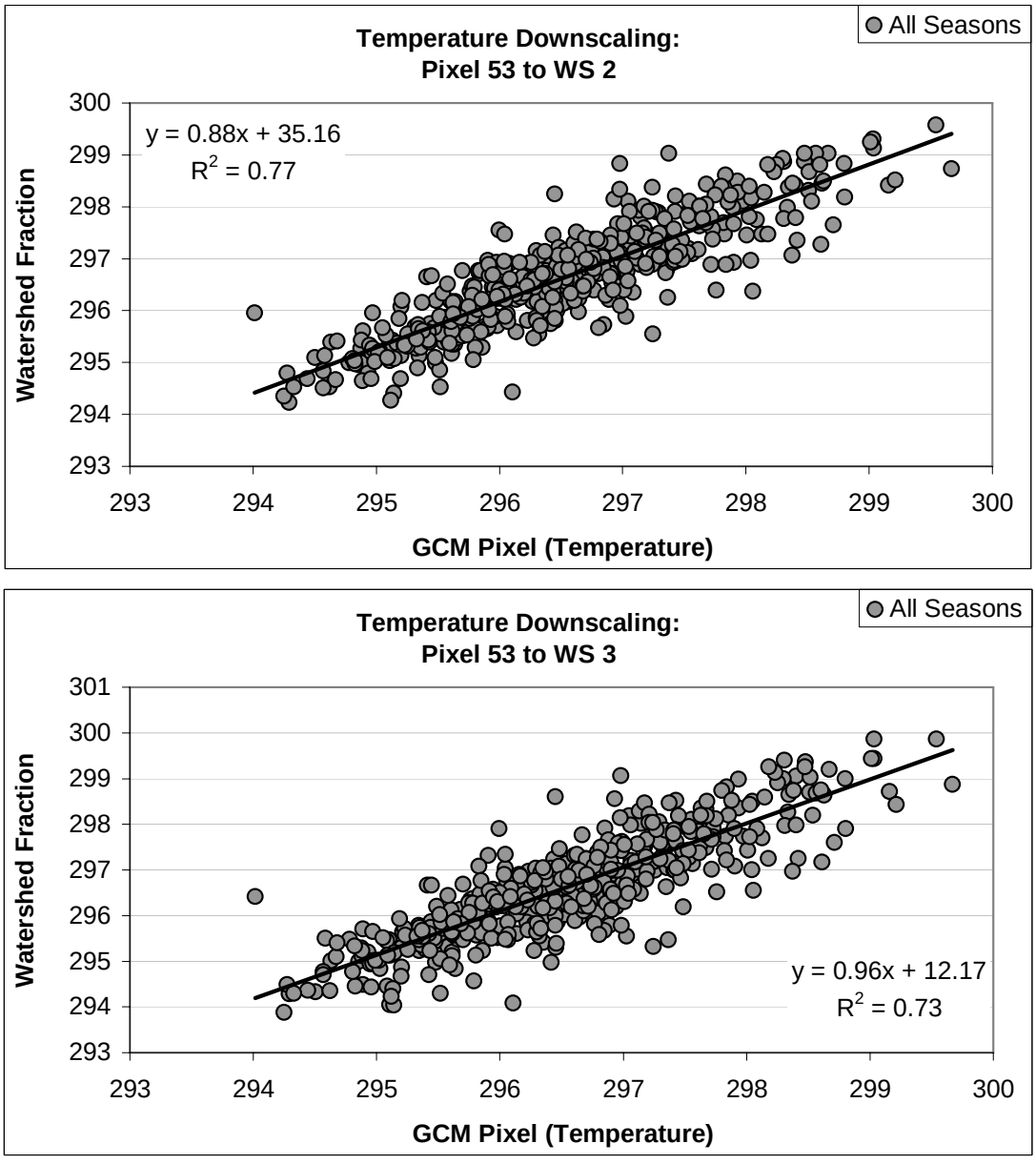

Figure A.7(e-f): Equatorial Lakes temperature downscaling relationships.

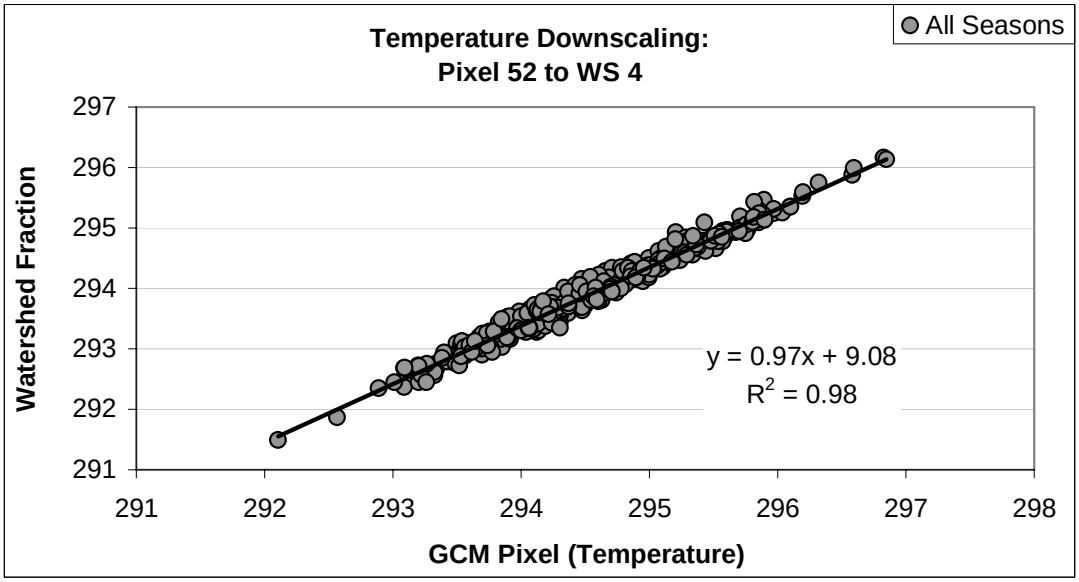

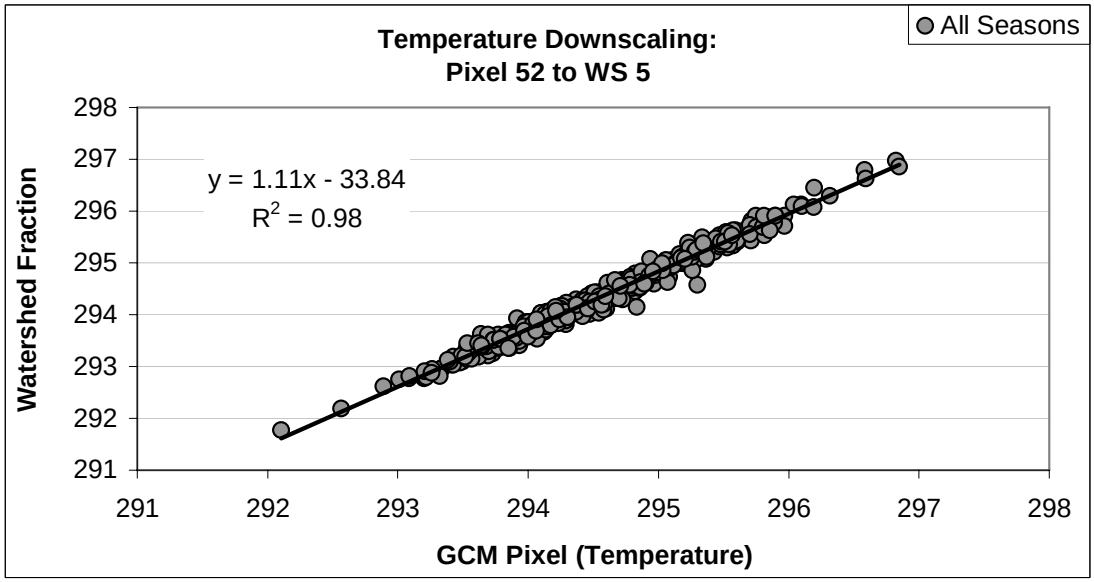

Figure A.7(g-h): Equatorial Lakes temperature downscaling relationships.

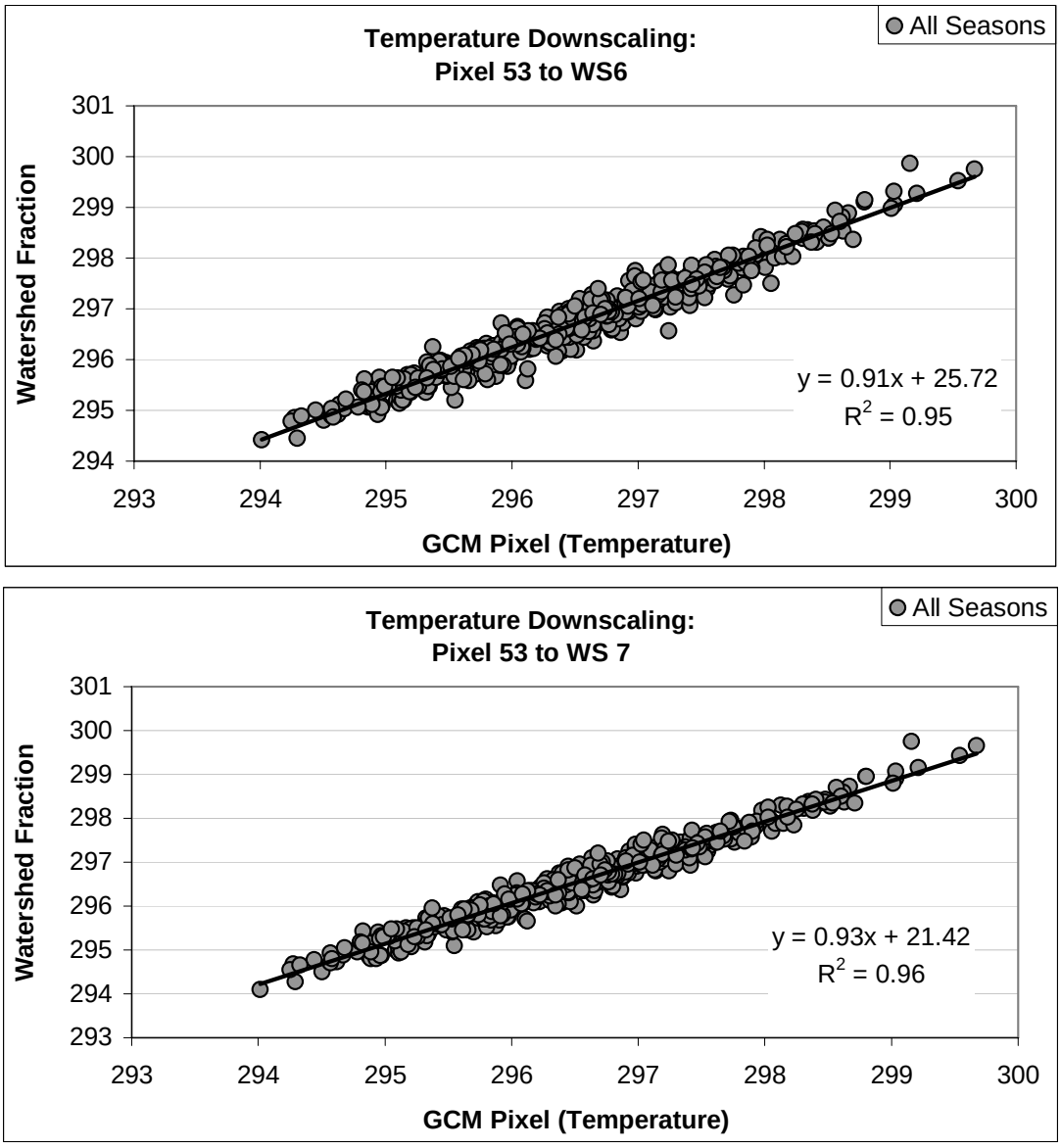

Figure A.7(i-j): Equatorial Lakes temperature downscaling relationships.

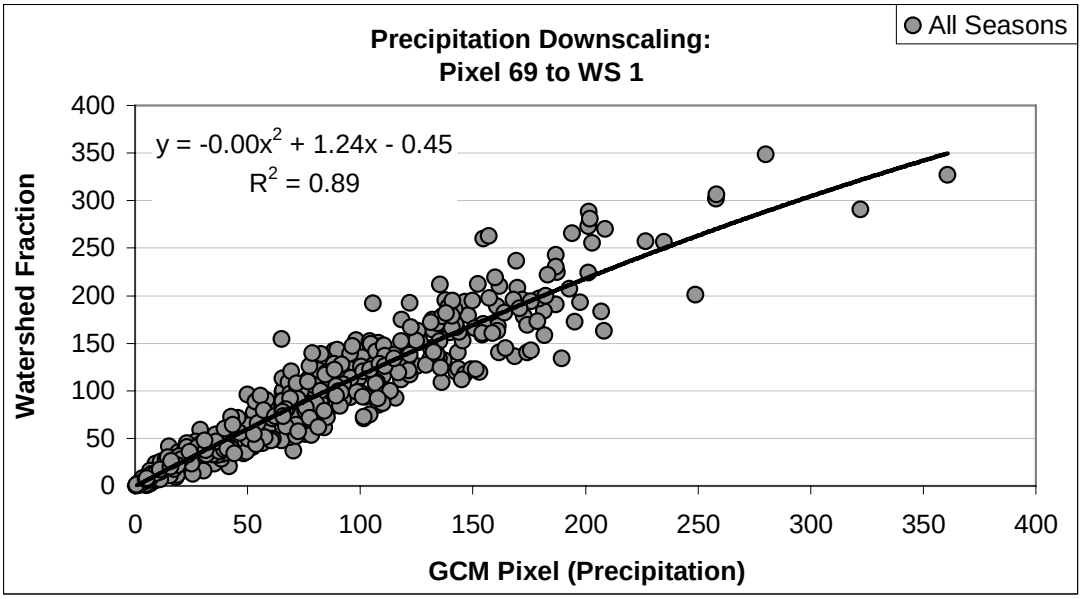

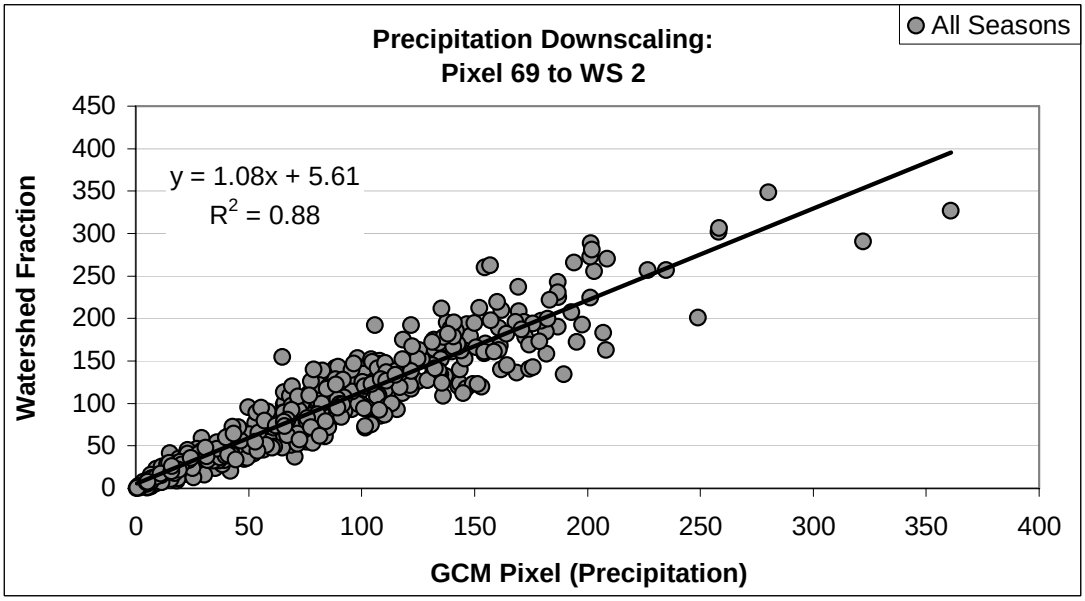

Figure A.8(a-b): Equatorial Lakes precipitation downscaling relationships.

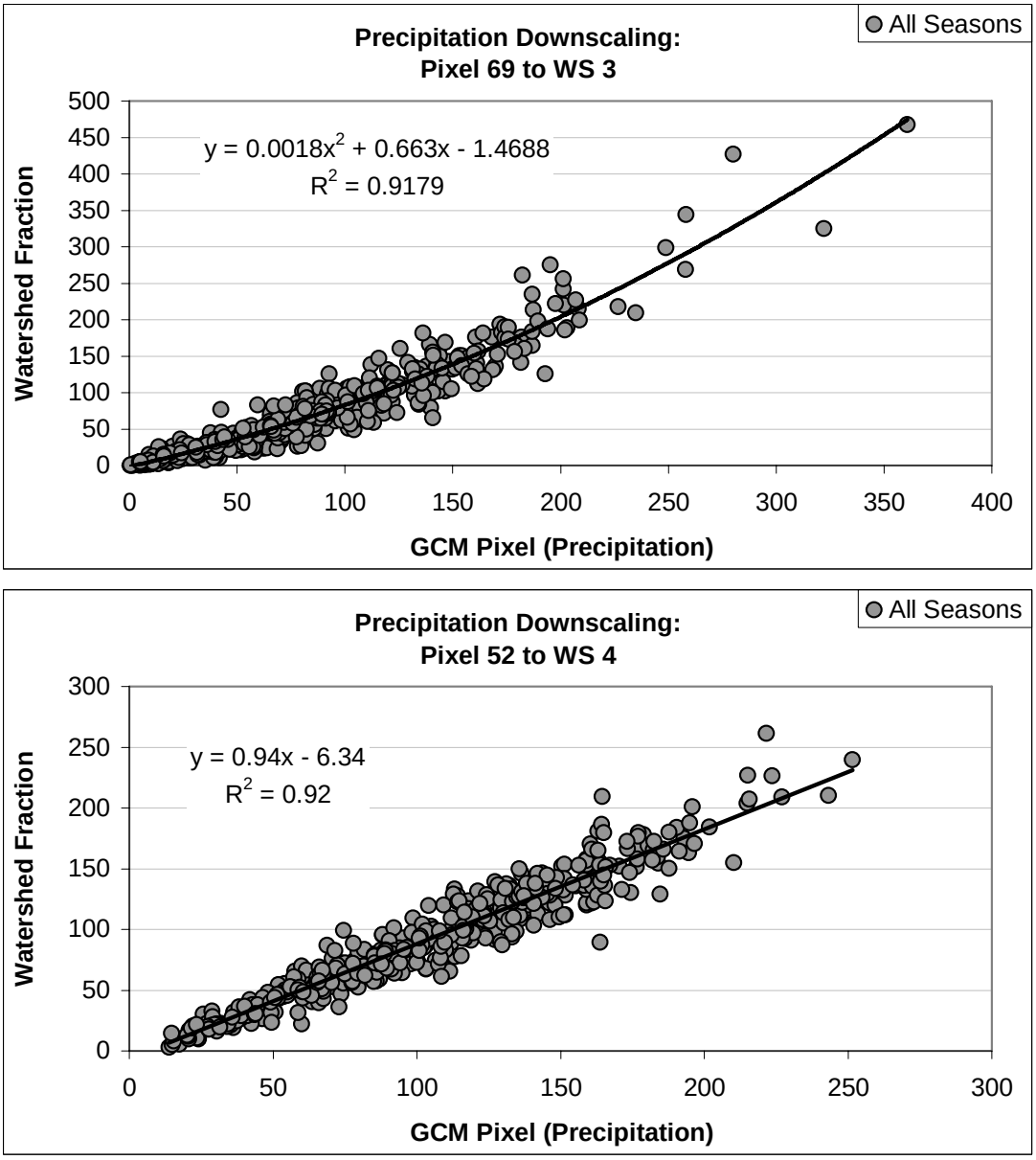

Figure A.8(c-d): Equatorial Lakes precipitation downscaling relationships.

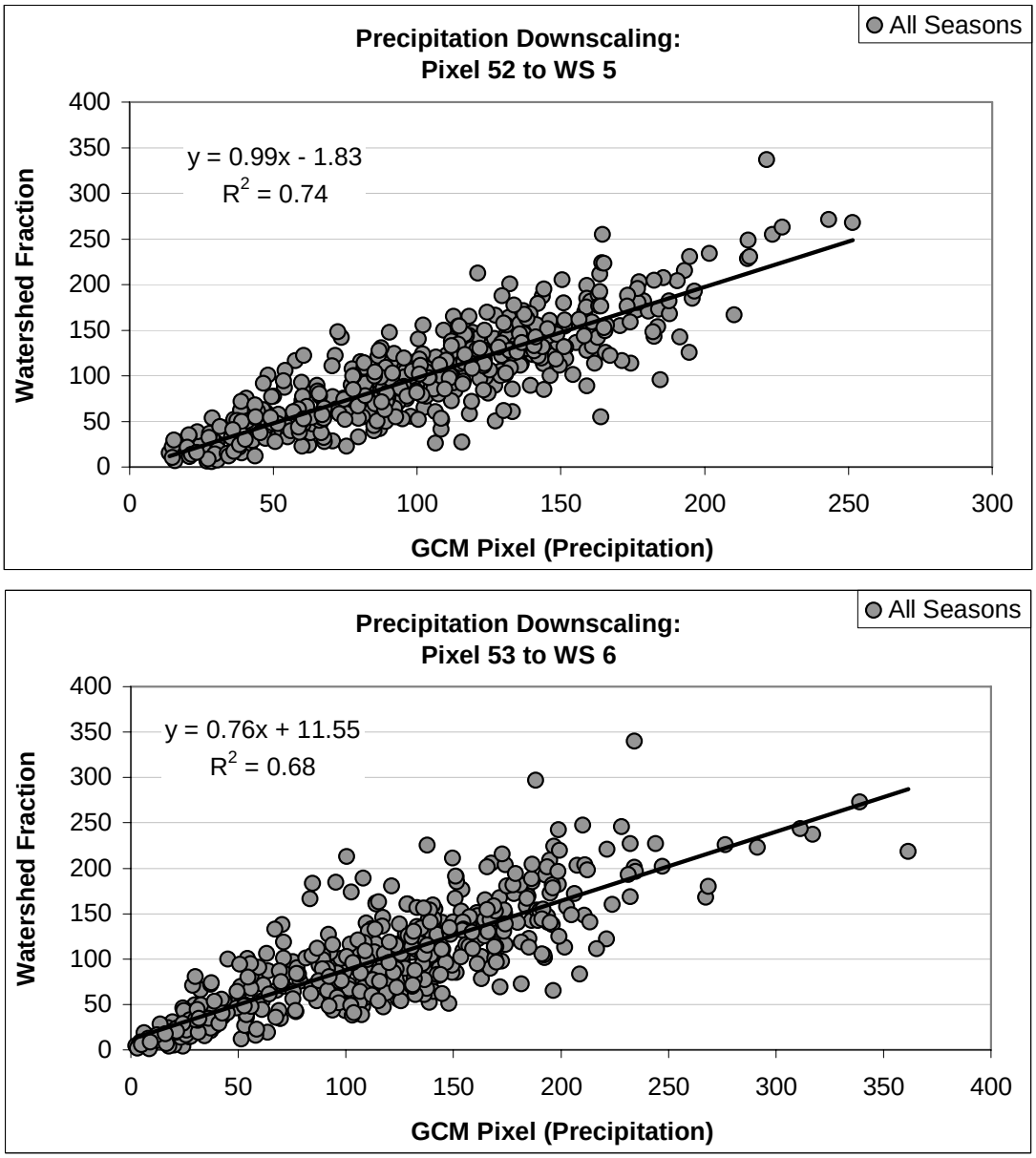

Figure A.8(e-f): Equatorial Lakes precipitation downscaling relationships.

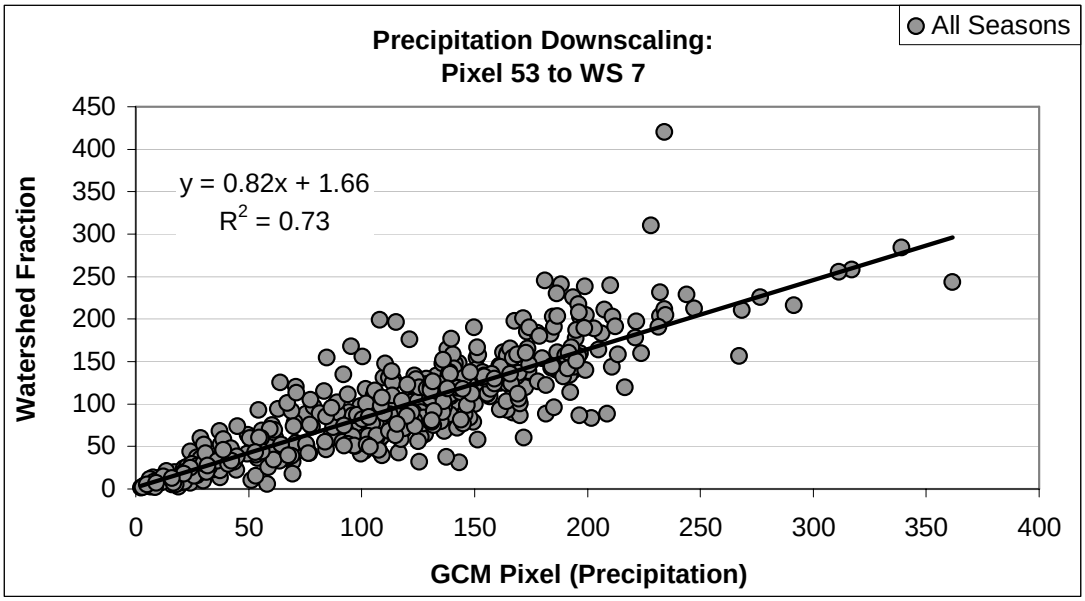

Figure A.8(g): Equatorial Lakes precipitation downscaling relationships.

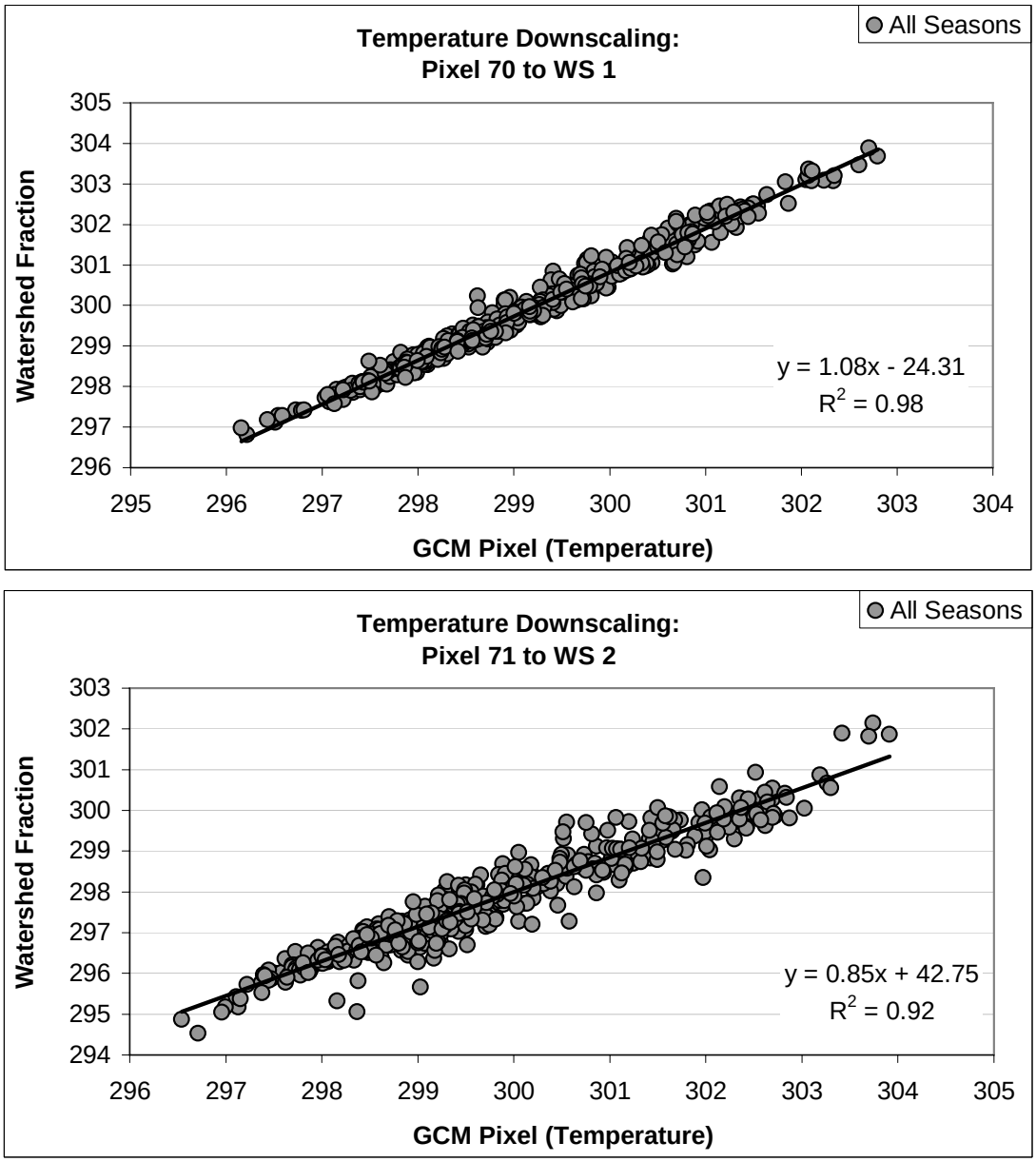

Figure A.9(a-b): Sobat temperature downscaling relationships.

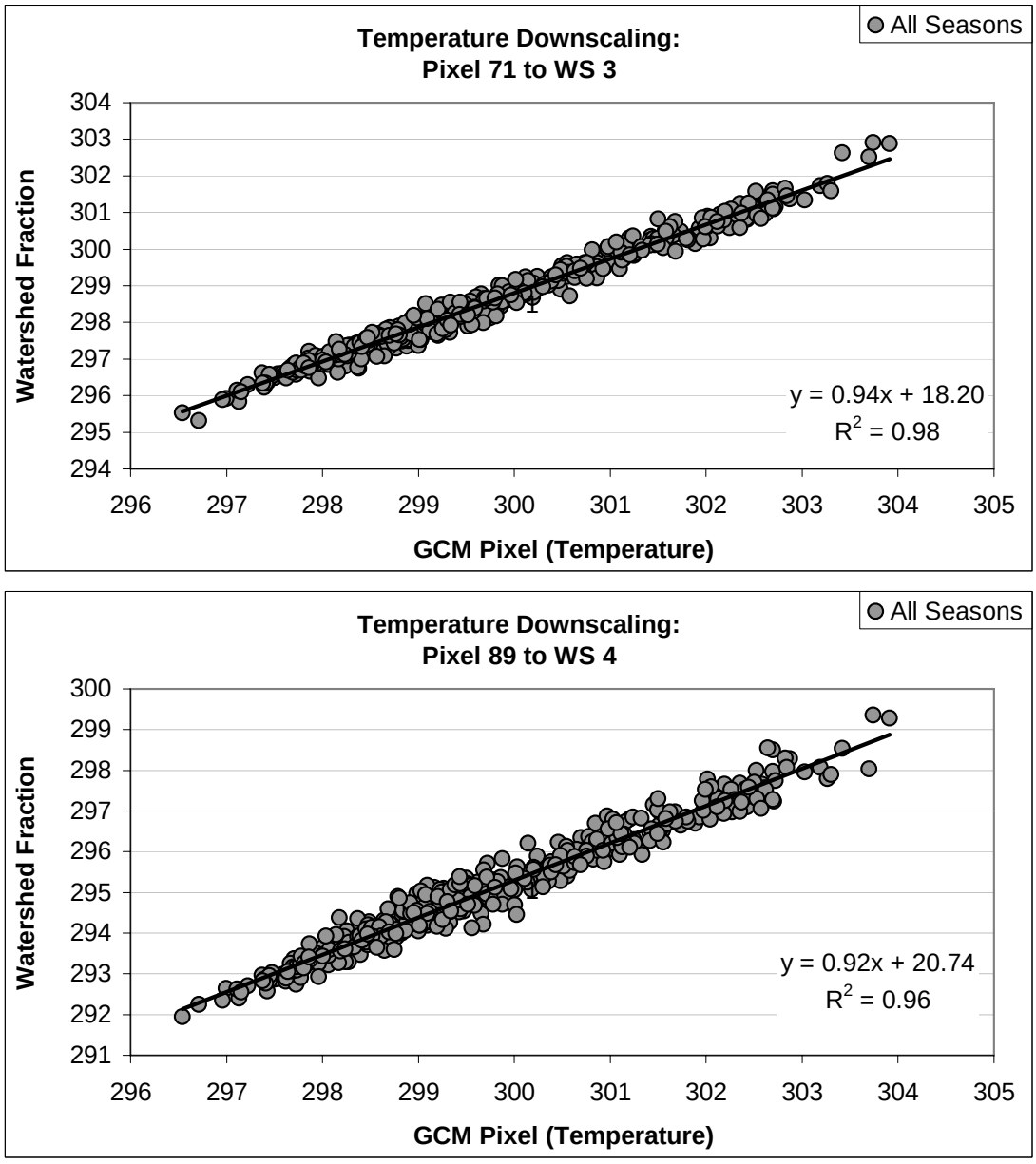

Figure A.9(c-d): Sobat temperature downscaling relationships.

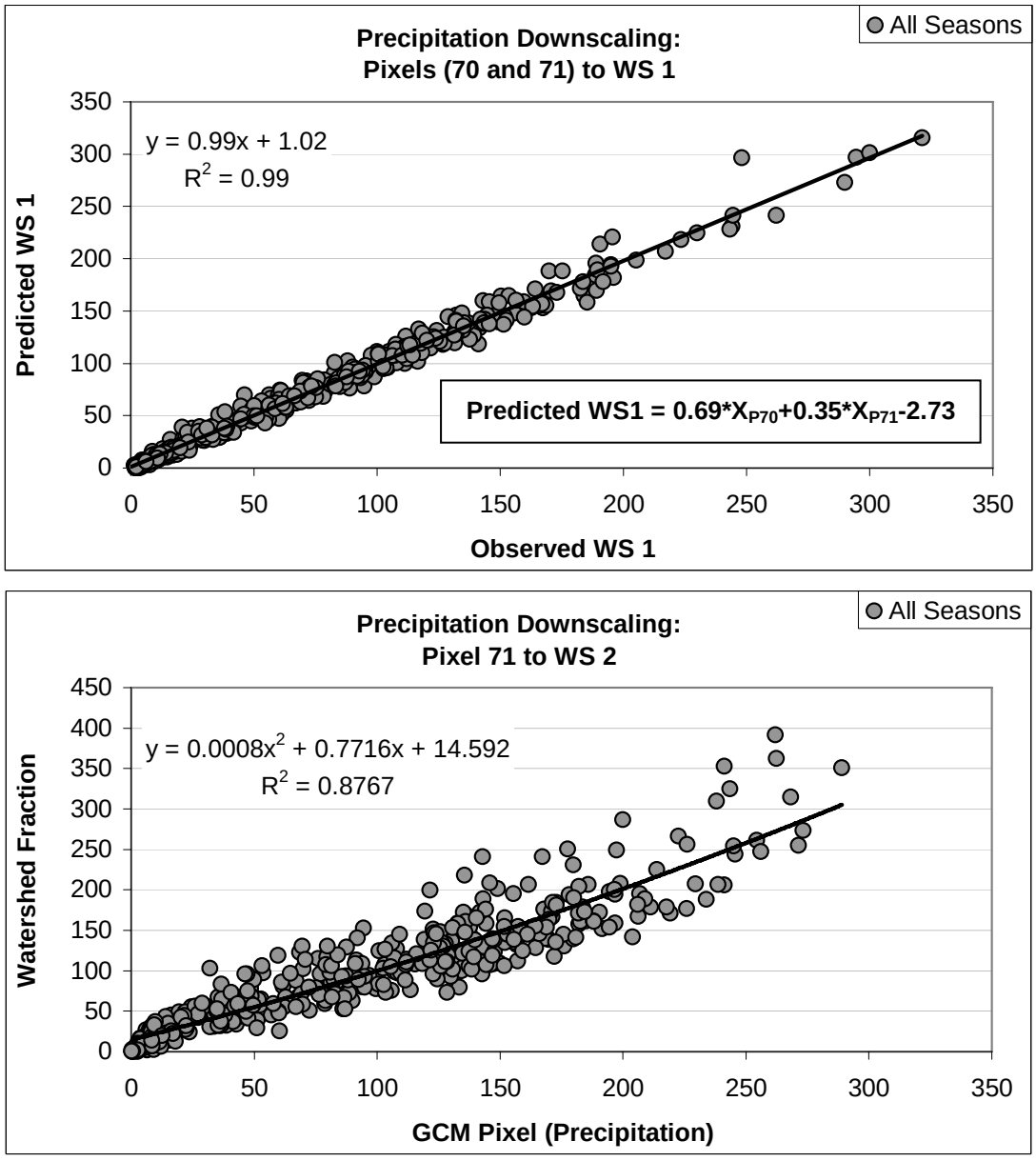

Figure A.10(a-b): Sobat precipitation downscaling relationships.

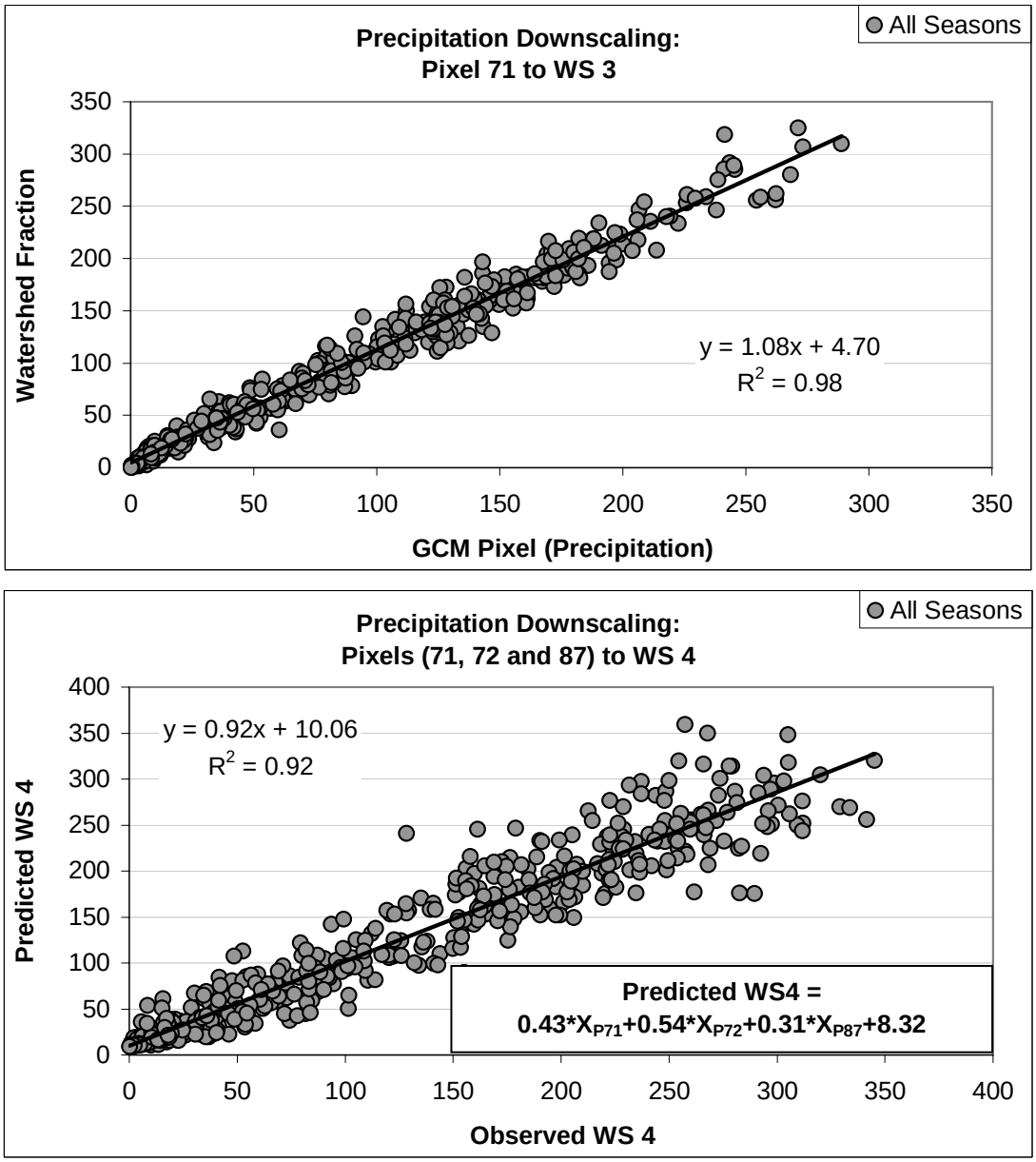

Figure A.10(c-d): Sobat precipitation downscaling relationships.

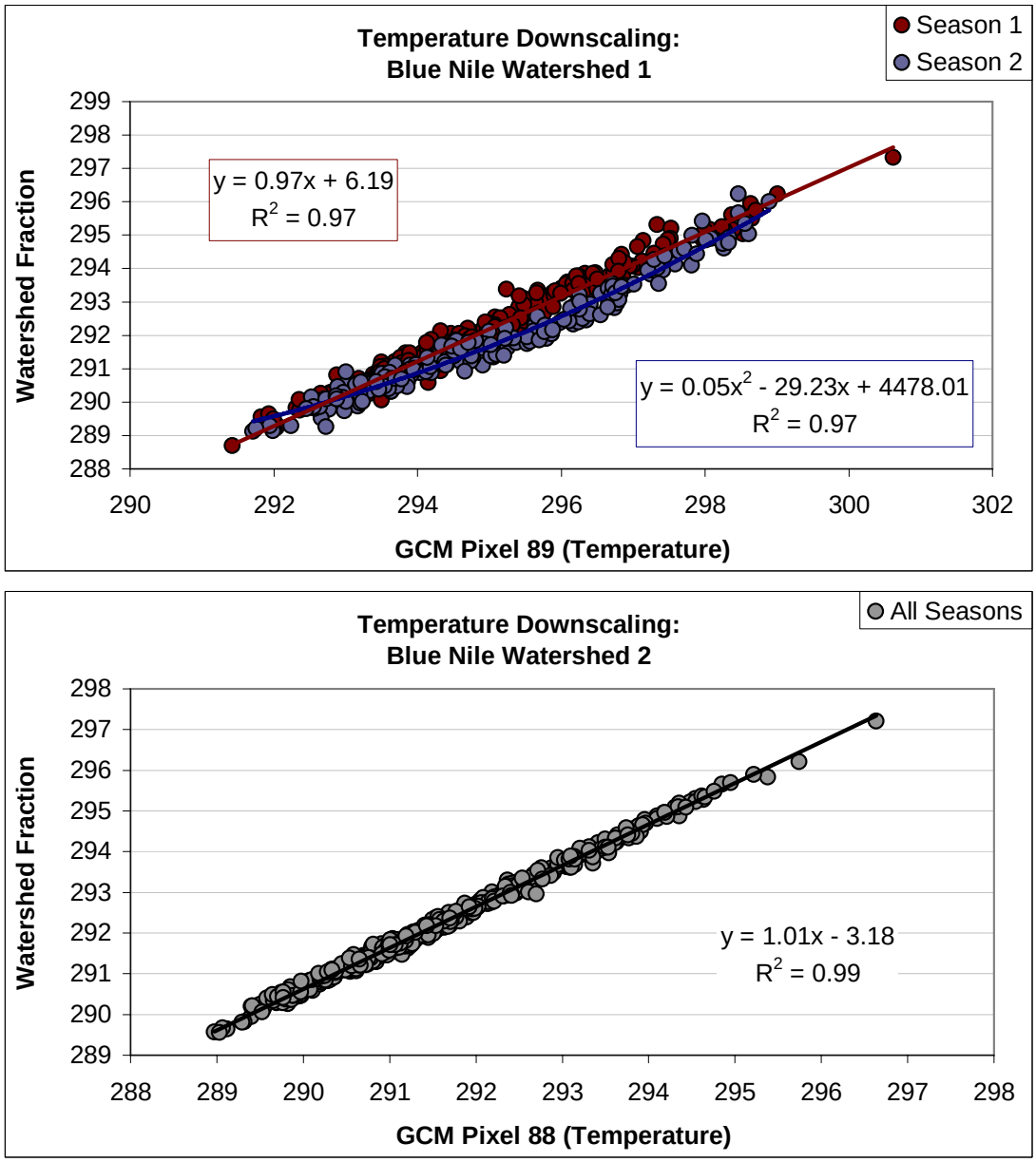

Figure A.11(a-b): Blue Nile temperature downscaling relationships.

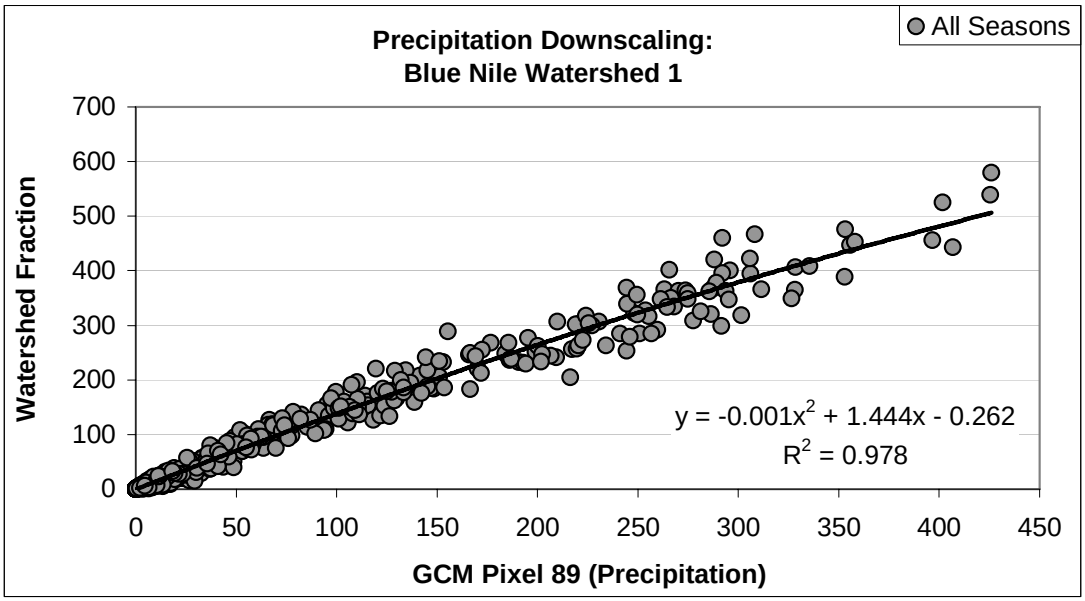

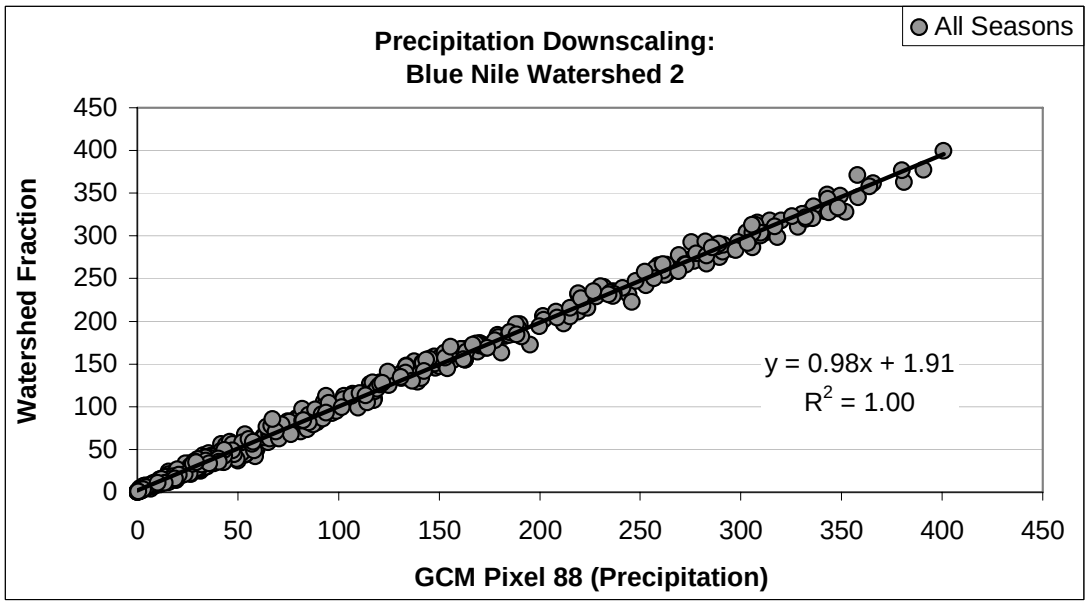

Figure A.12(a-b): Blue Nile precipitation downscaling relationships.

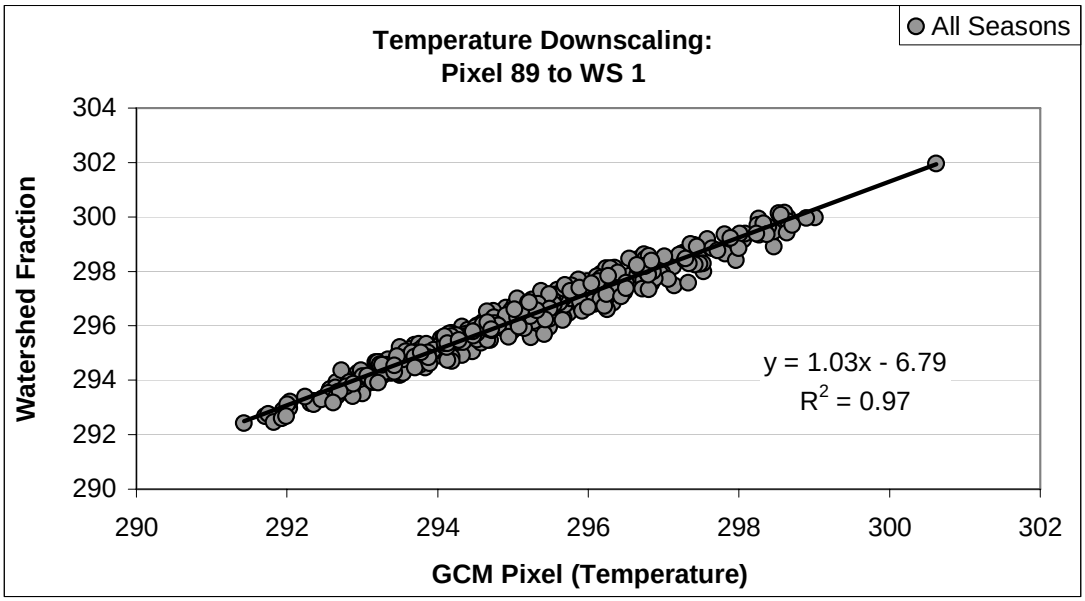

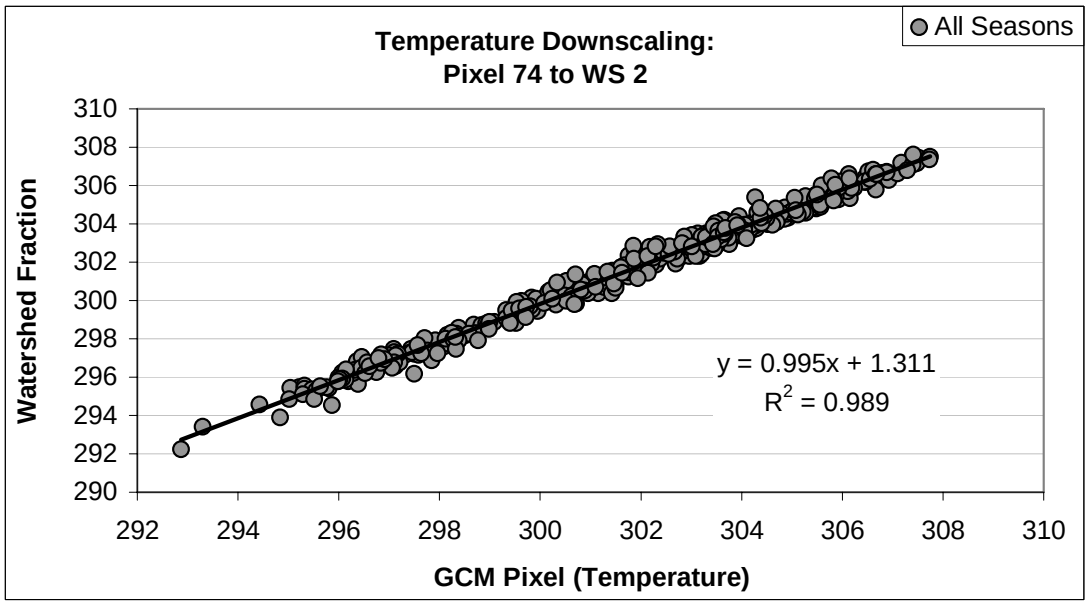

Figure A.13(a-b): Atbara temperature downscaling relationships.

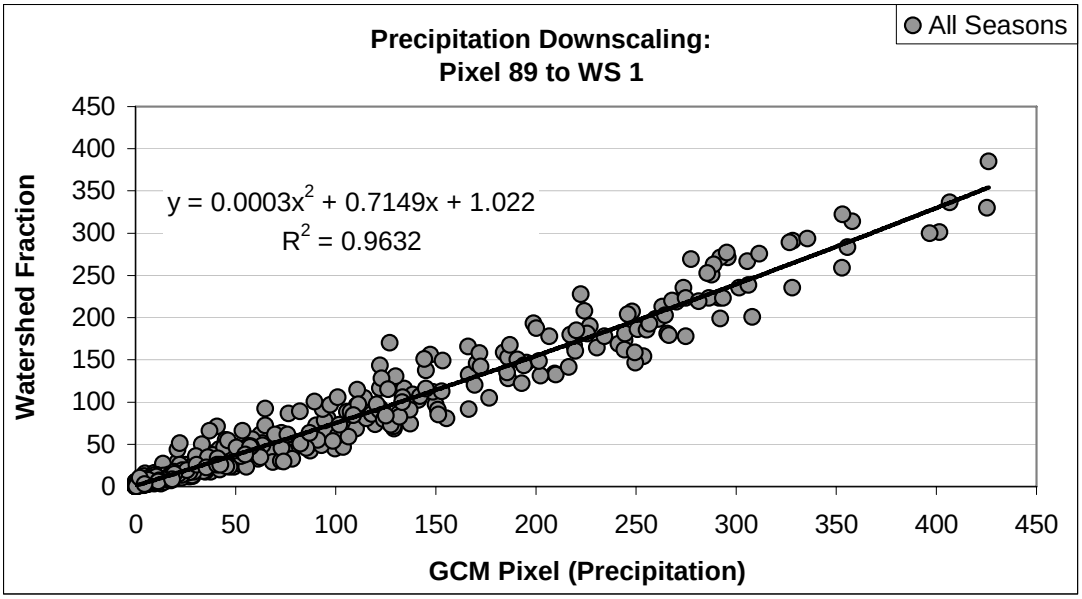

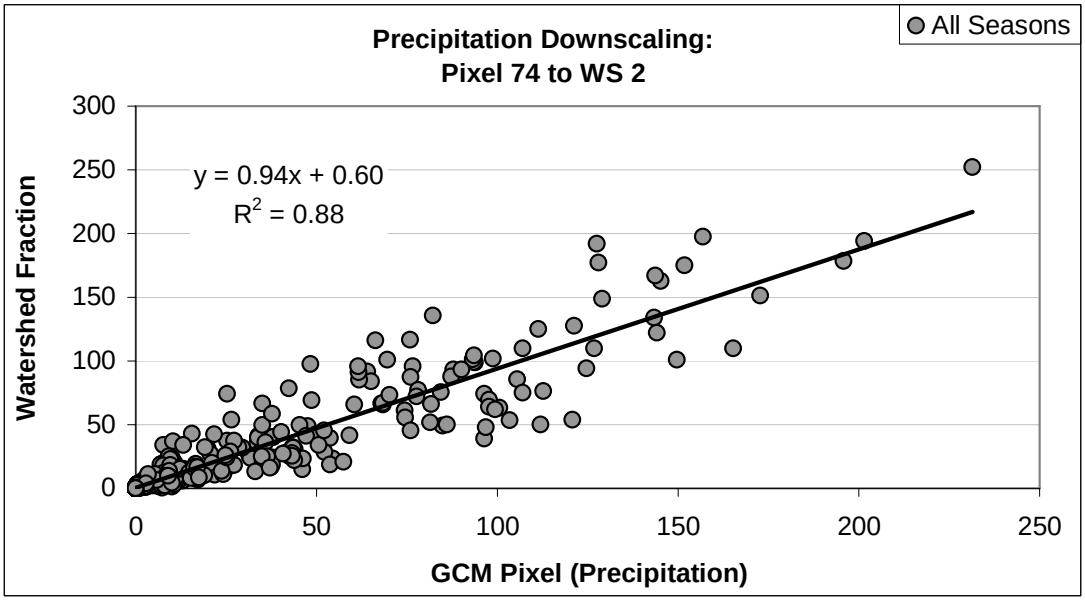

Figure A.14(a-b): Atbara precipitation downscaling relationships.

Appendix B

Hydrologic Ensembles

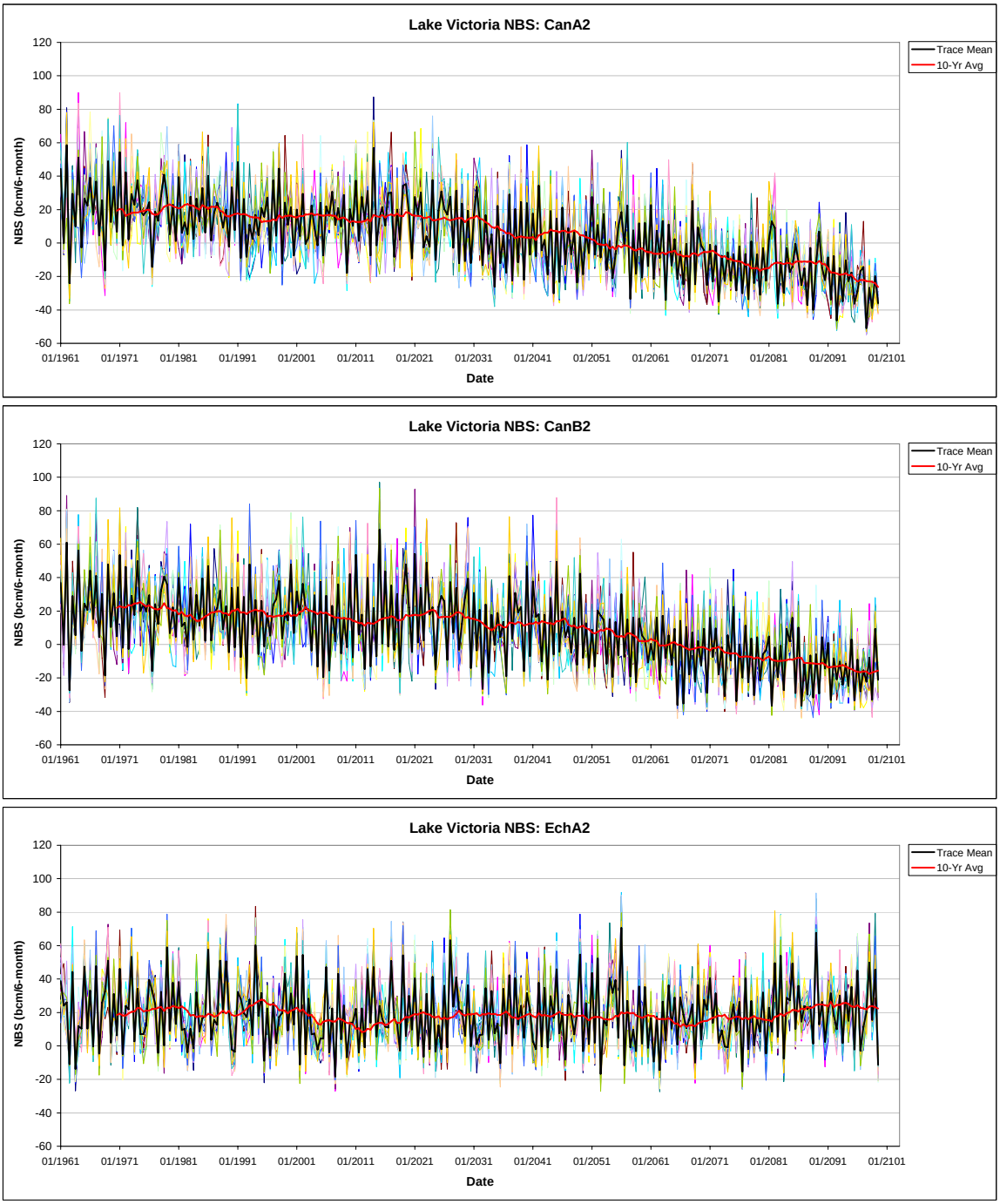

Figure B.1(a-c): Lake Victoria net basin supply ensembles by scenario.

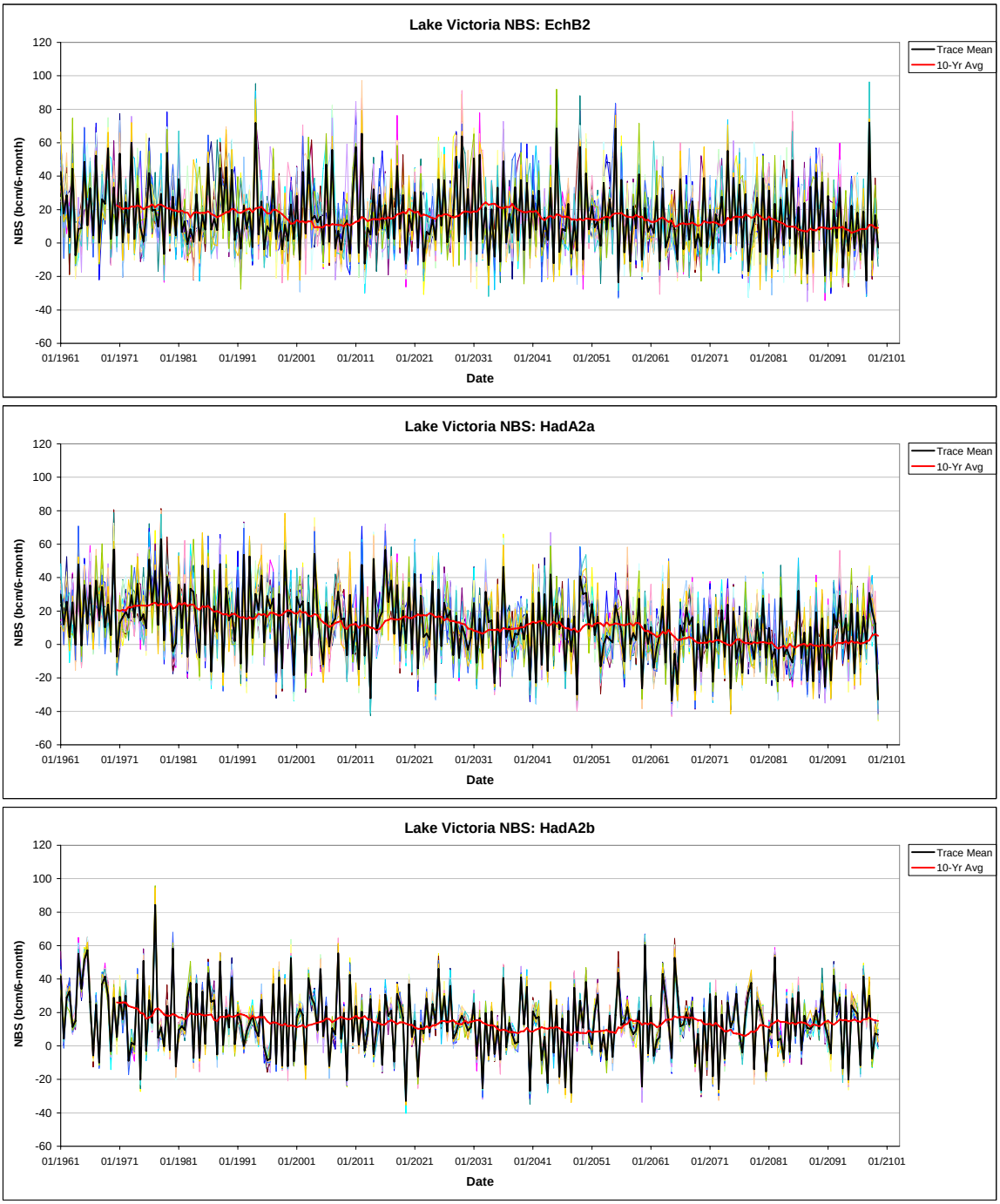

Figure B.1(d-f): Lake Victoria net basin supply ensembles by scenario.

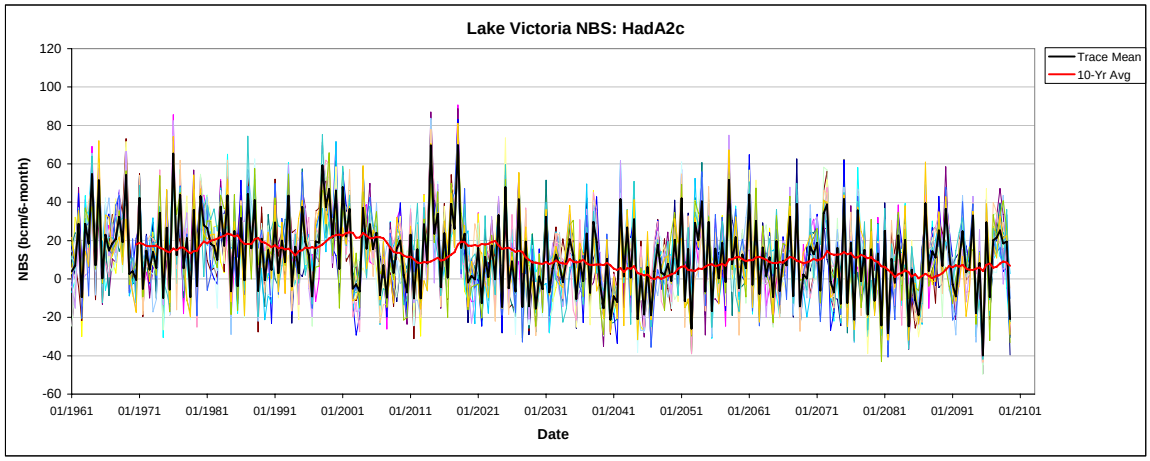

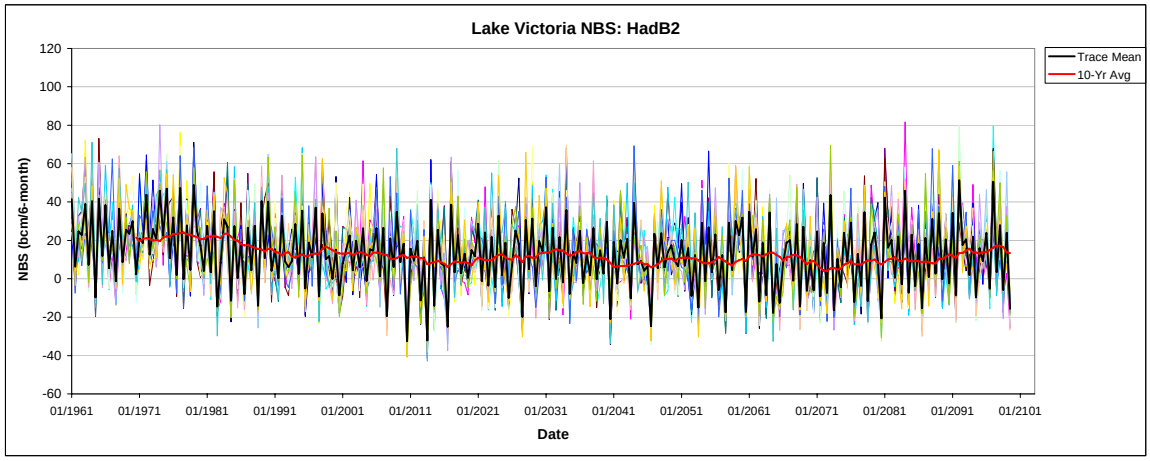

Figure B.1(g-h): Lake Victoria net basin supply ensembles by scenario.

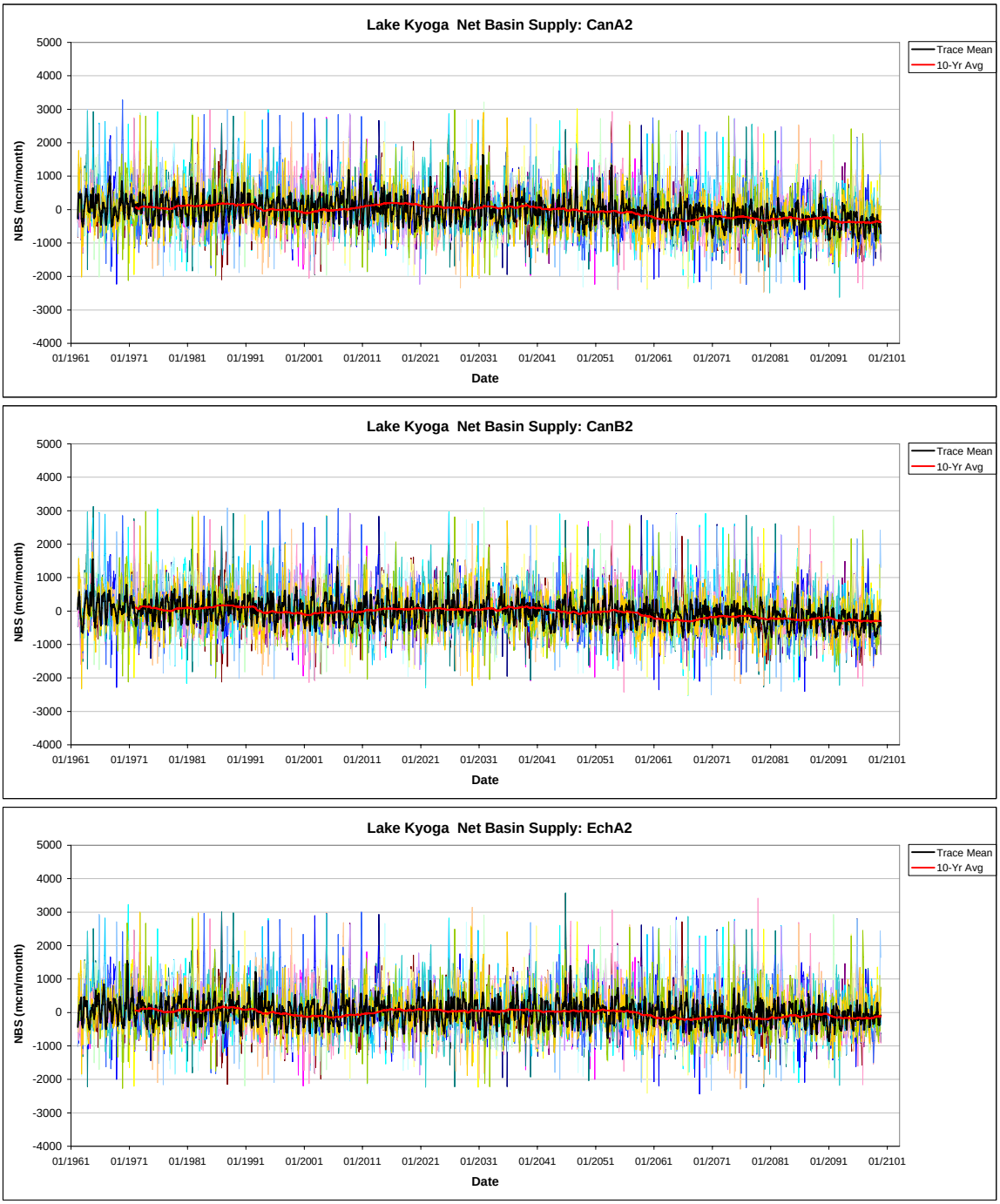

Figure B.2(a-c): Lake Kyoga net basin supply ensembles by scenario.

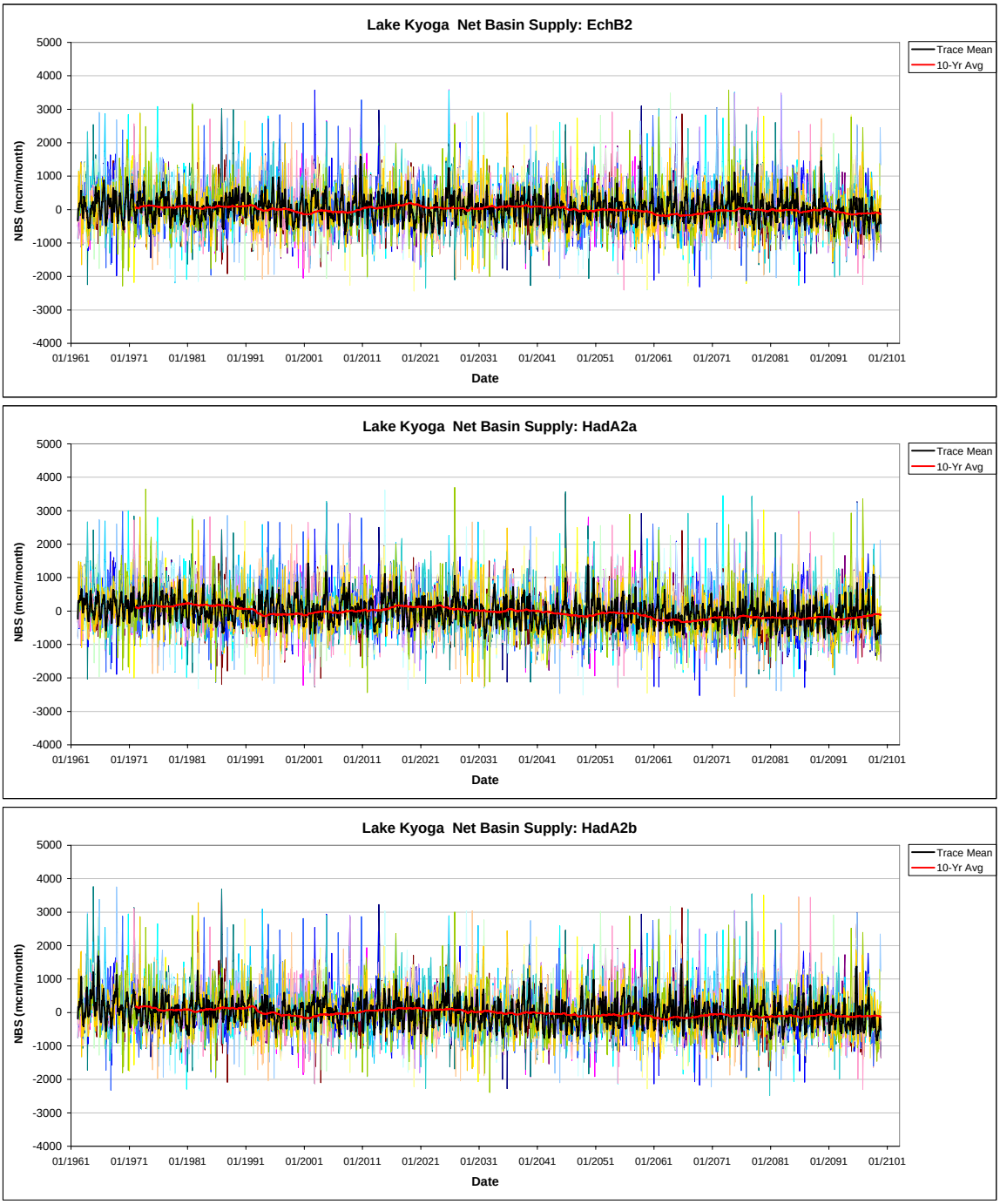

Figure B.2(d-f): Lake Kyoga net basin supply ensembles by scenario.

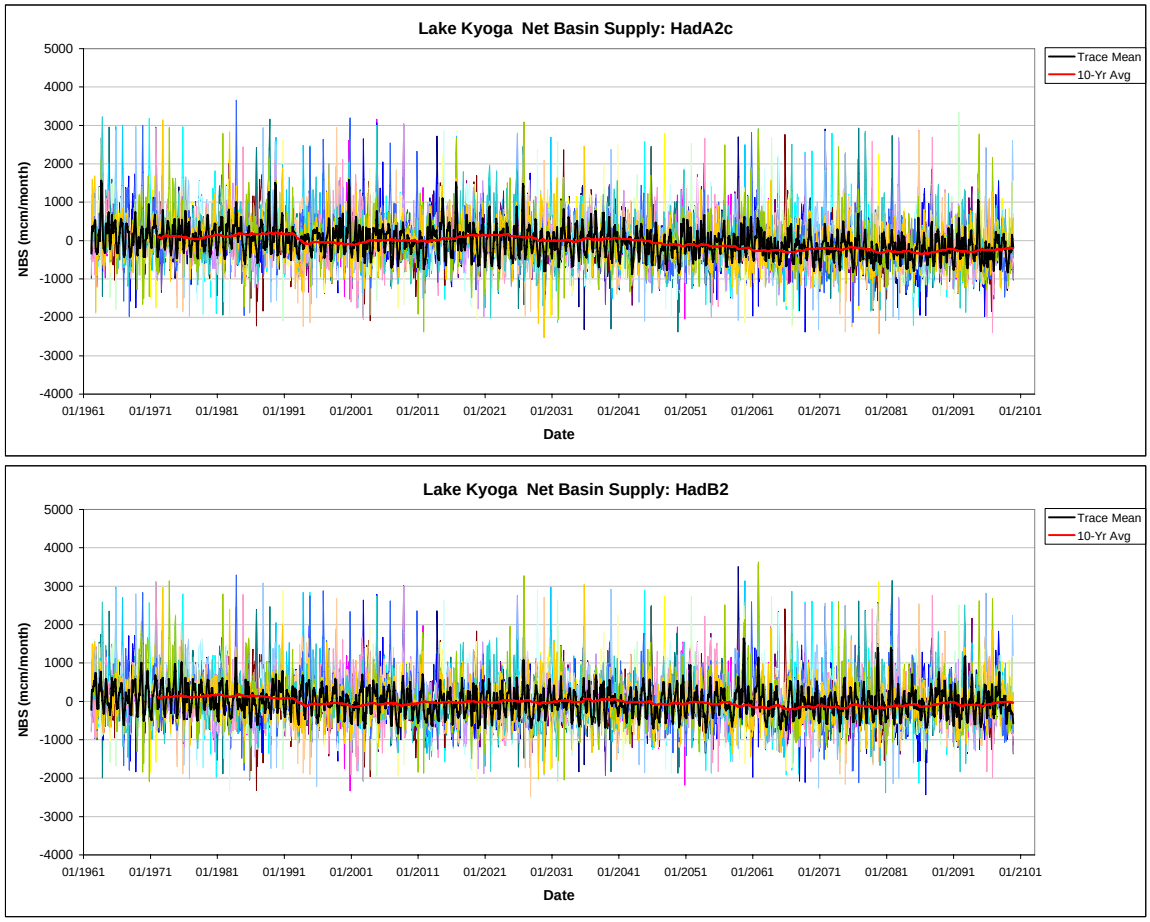

Figure B.2(g-h): Lake Kyoga net basin supply ensembles by scenario.

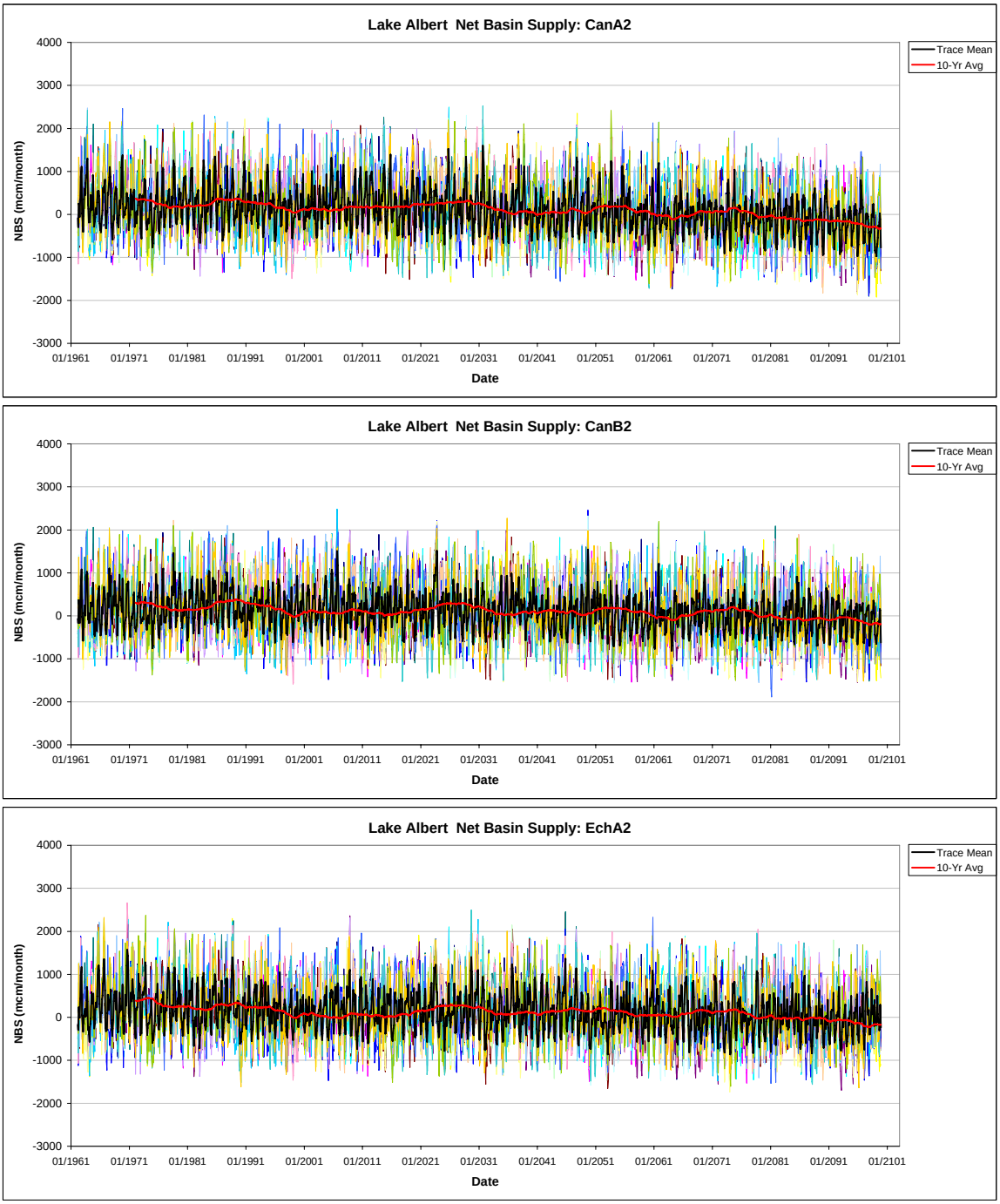

Figure B.3(a-c): Lake Albert net basin supply ensembles by scenario.

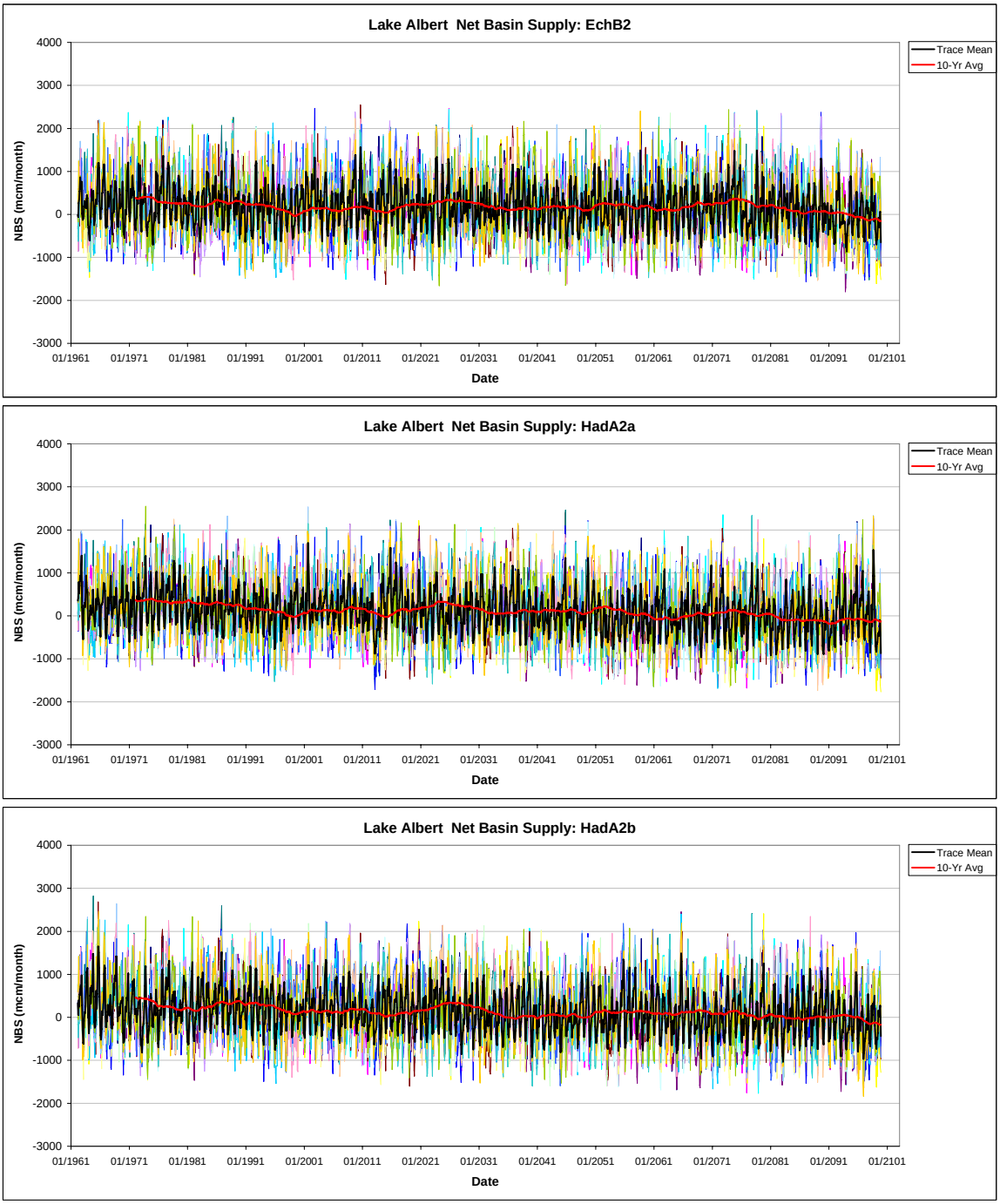

Figure B.3(d-f): Lake Albert net basin supply ensembles by scenario.

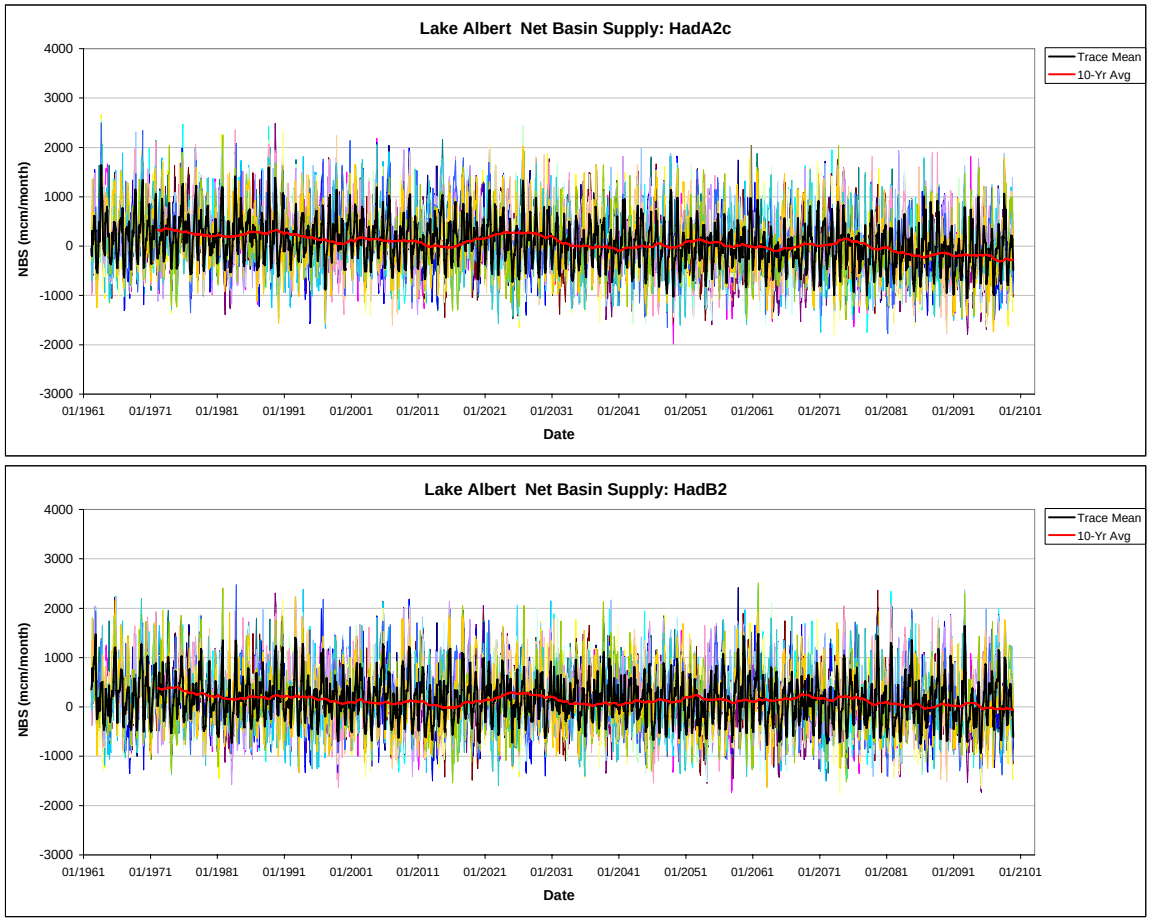

Figure B.3(g-h): Lake Albert net basin supply ensembles by scenario.

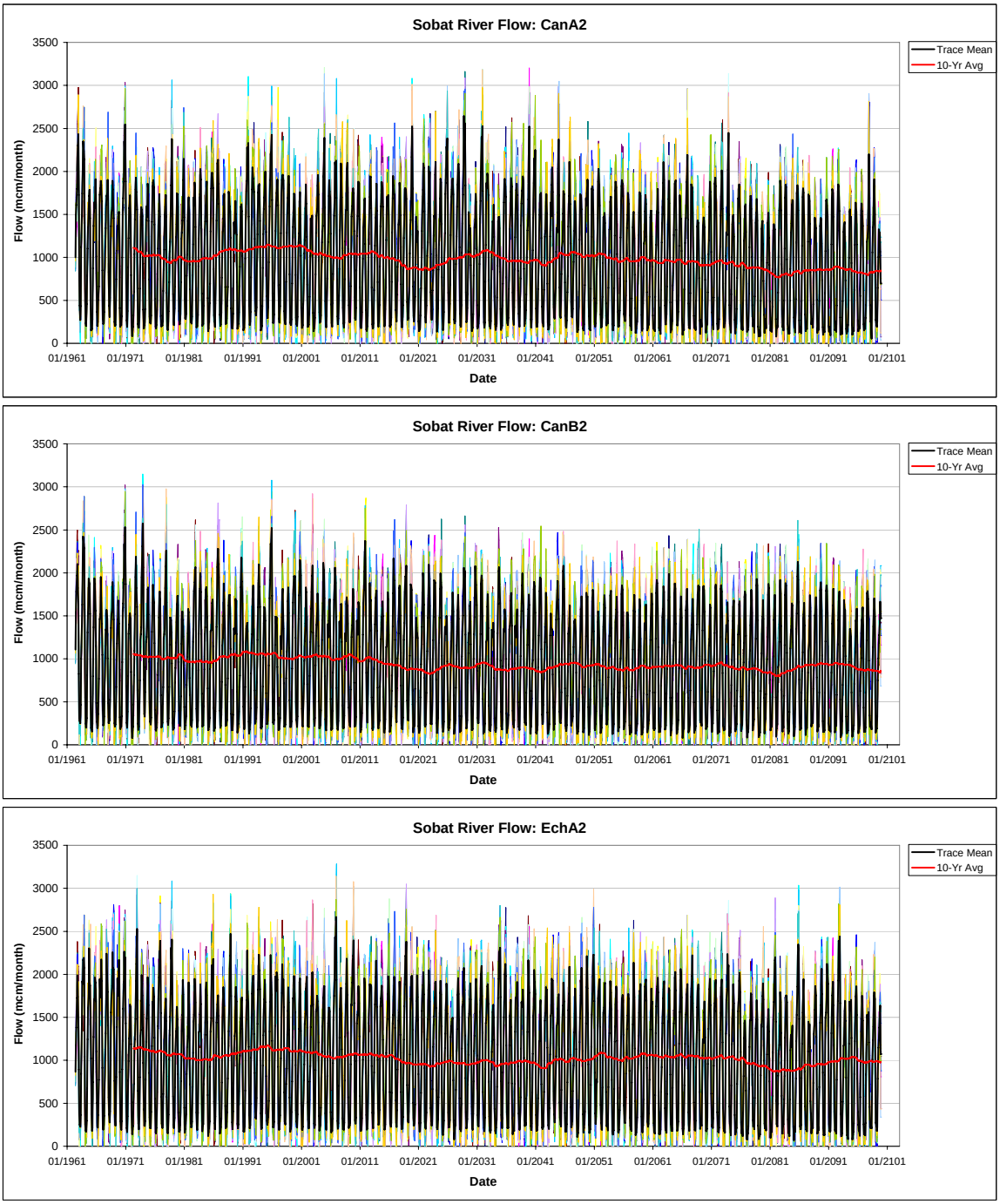

Figure B.4(a-c): Sobat River flow ensembles by scenario.

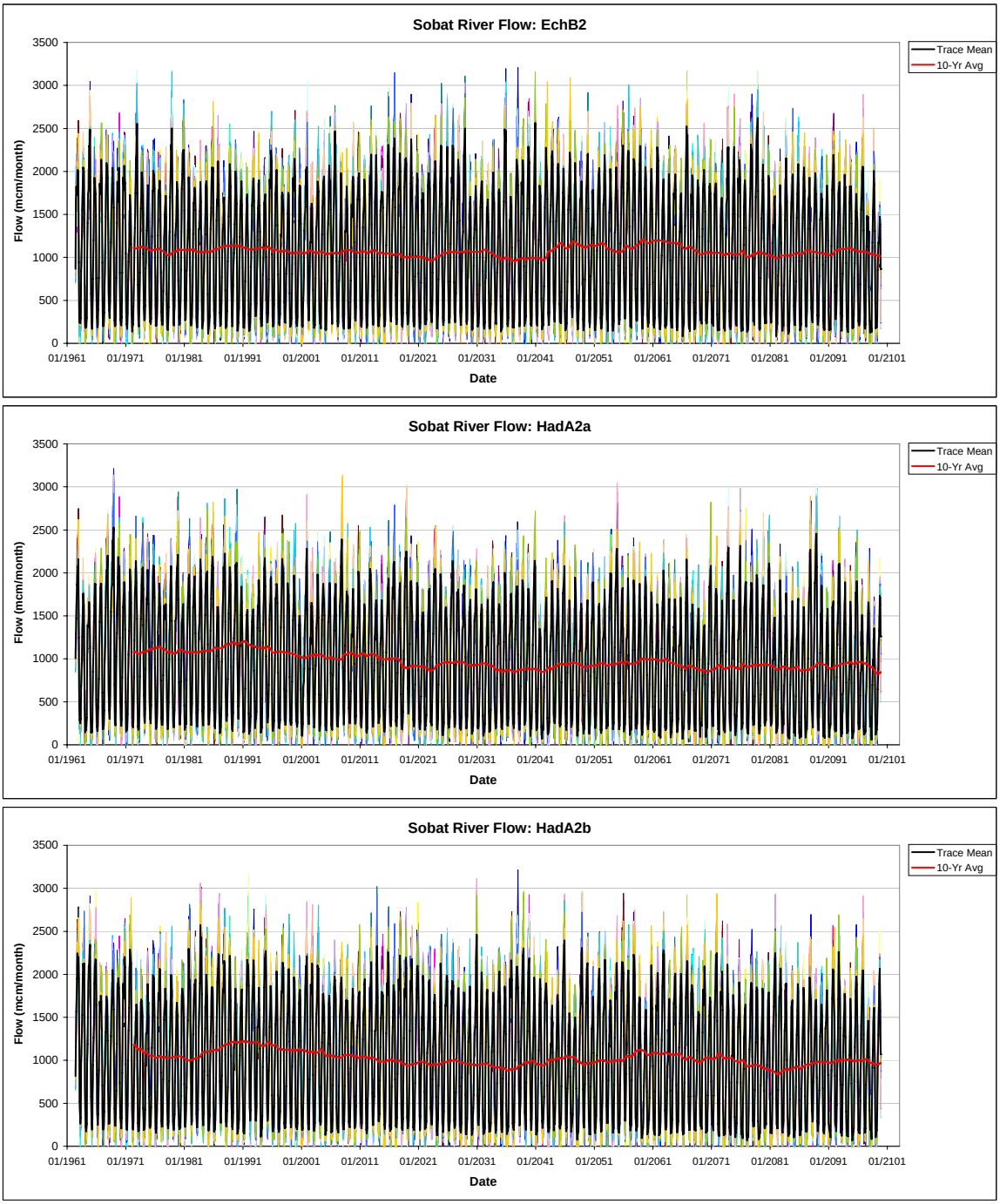

Figure B.4(d-f): Sobat River flow ensembles by scenario.

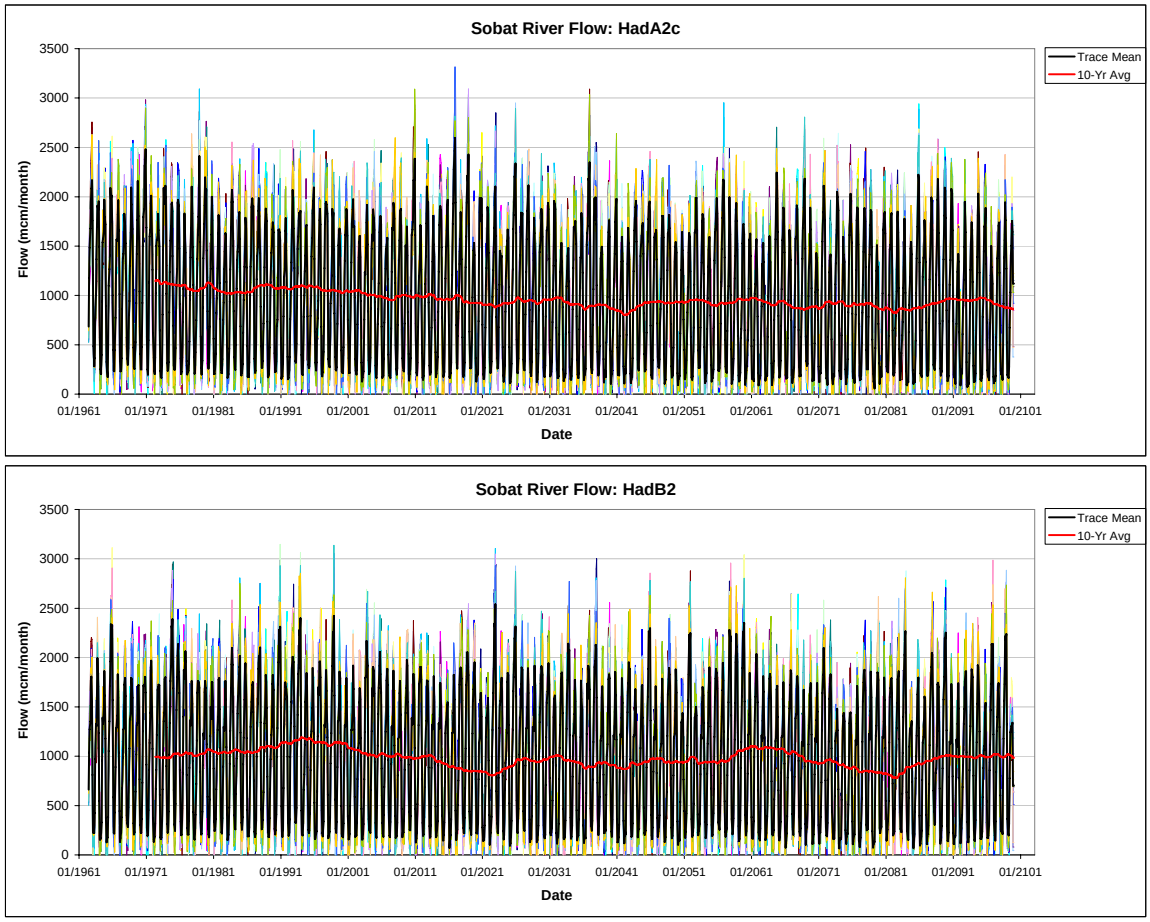

Figure B.4(g-h): Sobat River flow ensembles by scenario.

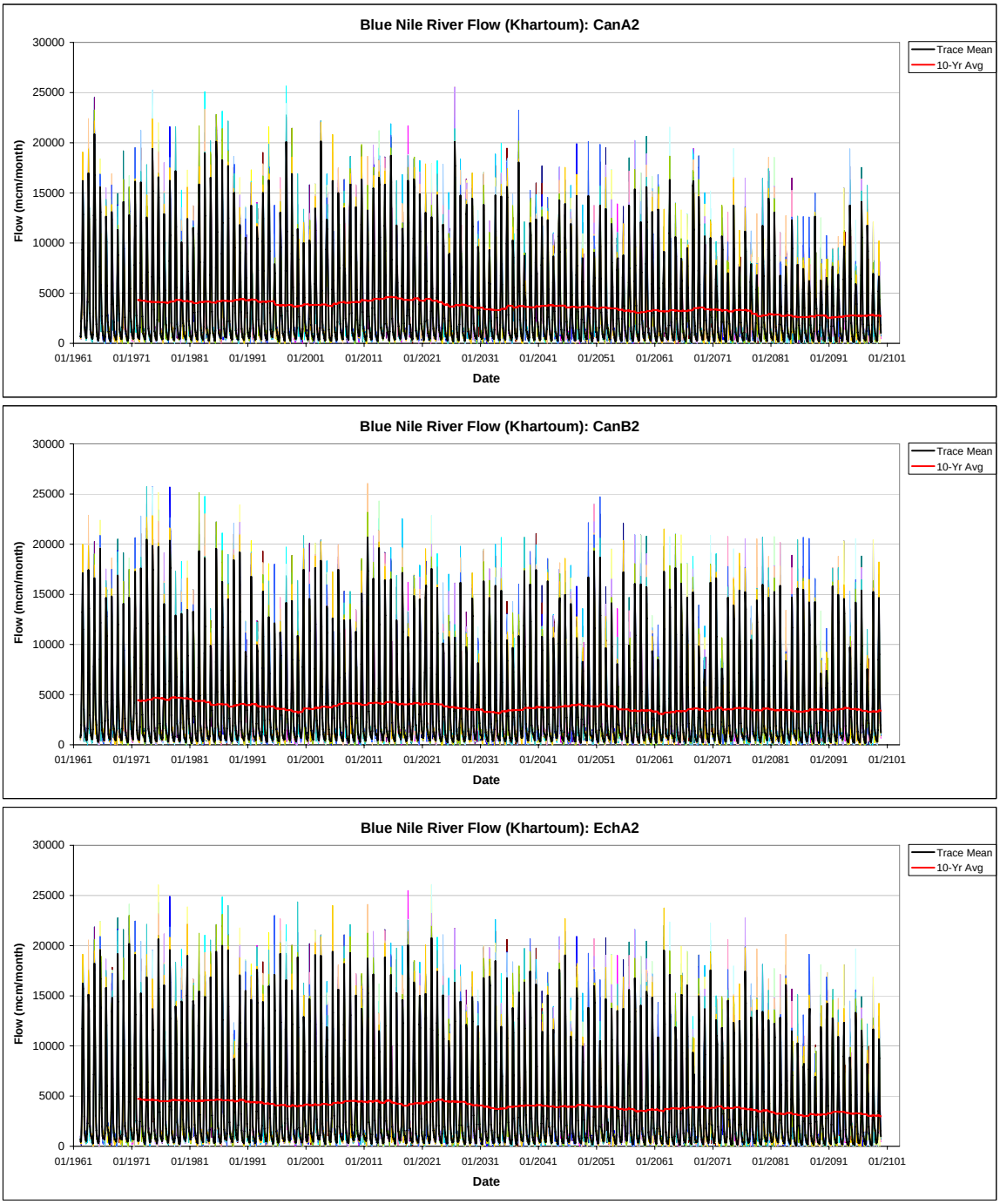

Figure B.5(a-c): Blue Nile flow ensembles by scenario.

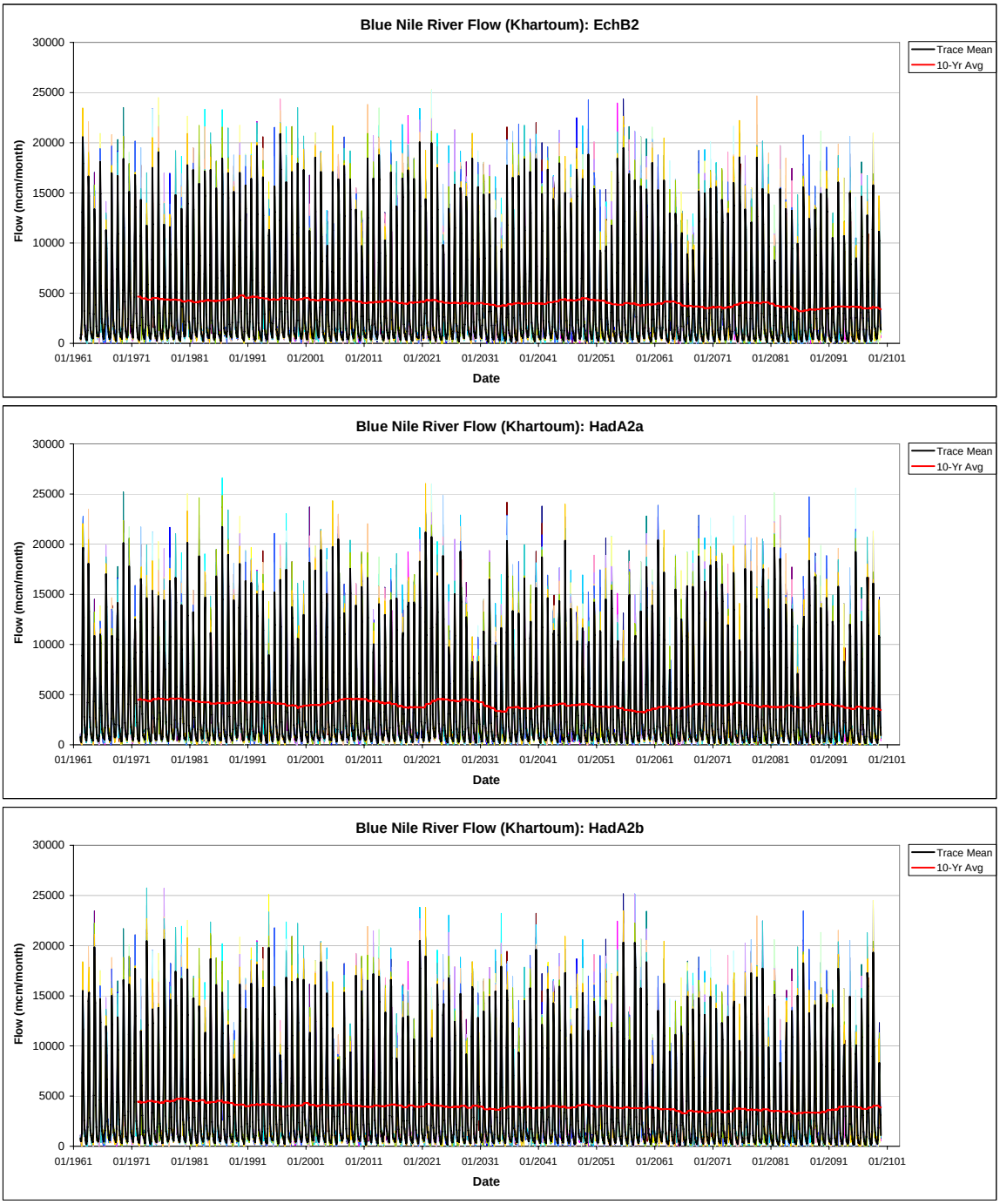

Figure B.5(d-f): Blue Nile flow ensembles by scenario.

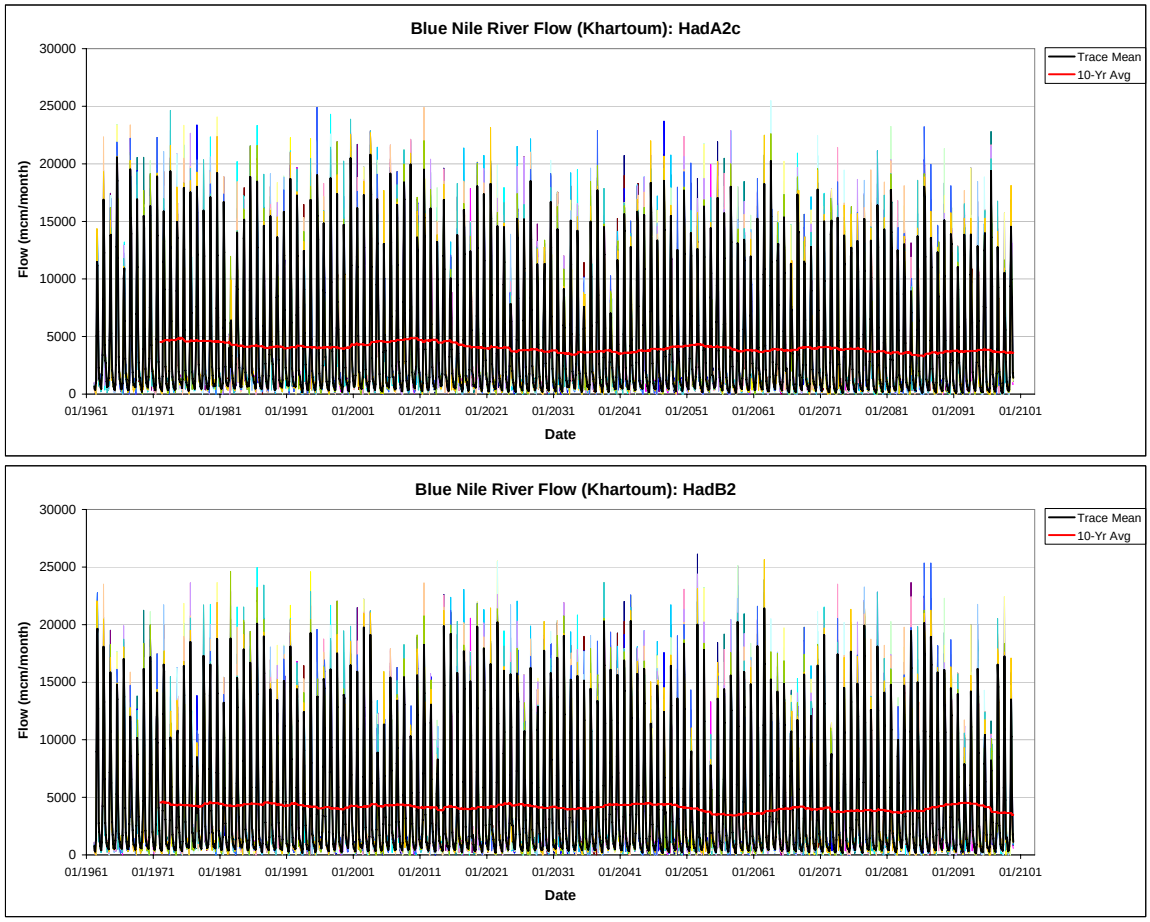

Figure B.5(g-h): Blue Nile flow ensembles by scenario.

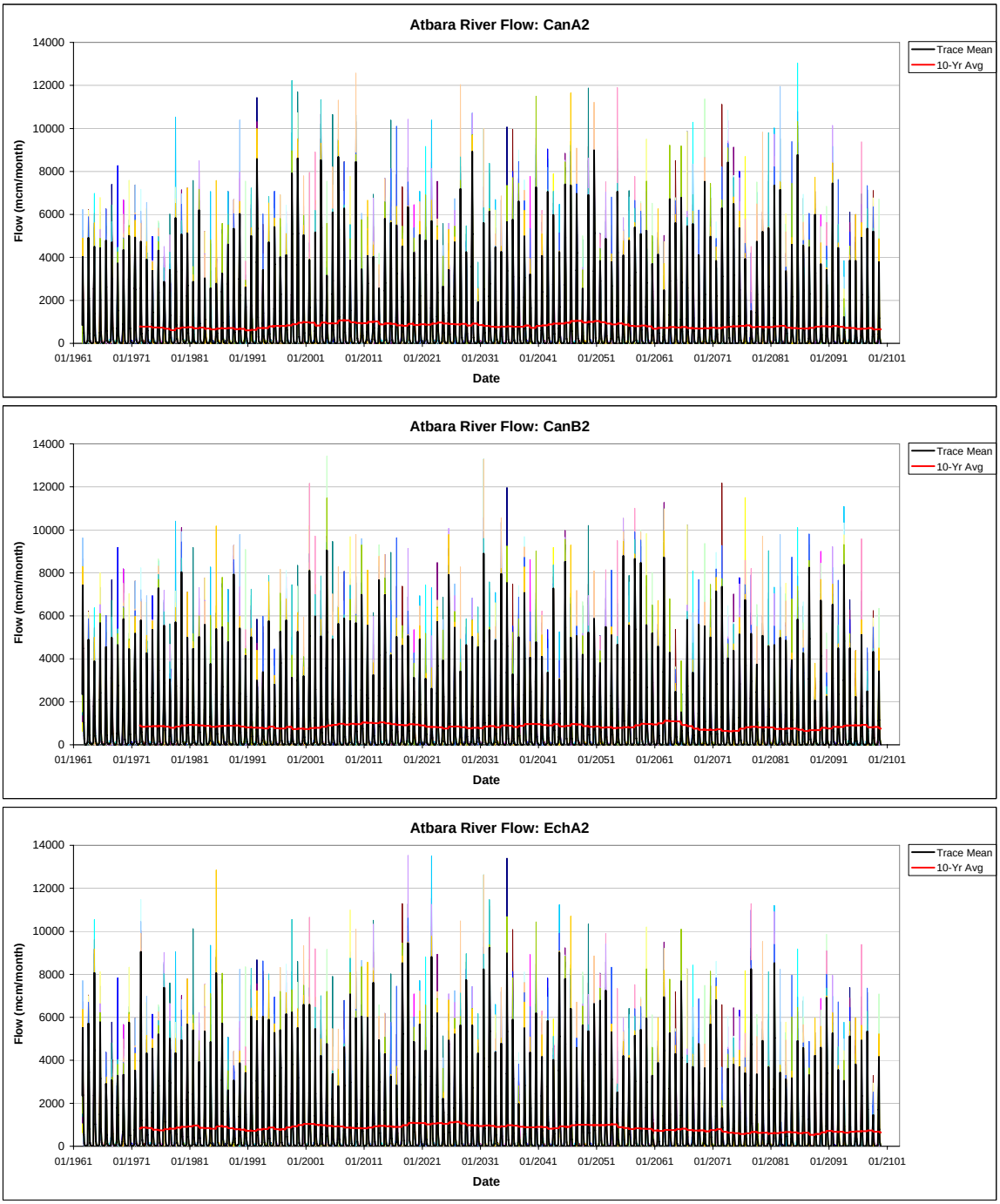

Figure B.6(a-c): Atbara River flow ensembles by scenario.

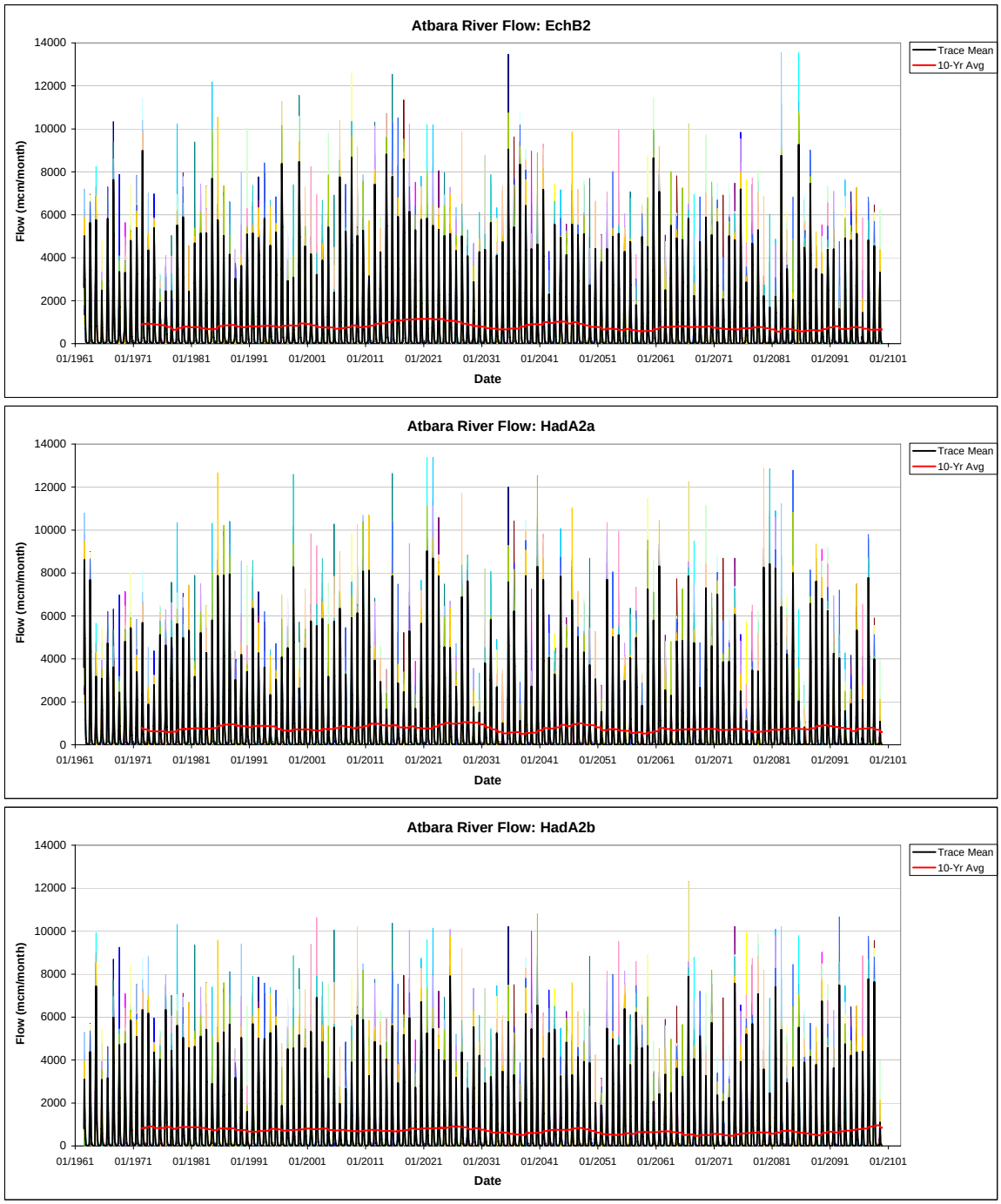

Figure B.6(d-f): Atbara River flow ensembles by scenario.

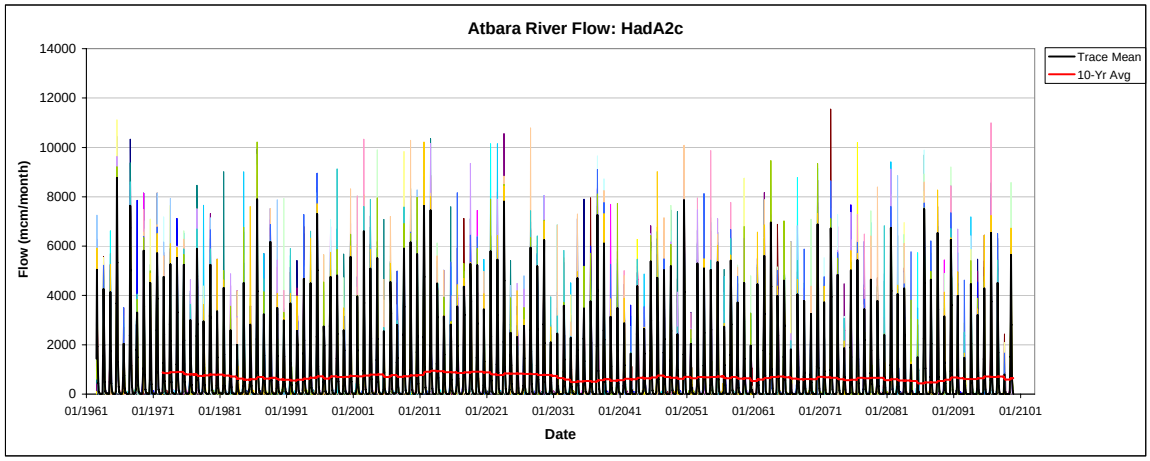

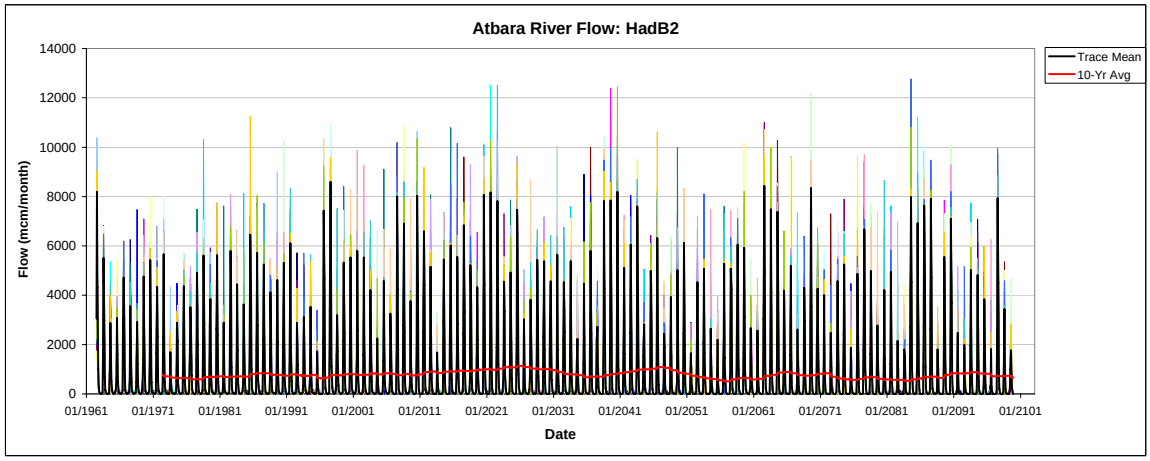

Figure B.6(g-h): Atbara River flow ensembles by scenario.

Appendix C

Nile System Specifications (after Georgakakos and Yao, 2000)

Table C.1: Storage and outflow specifications for the Equatorial Lakes.

		Lake Victoria [1900-1977]	Lake Kyoga [1912-1977]	Lake Albert [1905-1977]
	Level (m)	1133.08	1030.31	618.75
Minimum	**Storage (bcm)**	2905.73	5.44	145.88
	Outflow (bcm/yr)	10.94	8.83	10.82
	Level (m)	1134.28	1031.81	620.51
Mean	**Storage (bcm)**	2985.65	10.49	155.2
	Outflow (bcm/yr)	25.48	24.82	28.38
	Level (m)	1136.28	1034.11	623.97
Maximum	**Storage (bcm)**	3121.32	20.35	175.68
	Outflow (bcm/yr)	55.22	62.78	64.64

Table C.2: Existing and potential hydroelectric sites on the Victoria and Kyoga Niles.

	Hydroelectric Site	Power Capacity (MW)
	Owen Falls	380
Victoria Nile	Bujagali	320
	Kalagala	450
	Kamdini	180
Kyoga Nile	Ayago	538
	Murchison Falls	416

Table C.3: Existing and potential hydroelectric sites on the Blue Nile and Atbara Rivers.

	Max. Storage (bcm)	Min. Storage (bcm)	Desing Capacity (MW)
Lake Tana	13.84	2.34	200
Karadobi	34.2	3.94	1356
Mabil	14.11	3.22	1200
Mendaia	16.72	11.39	1620
Border	10.75	6.30	1400
Roseires	2.72	0.156	250
Sennar	1.07	0.180	15
Khashm el Girba	1.35	0.061	13

Table C.4: Storage and hydroelectric specifications for the Aswan Complex.

	High Aswan Dam	Old Aswan Dam
Max. Level (m)	178	113
Max. Storage (bcm)	137.5	0.10
Min. Level(m)	147	107.5
Min. Storage (bcm)	31.6	0.044
Design Capacity (MW)	2100	621

References

Achuta Rao, K., Covey, C., Doutriaux, C., Fionino, M., Gleckler, P., Philips, T., Sperber, K., and Taylor, K., 2004. An Appraisal of Coupled Climate Model Simulations, edited by: Bader, D., 20 University of California, Lawrence Livermore National Laboratory, UCRL-TR-202550.

Camberlin, P. and N. Philippon, 2002. The East African March-May Rainy Season: Associated Atmospheric Dynamics and Predictability over the 1968-97 Period. Journal of Climate, 15: 1002-1019.

Chan, S-O. and P.S. Eagleson, 1980. Water Balance Studies in the Bahr el Ghazal Swamp. Department of Civil Engineering, MIT, Technical Report No. 261.

Conway, D., 2000. The Climate and Hydrology of the Upper Blue Nile River. The Geographical Journal, 166: 49-62.

Conway, D. and M. Hulme, 1993. Recent fluctuations in precipitation and runoff over the Nile sub-basins and their impact on Main Nile discharge. Climatic Change, 25: 127-151.

Conway, D. and M. Hulme, 1996. The impacts of climate variability and future climate change in the Nile basin on water resources in Egypt. Water Resources Development, 12: 277-296.

Conway, D., M. Krol, J. Alcamo, and M. Hulme, 1996. Future availability of water in Egypt: the interaction of global, regional, and basin scale driving forces in the Nile basin. Ambio, 25: 336-342.

Dingman, L., 2002. *Physical Hydrology*. 2nd Ed. Prentice Hall, Upper Saddle River, New Jersey, 646 pp.

Efron, B., and R. Tibshirani, 1993. *An Introduction to the Bootstrap*. Chapman & Hall/CRC, New York, 436 pp.

El-Hemry, I.I. and P.S. Eagleson, 1980. Water Balance Estimates of the Machar Marshes. Department of Civil Engineering, MIT, Technical Report No. 260.

Fahmy, A. and S. Fahmy, 1981. Mathematical Model of the Upper Nile System. Proceedings of the 2nd International Conference of Water Resources Planning, Cairo, Egypt.

Flato, G.M., G.J. Boer, W.G. Lee, N.A. McFarlane, D. Ramsden, M.C. Reader and A.J. Weaver, 2000. The Canadian Centre for Climate Modeling and Analysis global coupled model and its climate. Climate Dynamics, 16: 451-467.

Georgakakos, A. P., and D.H. Marks, 1987. A Stochastic Control Method for the Real-Time Operation of Reservoir Systems. Water Resources Research, 23: 1376-1390.

Georgakakos, A. P., 1989. Extended Linear Quadratic Gaussian (ELQG) Control: Further Extensions. Water Resources Research, 25: 191-201.

Georgakakos, A. P., 1993. Operational Tradeoffs in Reservoir Control. Water Resources Research, 29: 3801-3819.

Georgakakos, A. P., H. Yao, and Y. Yu, 1995. A Decision Support System for the High Aswan Dam. Georgia Water Resources Institute Report, Georgia Tech, Atlanta, GA.

Georgakakos, A. P., C. Barrett, and B. Attia, 1996. A Decision Support System for the High Aswan Dam. Proceedings of the Fifth International Workshop on Water Resources Operations Management, sponsored by ASCE, Georgakakos, A. P., and Q. W. Martin Eds., pg. 34-66, Arlington, VA, March 4-6, 1996.

Georgakakos, A. P., and W. Klohn, 1997a. A Decision Support System for the Nile River. Proceedings of the 5th Nile 2002 Conference, Addis Ababa, Ethiopia, February 24-28.

Georgakakos, A. P., H. Yao, and Y. Yu, 1997b. A Control Model for Dependable Hydropower Capacity Optimization. Water Resources Research, 33: 2349-2365.

Georgakakos, A. P., H. Yao, and Y. Yu, 1997c. Control Models for Hydroelectric Energy Optimization. Water Resources Research, 33: 2367-2379.

Georgakakos, A. P., H. Yao, and Y. Yu, 1997d. A Control Model for Hydroelectric Energy Value Optimization. ASCE J. for Water Resources Planning and Management, 123: 30-38.

Georgakakos, A. P., W. Klohn, and B. Appelgren, 1998a. Decision Support Systems for Water Resources Planning and Management in the Nile Basin. Proceedings of the 6th Nile 2002 Conference, Kigali, Rwanda, February 23-27.

Georgakakos, A. P., M. Andgelic, and K. P. Georgakakos, 1998b. A Decision Support System for Lake Victoria. Proceedings of the 6th Nile 2002 Conference, Kigali, Rwanda, February 23-27.

Georgakakos, A. P., M. Mullusky, H. Yao, and B. Attia, 1998c. El Nino/Southern Oscillation: Implications for Water Management in the Nile Basin. Proceedings of the 6th Nile 2002 Conference, Kigali, Rwanda, February 23-27.

Georgakakos, A. P., K. Brumbelow, S. Bourne, C. Demarchi, and H. Yao, 1999. A Decision Support System for Lake Victoria. Georgia Water Resources Institute Report, Georgia Tech, Atlanta, GA.

Georgakakos, A. P., and H. Yao, 2000. An Assessment of the Development Options, Management Strategies, and Climate Scenarios for the Nile Basin. Georgia Water Resources Institute Report, Georgia Tech, Atlanta, GA.

Georgakakos, A. P., and H. Yao, 2003. A Decision Support System for the Nile River. Georgia Water Resources Institute Report, Georgia Tech, Atlanta, GA.

Gordon, C., C. Cooper, C.A. Senior, H.T. Banks, J.M. Gregory, T.C. Johns, J.F.B. Mitchell, and R.A. Wood, 2000. The simulation of SST, sea ice extents and ocean heat transports in a version of the Hadley Centre coupled model without flux adjustments. Climate Dynamics, 16: 147-168.

Howell, P., M. Lock, and S. Cobb, 1988. *The Jonglei Canal: Impact and Opportunity*. Cambridge University Press.

Hulme, M. and T.R. Carter, 1999. Representing uncertainty in climate change scenarios and impact studies in ECLAT-2 Report No.1, Helsinki Workshop Proceedings, Climate Research Unit, Norwich, UK, 128 pp.

Hulme, M., R. Doherty, T. Ngara, M. New and D. Lister, 2001. African Climate Change: 1900-2100. Climate Research, 17: 145-168.

Hurst, H. E., and P. Philips, 1931. *Nile Basin Vol. I: General Description of the Basin, Meteorology, Topography of the White Nile Basin*. Government Press, Cairo.

Hurst, H. E., and P. Philips, 1938. *Nile Basin Vol. V: The Hydrology of the Lake Plateau and Bahr el Jebel*. Government Press, Cairo.

Hurst, H. E., R. P. Black, and Y. M. Simaika, 1946. *Nile Basin Vol. VII: The Future Conservation of the Nile*. Government Press, Cairo.

Hurst, H. E., 1950. *Nile Basin Vol. VIII: The Hydrology of the Sobat and White Nile and the Topography of the Blue Nile and Atbara.*. Government Press, Cairo.

Hurst, H. E., R. P. Black, and Y. M. Simaika, 1966. *Nile Basin Vol. X: The Major Nile Projects*. Government Press, Cairo.

IPCC, 1999. Guidelines on the Use of scenario data for climate impact and adaptation assessment. Version 1. Prepared by Carter, T.T., M. Hulme, and M. Lal, IPCC Task Group on Scenarios for Climate Impact Assessment, 69 pp.

IPCC, 2000. Special Report on Emissions Scenarios: A Special Report of Working Group III of the Intergovernmental Panel on Climate Change. N. Nakicenovic and R. Swart eds. Cambridge University Press, Cambridge, U.K., 599 pp.

IPCC, 2001. Climate Change 2001: The Scientific Basis, Contribution of Working Group I to the Third Assessment Report of the Intergovernmental Panel on Climate Change. Cambridge University Press, Cambridge, United Kingdom, 881 pp.

IPCC Data Distribution Center, http://ipcc-ddc.cru.uea.ac.uk/index.html, October 2006.

Jonglei Investigation Team, 1954. The Equatorial Nile Project and its Effects in the Aglo-Egyptian Sudan. Technical Report of the Jonglei Investigation Team, Government of Sudan.

Linacre, E.T., 1993. Data-sparse estimation of lake evaporation, using a simplified Penman equation. Agricultural and Forest Meteorology, 64: 237-256.

Mearns, L.O., F. Giorgi, P. Whetton, D. Pabon, M. Hulme, and M. Lal, 2003. Guidelines for Use of Climate Scenarios Developed from Regional Climate Model Experiments. Data Distribution Centre of the Intergovernmental Panel on Climate Change.

Mitchell, T.D., 2003. Pattern Scaling. Climatic Change, 60: 217-242.

Mitchell, T.D., 2005: An improved method of constructing a database of monthly climate observations and associated high resolution grids. International Journal of Climatology, 25: 693-712.

Nicholson, S. E., 1996. A review of climate dynamics and climate variability in Eastern Africa. *The Limnology, Climatology and Paleoclimatology of the East African Lakes*. T. C. Johnson and E.O. Odada, Eds., Gordon and Breach, 25-56.

Nyenzi, B.S., 1988. Mechanisms of East African rainfall variability. PhD Thesis, Department of Meteorology, Florida State University.

Oberhuber, J.M., 1993. Simulation of the Atlantic circulation with a coupled sea-ice-mixed layer-isopycnical general circulation model. Part I: model description. Journal of Physical Oceanography, 23: 808-829.

Ogallo, L., 1979. Rainfall variability in Africa. Monthly Weather Review, 107: 1133-1139.

Pike, J. G., 1964. The estimation of annual run-off from meteorological data in a tropical climate. Journal of Hydrology, 2: 116-123.

Pope, V. D., M. L. Gallani, P. R. Rowntree and R. A. Stratton, 2000. The impact of new physical parameterizations in the Hadley Centre climate model -- HadAM3. Climate Dynamics, 16: 123-146.

Rodhe, H. and H., Virji, 1976. Trends and periodicities in East African rainfall data. Monthly Weather Review, 104: 307-315.

Roeckner, E., K. Arpe, L. Bengtsson, M. Christoph, M. Claussen, L. Dümenil, M. Esch, M. Giorgetta, U. Schlese, and U. Schulzweida, 1996. The atmospheric general circulation model ECHAM4: Model description and simulation of present-day climate. Max Planck Institut für Meteorologie, Report No. 218, Hamburg, Germany, 90 pp.

Sadek, M.F., M.M. Shahin, and C.J. Stigter, 1997. Theoretical and Applied Climatology, 56: 57-66.

Shahin, M., 1985. *Hydrology of the Nile Basin*. Developments in Water Science, 21, Elsevier, Amsterdam, 575 pp.

Special Report of the Intergovernmental Panel on Climate Change, 2000. Nebojsa Nakicenovic and Rob Swart, Eds., Cambridge University Press, UK., 570 pp.

Sutcliffe, J.V. and Y.P. Parks, 1999. *The Hydrology of the Nile.* IAHS Press, Wallingford, UK, 180 pp.

Tate, E., J. Sutcliffe, D. Conway, and F. Farquharson, 2004. Water balance of Lake Victoria: update to 2000 and climate change modeling to 2100. Hydrological Sciences Journal, 49: 563-574.

United Nations Development Program, 1981. Mathematical Model of the Upper Nile. Water Master Plan Technical Report No. 15, Ministry of Irrigation, Egypt.

U.S. Bureau of Reclamation, 1964. Land and Water Resources of the Blue Nile Basin, Ethiopia. Main Reconnaissance Report and Appendices, prepared for the U.S. Agency for International Development and the Ethiopian Government.

WMO, 1974. Hydrometeorological Survey of the Catchments of Lakes Victoria, Kyoga, and Albert. WMO/UNDP, Geneva.

Yates, D. and K. Strzepek, 1998. Modeling the Nile basin under climatic change. Journal of Hydrologic Engineering, 3: 98-108.